Mixed Micelle Characterization of Pluronic and Gemini Surfactant – Based Gene Therapy Carriers and a Connection to Transfection Efficiency

by

Samantha Marisha Shortall

A thesis
presented to the University of Waterloo
in fulfillment of the
thesis requirement for the degree of
Doctor of Philosophy
in
Pharmacy

Waterloo, Ontario, Canada, 2020

Examining Committee Membership

The following served on the Examining Committee for this thesis. The decision of the Examining Committee is by majority vote.

External Examiner	DR. TODD HOARE Associate Professor, Chemical Engineering, McMaster University
Supervisor	DR. SHAWN D. WETTIG Professor; Associate Dean, Graduate Studies (Science)
Internal Member(s)	DR. PRAVEEN NEKKAR RAO Associate Professor; Graduate Officer (Pharmacy)
	DR. OWEN VAN CAUWENBERGHE Adjunct Assistant Professor
Internal-External Member	DR. MICHAEL K. C. TAM Professor, Chemical Engineering; University Research Chair

Author’s Declaration

I hereby declare that I am the sole author of this thesis. This is a true copy of the thesis, including any required final revisions, as accepted by my examiners.

I understand that my thesis may be made electronically available to the public.

Abstract

Non-viral gene therapy formulation development often relies on a rational design approach, where vector components are selected based on individual characteristics known to favour transfection efficiency. However, these mixtures do not necessarily result in additive or even synergistic effects on efficiency, leaving the vast majority of non-viral formulations limited by poor transfection. The development of successful non-viral gene therapy carriers is stunted by unpredictable results, even *in vitro*, and often poor correlations to external physical characterizations such as particle size, shape, and zeta potential to aid in effective screening of potential formulations.[1] This creates reliance on trial and error experiments that are not feasible long-term.[2] Current gene therapy studies fail to consider the internal mixing interactions involved in self-assembled systems and the effect of the presence of the intended active pharmaceutical ingredient (API), nucleic acids in this case. These factors have an irrefutable impact on transfection; hence, this work aimed to address this knowledge gap by exploring the interactions between the components of a self-assembled Pluronic/gemini surfactant-based nanocarrier for plasmid DNA delivery, and presents a link to transfection efficiency that may inform more effective vector design and screening for future formulation development.

In an effort to improve the transfection efficiency of gemini surfactant-based vectors for non-viral gene therapy, the addition of neutral block copolymers known as poloxamers (or commonly by their former commercial name, Pluronics, BASF Corp.) to the *N*,*N'*-bis(dimethylhexadecyl)-1,3-propanediammonium dibromide (16-3-16) gemini surfactant have recently been under investigation. Although preliminary studies of such formulations have shown limited transfection *in vitro*, the transfection efficiencies appear related to the nature and strength of mixed micelle formation in these systems, which may aid the optimization of these Pluronic/16-3-16, and related, systems in the future.

To study the plasmid DNA-loaded Pluronic and 16-3-16 gemini surfactant mixed micellization, the full formulations were treated as binary mixtures in water where the 16-3-16/pDNA condensate or complex (prepared at charge ratio N^+/P^- 10:1) was treated as a single component. A critical aggregate concentration (CAC) of the 16-3-16/pDNA complex in water was determined by surface tension, conductivity, and dynamic light scattering measurements over a range of 16-3-16/pDNA concentrations. Based on these studies, it was also proposed that the gemini surfactant molecules only partially dissociate from the pDNA upon dilution to concentrations below the CAC, leaving a “loose”,

electrostatically-bound 16-3-16/pDNA complex. At concentrations beyond the 16-3-16/pDNA CAC, the complex returns to a more condensed form.

A series of Pluronic block copolymers (F87, P84, L121, F127, P103, and L44) was used to study the effects of the Pluronic composition on its mixing behaviour with the 16-3-16/pDNA condensates. CAC values determined by tensiometry and application of Rubingh's mixed micelle theory indicated that Pluronic and 16-3-16/pDNA mixed micellization is generally synergistic in nature but the strength of this synergism decreases with increasing PPO block length. The non-ideal mixing behaviours were attributed to a greater presence of the 16-3-16/pDNA component in the mixed aggregates involving the larger PPO blocks (60 PO units and above), as opposed to Pluronic-rich aggregates for polymers with lower PO content. Presumably, micellization is hindered by the bulkiness of larger PPO blocks.

Transfection efficiency was evaluated by expression of enhanced green fluorescence protein (eGFP) as a reporter gene for plasmid expression in COS-7 cells *in vitro*, and cytotoxicity was determined by propidium iodide staining. Transfection varied with the Pluronic composition and Pluronic mole fraction in the formulation, but there was no significant decrease in the cell viability compared to non-treated cells. The Pluronic/16-3-16/pDNA formulations produced self-assembled nanoparticles with sizes generally below 250 nm and positive zeta potentials that appeared to decrease linearly with increasing Pluronic PEO chain lengths. Although there was no clear relationship between the transfection efficiency and the particle size and zeta potentials, higher transfection was associated with stronger synergism and aggregates enriched with the Pluronic-component. These findings could be used for future optimization.

Acknowledgements

First and foremost, thank you to my supervisor, Dr. Shawn Wettig, who has been a supportive, encouraging, and patient mentor. Over my many years of working in the Wettig Lab I have appreciated the numerous opportunities for professional growth and the chance to explore and build new ideas together. I am also indebted to my advisory committee members Dr. Praveen Nekkar, and Dr. Owen Van Cauwenberghe for sharing their professional guidance and technical expertise throughout the progress of this research and graduate program. Financial support from the CIHR Drug Safety & Effectiveness Cross-disciplinary Training Program, Ontario Graduate Scholarship, University of Waterloo, and School of Pharmacy were also greatly appreciated throughout this research program.

Dr. Roderick Slavcev is gratefully acknowledged for providing the plasmid used in this work and for his mentorship and collaboration during my graduate studies. Thank you to members of the Slavcev Lab, Jessica Nicastro, Shirley Wong, Nafiseh Nafissi, and Farah El-Zarkout for their helpful direction in microbiology biology techniques and troubleshooting some plasmid-related challenges at the start.

Thank you to Dr. Monica Tudorancea (School of Pharmacy, University of Waterloo) for her assistance with the School of Pharmacy Core Research Facility equipment used during the course of this research. I also thank Dr. Terence Tang (Biology, University of Waterloo) and Mishi Groh (Biology, University of Waterloo) for their guidance in experiment planning and execution of the flow cytometry and transmission electron microscopy analyses, respectively.

Zameer Bharwani, Fatum Abdullahi, and Disha Bhagat are acknowledged for their contributions to the surface tension, particle size and zeta potential data in this thesis. I am also grateful to Monica Hoang and Nyasha Gondora for sharing their knowledge of mammalian cell culture techniques and *in vitro* cytotoxicity assays.

My gratitude goes to all members of the Wettig Lab, with special thanks to: Haitang (Lizzie) Wang for her guidance during the early stages of my research journey; Osama Madkhali for collaborative efforts in transfection experiments and early work on Pluronic/16-3-16 formulations; Aula Al-Muslim for her assistance with multiple physical chemistry techniques; and Shannon Callender for helping me troubleshoot many technical problems in the lab, and for joining me in brainstorming and allowing me to work through new ideas aloud!

Thank you to the School of Pharmacy graduate student community – it has been a privilege to learn and laugh with so many of you. Thanks to all my friends and family for their cheers of encouragement.

Finally, I would like to acknowledge my fiancé, David Francis, for his patience and unlimited support with every new step I take, and most of all, for reminding me to just be myself.

Dedication

I dedicate this thesis to my mother, Fazeeda Baksh.

Mom, thank you for making learning fun, encouraging my creativity, and teaching me to consider multiple perspectives of an argument. Needless to say, some of it came in handy throughout this journey. And as my interests and aspirations continue to evolve I find strength in your unconditional love and support.

Table of Contents

List of Figures

List of Tables

List of Abbreviations

16-3-16	*N,N'*-bis(dimethylhexadecyl)-1,3-propanediammonium dibromide
16-3-16/pDNA	16-3-16 gemini surfactant - plasmid DNA complex
ANOVA	analysis of variance
ATP	adenosine triphosphate
CAC	critical aggregate concentration
CMC	critical micelle concentration
CMC_i	critical micelle concentration of surfactant i
CMC_{ION}	critical micelle concentration of ionic surfactant in ionic/non-ionic surfactant mixtures
CMC_{NON}	critical micelle concentration of non-ionic surfactant in ionic/non-ionic surfactant mixtures
CTAB	Cetyltrimethylammonium bromide
Dc-chol	3β-(*N*-[*N*',*N*'-dimethylaminoethane]-carbamoyl)cholesterol hydrochloride
DLS	dynamic light scattering
DMEM	Dulbecco's Modified Eagle Medium
DNA	deoxyribonucleic acid
DODAB	Dimethyldioctadecylammonium
DOSPA	2,3-dioleyloxy-*N*-(2-[sperminecarboxyamido]ethyl)-*N*,*N*-dimethyl-1-propaniminium bromide
DOTMA	*N*-[1-(2,3-dioleyloxy)propyl]-*N*,*N*,*N*-trimethylammonium chloride
DOTAP	*N*-{1-(2,3-dioleoyloxy)propyl}-*N*,*N*,*N*-trimethylammonium chloride
eGFP	enhanced green fluorescence protein
EMA	European Marketing Association

EO	ethylene oxide
FDA	(United States) Food and Drug Administration
i.m.	intramuscular
i.v.	intravenous
MPS	mononuclear phagocytic system
NLS	nuclear localization signal
pDNA	plasmid deoxyribonucleic acid
PEI	polyethyleneimine
PEO/PEG	poly(ethylene oxide) / poly(ethylene glycol)
PI	propidium iodide
PO	propylene oxide
PPO	poly(propylene oxide)
RES	reticuloendothelial system
RNA	ribonucleic acid
RST	Regular Solution Theory
TEM	transmission electron microscopy
X_1	mole fraction of component 1 in the mixed micelle
X_{ION}	mole fraction of ionic component in ionic/non-ionic mixed micelles
X_{ideal}	ideal mole fraction of component 1 in the mixed micelle
α_i	solution mole fraction of component i
β	interaction parameter
γ	Surface tension

Chapter 1
Introduction

This chapter provides a detailed review of the background literature relevant to the work presented in this thesis. While each body chapter also includes a short introduction to provide some context to the results and a relationship to current knowledge in a particular field, this chapter provides a more comprehensive summary of the topics.

1.1 Surface Active Agents Form Micelles

Surface active agents, also known as surfactants, are materials that preferentially adsorb at the boundary (interface) between two immiscible phases, which alters the surface or interfacial properties of the system.[3] Surfactants are amphiphilic, possessing both hydrophilic and hydrophobic regions within their molecular structure, which allows for this surface/interfacial activity. (Note the term "surface" is used in reference to systems where one phase is a gas. In this work, "surface" and "surface tension" refer to that between air and water.)

Due to their "split nature", surfactants must reorganize themselves in solution in order to reduce the occurrence of energetically unfavourable hydrocarbon-water interactions. For example, when a surfactant is dissolved in water, there is a distortion of the solvent structure, which increases the overall free energy of the system.[3] Since the hydrophobic chains of the surfactant molecules are unable to hydrogen bond with water, water molecules of the bulk phase form a cage structure around the hydrophobic groups.[4] These cavities in the bulk water structure result in more order and in a significant entropy decrease.[4] Therefore, the surfactant molecules concentrate at the surface where they orient in such a way that the lyophobic groups are directed away from the bulk solvent, thus minimizing the free energy of the system.[3]

Once a sufficient amount of surfactant is added to the system and the surface is saturated, the free energy of the system must be minimized in other ways. Phase separation from solution could also eliminate the unfavourable hydrocarbon-water interactions, but this would also involve removal of the hydrophilic portions of the surfactant structures, which would not be energetically favourable. Aggregation of the surfactant molecules into clusters known as micelles offers a feasible means of minimizing the free energy of the systems.[5] Micellization allows the hydrophobic groups to be removed from the water and combine into a hydrophobic core, while the surfactants' hydrophilic groups face outward to form a shell that remains in contact with water.[4] The return of water molecules formerly

making up the highly ordered cavities to the normal hydrogen-bonding environment of the bulk water results in an entropy increase which drives the micellization process.[4] Therefore, the driving force for micellization comes from a gain in entropy; however, when all factors are considered, the occurrence of micelle formation and the concentration at which micellization takes place is governed by a balance of forces that either favour or oppose this aggregation process.[4]. For example, a loss of freedom experienced by the surfactant molecule in being transferred from solution to confined to a micelle, and electrostatic repulsion between ionic surfactant head groups result in increased free energy.[3,5] Additional considerations in the head group region include the tendency for head groups to crowd together to minimize water contact with the micelle core, but also electrostatic, steric, and hydration considerations that create a tendency for head groups to spread apart.[6] Nonetheless, micellization still occurs when the gain in entropy for the bulk solvent is greater and leads to an overall minimization of free energy for the system as a whole.

Although micelles are typically depicted as spherical, the micellar structure depends on the relative shape and space occupied by the headgroup and hydrophobic groups (Figure 1.1-1). An approximation of the micelle structure in aqueous solution is given by the critical packing parameter, calculated according to the equation $P = \frac{v}{a_0 l_c}$, where v is the volume of the hydrophobic portion, a_0 is the area occupied by the headgroup, and l_c is the maximum length the hydrocarbon tail can stretch according to factors such as the molecular structure and environment.[3] The critical packing parameter for some general surfactant structures and the predicted aggregate structure are listed in Table 1.1-1.

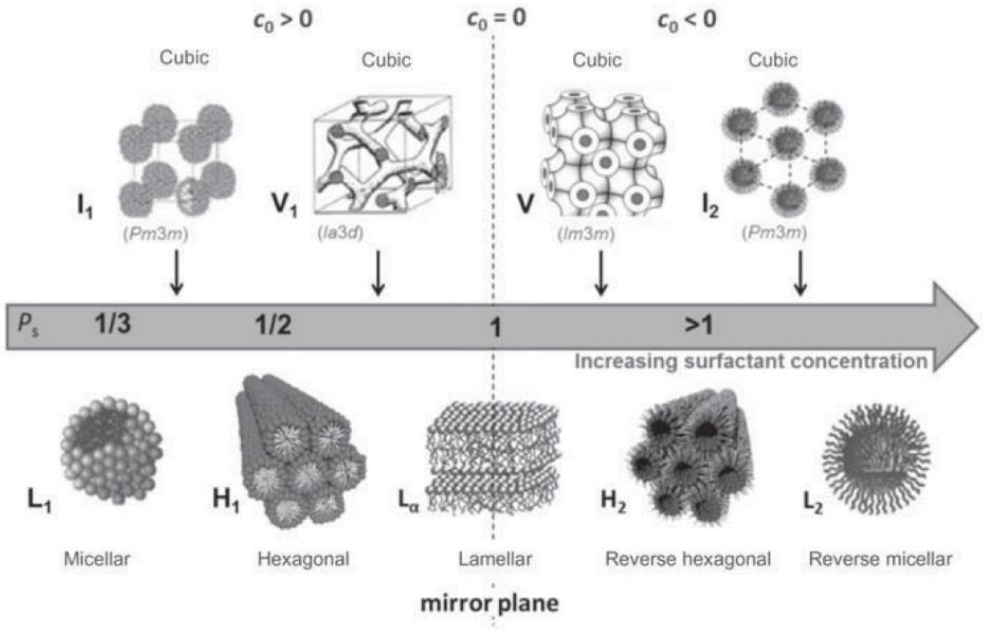

Figure 1.1-1 Idealized sequence of surfactant aggregate structures as a function of surfactant concentration, critical packing parameter (P_s) and preferred surfactant membrane curvature (c_0). Reprinted from 5, with permission from Elsevier.

Table 1.1-1 Predicted surfactant aggregate structures in aqueous media according to critical packing parameter values[3]

Critical Packing Parameter	General Surfactant Structure	Aggregate Structure
< 0.33	Single chain and relatively large headgroup	Spherical micelles
0.33 – 0.5	Relatively small headgroup, or ionic surfactant in presence of excess electrolyte	Cylindrical micelles
0.5 – 1.0	Double chains (flexible) with large headgroup	Vesicles and flexible bilayer
1.0	Double chain with small headgroup or immobile chains	Planar bilayer structure
>1.0	Double chain with small headgroup, bulky hydrophobic groups	Inverted micelles

These micellar structures may be considered the simplest forms of surfactant aggregates, which generally consist of 30-100 surfactant monomers (depending on their molecular structure), and occur at low concentrations.[7] As the surfactant concentration is increased, the micelles grow in size, adopt other shapes, and eventually form higher order liquid crystalline phases. While the micellar solutions show little structure beyond the micellar aggregate, these lyotropic mesophases are referred to as liquid crystal since they are highly ordered, at least in one dimension, but are not truly crystalline.[3] As surfactant concentration increases, and the amount of solvent available between micelles in solution decreases, there is an increase in the interactions between adjacent micellar structures until coalescence occurs.[3] Typically, spherical or ellipsoidal micelles become rod-shaped, and as the concentration increases, a hexagonal array of close-packed cylindrical aggregates appears, referred to as the "normal hexagonal" or hexagonal phase (Figure 1.1-1)[3] With further increase in concentration, it may become energetically favourable to form a bilayer structure known as the lamellar phase through coalescence of parallel cylinders with solvent separating the bilayers.[3] Eventually, a reversed or inverted hexagonal phase may occur, which consists of a hexagonal array of cylindrical aggregates of surfactant molecules in an inverse orientation (with the aqueous phase and surfactant head groups making up the aggregate interior).[3] Another type of liquid crystalline structure known as the cubic phase has also been reported, typically in the transition regions.[3,7] This cubic phases consists of either a cubic arrangement of globular micelles or a cubic bicontinuous phase.[3,7] The formation of these phases is dependent on the solvent properties as well as the surfactant structure; for example, greater charge repulsion between adjacent surfactant molecules tends to result in a delay in the formation of the liquid crystalline phases.[3]

The concentration at which micelle formation begins is called the critical micelle concentration (CMC), which is characteristic of a given surfactant and is accompanied by dramatic changes in the physical properties of the solution[3,5]. The micellization process and estimation of the CMC can be experimentally detected by a number of methods – surface tensiometry, conductivity, light scattering, rheology, and isothermal titration calorimetry to name a few.

Since the majority of the work presented here relies on CMC measurements obtained through surface tension studies conducted in water, a brief description of this phenomenon is described here. The interfacial tension occurring at the interface between two immiscible phases reflects the net asymmetric force field experienced by the molecules at the interface, which arises from the

difference in forces of attraction acting on the molecules at the interface/surface.[3] Molecules in the bulk water phase experience attractive forces of equal strength to neighbouring molecules in all three dimensions, resulting in a net force of zero.[3] On the other hand, surface molecules typically have a stronger attraction to identical units in their respective bulk phase rather than the "foreign" units in the adjacent phase; this imbalance of forces creates the apparent force of tension (a net downward pull) and higher potential energy of these molecules at the surface.[3,8] Since surface tension is determined by the energy of the surface molecules, displacement of these molecules by adsorption of solute molecules at the surface affects the measured surface tension. As surfactant is progressively added to a volume of water, the surface tension will gradually decrease until the surface is saturated with surfactant and the surface has effectively changed from a water surface to a hydrocarbon surface.[8] Surfactant adsorption to the air-water interface introduces more favourable air-surfactant tail and water-surfactant headgroup interactions. At this point, the surface tension reaches a minimum, which signifies the CMC (as depicted in Figure 1.1-2), and remains relatively constant even with added surfactant.

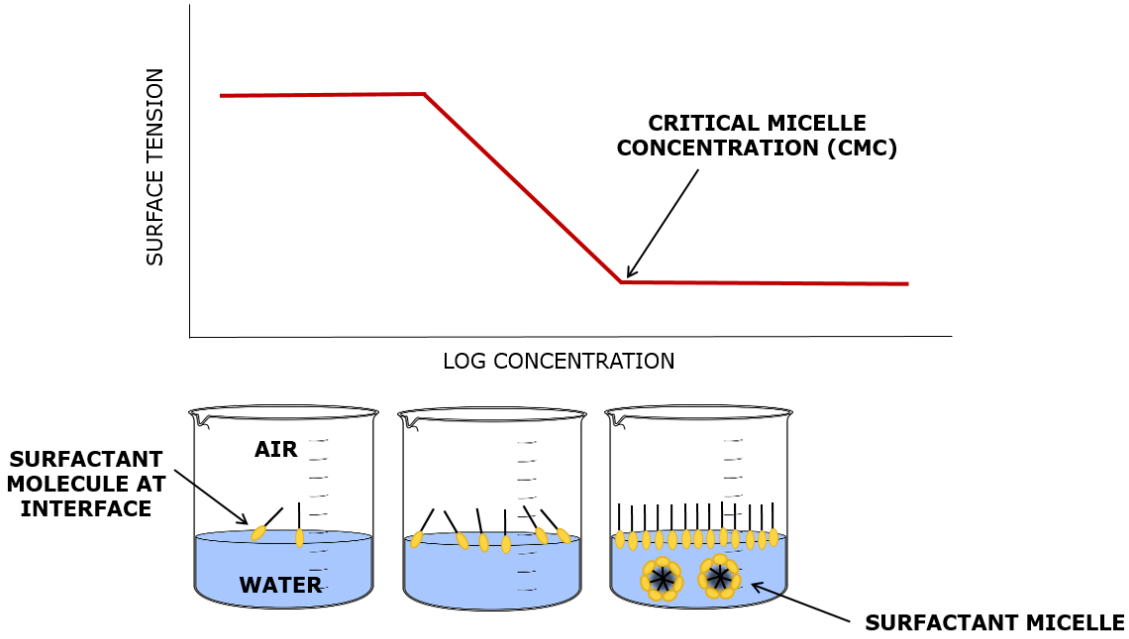

Figure 1.1-2 Schematic of surfactant adsorption and micellization detected by surface tension

In the du Nouy ring method, the force required to remove a wire ring/loop from the interface is measured.[9] To a first approximation, the detachment force is equal to the surface tension multiplied by the perimeter of the ring (the perimeter of the detached surface), represented by $F = W + 4\pi r\gamma$, where W is the weight of the ring, r is ring's radius, and γ is the surface tension.[9]

In order to describe the energetic basis of the micellization process, there are two generally accepted models that can be used. The phase separation model (also called the pseudo-phase separation model) treats micelles as a separate phase, where the CMC is the saturation concentration of surfactant monomers in solution and the micelles form a separate but soluble phase (a pseudo-phase).[3,9] Above the CMC, the monomer surfactant activity is assumed to remain constant (as might be observed by the near-constant surface tension value in surface tension measurements for some but not for all systems).[6,9] Another criticism of this model is that a sharp break point or discontinuity should be observed in the physical properties (e.g. surface tension, turbidity) of a surfactant solution at the CMC, however this is not always observed experimentally.[9] Mixed micellization theories based on the pseudo-phase separation model will be discussed later on. On the other hand, the mass action model provides a more appropriate description of micellization as it assumes the surfactant monomers and the micelles are in a dissociation-association equilibrium.[3] Therefore, an equilibrium constant can be used to calculate the free energy of micellization per monomer.[9]

In general, either approach produces similar results in describing the energy change associated with micelle formation. For nonionic surfactants, or an ionic surfactant with counterion-bound micelles, the standard free energy of micellization is given by Equation 1.1-1, where R is the gas constant, T is the solution temperature.

$$\Delta G_m^\circ = RT\ln(CMC) \qquad \textbf{Equation 1.1-1}$$

For ionic surfactants, the degree of counterion association with the micelles also needs to be considered since a portion of the counterions will transfer into the micellar phase.[3] For a typical 1:1 ionic surfactant micelle with the degree of micelle ionization represented by α, the Gibbs energy change of micellization is given by Equation 1.1-2.[3]

$$\Delta G_m^\circ = (2-\alpha)RT\ln(CMC) \qquad \textbf{Equation 1.1-2}$$

Also note, for a surfactant with two charged head groups and monovalent counterions, such as the gemini surfactants discussed later, which dissociate into 3 ionic species, the (2-α) becomes (3-2α).[6]

1.1.1 Surfactant Structure and Solution Conditions Influence Surfactant Self-assembly

Ultimately, a surfactant's chemical composition controls the micellization process because the magnitudes of the forces favouring or retarding micellization are determined by the chemical structure (with all other factors such as temperature, pressure, solvent kept constant).[3] The major determining factor of a surfactant's CMC is the hydrophobicity of the surfactant molecule. The CMC decreases logarithmically as the number of carbons in the alkyl chain of a hydrocarbon surfactant increases.[3] Changes to the hydrophilic group (for a series of surfactants having the same hydrophobic chain) can also impact the CMC, although this effect is much smaller than that achieved by changes to the hydrophobic component.[3] For ionic surfactants, the free energy of micellization is also influenced by the interaction between the head groups and solvent, which will depend on the degree of counterion binding.[3] Since counterions reduce the electrostatic repulsion between charged head groups, the CMC decreases with an increasing degree of counterion binding, which depends on the ion's radius of hydration and valency.[3] The larger the radius of hydration of the ion, the greater the decrease in the CMC.[3] Accordingly, the addition of salt reduces the CMC of an ionic surfactant also due to a reduction in electrostatic repulsion between head groups.[3] For nonionic surfactants, increasing the hydrophilicity of the head group, for example an increase in ethylene oxide content, tends to increase the CMC.[3]

Solution properties such as ionic strength (i.e. added salt), pH, and temperature can also affect micellization in water. Salt effects are much smaller for nonionic surfactant systems, and can produce either an increase or decrease in the CMC depending on the electrolyte's effect on the water structure.[3] Ions that strongly interact with water will induce greater hydrogen bonding and increase the organization of water, which would require more work to accommodate the surfactant monomer, leading to a "salting out" effect that lowers the CMC of the surfactant. For structure-breakers, which disrupt the water organization, less work is required so the surfactant is "salted in" and the CMC will increase.

Surfactants containing ionizable groups will demonstrate significant changes in the CMC as a result of changes in the electrostatic interactions between head groups.[3] Temperature can also have a complex effect on micellization, which differs between ionic and non-ionic surfactants.[3] In general, higher temperatures result in dehydration of the polar head groups, which favours micellization over solvation

of the surfactant molecule.[3] Conversely, increased temperatures disrupt the water structure surrounding the hydrophobic group, essentially increasing its solubility in water and making micellization less favourable due to decreases in the magnitude of the free energy attributed to the hydrophobic effect.[3] Therefore, the overall temperature effect will depend on the relative magnitudes of these two effects.[3] For non-ionic surfactants, which generally rely on hydrogen bonding between water and ethylene oxide groups in the surfactant head group region, there is an inverse temperature-solubility relationship.[3] In this case, the CMC decreases with increasing temperature, and increasing the temperature beyond the surfactant's cloud point leads to phase separation.[3] At this point, there is no longer sufficient solubility for effective surfactant action and a second phase dominated by surfactant is formed and its domains are significantly larger than typical micelles.[3]

1.1.2 Surfactant Aggregates Solubilize Additives

Most applications of surfactants involve their combination with additives such as salts, organic materials, polymers, drugs, and even additional surfactants (to improve the properties of a surfactant product). Therefore, it is also important to consider the effect of additives (other than electrolytes, which was already briefly discussed) on the micellization process, and the location of the solubilized molecules within the surfactant micelle/aggregate structure, which is determined by the molecular structures of the additive and the surfactant.

The spontaneous process of solubilization produces thermodynamically stable, isotropic solutions of a substance/additive that is typically insoluble or has limited solubility in a particular solvent through the addition of amphiphilic compounds at or above the CMC.[3] For example, as seen in Figure 1.1-3, in an aqueous solution the hydrophobic region of a surfactant micelle provides a compatible microenvironment for nonpolar additives (e.g. hydrocarbons, or aromatics) which would therefore associate with the hydrophobic core of the micelle (and result in a decreased CMC).[3] The extent of solubilization will depend on the size of the hydrophobic chain lengths, with solubilization increasing with increasing alkyl tail lengths and in the following order: anionic < cationic < non-ionic headgroups for the same tail length.[9] Further, solubilization power (molar ratio of solubilizate to surfactant) generally increases with increasing polyoxyethylene (PEO) groups, due to decreasing aggregation number which results in a greater number of micelles per mole of surfactant.[9] Reverse micelle formation in non-polar solvent systems provide an opportunity to solubilize polar additives within the core, made up of polar head groups, of the reversed micelle.[3]

In addition, additives may locate in the palisade region of non-ionic surfactant micelles or on the surface of ionic micelles (at the micelle-solvent interface).[3,10] The palisade layer is the transition zone between the hydrophobic and hydrophilic regions of the micelle, and accounts for a large portion of the micellar volume for non-ionic surfactants, especially those with PEO headgroups.[3] Due to the bulky nature of the PEO chains, steric crowding leaves little room for hydration water near the core. This creates a polyether chemical environment in the deeper regions of the palisade layer of these micelles; therefore, materials that are soluble in such environments will reside in that region of the micelle.[3] For example, as a polarizable additive, benzene can adsorb to cationic micelle surfaces or between the PEO chains of PEO non-ionics.[10]

Alternatively, slightly polar additives such as fatty acids or alcohols are usually located in the core-palisade boundary and expected to have a radial orientation with the carbon tail closely associated with the micellar core, and polar group oriented toward the surfactant headgroups.[3,10] As the carbon chain length of the alcohol additive increases, especially for four carbons and greater, there is a more rapid change in the surfactant solution properties and generally a decrease in the CMC, which is attributed to these materials having inherent surface activity, resulting in mixed micelle formation, where the alcohol acts as a second surfactant species in the micelle.[3] Mixed micelles will be discussed further in Section 1.5.

As seen with the effect of temperature, the net effect on the CMC depends on the magnitudes of these opposing effects.[3] Organic materials that are water-miscible such as short-chain alcohols, acetone, glycol, and polar organic solvents, can act as co-solvents when present at high concentrations, which reduces the dielectric constant of the bulk solvent, resulting in decreased electrostatic repulsions between ionic surfactant head groups and lower surfactant solubility, ultimately lowering the CMC.[3] However, solubility of the hydrophobic tail would increase, and lead to an increase in the CMC.

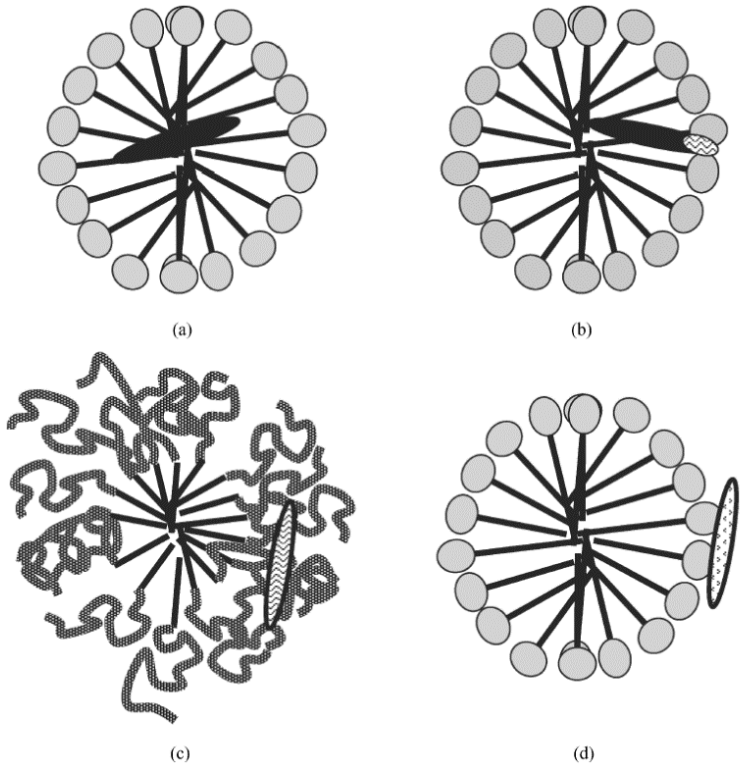

Figure 1.1-3 Solubilization of additives in different regions of a micelle: a) hydrophobic micelle core; b) core-palisade interface/mixed micelle formation; c) surface or palisade region of nonionic micelles; d) adsorption to ionic micelle surface.[3]

As discussed later on in this chapter, surfactant micelles (and other aggregate structures) can be applied in pharmaceutical formulations as a way of improving the overall delivery of drugs (and genetic material, as discussed in the next section). Surfactant self-assembly can be exploited to improve solubility of otherwise poorly soluble drugs in biocompatible solutions through micellar solubilization, or protect degradable APIs (e.g. protect deoxyribonucleic acid, DNA, from nucleases) and improve circulation through solubilization or encapsulation.

1.2 Gene Therapy Utilizes Genes as Medicine

The term gene therapy generally refers to the transfer of nucleic acids into target cells in order to produce a therapeutic effect.[11] This approach can involve introducing a correct copy of a missing or non-functional gene, silencing the expression of a non-functional or over-expressed gene (e.g. gene knockdown by ribonucleic acid, RNA, interference), or repairing a mutation (through gene editing).[12,13]

Gene therapy holds potential for treating monogenic disorders (e.g. cystic fibrosis, haemophilia, lipoprotein lipase deficiency) as well as for treating cancer, by addressing the root cause of these diseases. With recent successes in clinical trials and licensing in Europe and North America, the capacity of gene therapy to revolutionize human disease treatments is becoming a reality. The majority (66.6%) of gene therapy clinical trials in 2018 addressed cancer treatment, while monogenic diseases also accounted for a large portion (11.5%) of the indications addressed, followed by infectious diseases and cardiovascular diseases that accounted for 6.3% and 6.2%, respectively.[14]

Gene delivery techniques consist of vector-assisted delivery or physical methods like electroporation, sonoporation, microinjection, or particle bombardment via a gene gun.[15] Vector-assisted gene delivery consists of two major categories; viral and non-viral. The viral vector method exploits the natural ability of viruses to introduce their genetic load to target cells, but first requires replacement of essential genes for viral replication, assembly, or infection with the expression cassette encoding the therapeutic gene to be delivered.[16,17] Viral vectors have many advantages for gene therapy, including high transfection efficiency, persistent gene transfer, and the ability to infect dividing and non-diving cells, including many cell types considered difficult to transfect.[18] However, multiple patient deaths in earlier gene therapy clinical trials highlighted safety risks associated with viral delivery systems. For example, in 1999 18-year old Jesse Gelsinger died of an inflammatory reaction to the adenovirus-based vector used in a Phase I gene therapy clinical trial to treat ornithine transcarbamylase deficiency.[14] Another occurrence involved the development of a leukemia-like condition in 2002 in two children enrolled in a trial to treat X-linked severe combined immunodeficiency, and development of a similar condition in a third child when trials restarted with a revised protocol in 2005.[14] This condition was caused by retroviral vector integration near an oncogene promoter.[14] Although these events were largely seen as setbacks for gene therapy, continued basic and clinical research have led to improvements. In the case of adenoviral vectors, there has been wide use of these vectors in various clinical applications, and safer dosing and routes of administration have been established.[18] In fact, current approved gene therapy products, as well as the majority of ongoing gene therapy clinical trials, use recombinant viral vectors to achieve delivery (approximately 67% in September 2019).[14,19] In 2012, Glybera® (uniQure, Amsterdam, Netherlands) was approved by the European Marketing Association (EMA) for lipoprotein lipase deficiency treatment, which used a recombinant adeno-associated virus to deliver the therapeutic gene. This was followed by Strimvelis™ (GlaxoSmithKline, Middlesex, United Kingdom) in 2016 to treat adenosine deaminase deficiency using a retroviral vector for *ex vivo* transduction of hematopoietic

stem cells extracted from the patient.[13] In 2017, the United States Food and Drug Administration (FDA) approved Kymriah (Novartis Pharmaceuticals, Basel, Switzerland), the first chimeric antigen receptor T-cell (CAR-T) cell therapy product (for acute lymphoblastic leukemia), and shortly after in the same year, approval for Yescarta (Kite Pharma, Santa Monica, USA) for B-cell lymphoma followed.[13] CAR-T therapies generally rely on retroviral transduction or electroporation to introduce the CAR gene into patient T-cells *ex vivo*.[20] Luxturna, developed by Spark Therapeutics (Philadelphia, USA) also received approval by the FDA in 2017 for retinal dystrophy (also utilizing an adeno-associated virus).[13]

Despite the recent success of viral vectors, safety concerns and the relatively small capacity for therapeutic nucleic acids still motivate interest in non-viral vectors.[13] Non-viral vectors generally use synthetic materials to protect and deliver the therapeutic nucleic acids to the cells of interest, and generally offer advantages such as low immunogenicity, unrestricted plasmid size, low production costs, and can be produced on a large scale.[21] In spite of these advantages over viral vectors, the use of non-viral methods is typically impeded by poor efficiency.[13,21] Therefore, research endeavors to develop non-viral methods have not only focused on the use and development of different materials to achieve this goal, but also establishing structure-transfection relationships, which will be discussed in more detail in the following sections. Successful improvements in the efficiency of non-viral gene delivery have been made with the application of nanotechnology in the design of these vectors. Gene therapy nanoparticles can consist of inorganic materials such as silica, quantum dots, iron oxide, carbon, or gold, which are either directly conjugated to the therapeutic nucleic acids through an environment-sensitive linker, or are modified with cationic molecules for nucleic acid complexation.[21] Alternatively, "soft" nanoparticles made of lipids or polymers are used to complex with or encapsulate the nucleic acid cargo. Lipid nanoparticle formulations for drug delivery (e.g. polyethylene glycol-modified liposomal doxorubicin, Doxil®) offered reduced toxicity and/or increased efficacy (compared to the free drug), and the understanding of the requirements for successful delivery of these systems has been extended to the application of similar vehicles for gene delivery.[22] A recent breakthrough and proof-of-concept is Onpattro (Alnylam Pharmaceuticals, Cambridge, USA), which uses a lipid nanoparticle to deliver therapeutic small interfering RNA to the liver to treat peripheral nerve disease caused by hereditary amyloidosis received approval by the FDA and EMA in 2018[23]; demonstrating gene therapy by non-viral methods is commercially achievable.

The following section will discuss important features of nanoparticle design (mainly "soft" nanoparticles) for achieving successful gene delivery and transgene expression (known as transfection).

1.2.1 Non-Viral Vectors Require Rational Design to Overcome Barriers to Transfection

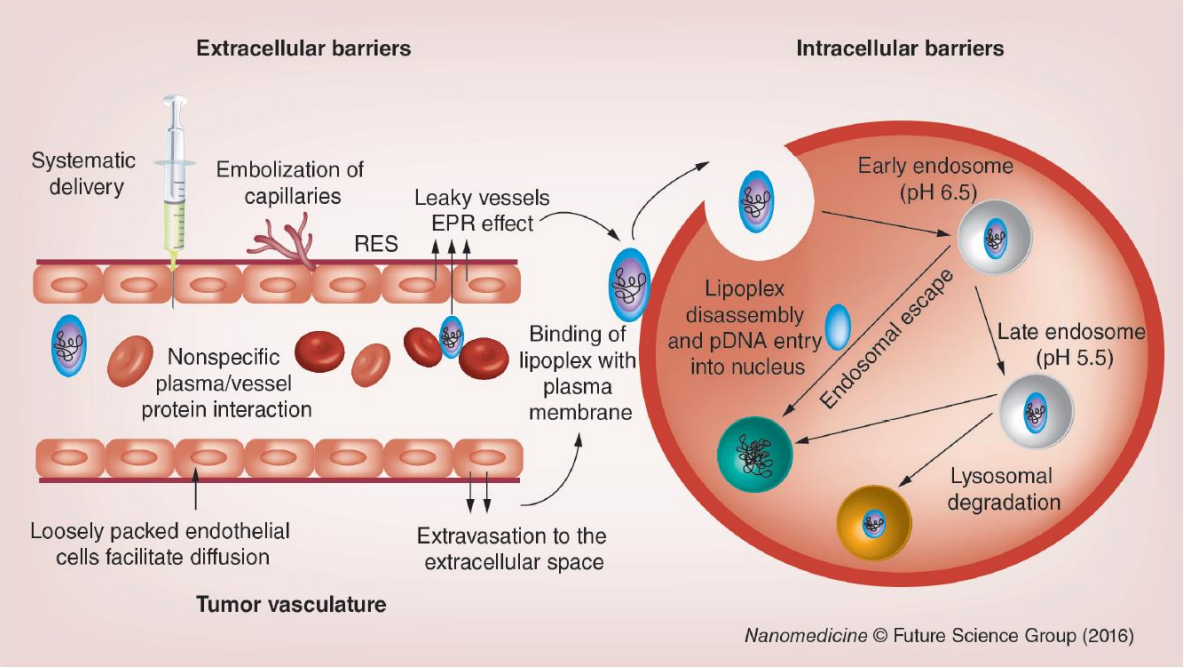

Figure 1.2-1 Schematic representation of extracellular and intracellular barriers to gene delivery. Reproduced from [142] with permission.

Transfection, the process by which nucleic acids are delivered to cells, can be hindered by a number of barriers that can limit the overall efficiency of the process. At the cellular level, these barriers include cellular internalization of the vector, escape from the endosome/lysosome before acidification of the compartment occurs, intracellular trafficking, dissociation of the nucleic acid-vector complex, and nuclear entry of the nucleic acid cargo (as illustrated in Figure 1.2-1).[1,24] In addition, extracellular barriers to transfection (following intravenous, i.v., injection) include vector instability due to components within the blood, adhesion to non-target tissues, clearance of the vector by the reticulo-endothelial system, and degradation by endonucleases in the blood and extracellular space.[25,26] The key to successful gene therapy is to protect the therapeutic nucleic acids (herein referred to as DNA, but

generally applies to other nucleic acid forms unless specified) from degradation and assist the therapeutic load in overcoming these barriers so that it can reach its intracellular target of the appropriate cells for treatment. Although viruses naturally overcome many of these obstacles, efficient transfection by non-viral vectors remains stalled by such factors; therefore, non-viral gene delivery systems often require a rational design approach.

1.2.1.1 Nucleic Acid Cargo Requires Compaction and Protection

Traditionally, non-viral gene delivery vectors generally require a component to bind and condense the DNA, usually with a cationic component, and usually some additional components are added to help evade or overcome the rest of the barriers mentioned above. The following discussion will cover the major barriers in more detail accompanied by typical strategies for addressing them in the context of non-viral vector design.

The most common vectors are those consisting of cationic lipids (which form "lipoplexes" with nucleic acids) or cationic polymers (forming "polyplexes"), which bind DNA through electrostatic and hydrophobic interactions.[27] This cationic component is important for: 1) neutralizing the negative charge of the nucleic acid phosphate backbone, 2) condensing the DNA size to enable cellular internalization, 3) when used in enough excess, providing a positive charge to facilitate interactions with the cellular membrane via electrostatic attraction and cellular uptake, and 4) protecting the DNA cargo from both extra- and intracellular degradation.[28] Some cationic materials that have been investigated for compacting and delivering nucleic acids include: spermine, cationic surfactants (CTAB, gemini surfactants), cationic lipids (DOTMA, DODAB, DOTAP), cationic cholesterol derivatives (Dc-Chol), chitosan, polyethyleneimine (PEI), polypropyleneimine, poly(L-lysine).[1,28] Poly(lactic-*co*-glycolic acid) (PLGA) has also been used to encapsulate DNA/RNA through a double-emulsion solvent evaporation technique rather than electrostatic interactions, and shows stability and an ability to protect the nucleic acid cargo *in vivo*.[25] Nontheless, novel materials, including polymers modified with a cationic component or other cationic polymer (e.g. chitosan-modified PLGA) continue to be developed for gene delivery purposes.[25]

The hollow compartments of liposomal structures also offer an opportunity to encapsulate DNA in the inner aqueous environment of the liposome, which would then have the ability to release the cargo

through fusion with biological membranes. Liposomes are also said to offer more stability upon dilution in the circulation following i.v. administration versus micelles that can disassemble once diluted below the CMC. However, there are some drawbacks to the use of liposomal structures and their preparation processes. For example, in the classical thin film hydration method, there is generally poor loading efficiency of hydrophilic molecules since the volume of hydration is larger on the outside of the liposomes rather than the aqueous core.[29] Additionally, the conventional methods for liposome formation are not easily applicable for industrial scale production due to inconsistent encapsulation efficiencies, and broad size distributions. In order to overcome these problems, more sophisticated methods, such as microfluidics technology, are required.[29] Furthermore, for temperatures above the phase transition temperatures of the particular lipids used, liposomes can also be leaky at body temperature (37°C) and the encapsulated contents may be released in circulation prior to reaching the target tissue. However, this might be reduced by choosing lipids with gel states under physiological conditions, or adding cholesterol to stabilize the lipid bilayer. Similarly, micellar delivery systems made from materials with a low CMC (e.g. polymers) would also be less affected by dilution, and has the advantage of simple preparation through self-assembly.[30]

1.2.1.2 Circulation and Clearance Are Influenced by Nanoparticle Size and Surface Characteristics

Although useful at the cellular level, the positive charge of many lipoplex and polyplex systems often results in interactions with serum components, leading to clearance by the immune system, which renders the delivery vector ineffective.[23,31,32] Foreign organisms or materials, such as gene or drug nanoparticle carriers, become covered with opsonin proteins in the blood serum, which makes the nanoparticle more visible to macrophages of the mononuclear phagocytic system (MPS, also known as the reticuloendothelial system, RES).[32] Following this process (known as opsonization), the nanoparticle is phagocytosed (engulfed) by the macrophage and digested in order to remove the foreign material from the bloodstream.[32] This can occur within seconds of i.v. injection.[32] Any nanoparticles that cannot be cleared by macrophages (typically polymeric nanoparticles) are sequestered in the liver and spleen.[23,32] Due to increased adsorption of serum proteins, hydrophobic particles reportedly undergo opsonization quicker than hydrophilic particles; while charged particles are opsonized faster than particles with a neutral charge.[23] Therefore, vectors often include “stealth groups”, such as polyethylene glycol (PEG), to decorate the surface of the delivery vector in order to mask the charge,

provide stability, reduce non-specific interactions, and prolong circulation times *in vivo*.[23,25] Although PEG and the PEG-containing polysorbate, poloxamine, and poloxamer (discussed later) are the most effective, numerous other polymers have also been used as shielding/stealth groups, including polysaccharides, polyacrylamide, poly(vinyl alcohol), and poly(N-vinyl-2-pyrrolidone).[23]

Even neutral nanoparticles can benefit from "PEGylation" since they too form large aggregates in physiological salt concentrations, which can adsorb to serum proteins.[25] PEG introduces an aqueous layer at the liposome surface, which confers colloidal stability and steric hindrance, leading to inhibition of adsorption of proteins and less recognition by macrophages.[33] As a result, sterically stabilized (e.g. PEGylated) delivery vehicles can have significantly longer blood circulation times after i.v. administration (which is also observed with the addition of PEG to drug delivery liposomes; for example, higher levels of accumulation in tumors with PEGylated liposomal doxorubicin versus free doxorubicin).[33] The thickness, charge, surface density, and conformation of the PEG layer can also impact the interaction with opsonins; therefore, optimization of the PEGylation is also required.[32] Nevertheless, it has been found that this "stealth method" works better *in vitro* than *in vivo*, where aggregation is still known to occur with these complexes.

Prolonged circulation is also desirable because it can result in enhanced accumulation in pathological sites such as solid tumors through the enhanced permeability and retention (EPR) effect, allowing for passive targeting.[33] In theory, this exploits the leaky vasculature of tumor tissue (which has a discontinuous or absent basement membrane due to rapid angiogenesis) and lack of lymphatic drainage, which allows small and even large macromolecules or nanoparticles to accumulate in the interstitial tumor space.[33] However, it is also important to keep in mind that the PEG layer on the surface of gene carriers has been known to reduce interactions with the cell surface and the increased stability introduced by PEG results in poor membrane fusion for endosomal escape[33]; therefore, additional strategies (e.g. ligands for cellular uptake, cleavable PEG systems, and endosomal fusogenic peptides) are required to compensate for these drawbacks.[33]

Furthermore, in regard to the EPR effect, early nanomedicine approaches to overcome the low specificity of traditional chemotherapeutics relied on the EPR effect as the major underlying mechanism to achieve drug accumulation in the tumor tissue while reducing side effects.[34] Naturally, anti-cancer gene therapy nanomedicines also adopted this approach, generally leading researchers to strive for gene nanocarrier sizes of approximately 20-200 nm. Not only would this size be large enough

to avoid renal clearance *in vivo* (which removes particles smaller than 30 nm from circulation), contributing to longer blood circulation times, the idea is also that these particle sizes would achieve passive targeting to tumor tissues by extravasation through the discontinuous, hyperpermeable tumor vasculature that allow passage of particles of 10-500 nm (but not through normal vasculature, which requires 2-4 nm sizes).[34–36] However, a few caveats exist with this approach. First, although smaller particles would accumulate faster and diffuse deeper into the tumor compared to larger particles, a smaller size also allows for more rapid diffusion back to the vascular compartments; this of course, reduces its accumulation in the tissues.[37] Second, large tumors show pathophysiological heterogeneity; in particular, the central region of metastatic tumors does not exhibit the EPR effect, also leading to less nanoparticle accumulation throughout the tumor tissue.[38] Third, loss of effective dose within tumours may also occur due to the tumour core having a higher interstitial pressure than the periphery, allowing the nanoparticles to flow outward.[38] Similarly, a negative pressure gradient of the tumor interstitium may also limit movement of nanoparticles from the intravascular to extravascular space.[38] As a result, the EPR effect is better documented in small animal models, but fails to translate in the clinic.[34] Therefore, use of the EPR effect in the rationale of nanoparticle designs is likely only appropriate for some tumors known to show a strong EPR effect (e.g. Kaposi sarcoma and head and neck tumors), and other approaches that exploit the tumor microenvironment instead may be more promising. Although outside the scope of this work, some methods include stimuli-responsive nanoparticles to take advantage of gradients in the tumor regions such as pH, or hypoxia.[34]

Opsonization and phagocytosis form the main clearance mechanism for removing undesired elements from the blood when they are larger than the renal threshold.[32] Hence size can also play a role in whether a gene delivery vector remains in the body long enough to achieve its desired benefit, even for PEGylated/stealth nanoparticles.[32] In general, for nanoparticles that cannot be cleared by the renal system, nanoparticles with a hydrodynamic size over 200 nm are typically cleared faster than those under 200 nm.[23] Taking PEGylation into consideration, poloxamer-coated nanoparticles smaller than 150 nm showed increased uptake in the bone marrow of rabbits versus the liver and spleen (the major sites of clearance for 250 nm particles), which may be due to the steric barrier having greater effectiveness on the smaller particles despite having a lower concentration of adsorbed polymer (as opposed to a more crowded arrangement and lower mobility of the polymer chains on larger particles with a smaller surface curvature).[39] Furthermore, in most systems, size also affects the ability to overcome cellular barriers; however, the relationship between size and efficiency is not always

consistent across systems. Gene delivery particles can range from "small", ≤100 nm, to "giant", ≥1000 nm.[1] Small particles have shown high transfection efficiency *in vivo* due to their ability to cross capillary networks, for example in the spleen, lungs, liver, and kidney.[1] On the other hand, once at the cellular level, larger lipoplexes may be capable of releasing their contents into cells through fusion with the cellular membrane, which by-passes the barriers associated with cellular entry through endocytosis pathways (discussed later).[1]

1.2.1.3 Gene Delivery Vectors Achieve Internalization

The first obstacle encountered by the delivery complex at the cellular level is the plasma membrane. Passive diffusion into the cell is not possible due to the size restrictions of transmembrane pores and channels; therefore cellular uptake strategies take advantage of the natural cellular mechanisms used to internalize macromolecules, specifically, the process of endocytosis.[28] Cellular internalization of the complex can occur through non-specific uptake following ionic interactions with negatively charged membrane-bound proteoglycans, receptor-ligand binding at the cell surface, lipophilic interactions between lipophilic residues in the delivery vector and cellular membrane phospholipids, or through the use of cell-penetrating peptides originally derived from cationic, amphipathic viral proteins capable of membrane translocation.[28] The mechanism by which cellular internalization occurs can determine the intracellular pathway and fate of the delivery vector and DNA cargo; therefore, it is important to consider and can contribute to more rational design.

Similar to many macromolecules and solutes that are unable to permeate the plasma membrane, gene delivery vectors are most commonly internalized/engulfed through clathrin-mediated, caveolae-mediated, or micropinocytosis pathways.[40] These pathways differ in the composition of the structures or coat (if any), size of the vesicle, and the fate of the particles that are internalized.[41] Firstly, clathrin-mediated endocytosis is triggered by binding of a ligand to its high-affinity transmembrane receptor, which triggers clustering of these ligand-receptor complexes into membrane structures known as clathrin-coated pits.[40–42] These pits then invaginate and are pinched off from the plasma membrane, forming intracellular clathrin-coated vesicles that reportedly have a cargo size upper limit of 150-200 nm in diameter.[42,43] Depolymerization of the vesicle's clathrin coat then results in an early endosome and acidification in the lumen to pH 5.9-6, which dissociates the ligand from the receptor.[41] The early endosomes fuse with each other or with other pre-existing endosomes, forming a late endosome that later fuses to lysosomes, and leads to further acidification to pH 5.[41] Therefore, for gene therapy, the

DNA needs to escape the endosome and avoid degradation by the lysosome in order to be effective. Strategies for endosomal escape will be discussed in the following section.

Caveolae-mediated uptake occurs through small, hydrophobic domains in the plasma membrane that are rich in cholesterol and glycosphingolipids.[41,42] Unlike the clathrin-mediated pathway, the caveosome does not follow an acidic or digestive route.[44] Therefore, the pathogens and particles taken up by this route will be transported directly to the Golgi apparatus or endoplasmic reticulum without undergoing degradation.[44] For gene therapy purposes, caveolae-mediated uptake could be advantageous if internalization by this route (e.g. through exploitation of specific receptors) can be increased; however, it is also important to keep in mind that internalization of caveolae is generally slower and their size is more appropriate for 50-80 nm vehicles.[43]

Finally, in micropinocytosis a large volume of extracellular medium is non-selectively internalized by membrane protrusions that collapse and fuse with the plasma membrane.[42,43] Contrary to the other mechanisms mentioned, this process is not directly driven by receptors or by the cargo, but can be induced by mitogenic factors.[41,44] The resulting vesicles, known as macropinosomes, can vary in size up from 0.5 to 10 μm.[43] The fate of macropinosomes remains unclear but appears to be cell type dependent, where some fuse with lysosomes, and others do not mature beyond the early endosome stage.[44] Although not covered in this discussion, other endocytosis pathways include: phagocytosis; which occurs in specialized cells such as macrophages, neutrophils, and monocytes; and caveolae- and clathrin-independent, which are not very well characterized.[40]

Manifestly, the fate of the DNA cargo depends on the size of the gene delivery nanoparticle and endocytosis pathway. Furthermore, when administered intravenously, the non-viral delivery vector likely has a negative charge following interactions with serum components; therefore, there may not be much electrostatic interaction with cell membranes to rely on.[45,46] However, while lipoprotein particles inhibit uptake, adsorption of fibrinogen on the surface of lipoplexes stimulates uptake through interaction with specific cell surface receptors.[45,46]

Cellular uptake can also be improved through receptor targeting and receptor-mediated endocytosis.[28] This generally results in faster internalization compared to non-specific uptake (without a ligand) and accumulation of the DNA cargo inside the cell (which is expected to decrease the amount of cargo required to achieve efficient transfection due to greater accumulation of the DNA within the cells).[11,27] In the receptor-mediated endocytosis approach, the diversity of cell receptors on cell surfaces

are exploited to enhance internalization and transfection activity by coupling targeting molecules (ligands) to gene delivery vectors.[27] These ligands bind surface markers exclusively present or up-regulated on specific cells, and facilitate receptor-mediated endocytosis into the intended cells. Additionally, the ligand-receptor binding should be particularly strong in order to be effective.[25] Incorporating targeting molecules in transfection formulations is also thought to decrease the non-specific delivery to normal cells outside of the target tissue that can often lead to toxicity of the gene therapy in *in vivo* applications, contributing to a safer and more efficient therapeutic.[11,47] Some common ligands include transferrin (recognized by transferrin receptors upregulated in many cancer cells), arginine-glycine-aspartic acid (RGD) peptides (recognized by tumor vasculature integrins), lactose (recognized by hepatocytes), mannose (recognized by macrophages and dendritic cells), folate (recognized by certain tumor cells), as well as receptor-targeting antibodies (e.g. an anti-transferrin receptor single chain antibody fragment, which was incorporated in a cationic liposome currently under phase II trials for targeted p53 gene therapy for metastatic pancreatic cancer, in combination with nab-paclitaxel).[25,27] The choice of ligand can also be used to target the caveolin-dependent versus clathrin-dependent pathway. While the clathrin pathway is receptor-mediated, this does not mean all ligand-receptor binding results in cellular uptake through this pathway. Rather, the internalization pathway depends on the cell type and receptor. For example, transferrin receptor binding triggers clathrin-mediated endocytosis, whereas folic acid uptake occurs through caveolae.

Cell-lipoplex fusion is thought to be a secondary pathway for internalization of lipid-based vector contents into cells, but accounts for only a small fraction of internalization events.[1] The surface of gene therapy nanocarriers can also be decorated with cell-penetrating peptides to accelerate cellular entry, such as that derived from the HIV-1 TAT protein which enters cells by interacting with negatively charged components of the cell membrane.[25,48] These peptides consist of 5-30 amino acids, and are cationic and/or amphipathic.[48] Cationic peptides interact with anionic/acidic motifs on the cell membrane, whereas amphipathic peptides adsorb to the cell membrane.[48] Depending on the features of the peptide, the conjugated cargo, cell type, and the lipid composition of the membrane, the cell-penetrating peptides can increase uptake through direct translocation (conjugated to small cargo) or through endocytic pathways (usually energy-dependent micropinocytosis for large cargo).[48]

1.2.1.4 Endosomal Escape Must Occur to Avoid Degradation

If internalized through endocytosis, the next intracellular hurdle to be conquered is escape from the endosome before the encapsulated delivery vector is either recycled back to the cell surface, shuttled to an acidic lysosome (pH decreases to approximately 5), or delivered to other organelles such as Golgi apparatus or endoplasmic reticulum.[28] In any case, release from the endosome is vital in order to avoid degradation and for the DNA to make its way to the nucleus. Some methods that facilitate endo-lysosomal escape are to incorporate endosomal release peptides (peptides that adopt a membrane-disrupting conformation with decreases in pH), protonatable groups with a pK_a generally between 5 – 7 (known as the proton sponge effect), or encourage interaction of hydrophobic alkyl chains able to interact with the endosomal membrane.[28]

Endosomal release peptides undergo a conformational change at low pH, which leads to interaction and disruption of the endosomal membrane.[28] The protonatable carboxyl groups and alkyl chains of these peptides are suspected to be responsible for this function, which has been mimicked in synthetic pH-sensitive polymers.[28]

With the proton sponge effect, as the endo-lysosomal vesicle acidifies, functional groups, such as secondary and tertiary amines or imidazole, of the delivery vector become protonated, acting as a "proton sponge", and prevents the desired pH from being reached inside the vesicle.[28] As protons continue to enter the endosome, water follows; this eventually causes the endo-lysosomal vesicle to osmotically swell, rupture, and release its contents into the cell cytoplasm.[28,49] PEI is a notable example of a gene delivery material capable of inducing this proton sponge effect under the acidic conditions of the endosome, which has been credited, in part, with the high transfection efficiency achieved by PEI gene delivery systems, including the commercially available reagents jetPEI and ExGen500.[50] Some other chemicals capable of this effect are ammonium chloride, chloroquine, methylamine, poly-L-histidine, polyamidoamines, and polypropylacrylic acid.[51]

Lipid-based vectors can also disrupt the endosomal membrane by interacting with the membrane lipids; however, the mechanism of this process remains unclear. It has been hypothesized that cationic lipoplex interaction with endosomal membranes induces reorganization of the phospholipids where lipids from the cytoplasmic-facing layer of the membrane flip inward, neutralize the cationic lipids in the vector, and results in dissociation of the DNA and its release into the cytoplasm.[52] Alternatively, the vector/DNA complex may escape from the endosome following destabilization of the membrane,

and subsequent DNA release from the vector occurs in the cytoplasm following interactions with lipids of other organelles in the cytoplasm.[45]

Furthermore, addition of lipids such as dioleylphosphatidylethanolamine (DOPE), known as helper lipids, to cationic lipid transfection complexes aids in forming stable, liposomes that are fusogenic and initiate endosomal escape and tissue penetration.[1] The transfection efficiency achieved by such lipid carriers has been correlated to the structural transformation of the lipoplexes accompanied by their interaction with the anionic lipids of cellular membranes, for example, bilayer-to-micelle transitions or the lamellar-to-inverted hexagonal phase transition achieved by DOPE-containing bilayers.[1,53] Koynova et al. suggested that lipoplexes with a lamellar phase, but close to a lamellar-nonlamellar phase boundary would optimally protect the DNA and subsequently release it upon mixing with membrane lipids; otherwise, lamellar lipoplexes would likely maintain their structure after contact and may not release the DNA.[53] Comparatively, formulations that form phases with a highly negative interfacial curvature (such as inverted micellar cubic or inverted hexagonal) would be the most effective carriers.[53] The commercially available transfection reagent Lipofectamine (consisting of DOPE and DOSPA) is also expected to have a pH-dependent transition due to the polyamine region of DOSPA.[54]

Increased transfection can also be achieved upon conjugation of whole, inactivated virus particles (e.g. adenovirus[55]) to a synthetic gene carrier, possibly due to virus-mediated endosomal escape; however, the virus' presence raised safety concerns, which is also an important consideration in vector design.[45,51] Likewise, it is also important to consider excessive damage to lysosomes can reduce the safety of the method despite its efficiency.[45,51]

1.2.1.5 Nuclear Entry is Essential for Plasmid DNA Transfection

Depending on the vector composition, the DNA may dissociate from the vector at the endosomal-stage or within the cytoplasm following interaction or fusion with the cytosolic membrane network (i.e. the endoplasmic reticulum, Golgi, mitochondria, or nuclear membrane).[45] However, cytoskeletal elements such as microtubules, intermediate filaments, and microfilaments within the cell cytosol greatly hinder diffusion of the DNA or the DNA/vector complex, and carrier-mediated gene delivery is unable to take part in microtubule-mediated transport as some viruses do.[28,50] Cationic vectors that compact the DNA into small enough particles could aid in nuclear localization and protection of the nucleic acid cargo from degradation by endonucleases in the cytoplasm; meanwhile, diffusion of naked DNA through the cytoplasm is considered negligible.[50]

Once localized at the cell nucleus, passage of the DNA into the nucleus must occur rapidly before the unbound, de-condensed DNA is degraded by cytoplasmic DNA nucleases.[1] A double membrane surrounds the nucleus.[45] Transport structures known as nuclear pores regulate passage across the nuclear membrane, and the size threshold for molecules to freely pass through the nuclear pore complex is approximately 9-11 nm in diameter.[50] Plasmid DNA, commonly used for transfection, is typically too large to enter the nucleus unassisted and is therefore thought to either i) enter during mitosis when the nuclear membrane structure disappears in dividing cells, or ii) be imported through an ATP-dependent pathway.[50]

These energy-dependent modes of nuclear transport can occur through a DNA sequence-dependent transport or through addition of peptides carrying a nuclear localization signal (NLS).[45] The presence of protein-binding sequences in the plasmid DNA, for example sequences derived from the SV40 viral genome such as the SV40 origin of replication or early and late promoters, bind to cytoplasmic proteins (e.g. transcription factors) that contain NLSs. These proteins then couple the plasmid DNA to the NLS import machinery.[45] As such, nuclear import, and therefore transfection, can be increased by strategic selection of sequences in the therapeutic DNA molecule that can be recognized by transcription factors expressed in the cells of interest.[45] Another strategy involves coupling NLS peptides to the DNA or the chemical vector.[45] For example, coupling an SV40-derived NLS-containing peptide resulted in an eight-fold increase in PEI-mediated plasmid transfection.[45,56] Alternatively, some pharmaceutical excipients, such as Pluronics, can activate certain cellular signaling pathways that enhance nuclear transport of plasmid DNA (pDNA) containing specific sequences without additional modification of the DNA (discussed later on).[57]

It is also worth acknowledging that there are a number of other important elements in the pDNA structure that generally impact transfection. Briefly, and specifically relating to pDNA transfection, the plasmid is composed of a bacterial backbone and a eukaryotic expression cassette.[58,59] The bacterial backbone consists of an origin of replication for pDNA replication in bacteria, and a drug resistance gene, such as kanamycin or ampicillin resistance, which allows for the selection of plasmid-transformed bacteria.[58,59] The eukaryotic expression cassette consists of everything necessary for successful gene expression in the transfected cells. Firstly, there is a promoter, which contains a DNA sequence capable of recruiting RNA polymerase II for the transcription of the pDNA.[59] This promoter may also contain enhancer sequences which bind proteins known as transcription factors that aid in the recruitment of

RNA polymerase II.[59] The expression cassette is also comprised of a 5' untranslated region, including at least one intron (to ensure the pre-mRNA is processed into a mature mRNA, and exported into the cytoplasm) and a Kozak sequence (that provides the ribosome with a signal to start translation); the open reading frame, which encodes the gene to be expressed; and a 3' untranslated region with a polyadenylation sequence.[59] Polyadenylation promotes nuclear export and translation of the mRNA and inhibits its degradation.[59]

While this work focuses on pDNA delivery, a significant number of gene therapy efforts involve RNA interference methods where small interfering RNA, microRNA, or antisense oligonucleotides are used for the post-transcriptional regulation of a gene of interest. In this case, only delivery to the cytosol is required – eliminating the need to overcome the challenges to nuclear entry.

1.2.1.6 Safety Must Also Be Considered

Although non-viral vectors are generally considered safer than viral vectors due to lower immunogenicity, the safety of these vectors must still be considered and characterized along with their efficacy. Factors such as the chemical composition of the materials used, particle size, nanoparticle surface properties, and shape also contribute to the safety profile of gene therapy nanoparticles. For instance, the cationic charge often necessary for efficient transfection (as discussed above) is often a double-edged sword, where delivery vehicles carrying a higher cationic surface charge are generally more cytotoxic, which has been attributed to interactions with critical enzymes such as protein kinase C and substantial cell membrane permeabilization.[60,61] Administration of highly cationic materials such as PEI in the circulatory system can also cause toxicity by adhering to and destabilizing the plasma membrane of red blood cells (hemolysis).[60] The presence of particles carrying a high cationic surface charge also have the potential to induce platelet aggregation in the blood.[35] Similarly, lipid materials containing ether linker bonds have been shown to produce greater transfection *in vitro*, but these bonds are generally too stable for biodegradation, which can also pose a toxicity risk.[60] Non-degradable materials can accumulate in organs such as the liver and spleen, which leads to toxicity.[23] On the other hand, amide and ester linkers are associated with less cytotoxicity since they are more biodegradable but these gene carrier materials would also be more susceptible to decomposition in systemic circulation.[60] In terms of particle size, formulations administered intravenously should not possess particle sizes larger than 0.5 μm and should have a maximum aggregation limit of 5 μm in order to avoid blockages of blood vessels (embolisms).[23]

As previously mentioned, the incorporation of materials such as PEG could mitigate some of these challenges; however, although PEG is generally well-tolerated by the body (due its hydrophilicity), these molecules may turn out to be immunogenic considering anti-PEG antibodies having been identified in approximately 25% of patients following administration of PEG conjugates.[23]

All in all, an ideal non-viral vector would be able to overcome all of the above mentioned barriers. Of course this is where rational design and structure-activity approaches play a role and plenty of effort towards optimization is required, since a component incorporated to overcome one barrier could hinder the system's ability to overcome another.[1,28,50] For example, as discussed above, a delivery complex with an overall positive charge allows for favourable interactions with the cell surface; however, excess positive charge can lead to serum instability or toxicity.

1.3 Cationic Gemini Surfactants Can Act as Non-Viral Transfection Vehicles

A number of cationic lipids and surfactants have been investigated for non-viral DNA delivery, including: monocationic lipids with ammonium head groups, cationic cholesterol derivatives, dicationic lipids and surfactants, polycationic lipids, and cationic lipid hybrids (containing sugar, peptide or polymer residues).[1] Of particular interest for the work present here, is the application of a family of dimeric cationic surfactants commonly referred to as "gemini" surfactants. The general structure of gemini surfactants consist of two amphiphilic monomers covalently linked at or near their positively charged head group by a spacer.[62] The most commonly studied series of gemini surfactants is the dicationic *N,N'*-bis(dimethylalkyl)-alkane-diammoniumdibromide series, or "*m*-*s*-*m*" type (where *m* in this notation refers to the number of carbon atoms in the alkyl tails, while *s* denotes the number of atoms in the spacer group connecting two quaternary ammonium head groups).[62] The structure of 16-3-16 used in this work is depicted in Figure 1.3-1 below.

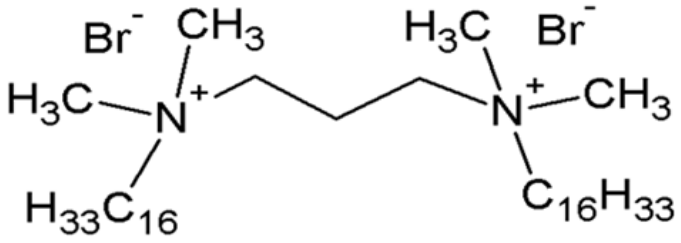

Figure 1.3-1 Structure of the *m*-*s*-*m* gemini surfactant known as 16-3-16

As a group, gemini surfactants display unique solution properties compared to conventional surfactants; making them attractive for building gene delivery carriers. These properties include CMC values that are at least one order of magnitude lower than that of comparable monomeric surfactants, and the ability to form a wide variety of aggregate morphologies in solution through manipulation of the molecular structure.[62] The unique structure of gemini surfactants also offers advantages like CMC control which is important when designing transfection vectors. For example, a high CMC is important in order to have a sufficiently high monomer concentration to form DNA complexes with an overall positive charge; meanwhile, a low CMC can increase micelle stability and keep the delivery complex together during the delivery process.[63] Since the CMC of a gemini surfactant is more sensitive to changes in alkyl tail length than variations in the spacer size, its properties can be fine-tuned by manipulating the spacer, without affecting the CMC.[62]

1.3.1 DNA Binding and Transfection Efficiency Depend on Gemini Surfactant Structure and Aggregation Properties

In regard to gene therapy application, cationic gemini surfactants are known to bind nucleic acid molecules, leading to compaction and protection against enzymatic degradation and ultimately successful delivery to cells. Atomic force microscopy studies of gemini surfactant-plasmid DNA complex formation showed 16-3-16 binds to naked plasmid DNA and compacts the large loop structure of the plasmids within 30 seconds, and more compact particles form within 15 minutes.[64] The process of surfactant-mediated DNA compaction is discussed in more detail in Section 1.5.3.

Gemini surfactants, either alone or in combination with helper lipids have exhibited transfection efficiencies comparable to commercially available reagents. The ability of gemini surfactants to

condense DNA has been associated with the spacer length, where the most condensed DNA form is achieved with surfactants having spacers shorter than 4 carbons or longer than 10 carbons, for a given series of constant alkyl tail length.[62] Intermediate lengths of s = 5 – 10 are generally less efficient.[62] Similar correlations are seen between spacer length and transfection efficiency (highest transfection efficiencies are achieved with $s \leq 4$ or $s > 12$). These effects are attributed to the distance between the cationic nitrogen centres in the surfactant headgroups; the shorter spacer lengths create optimal spacing for the amine groups to interact with adjacent phosphates on the DNA backbone.[62] The increased transfection with long spacer groups may be due to the spacer bending into a U-shape, which subsequently decreases the headgroup distance that allows for improved DNA binding, or membrane disruption via folding of the spacer into the alkyl tail region of biological membranes.[62,63]

Binding of gemini surfactant micelles to DNA is entropy-driven, which is attributed to the release of counterions from the micelles and the DNA upon binding; therefore, changes in the counterions associated with the gemini surfactant headgroups are reported to alter the concentration at which gemini micelles begin to form along the DNA molecule.[65] For example, one of the most effective decreases in this concentration is achieved by replacing the bromide ions with a divalent sulfate.[65] Differences in transfection efficiencies have also been observed with variations in the associated counterions.[66]

Transfection efficiency has also been associated with gemini surfactant CMCs, where transgene expression increases with decreasing surfactant CMC.[63] This trend has been attributed to the ability of the surfactant/DNA complex to hold together due to micellar aggregation, providing stability during the delivery process.[7,63] However, this trend may be more complicated depending on the surfactant series; for 12-s-12 geminis with s = 3-10, lower CMC values were associated with lower in vitro transfection efficiency, but transfection increased with decreasing CMC for spacer lengths 12-16.[63]

The ability of the carrier to adopt various morphologies has also been correlated to increased transfection efficiencies, owing to greater endosomal escape.[62] In particular, the ability to form an inverted hexagonal or cubic phase facilitates DNA release when the lipoplex interacts with anionic membrane lipids.[67] Gemini surfactant-based delivery systems with polymorphic phases (not necessarily inverse hexagonal) generally produce greater transfection efficiency than those systems that show a particle-like morphology and lack long-range order.[64] Gemini surfactants that form vesicle structures in aqueous solution have also been associated with better transfection efficiencies than those with micelle structures.[67] This trend can be explained in terms of the surfactant packing parameter.[3,67] For

instance, lamellar lipoplexes can bind anionic lipids of cellular membranes, which increases the packing parameter of the cationic surfactant and allows the formation of inverted hexagonal or cubic structures because the electrostatic attraction between the positive and negative head groups results in the total volume of hydrophobic tails of the molecules increasing faster than that of the head group areas; v increases faster than a_0 in the packing parameter equation.[67] Although these non-lamellar structures are not favourable for binding DNA, they are favourable for releasing DNA once the lipoplex is within, or after it leaves, the endosome; a key factor in vector-assisted DNA delivery.[67] Correspondingly, a neutral helper lipid such as 1,2-dioleoyl-sn-glycero-3-phosphatidylethanolyamine (DOPE) is often added to gemini surfactant-based gene delivery formulations in order to enhance transfection.[67] Addition of DOPE creates mixed aggregates and increases the packing parameter of the systems; shifting micelle systems towards vesicles or inverted hexagonal structures, and vesicle systems toward the inverted hexagonal or a cubic phases.[67] DOPE is also believed to contribute to increased transfection efficiency by increasing the fluidity of cellular membranes and aid in destabilization of the endosomal membrane.[67] In fact, DOPE is required for transfection depending on the structure of the surfactant molecule. For example, the 12-s-12 series does not show transfection without the addition of DOPE, but longer alkyl tails such as those of 16-3-16 or 18:1-3-18:1 can transfect in the presence or absence (albeit with lower efficiency) of helper lipid.[68]

Early efforts to optimize pDNA/gemini surfactant/DOPE formulations for *in vitro* transfection to PAM 212 murine keratinocytes based on transfection efficiency and cell viability simultaneously revealed an optimal plasmid/gemini charge ratio of 1:10 for the 16-3-16 surfactant (2.4% cells transfected vs. 5.9% by Lipofectamine Plus reagent).[63] Although a 1:40 charge ratio produced the highest percentage of transfected cells (3.1%), the cell viability was significantly reduced to 20%.[63] It was also reported that gemini surfactant-DNA complexes must be allowed to form first, followed by addition of pre-formed DOPE vesicles.[63] Otherwise, combining the gemini surfactant with DOPE and then adding plasmid does not form complexes that are appropriate for transfection.[63] Cationic 16-3-16 delivery formulations have also shown significant increases in transgene expression in the intact skin and lymph nodes of mice treated topically with a total of 75 μg pDNA over three daily treatments compared to the naked DNA and a liposomal 3β-[N-(Dimethylaminoethane)carbamoyl]cholesterol formulation known to deliver plasmid DNA to various tissues *in vivo*.[63] This work demonstrated that topical plasmid DNA delivery using gemini surfactant-based systems is feasible.

Progress in understanding gemini surfactant structure-transfection activity relationships has also led to modification of the gemini surfactant structure in an effort to achieve more favourable effects both *in vitro* and *in vivo*. For example, functional groups have been added in the spacer region in order to influence transfection. Incorporation of secondary or tertiary amines in the spacer resulted in increased transfection efficiencies; most notably, with a 9-fold increase *in vitro* (resulting in levels comparable to the Lipofectamine Plus commercial control) achieved by 12-7NH-12/DNA/DOPE complexes compared to complexes containing the corresponding unsubstituted 12-3-12 structure.[54] In particular, the improvements achieved by 12-7N-12 and 12-7NH-12 (structures shown in Figure 1.3-2) are likely due to the spacing between the nitrogen groups in these structures which allows for more favourable interactions with adjacent phosphate groups of the DNA.[54] Meanwhile, the 3-fold improvement of 12-7NH-12 over 12-7N-12 may be related to less steric hindrance and increased pH activity from the secondary versus the tertiary substitution.[54] 12-7NH-12/pDNA/DOPE nanoparticles show transitions in size and zeta potential at pH 5.5, and show the presence of multiple phases that make the gemini-DNA-lipid complexes more amenable to endosomal membrane fusion.[54] Addition of a hydroxyl functional group in the spacer also increased transfection over the unsubstituted structures, which is thought to be due to enhanced interactions with the DNA through hydrogen bonding.[62] However, addition of a second hydroxyl group or addition of one to three ethylene oxide substitutions in the spacer did not produce significant increases in transfection (Figure 1.3-2).[62] More recently, amino acid moieties have been introduced at the N-position of the 12-7NH-12 spacer to improve biocompatibility.[69] Grafting of the amino acids or short peptides provided significant enhancements to transfection efficiency in epithelial cell lines compared to the 12-7NH-12 parent compound, without any significant changes to cytotoxicity, the particle size or zeta potential of the complexes.[69,70] In

particular, glycyl-lysine substitution was credited with an increased buffering capacity that allows the nanoparticles to escape endosomes.[42]

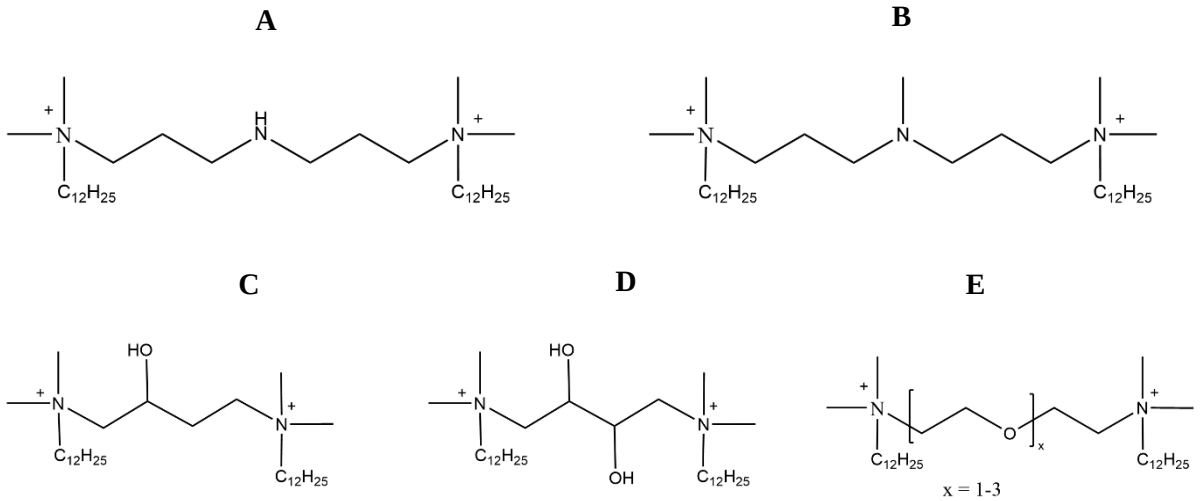

Figure 1.3-2 Chemical structures of 12-s-12 substituted analogues. **A)** secondary amine substitution (12-7NH-12); **B)** tertiary amine substitution (12-7N-12); **C)** monohydroxyl substitution (12-4(OH)-12); **D)** dihydroxyl substitution (12-4$(OH)_2$-12); **E)** ethylene oxide substitution (12-$(EO)_x$-12)

Compaction of the DNA through electrostatic binding of cationic gemini surfactants inhibits intercalation of ethidium bromide (EtBr) between DNA base pairs (indicated by a loss of fluorescence emission).[70] Therefore, strong binding results in greater loss of fluorescence, which is associated with greater transfection efficiency for the first generation of geminis (having alkyl spacers).[70] However, this correlation is not necessarily true for all gemini surfactant series. For example, the amino acid-substituted gemini derivatives showed the highest EtBr-DNA binding (less compaction) but were associated with greater transfection efficiency.[70] This effect is thought to be an indication of balanced binding, where there is sufficient protection of the DNA against degradation while allowing intracellular release of the DNA cargo, which is necessary for gene expression.[70] The introduction of van der Waals forces and hydrogen bonding accompanied by the amino acid-substitution may play a role, and increased hydration due to an increased number of amine groups may result in greater DNA and cell surface interactions.[70] The terminal amine groups may also act as polycations at physiological or acidic pH and encourage membrane fusion that leads to cellular uptake or endosomal escape, or improve endosomal escape through the proton sponge effect.[70] However, lysyl-lysine-substituted

gemini surfactants having three terminal amine groups resulted in the smallest mean particle diameter, but the lowest transfection efficiency of all the amino acid derivatives.[70]

Furthermore, the gemini-DNA binding may also influence the cytotoxicity of the formulation. For example, the weaker binding and more efficient release of DNA encapsulated by the glycyl-lysine substituted gemini 16-7N(GK)-16 (compared to 16-3-16 or the pyridine head group surfactant 16(Py)-S-2-S-16(Py)) is thought to contribute to the reduced cytotoxicity of these lipoplexes since earlier release of the DNA allows translocation of free DNA to the nucleus, whereas stronger binding (by 16-3-16 or 16(Py)-S-2-S-16(Py)) may result in greater accumulation of the intact lipoplex at the nucleus.[71] Although localization at the nucleus is important for gene expression, it was hypothesized that nuclear accumulation of gemini surfactants may contribute to higher toxicity since the surfactants could impact the membrane integrity and function of the nucleus.[71] This could explain the observed correlation between nuclear accumulation and cytotoxicity, again emphasizing a need for balance.[71]

Clathrin- and caveolae-mediated endocytosis are the most common cellular uptake pathways for gemini surfactants.[71] Interestingly, pDNA/gemini/DOPE nanoparticles of either the 12-7NH-12 or its glycyl-lysine-substituted derivative, recruit both clathrin-mediated and caveolae-mediated uptake, but micropinocytosis does not appear to play a major role in uptake (based on comparison of gene expression following transfection in the prescence of various uptake pathway inhibitors).[42]

Considering the interest and notable success of using gemini surfactant/DOPE mixed systems for gene therapy, an evaluation of the interaction properties between a series of gemini surfactants and DOPE was previously completed. Based on CMC determinations of gemini surfactant/DOPE mixtures, the tendency toward mixed aggregate formation between these two amphiphiles was found to be antagonistic, meaning the net interactions in the mixture are repulsive in nature.[72] This was thought to be due to the two amphiphiles having different preferred aggregate structures (based on their packing parameters) and, as seen with other mixed systems, may be an indication that mixed gemini/DOPE aggregates would dissociate into separate gemini-rich and DOPE-rich aggregates over time.[72] However, the strength of this antagonistic interaction (repulsion) was dependent on the gemini's spacer group, with 16-3-16 showing the strongest antagonism, followed by 16-7NH-16, then 16-7-16.[72] DNase sensitivity assays also indicated that the lipoplex's membrane integrity degrades over time, with nearly complete degradation of the incorporated DNA after 4 weeks (or increased storage temperature).[72] Although this study was informative as an initial characterization of the mixing involved in forming

this delivery vehicle, the relationships between mixing behavior and transfection efficiency remain unknown.

While numerous alterations to the gemini surfactant structure have been evaluated in the context of transfection, only a few notable examples were mentioned here. Structural modifications and elucidation of structure-activity relationships continue to fill this research space. Likewise, other approaches to improve the transfection efficiency of gemini surfactants have been dedicated to incorporating alternative components to the gemini/DNA or gemini/DNA/helper lipid complexes to enhance the formulation properties to favour transfection. One such effort involved the addition of neutral tri-block copolymers known as poloxamers or Pluronics® (BASF Corp.) to 16-3-16/pDNA complexes in the presence and absence of DOPE (as discussed in Section 2.1).[73] Accordingly, the work presented in this thesis examined the aggregation tendencies and transfection efficiencies of pDNA-loaded 16-3-16/Pluronic nanoparticle systems.

1.4 Pluronic Block Copolymers Enhance Drug and Gene Delivery

There are a variety of polymers that have been investigated for use as non-viral gene delivery vectors, including: polyethyleneimine (and derivatives), poly(L-lysine), polymethacrylate, poly(amido-amine), poly(D,L-lactide-co-glycolide), and carbohydrate-based polymers (e.g. chitosan, dextran, β-cyclodextrin).[50,74] In addition, a class of water-soluble, non-ionic block copolymers known as Pluronics®, Synperonic®, or under the non-propriety name poloxamer (shown in Figure 1.4-1), have been used in gene delivery applications. Herein, these polymers will be referred to as Pluronics.

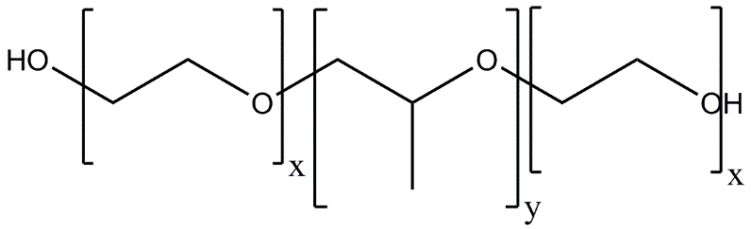

Figure 1.4-1 General Pluronic structure

Pluronic block copolymers have the general structure: PEO_x– PPO_y – PEO_x, where a hydrophobic poly(propylene oxide), PPO (also known as polypropyleneglycol), block is flanked by two hydrophilic poly(ethylene oxide), PEO (also known as polyethyleneglycol) chains. The number of EO (ethylene oxide) and PO (propylene oxide) repeating units, represented by *x* and *y*, respectively, can be varied in

order to alter the water-solubility and physicochemical properties of the copolymer. The nomenclature used by the Pluronic manufacturer BASF Corp. (Parsippany, NJ, USA) begins with a letter indicating its physical state under ambient conditions (F = flake, P = paste, L = liquid) followed by a two or three-digit code referring to the chemical structure[75,76]. The last digit represents the weight fraction of the EO content, while the first two or three numbers approximate the molecular mass of the PPO block (in Da) when multiplied by 300[75,76]. For example, Pluronic F127 is present as a flake and consists of a PPO block of approximately 3600 Da and approximately 70% wt. EO.

Due to the block copolymer structure, which imparts an amphiphilic nature, the Pluronics act as surface active agents. Individual copolymer molecules, referred to as unimers, self-assemble into micelles in selective solvents (a good solvent for one type of block and a poor solvent for the other type) at concentrations at or above the CMC.[75] In aqueous solution, the micellization is driven by the hydrophobic interaction between unimer PPO blocks, which segregate into the micelle core, and leaves the hydrated PEO chains to form the outer, hydrophilic shell, or corona.[75] As expected, increases in the PPO block length (with constant PEO) favours micellization and results in a decreased CMC, while increased PEO lengths increase the CMC (albeit to a lesser extent than PPO, on a per unit basis).[77] This is thought to be due to increased probability of the EO units to interact with the PO units within the micellar core, which decreases the hydrophobicity of the core and destabilizes the micelle.[78] Similarly, Pluronics show a strong temperature dependence and have a characteristic critical micelle temperature (CMT) at which micelle formation occurs for a given Pluronic concentration due to temperature-dependent differences in hydration of the PEO and PPO blocks.[79] At low temperatures, Pluronics are present as unimers (even for high concentrations) and increases in temperature cause dehydration of the PPO block, leading to micellization.[80] Therefore, micelle formation can be achieved by two approaches – either by exploiting the influence of concentration or influence of temperature.[80] In fact, an increase in temperature as small as 10°C can reduce the CMC by a factor of about 10-100.[80] PPO and PEO chain lengths also influence the CMT in the same way they do the CMC. Total molecular weight can also play a role; at constant PPO/PEO ratio, an increase in molecular weight produces a decrease in the both the CMC and CMT.[77] This effect is greater with lower relative PEO content, so for the same change in CMC, a 50 EO-unit change is required for 80% EO Pluronics versus only about 10 EO units for 40% EO Pluronics.[77] Further, in aqueous solution, the micellization process is endothermic and therefore entropy driven (owing to the release of hydration water from the PPO blocks during aggregation).

Pluronic unimers generally have a hydrodynamic radius of approximately 1 nm, while micelles are approximately 10 nm in size.[75] Dynamic light scattering studies also show the co-existence of unimers, micelles, and aggregates at higher concentrations.[75] Interestingly, the micelle size typically remains constant with increased temperature even though the aggregation number increases.[75] This effect is attributed to dehydration of nonionic unimers which results in a greater tendency to separate from the solvent, as well as dehydration of micelles at higher temperatures.[75]

The diverse compositions of the Pluronic series also allow for a variety of structures to be reached. Depending on the Pluronic structure, the concentration and temperature, Pluronics can form the various mesophases that are typically observed with normal hydrocarbon surfactants. For example, between 0 to 50°C, increasing the concentration of an aqueous P104 solution results in transitions from spherical micelles to a cubic phase, then hexagonal phase, and eventually lamellar phase, with two-phase transition regions in between.[80,81] Likewise, some liquid crystalline mesophases can be reached with increasing temperature at a fixed concentration, since the polymers become more lipophilic at higher temperatures.[80,81] In particular, this sequence of mesophases occurs for EO/PO molar ratios of 0.5 or greater.[80] Meanwhile, the hexagonal phase is the first mesophase (cubic phase disappears) for more hydrophobic Pluronics having an EO/PO ratio of 0.25 and the lamellar phase appears first for ratios of approximately 0.15.[80] Furthermore, Pluronic micelles are typically spherical in shape for those polymers with 40% PEO content and above[82]; meanwhile, Pluronics with approximately 30% PEO form cylindrical/rod-like aggregates.[82] Those polymers containing up to 20% PEO, or having a low cloud point form bilayers or lamellar aggregates.[80,82] Spherical micelles can also transition to cylindrical micelles at increased temperatures, even at dilute concentrations (for example, P85 forms cylindrical micelles at 70-85°C for concentrations less than 1% w/w/).[80] Finally, another important characteristic of aqueous Pluronic solutions for pharmaceutical applications is the ability to form gels at appropriate concentrations and temperatures. However, this only applies to Pluronics with a PPO molar mass of at least 1750.[80] The crystalline mesophase regions have generally coincided with the gel formation regions of Pluronics in water.[80]

Water-insoluble compounds, for example drugs, can be solubilized into the PPO core of Pluronic aggregates in order to increase the solubility, metabolic stability, and circulation time of the compound. Therefore, Pluronics have been under investigation as drug delivery carriers and formulation aids for various routes of administration for a wide variety of hydrophobic drugs.[2,83–85]

Currently, five Pluronics (listed as poloxamers) are listed in the FDA Inactive Ingredient Database: Pluronic L44 (poloxamer 124), F68 (poloxamer 188), L101 (poloxamer 331), F127 (poloxamer 407), and L62 (poloxamer 182).[86] Overall, Pluronic block copolymers are generally regarded as non-toxic for all routes of administration except intravenous injection.[87] Early metabolic studies using a single intravenous injection of F38 in rats showed 94% was excreted in the urine and 6% in feces within 3 days, with no breakdown of the polymer, as indicated by the presence of only the parent compound in the urine.[88] In addition, longer retention in organs was observed after intravenous administration for more hydrophobic Pluronics with longer PPO blocks, and Pluronic plasma concentrations remained high for dozens of hours, which suggests recirculation of the copolymer in blood and organs.[89] Despite a lack of metabolic change to the material, histologic lesions were observed in liver, lungs, and kidneys, which are generally attributed to the surface activity of the polymer.[87] Nonetheless, Pluronic F68 currently appears in intravenous injection formulations approved by the FDA.[86] Although Pluronic toxicity by other routes of administration have been assessed, this discussion was limited to a brief summary of studies using the intravenous route. The reader is referred to an early discussion presented by Rodriguez and Singer, which includes summaries of acute toxicity studies conducted by the manufacturers of various polymers.[87]

Pluronics are also known to act as biological response modifiers in both drug and gene therapy applications, capable of overcoming multidrug resistance in cancer cells and altering cellular membrane integrity, nuclear transport, and transcription (discussed in Section 1.4.1). While Pluronic micelles have proved useful as drug carriers, the presence of Pluronic unimers is also important since they show notable activity at the cellular level.

1.4.1 Pluronic Properties Contribute to Improved Transfection

The addition of Pluronic to various gene delivery systems (both viral and non-viral methods) has been associated with significant increases in transgene expression both *in vitro* and *in vivo*, examples of which will be discussed in further detail throughout this section. For now, it is worthwhile noting that unlike cationic polymers and lipids traditionally used for gene delivery, Pluronics do not bind and condense the nucleic acid cargo. This was demonstrated by a lack of observable attractive forces in small angle neutron scattering studies of a DNA-L64 Pluronic mixture.[90] Additionally, fluorescence produced by the intercalation of EtBr with free DNA, and the DNA electrophoretic mobility remain unchanged in the presence of Pluronic, indicating the DNA is not condensed by Pluronic.[90,91] The

presence of Pluronic P85 also did not impede DNA digestion by DNase I.[91] Therefore, Pluronics generally improve transfection through other modes of action.

Addition of LentiBOOST reagent (containing Pluronic F108 as the active component) to lentiviral transduction of human mesenchymal stem cells produced a significant increase in transduction (gene transfer by a virus) to rates greater than 80% gene expression, while cell viability remained high and transduced cells maintained their ability to differentiate into hematopoietic lineages.[92] It is thought that use of the reagent below the CMC increases fusion between the vector and cell membranes.[92] Further, this improvement was achieved with the use of low amounts of viral vector, which could improve the cost of production and overall safety of this method.[92]

The temperature sensitivity and ability of some Pluronics to form gels, have also been exploited to enhance the physical properties of gene delivery formulations. For example, adenoviral vectors used for gene delivery in vascular smooth muscle cells showed increased transfection efficiencies owing to the formation of a Pluronic gel under the conditions of the transfection experiment which acts as a reservoir for the virus, leading to high vector concentrations in the area surrounding the cells and the opportunity for reduced incubation times.[93] This combination also had the added advantages of vector specificity (which remained unchanged with the introduction of Pluronic), and no specific tissue toxicity even with concentrations of copolymer as high as 20% w/v.[93] More recently, F127 was added to a non-viral, gemini surfactant/lipid formulation as a gelling agent for noninvasive pDNA delivery in the vaginal cavity of rabbits.[94] The thermogelling properties introduced by F127 allowed for easy handling and administration at room temperature and reduced leakage from the vaginal cavity for increased the residence time of the pDNA-loaded nanoparticles.[94]

1.4.1.1 Pluronics Provide Formulation Stability and Stealth

Owing to the presence of PEG (or PEO) chains in the Pluronic structure, addition of Pluronics to gene delivery formulations can enhance vector stability in solution and under physiological conditions.

For example, conjugation of P85 to cationic poly{*N*-[*N*-(2 -aminoethyl)-2-aminoethyl] aspartamide (P85-*b*-P[Asp(DET)]) produced samples that did not show any aggregation, even for those with close-to-neutral zeta potentials and had low polydispersity in dynamic light scattering measurements taken over 12 hours at physiological salt concentration.[95] Also, addition of F68, as an alternative stabilizer to poly(vinyl alcohol) which can decrease cellular uptake, in poly(D,L-lactide-co-glycolide)/chitosan

nanoparticles created smaller diameters and more narrow size distributions.[74] These F68-containing nanoparticles showed greater internalization and transgene expression than those containing Tween 80 (possibly due to F68 interactions with the cell membrane, as discussed later).[74]

In the presence of 10 – 50% fetal bovine serum, addition of Pluronic to PEI-DNA complexes showed a notable increase in the *in vitro* transfection efficiency of the complexes, which was considered to be due to the steric barrier introduced by the Pluronics.[96] This serum-stabilization was associated with Pluronics that have a high hydrophilic-lipophilic balance (HLB) value, such as F127 (HLB = 22), F68 (HLB = 29), and P105 (HLB = 15).[96] Similarly, addition of Pluronic P123 to a pDNA delivery vector consisting of Pluronic L92 conjugated to poly[2-(dimethylamino)ethyl methacrylate] (L92-pDMAEMA) resulted in increased transfection and a reduction in the serum-mediated inhibition of transfection, even at P123 concentrations as low as 0.005%.[97] Hemolysis measurements also showed F127-PEI had better blood compatibility than PEI, which is also promising for *in vivo* stability.[98]

Even the encapsulation of a recombinant adeno-associated viral gene carrier in Pluronic F68 micelles prevented neutralization by a viral capsid-specific antibody and potentially allowed for more interaction with cell membranes by shielding of the negatively charged rAAV surface by the PEO chains.[99]

1.4.1.2 Pluronics Interact with Lipid Membranes

As previously mentioned, PEGylation of vectors is known to enhance colloidal stability and reduces recognition by the reticuloendothelial system; however, this method presents a dilemma as the PEG layer can reduce interactions with cells and hinder cellular uptake and the improved stability of these nanoparticles can reduce opportunities for membrane fusion that are necessary for endosomal escape.[33] While the PEG chains of the Pluronic structure can provide some of the benefits of PEGylation, the Pluronic's amphiphilic nature offers an advantage for cellular uptake via PPO-cell membrane interactions. This was demonstrated by higher transfection efficiencies of P85-b-P[Asp(DET)] (mentioned above) compared to the PEG conjugate (PEG-*b*-P[Asp(DET)]) in both the MDA-MB-231 human breast cancer cell line and A549 human lung cancer cell line, which was attributed to greater cell membrane interactions (within 30 minutes) and more efficient cellular uptake and accumulation within 24 hours.[95]

Several reports have suggested Pluronics contribute to enhanced transfection efficiency improvements through interaction with cellular membranes; either by inducing pore formation in the

plasma membrane which enhances uptake of the nucleic acid, or through surfactant activity in the endosome which allows for escape from degradation. Electrical measurements with model lipid membranes showed Pluronic L64 induces formation of ionic channels with discrete conductance levels similar to that of biological channels, and these structures are transiently stable in the open state for several seconds.[90] Interestingly, pore formation was also observed for low L64 concentrations (less than 10 μg/mL).[90] It is hypothesized that once a threshold polymer concentration is reached at the membrane surface, a change in the local membrane curvature is induced, and small-angle X-ray scattering suggests the Pluronics fold so that the hydrophobic PPO region is anchored in the lipid bilayer and the hydrophilic PEO chains protrude out from the membrane (on the same side of the bilayer).[90,100] However, these Pluronic effects appear to be structure-dependent as well as dependent on cell type.[101] PPO chain lengths that approximate that of the acyl chain region of the bilayer (requires approximately 39 PO units) create strong anchoring of the polymer to the membrane with the PPO block spanning the length of the bilayer and the PEO chains normal to the membrane surface; whereas shorter PPO blocks have poorer integration and create the more flat PEO chain orientation previously described for L64.[100] According to molecular dynamics simulations, long PEO chains in the Pluronic structure anchor to the polar head group region of the lipid bilayer of dipalmitoylphosphatidylcholine (DPPC) model membranes, and provide temporary stabilization to the membrane structure through interactions with several lipid molecules.[102] In contrast, short PEO chains quickly pull the lipid head groups internally, causing membrane instability, leading to bending of the membrane and increased permeability, which is consistent with erythrocyte haemolysis assays that show hemoglobin release occurs earlier for Pluronics with short PEO chains.[102] Hydrophobic interactions between the lipid acyl tails and the central PPO block of the Pluronic structure are said to stabilize the membrane structure and keep the two leaflets together.[102] The oxygen atom in the PO units can also interact with the polar head groups of the lipids of the other leaflet (the leaflet not in direct contact with the PEO), which can also contribute to membrane bending.[102] These computational simulations are also consistent with observations of the Pluronic influence on lipid flip-flop activity of liposomes where decreases in the PEO chain length (of Pluronics with equal PPO lengths) increased lipid flip-flop between the liposome inner and outer leaflets, whereas flip-flop activity increased with growth of the central hydrophobic PPO block.[103]

In addition to the PPO length, the overall HLB of the Pluronics also influences membrane permeability. In bovine brain microvessel endothelial cells, hydrophilic polymers with HLB > 20 (e.g. F38, F88, F108, and F127) adhered to the plasma membrane surface and caused membrane

solidification, showed limited cellular internalization and intracellular accumulation that was limited to endocytic compartments.[104] Conversely, Pluronics with PPO blocks of intermediate length and an HLB < 20 (L64, P85, L81, and P105) fluidized cell membranes by incorporating into them. This group of polymers also spread into the cytoplasm, even reaching the nucleus in some cases, and also fluidized mitochondrial membranes.[104] Hydrophobic polymers with a short PPO block (e.g. L35 and L43), adhered to cell membranes, spread into the cytoplasm easily and reached the nucleus, but did not appear to impact the mitochondria.[104] Meanwhile, owing to a large PPO block and short PEO chains, hydrophobic Pluronics such as L121 and L101 caused the highest plasma membrane fluidization.[104,105] However, these polymers tend to anchor into the plasma membrane and remain localized in endocytic compartments, which suggests an ability to fluidize plasma membranes but not intracellular membranes.[104] It is also important to note that the relationships between Pluronic structure and membrane binding and fluidization can also influence cell viability; cytotoxicity in Caco-2 and HMEC-I cell lines was related to the polymer's ability to form ion traversable pores in cell membranes.[105]

Pluronic interactions with cell membranes also vary depending on the cell type, which has been attributed to differences in membrane composition. For example, mouse myeloma cells show a greater accumulation of Pluronic and decrease in membrane microviscosity compared to splenocytes and erythrocytes which adsorb most of the polymers to their surface and show an increase in membrane microviscosity.[101] Tumor cells are known to have less cholesterol content and a larger amount of unsaturated fatty acids, which both increase membrane fluidity (decrease membrane microviscosity), and may account for the variations in Pluronic interaction with different cells types.[106] Addition of phosphatidic acid to phosphotidylcholine liposomes led to a decrease in the microviscosity of the bilayer, which favoured the incorporation of Pluronic L61 and subsequent membrane destabilization by the polymer.[106] Correspondingly, increases in membrane microviscosity by addition of cholesterol, ganglioside GM1, or phosphatidylethanolamine (to a lesser extent) reduced Pluronic binding and suppressed the Pluronic-induced acceleration of lipid flip-flop and reduced membrane permeability.[106]

In another example, treatment of cells with Pluronic L64 two hours after transfection with PEI/pDNA did not influence cellular uptake but demonstrated increased survival of the internalized pDNA by accelerated escape from the endosome.[51] Based on co-localization of fluorescently labeled lysosomes, pDNA, and PEI, and confirmation that L64 and PEI/pDNA enter cells through the same endocytic

pathways (clathrin-mediated and caveolin-mediated endocytosis), it was concluded that L64 increased the permeability of the endosome/lysosomes, which facilitated the escape of PEI and DNA.[51]

1.4.1.3 Pluronics Act as Biological Response Modifiers

Pluronic binding to cell membranes not only influences cellular uptake and distribution, but has also been shown to improve transfection through activation of cell signaling pathways involved in cellular uptake and nuclear transport of DNA containing specific elements.

Co-administration of pDNA with Pluronic P85 or a L61/F127 mixture (known as SP1017) by intramuscular injection in mice increased transgene expression up to 20-fold (with the P85 formulation, 1-day post-injection) compared to injection of the naked pDNA.[91] P85-formulation of the pDNA also resulted in prolonged transgene expression.[91] However, there was no evidence of binding and condensing the pDNA, nor did the Pluronic protect the DNA against degradation.[91] Instead, the ability of P85 to enhance gene expression depended on the type of promoter controlling the gene of interest.[91] Most notably, a cytomegalovirus (CMV) promoter, or a basic promoter element (TATA-box) and an inducible *cis*-enhancer element responding to either NF-κB or p53 transcription factors produced a 20-, 8-, and 21-fold increase in gene expression 24 hours after injection, respectively.[91] Conversely, other promoters (e.g. SV40), which lack an NF-κB binding site, did not produce a statistically significant increase in expression.[91] A similar selectivity toward promoters containing stress response elements (e.g. CMV promoter) causing upregulated transgene expression was also observed with i.m. injection of pDNA formulated with SP1017 (a mixture of 0.25% Pluronic L61 and 2% Pluronic F127)[91], as well as in vitro with stably transfected mouse myoblasts treated with either P85 or L64[107], or administration of P123 following polyethyleneimine-based polyplex transfection.[57] The promoter-selectivity, along with a lack of response to Pluronic in athymic nude mice[91], and evidence of IκB-α phosphorylation in treated cells suggest Pluronics act as biological response modifiers in transfection through activation of the NF-κB signaling pathway.[57,91,107] NF-κB is known as a key regulator in inflammation, and a range of inflammatory diseases, where it is essential in transcriptional activation of pro-inflammatory cytokines, cell proliferation, and cell survival, and has also been shown to participate in oncogenesis and regulation of programmed cell death. [108,109] Hence, targeting and exploiting NF-κB has emerged in a number of gene therapy approaches.[108]

The Pluronic is thought to interact with the cell plasma membrane which leads to the rapid phosphorylation of IκB and activation of NF-κB.[57] NF-κB can bind pDNA that contains a NF-κB-

binding site in the cytosol, and transport it to the nucleus through the nuclear import machinery.[57,91] Following transport into the nucleus, activation of the NF-κB signaling pathway by Pluronics is also thought to increase transcription.[57] Furthermore, NF-κB's nuclear localization signal has been shown to import DNA into the cytoplasm across the cell membrane, which may also account for the enhanced transfection efficiency.[91] Interestingly, confocal microscopy studies showed Pluronics were not transported along with the DNA, but co-localizes with caveolin-1, which may be evidence that NF-κB activation by Pluronics occurs through disruption of caveolae.[57]

As mentioned, p53 binding sites can also produce an increase in transgene expression in the presence of Pluronic P85. Therefore, it is also possible Pluronics activate both transcription factors.[91] It is noteworthy that despite both transcription factors being involved in inflammatory events, the inflammatory responses to Pluronic are reportedly mild and generally no cytotoxic effects are observed in cell lines.[57]

Although Pluronics have generally displayed transfection-enhancing effects as biological response modifiers, it is also important to note that the opposite effect can occur under certain conditions. For example, P85 is known to have an ATP-depletion effect, which may inhibit DNA uptake by endocytosis, a process which requires energy through ATP.[91]

In summary, previous investigations show that Pluronics, or at least those with the appropriate structural properties, are capable of increasing transfection efficiencies by creating pores in the cellular membrane, activating signaling pathways within the cell to enhance DNA internalization, trafficking, and expression within the cell, and/or possibly by acting as a surfactant within the endosome to induce membrane disruption and DNA release.

1.5 Mixed Surfactant Systems Provide Opportunities for Optimized Performance

As previously mentioned, surfactant systems consisting of two (or more) surfactants in solution can introduce new properties that would not be possible for either component on its own; it essentially provides an opportunity to optimize the surfactant performance in a particular application. For example, introduction of an ionic surfactant to a non-ionic surfactant system results in an increase in (or complete elimination of) the cloud point of the nonionic component, as a result of mixed micelle formation.[3] This increases the solubility of the non-ionic surfactant at higher temperature, and allows for use under

solvent conditions (e.g. added electrolytes and high temperature) in which neither component would be effective alone.[3]

1.5.1 Mixed Micelle Theories Characterize Surfactant Mixing Behaviours

Mixtures containing two or more surfactants in solution can result in mixed micelle formation; however, the nature of the final mixed aggregates depends on the surfactants present and the interactions occurring between them. The stability of mixed micelles has been estimated by a number of different models, which typically take a molecular thermodynamics approach, a phenomenological approach, or a combination of both.[110,111] Thermodynamic characterizations based on the pseudo-phase separation model (which considers micelles as separate but soluble phase that appears when the surfactant concentration reaches the CMC, and is in equilibrium with monomers in the bulk) requires experimental determination of the mixed micelle composition. However, in some cases this parameter cannot be directly measured.[110,111] Therefore, phenomenological models of micellization (also based on the pseudo-phase separation model) can be applied, which will be the focus of the discussion from this point on.

In an "ideal" mixed micelle scenario, there is no net interaction between the surfactant molecules, which usually occurs with nonionic surfactants or in the case of both surfactants possessing the same polar head group but have different hydrophobic chain lengths.[9,112] The concentration (CMC_{ideal}) corresponding to mixed micelle formation of a surfactant mixture (at particular mole fractions of each surfactant) is reflected by the average of the CMC values of the individual components, as seen in Equation 1.5-1 where α_1 is the mole fraction of surfactant 1 in the solution (often referred to as Clint's model).[9] According to Motomura et al., the mixed micelle composition of the ideal systems would be given by Equation 1.5-2 where X_{ideal} is the mole fraction of component 1 within the mixed micelle.[9]

$$\frac{1}{CMC_{ideal}} = \frac{\alpha_1}{CMC_1} + \frac{(1-\alpha_1)}{CMC_2} \qquad \textbf{Equation 1.5-1}$$

$$X_{ideal} = \frac{(\alpha_1 CMC_2)}{[\alpha_1 CMC_2 + (1-\alpha_1) CMC_1]} \qquad \textbf{Equation 1.5-2}$$

The greater the difference in the CMCs of the two surfactants, the more dramatic the changes in the CMC of the mixture and the mixed micelle composition as the solution composition is varied.

In real systems (as opposed to ideal), mixtures consisting of different surfactant types tend to have net interactions occurring between the two components due to changes in the head group electrostatic

repulsion, counterion binding, and steric interactions.[112] For example, mixtures of a cationic and an anionic surfactant are expected to have strong electrostatic attraction between the oppositely charged head groups.[9] In the case of ionic and nonionic surfactant mixtures, the presence of the nonionic surfactant within a mixed micelle is thought to reduce the repulsion between ionic surfactant head groups, which would also contribute to an overall net interaction between the two components.[9] Therefore, activity coefficients (f_i) of each component, *i*, in the micelle are introduced to Equation 1.5-3 in order to account for the net interactions within the mixed system.[9,112]

$$\frac{1}{CMC} = \frac{\alpha_1}{f_1 CMC_1} + \frac{(1-\alpha_1)}{f_2 CMC_2} \qquad \textbf{Equation 1.5-3}$$

According to Rubingh's mixed micelle theory (based on regular solution theory, RST), the activity coefficients can be related to an interaction parameter, β, as represented in Equation 1.5-4 and Equation 1.5-5.[113]

$$lnf_1 = \beta(X_2)^2 = \beta(1 - X_1)^2 \qquad \textbf{Equation 1.5-4}$$

$$lnf_2 = \beta(X_1)^2 \qquad \textbf{Equation 1.5-5}$$

X_1 and X_2 in the above equations are the mole fractions of surfactants 1 and 2, respectively, within the resulting mixed micelles at the CMC of the mixed system. Rubingh's interaction parameter (β), characterizes a mixed micellar system's deviation from ideal (zero net interactions) mixing, or in other words quantifies the nature and strength of the molecular interactions between surfactants within the mixed micelles.[9,10] This can be expressed as follows in Equation 1.5-6:

$$\beta = \frac{N_A(w_{11}+w_{22}-2w_{12})}{RT} \qquad \textbf{Equation 1.5-6}$$

where w_{11} and w_{22} are the interaction energies between the surfactant molecules of the same kind within the pure surfactant micelles, w_{12} is the interaction energy between the unlike surfactant molecules within in the mixed micelles.[112,113] N_A is Avogadro's number, R is the gas constant, and T is temperature in the above equation.

In order to allow one to calculate the interaction parameter from experimental CMC data of mixed surfactant systems, Rubingh devised Equation 1.5-7.

$$\beta = \frac{ln\left(\frac{CMC_{exp.}\alpha_1}{CMC_1 X_1}\right)}{(1-X_1)^2} \qquad \textbf{Equation 1.5-7}$$

A negative β value indicates a net attraction (synergism) between the surfactants; meanwhile, a positive β value means there is net repulsion (antagonism). For true synergism, $|\beta| > |\ln(C_1/C_2)|$.[10] A value of zero indicates no net interactions. The magnitude of β signifies the strength of the interaction, where a larger magnitude indicates stronger interactions. Therefore, as seen from Equation 1.5-6, a large negative β value suggests the interaction between the two different surfactants in the mixed micelles is stronger than the interaction within the pure micelles, and the mixed micelles are stabilized.[112]

Once the actual CMC of the mixture is known (determined experimentally), X_1 is calculated through an iterative process from Equation 1.5-8.

$$\frac{(X_1)^2 ln\left(\frac{CMC_{exp.}\alpha_1}{CMC_1 X_1}\right)}{(1-X_1)^2 ln\left[\frac{CMC_{exp.}(1-\alpha_1)}{CMC_2(1-X_1)}\right]} = 1 \qquad \textbf{Equation 1.5-8}$$

The X_1 value can then be compared to the calculated X_{ideal} to give further description of the mixed micelles in comparison to the ideal mixing state. For $X_1 < X_{ideal}$, the mixed micelles are said to be enriched with component 2 (poor in component 1); meanwhile, $X_1 > X_{ideal}$ indicates the mixed micelles are enriched with component 1. Contrary to the ideal systems, as the CMCs of the individual surfactants get less similar, the micellar composition becomes less sensitive to variations in the interaction parameter.[9]

Using the X_1 value, the excess free energy of micellization can then be calculated according to Equation 1.5-9.

$$\Delta G_{ex} = RT[X_1 ln f_1 + (1 - X_1) ln f_2] \qquad \textbf{Equation 1.5-9}$$

In turn, the above calculated parameters can also be used to estimate the monomer concentration in the bulk (C_1^m and C_2^m) and the mixed micelle composition (X_1) at a surfactant concentration above the CMC according to Equation 1.5-10, Equation 1.5-11 and Equation 1.5-12, respectively.

$$C_1^m = \frac{-(C-\Delta)+\sqrt{(C-\Delta)^2+4\alpha_1 C\Delta}}{2\left(\frac{f_2 CMC_2}{f_1 CMC_1}-1\right)} \qquad \textbf{Equation 1.5-10}$$

$$C_2^m = \left(1 - \frac{C_1^m}{f_1 CMC_1}\right) f_2 CMC_2 \qquad \textbf{Equation 1.5-11}$$

$$X_1 = \frac{-(C-\Delta)+\sqrt{(C-\Delta)^2+4\alpha_1 C\Delta}}{2\Delta} \qquad \textbf{Equation 1.5-12}$$

where $\Delta = f_2 CMC_2 - f_1 CMC_1$ and C is the total surfactant concentration of the mixture. At high concentrations above the CMC, the mixed micelle composition approaches that of the bulk mixture.

Typically, the largest experimentally determined β magnitude is found with mixtures of an anionic and cationic surfactant, giving β values of -20 or less.[114] Mixtures of a monovalent ionic surfactant with a nonionic surfactant are usually much smaller, between -1 to -5, and mixtures of two non-ionic surfactants are usually quite small ($-1 < \beta < 0$).[114] Synergism can also be reduced (β becomes less negative) by steric effects due to either an increase in the size of the hydrophilic head group (or branching near the head group) or due to branching in the hydrophobic group.[10] Examples of antagonistic mixing (i.e. greater repulsion or small attractions between the two components after mixing than before mixing) include i) anionic-anionic surfactant mixtures, or ii) mixtures of hydrocarbon-chain surfactants with perfluorocarbon-chain surfactants having the same charge type.[10]

It is important to note there have been some criticisms of applying regular solution theory to describe non-ideal mixed micelles, therefore these approaches should only be considered as useful empirical models.[112] For example, RST assumes the excess entropy of mixing is zero, but for some mixtures, β has been found to vary depending on the solution composition. In this case, the assumption of zero excess entropy of mixing is invalid.[2] The theoretical development of Rubingh's non-ideal mixed micelle model also did not include the effect of counterion binding in surfactant mixtures involving ionic surfactants.[113] However, some ionic-nonionic surfactant mixtures show agreement between the predicted the experimental CMC data, which implies the deviation from ideality caused by the effect of counterion binding is either small, or is accounted for in the activity coefficients.[113]

Additionally, in the absence of salt or combination of ionic surfactants, the interaction parameter, β, determined by Rubingh's RST approach is dependent on the micelle composition, and only considers long-range electric interactions.[115] For high ionic strength solutions, the electrostatic interactions are short-range since there is sufficient shielding of the electrostatic repulsions around each charged site; therefore, β is assumed to be independent of micelle composition.[115] However, with medium ionic strength long-range electric interactions are no longer negligible (although the solution's ionic strength is independent of micelle composition), and for low ionic strength solutions, the ionic strength varies significantly with the micelle composition.[115] More recently, Maeda described the thermodynamic mixed micelle stability (ΔG_{Maeda}) of ionic/nonionic surfactant systems as a function of the ionic

surfactant mole fraction within the mixed micelle (X_{ION}). As seen below, Maeda's theory (Equation 1.5-13), takes both the hydrophobic chain-chain and electrostatic interactions into account.[116] Once B_2 is determined through the relationship $B_2 = -\beta$, where β is Rubingh's interaction parameter, Maeda's B_1 parameter can be calculated as shown below. B_1 represents the free energy change associated with the replacement of a non-ionic monomer within a non-ionic micelle with an ionic monomer, which involves short-range interactions between the hydrophobic chains and between the head groups.[116] Negative values of B_1 indicate an important contribution by the hydrophobic chain interactions, which is typically seen with hydrocarbon tail dissimilarity between the components.[116]

$$\Delta G_{Maeda} = RT(B_0 + B_1 X_{ION} + B_2 X_{ION}^2) \qquad \textbf{Equation 1.5-13}$$

$B_0 = ln\ CMC_{ION}$

$B_2 = -\beta$, where β is the interaction parameter from Rubingh's theory

$B_1 = ln\left(\frac{CMC_{NON}}{CMC_{ION}}\right) + B_2$

Despite their limitations, the above theories and equations continue to be applied as tools to help describe and quantify the non-ideal mixing behaviours of mixed surfactant systems in the literature. In particular, the β value provides a quantitative description of mixed micelle systems, and a way to compare different surfactant pairs.[2] For example, as discussed in Section 1.3.1, characterizations of gemini surfactant/DOPE mixtures previously reported by the Wettig lab used Clint's, Motomura's and Rubingh's mixed micelle theories.[72] Likewise, descriptions of gemini surfactant and Pluronic mixed micelle systems using these models will be summarized in Section 1.5.4 and the non-ideal mixing behaviour of pDNA/16-3-16/Pluronic systems investigated in this work will also be described according to Rubingh's and Maeda's theories in Chapter 3.

1.5.2 Surfactant-Polymer Interactions

Similar to mixed surfactant systems, surfactant-polymer mixtures also have the potential to improve the properties of a formulation compared to what either component would achieve when used alone.[117] Consequently, many surfactant-based formulations, for example in pharmaceutical, cosmetic, and detergency applications, also include a water-soluble polymer.[117] Therefore, it is important to understand the physicochemical interactions between the surfactant and polymer components within

such mixtures as it can provide valuable insights into how these systems work and may be helpful in designing mixtures to achieve more desirable properties.[117] Accordingly, understanding the self-assembled Pluronic/16-3-16/pDNA transfection nanoparticles discussed in this work requires consideration of the interactions occurring within these mixtures. Existing literature describing the interactions between the dicationic gemini surfactants interactions with plasmid DNA, and gemini surfactant interactions with Pluronic block copolymers are discussed later on in this section.

The same forces controlling the solution and interfacial properties of single-amphiphile systems are also responsible for surfactant-polymer interactions, and the nature of the polymer and surfactant will determine the relative importance of each interaction type (i.e. van der Waals forces, dipolar interactions, electrostatic interactions, and hydrophobic effect).[3] The interactions are further complicated by the aggregation properties of the polymer and order of addition (for example, addition of the polymer into a micellar surfactant solution).

Surfactant-polymer interactions can occur as complexes formed between the polymer chain and a surfactant micelle or other aggregate structure (e.g. pre-micellar aggregates, liquid crystals, or bicontinuous phases) or between individual surfactant molecules and the polymer resulting in direct formation of micelles along the polymer chain.[3] Typically, the addition of surfactant to a solution of free polymer chains in water results in surfactant micellization below the surfactant's CMC.[3] This concentration is often referred to as the critical aggregate concentration (CAC), which is the surfactant concentration corresponding to the onset of surfactant molecules binding to the polymer.[3,4] Depending on the nature of the polymer and surfactant, the CAC can be lower than the CMC by a factor of 10 to 1000 in some cases.[3] This significant difference in CAC vs. CMC values can be attributed to stabilization of the aggregates provided by the polymer.[3] Upon addition of polymer to a surfactant solution already containing micelles or other aggregate structures, polymer adsorption onto or into the aggregates may be expected.[3]

Anionic surfactant interactions with nonionic polymers such as polyvinyl pyrrolidone or polyethylene glycol, are expected to rely on van der Waals forces and hydrophobic interactions. Of course, the hydrophobic effect would depend on the polymer's ability to undergo hydrogen bonding with water, as well as the availability of nonpolar sites along the polymer chain.[3] When hydrophobic interactions are the primary mechanism, these would occur between the surfactant tail and the polymer chain.[3] This typically forces the polymer chain to uncoil or expand due to electrostatic repulsion

between ionic surfactant head groups and the resulting polymer-surfactant aggregates resemble a string of pearls.[3] This complex acts similar to a polyelectrolyte in solution, where addition of a salt would neutralize the electrostatic repulsions and allow the chain to collapse or contract.[3]

Not surprisingly, interactions between surfactants and polymers of the same charge are usually minimal (due to electrostatic repulsions that would inhibit any non-electrostatic attractions), especially for polymers with a relatively uniform charge distribution along the chain.[3] Nevertheless, if the charges happen to be concentrated in specific regions along the chain, there may still be an opportunity for hydrophobic interactions in the non-ionized regions.[3]

Interactions between surfactants and polymers of opposite charge occur predominantly through electrostatic attraction, and are considered co-operative due to hydrophobic interactions between the surfactant molecules.[3,118] Initially, the surfactants "coat" the charged sites of the polymer chain through electrostatic interaction with the surfactant headgroup, creating a "hairy worm" appearance.[3] With the hydrophobic chains projecting outward and free to interact, seed regions along the chain can form and the addition of more surfactant molecules leads to polymer-associated micelles.[3] The initial electrostatic binding also leads to collapse of the ionic polymer coil (as seen in Figure 1.5-1) and a decrease in solubility and eventually precipitation due to charge neutralization.[3] With high surfactant binding, both the surfactant's charged head group and hydrophobic tail are involved in binding.[3] Eventually, a reversal of the polymer's charge and coil expansion can occur at higher surfactant-polymer ratios.[3]

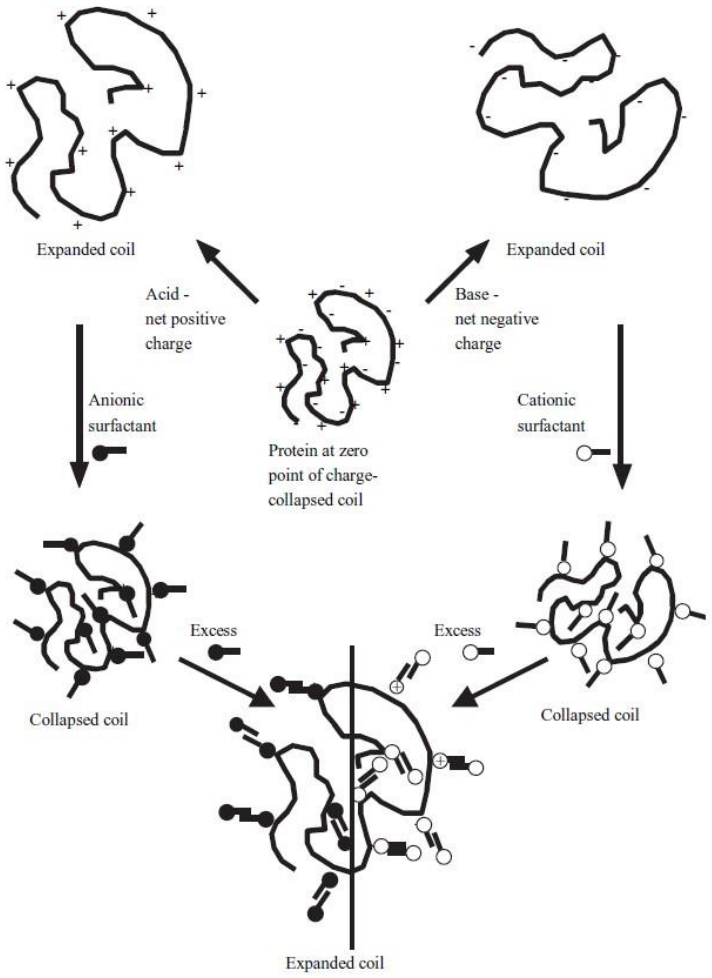

Figure 1.5-1 Expanded and collapsed coil configurations of a charged polymer (e.g. protein) following adsorption of surfactant of opposite charge.[3]

1.5.3 Surfactant-DNA Interactions

Surfactant-DNA complexes often exist in aqueous solution (which is the focus of this work), but can also be prepared as thermotropic liquid crystals, and bulk films.[119] Aside from their application in gene delivery, surfactant-DNA complexes can also be exploited for a large number of purposes such as: drug delivery vehicles or depots *in vivo*, scaffolds for DNA-templated reactions and functionalization of nucleic acids, scaffolds for fluorescence resonance energy transfer, prevention of concentration

quenching of fluorescent dyes, or even incorporation into optoelectronic devices like OLEDs and solar cells.[119]

Cationic surfactant interactions with DNA are similar to polyelectrolyte-oppositely charged surfactant systems, where the DNA can be considered as an amphiphilic polyanion. These interactions result in compaction of DNA and reduction of its charge, which is important for non-viral gene therapy applications (as discussed above).

Early studies found that a single DNA molecule undergoes a discrete transition between an elongated coil state and compacted globule state (plus a coexistence region) with the addition of cetyltrimethylammonium bromide (CTAB) in solution.[120] Binding of the surfactants to the DNA molecule is primarily through electrostatic attraction, occurring below the CMC of the surfactant.[118] This is supported by findings that addition of salt increases the CAC of DNA-cationic surfactant systems in solution.[118] In addition, ^{23}Na NMR showed displacement of sodium with surfactant binding, which implies the cationic surfactants replace sodium as the DNA counterions, and likewise, DNA replaces the anionic counterions of the cationic surfactants.[118]

DNA-cationic surfactant interactions are highly co-operative, according to binding isotherms that show a sigmoidal shape.[118] The binding mechanism is similar to that described in surfactant-polymer systems (above). Following individual surfactant binding to DNA through electrostatic interactions, the complex becomes stabilized through hydrophobic interactions[118,120]. Formation of DNA-associated surfactant micelles through hydrophobic interactions between surfactant molecules occurs once a sufficient surfactant concentration is reached.[118] These micelles then act as multivalent ions and induce compaction through electrostatic attraction to different areas of the DNA chain.[118]

1.5.3.1 Surfactant structure influences interactions with DNA

Surfactants with a larger alkyl chain length induce DNA compaction at a much lower concentration compared to those with a shorter alkyl chain (e.g. 8.0 vs. 80 μM for CTAB versus dodecyl-trimethylammonium bromide (DTAB), respectively).[118] Further, according to force-measuring optical tweezer studies, short-chain surfactants, such as octyl-trimethylammonium bromide (OTAB) do not induce condensation, likely due to an ability to "lie down" on the DNA surface and interact directly with the DNA groove through hydrophobic interactions.[121] In contrast, surfactants with a sufficient

aliphatic tail length, for example DTAB, promote DNA condensation through inter-molecular interactions between hydrophobic tails, which likely orient away from the DNA surface.[121]

In addition to hydrophobic chain lengths, alterations in the surfactant head groups can also impact the compaction efficiency. For instance, modification of the head group region that increases the hydrophobicity of the surfactant (e.g. addition of an aromatic ring between the head group and tail) will increase the surfactant's efficiency in compacting DNA. This effect is similar to that seen with increasing the hydrophobic tail of the surfactant, resulting in decreases in both the CMC and CAC.[118] Increased valency of a surfactant's polar head group also increase compaction efficiency.[118,122] Alternatively, increasing the surfactant hydrophilicity, for example by introduction of hydroxyl substituents in the CTAB headgroup, preserved the EtBr access to the DNA to a significantly larger extent.[118] This result is thought to be due to surfactant packing effects that increase the curvature of the aggregates, on account of the increased effective size of the polar headgroup (based on presence of bulkier groups and also due to increased hydration of a more polar group), producing smaller and more globular micelles on the surfactant-DNA complex as opposed to the typical rod-like CTAB micelles.[118] This increased curvature of surfactant aggregates likely produce less efficient, patch-like coverage of the DNA, which allows for EtBr binding.[118]

DNA compaction efficiency can also be enhanced by use of cationic gemini surfactants. Introduction of a second alkyl tail improves the hydrophobic tail interactions that are important for compaction. In fluorescence microscopy studies of bacteriophage T4 DNA interaction with gemini surfactants of varying architecture, DNA globules were detected at a much lower surfactant concentration (almost two orders of magnitude) with the 12-3-12 gemini surfactant compared to its divalent, single-tail equivalent 12-3-1.[122] As previously discussed, spacer length also influences compaction efficiency with either short ($s < 4$) or long ($s > 10$) spacers showing the highest DNA compaction efficiency.[122] This trend also appears to correspond to the trends in the observed CMCs of the 12-s-12 series studied, where the minimum in DNA compaction corresponds to the maximum CMC value in this gemini surfactant series.[118,122] This effect is thought to be due to greater flexibility as the spacer length increases, and presumably the conformation is restricted upon interaction with the DNA, which leads to a loss of entropy.[118,122] However, with further increases beyond $s=10$, the spacer becomes long enough to associate with the hydrophobic tails, and surfactant self-assembly becomes favourable again, leading

to decreases in the CMC values and increases in the surfactant's DNA compaction efficiency once again.[118,122]

In general, the structure of surfactant and oppositely charged polyelectrolyte complexes is dictated by that of the pure surfactant aggregates in solution, given that the polymer is sufficiently flexible to adapt to the surfactant's structure.[118] However, in the case of DNA as the polyelectrolyte, this may not be possible – although the surfactant aggregate structure does not necessarily need to deviate significantly from the structures they form on their own.[118] Hence, the rod-like structures of CTAB aggregates are slightly distorted in order to match with the phosphate groups on the DNA.[118] Overall, the CTAB/DNA complex shows a hexagonal structure (H_I), which can be described as hexagonally-arranged cylindrical micelles surrounded by DNA rods.[118,123,124] As the surfactant alkyl tail length decreases (for example, in DTAB), the aggregates, and therefore the DNA-surfactant complexes, become more spherical and less ordered.[118] For surfactants that form lamellar structures, the DNA will reside in the water region between two lamellar bilayers.[118]

Since surfactant-mediated DNA compaction relies on surfactant self-assembly, the compaction can be controlled or reversed.[118] Decompaction/decondensation can be induced with the addition of non-ionic or anionic surfactants, liposomes, polymers, or salts.[52,118,125,126] The interaction between the surfactants is more favourable than the surfactant-DNA interactions.[118] The addition of cylcodextrins can also decondense the surfactant-DNA complex through formation of inclusion complexes with the surfactant hydrophobic chains and increase steric hindrance inside the complex.[125] However, unlike addition of an anionic surfactant such as sodium dodecyl sulfate, this mechanism does not result in complete release of the surfactant from the DNA.[125]

Important for the work presented here, Pluronics have also demonstrated the ability to dissociate gemini surfactant/DNA complexes.[127] Similar to other anionic or non-ionic surfactant-mediated DNA decompaction, the 12-3-12 gemini surfactant shows preferential interaction with Pluronic P123 micelles.[127] As the gemini surfactant is added into a Pluronic/DNA solution (note these two components don't show any significant interaction), EtBr binding to the DNA appears uninterrupted.[127] Gemini-DNA complex formation is hindered until the Pluronic/gemini aggregates are saturated with gemini surfactant.[127] Further addition of the gemini surfactant then leads to gemini-DNA binding, and a reduction in the EtBr-DNA intercalation.[127] With the addition of Pluronic to gemini surfactant/DNA complexes in solution, it has been proposed that titration of Pluronic P123 to a 12-3-12/DNA solution

first results in Pluronic binding of free gemini surfactant in the bulk, which disrupts the thermodynamic equilibrium between DNA-bound and free surfactant in solution, leading to release of surfactant from the DNA into the bulk.[127] As more Pluronic is added, more 12-3-12/P123 complexes are formed and the DNA is eventually decondensed.[127]

1.5.4 Gemini Surfactants and Pluronics Show Non-Ideal Mixing Behaviour

In terms of surfactant-Pluronic interactions specifically, there are many studies in the literature reporting the interaction between Pluronic block copolymers and ionic surfactants (either traditional or gemini structures), as well as how changes to either molecular structure influences the interactions. For the purposes of relating to the work presented in this thesis, the following discussion focuses only on quaternary ammonium surfactants.

Early studies of the monomeric cationic quaternary ammonium surfactant (essentially half a gemini surfactant), tetradecyltrimethylammonium bromide, TTAB, with Pluronic F127 showed the interactions between the surfactant and polymer somewhat vary according to the aggregation state of the polymer. In the presence of unassociated F127 monomers in solution, the TTAB molecules bind to the polymer and form micelle-like aggregates which grow during a co-operative binding process.[79] This is the result of hydrophobic interaction where the methyl group of the PO units are in direct contact with the surfactant micelle palisade layer where the hydrophobic groups are in contact with water, which is thought to remove water from the micellar surface and also possibly from the hydrated parts of the polymer.[79] In the presence of F127 micelles, the surfactant initially binds to the micelles, forming F127/TTAB mixed aggregates (which are relatively stable according to constant light scattering intensities).[79] However, these mixed aggregates eventually break down into smaller mixed aggregates as F127 monomers are released into solution and the aggregates become richer in TTAB content.[79] This effect is likely due to destabilization of the mixed aggregate by electrostatic repulsions between TTAB headgroups.[79] Just before all the F127 micelles are dissociated into monomers, the added TTAB simultaneously begins binding to the F127 monomers in solution.[79] This continues until all F127 micelles are dissociated and the F127 monomers become saturated with TTAB.[79] At this point, further addition of TTAB will form free TTAB micelles.[79] Differential scanning calorimetry studies also revealed that small amounts of TTAB reduce the CMT of F127, as a result of F127-rich mixed micelle formation, whereas higher TTAB concentrations destabilize the mixed micelles and increase the CMT.[79]

CTAB and TTAB have also demonstrated synergistic interactions (according Rubingh's theory) with Pluronic-like triblock copolymers having the structures $(EO)_{18}(PO)_{31}(EO)_{18}$ and $(EO)_2(PO)_{15.5}(EO)_2$, which resulted in mixed micelles rich in the polymer component rather than the surfactant component.[128] The synergism observed was attributed to favourable reduction of the electrostatic repulsion between surfactant headgroups by intercalation of the copolymers in the mixed micelles.[128] However, differences in these interactions were observed based on the chemical structures of each component. Specifically, in comparison to the TTAB mixtures, the CTAB mixtures had stronger interactions with the triblock copolymers, likely due to stronger hydrophobicity imparted by a longer alkyl chain.[128] Greater synergism was also observed for the copolymer possessing longer PEO chains, which was attributed to more effective reductions in surfactant headgroup repulsion.[128]

The gemini surfactant and Pluronic mixtures previously studied indicate non-ideal mixing between these materials that are more complex than the interactions observed with traditional surfactant structures. The net interactions observed in these systems and the strength of these interactions are dictated by changes to the molecular structure of either component. Unfavourable (antagonistic) mixing behaviours were observed in mixtures of 12-2-12, 14-2-14, and 16-2-16 gemini surfactants with Pluronics of varying hydrophobicity (based on PEO/PPO ratio), as indicated by micellization occurring at surfactant concentrations higher than the expected ideal.[129] This effect was thought to be due to differences in hydrophobicity of the two materials.[129] The mixed micelles were determined to have a greater presence of Pluronic; however, the gemini surfactants have stronger hydrophobicity than the Pluronics (demonstrated by comparisons of the micropolarity of the pure components).[129] Therefore, an increased amount of Pluronic in the mixed state is thought to weaken the hydrophobic environment of the mixed state, leading to de-mixing of the components.[129] This effect appears greater with increasing hydrophilicity of the block copolymer.[129] In contrast, increases to the tail length of the gemini surfactant are said to strengthen the hydrophobic environment of the Pluronic-rich mixed micelles, leading to weaker antagonism.[129] The antagonism observed in these systems is consistent with other gemini surfactant – Pluronic interactions that consider the Pluronic as a neutral polymer rather than a nonionic surfactant.[129,130] In general, titration of gemini surfactant into a monomeric Pluronic solution (at a concentration and temperature below the copolymer's CMC or CMT, respectively) results in formation of gemini aggregates on or near the hydrophobic region of free Pluronic monomers.[130,131] This process results in a steep endothermic increase in the enthalpy, which is likely a result of dehydration of the polymer PPO segments.[130] Continued addition of surfactant results in the formation

of more or larger aggregates, until electrostatic repulsion between the gemini headgroups hinders this process and further addition of gemini at this point leads to the formation of free gemini micelles.[130] When the copolymer is present at concentrations above its CMC, two endothermic process are observed.[130] Copolymer micelles and copolymer micelle clusters are initially present; however, the presence of even a small amount of gemini surfactant breaks down the Pluronic micelle clusters.[130] Further addition of gemini leads to swelling of the Pluronic micelles as the gemini enters the hydrophobic core of the polymer micelles.[130] This is also accompanied by release of Pluronic monomers and formation of smaller sized mixed micelles due to an equilibrium of the hydrophobic interactions between the two components and electrostatic repulsion between the gemini surfactant headgroups.[130,131] Eventually, the unassociated Pluronic monomers form mixed aggregates with the gemini.[130] In the presence of both Pluronic monomers and micelles (e.g. at the CMT), the gemini surfactant alkyl tails penetrate the Pluronic micelle hydrophobic core, leading to gemini/Pluronic mixed micelle formation.[131] As seen with micellar Pluronic solutions, further addition of the gemini surfactant destabilizes the mixed micelles due to electrostatic repulsion between the gemini head groups, leads to smaller mixed micelles consisting of gemini surfactant as the richer component in the aggregate, and releases Pluronic monomers into the solution (as depicted in Figure 1.5-2).[131] Added gemini surfactant begins to bind the free monomers until saturation is reached, and free gemini surfactant micelles form.[131] As previously mentioned, the nature of the Pluronic has some influence on these events; addition of 12-6-12 to monomer and micellar F127 (solution temperature = CMT) proceeds to gradual breakdown into small mixed micelles (as described) and eventually dissociation into F127 monomers and 12-6-12 micelles, whereas with P123 the gemini surfactant does not completely dissociate the mixed micelles.[131]

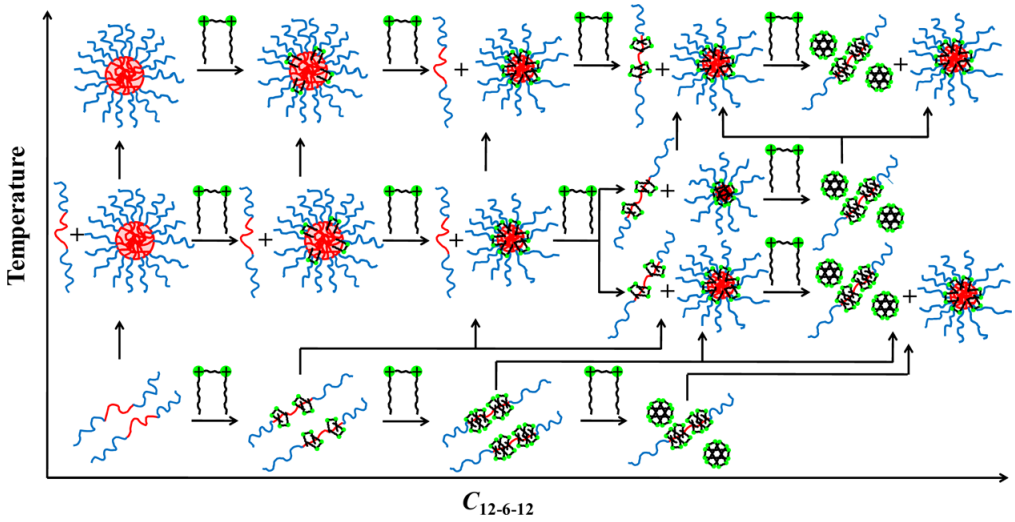

Figure 1.5-2 Schematic depiction of mixed aggregate formation during titration of cationic gemini surfactant into monomeric and micellar Pluronic block copolymer solutions (under different temperatures). Reprinted (adapted) with permission from [131]. Copyright (2014) American Chemical Society

Contrary to the interactions summarized above, binary mixtures of L64 with either 10-2-10, 12-2-12, or 14-2-14 cationic gemini surfactants are reported to show synergistic mixing behaviour.[132] Nonetheless, similar to previous reports, mixing became more favourable with increased gemini surfactant tail length.[132] Overall, the synergism was attributed to greater hydrophobic effect and reduced electrostatic repulsion on account of intercalation of the Pluronic PEO chains between the cationic gemini headgroups in the mixed micelle stern layer.[132] This is also consistent with the increased specific conductance measured during the titration of gemini surfactant into copolymers solutions; Pluronic interaction at the surface of gemini surfactant micelles was thought to disrupt the binding of counterion (bromide ions in this case) to the surfactant headgroups, and result in the release of additional bromide ions into solution, and thus an increase in conductance.[133] Fluorescence studies also revealed a decrease in the polarity of the micelles, which also suggests the copolymer interacts at the surface and palisade layer of the micelle, and displaces hydration water (which also provides further explanation of the increase in conductance).[133] These effects did not appear to be influenced by changes in headgroup size from 12-3-12 to 12-6-12 surfactant structures, but greater interactions appeared for the more hydrophobic P103 versus F108 and F68.[133]

In another study by Bakshi and Sachar, F127/12-2-12 and P103/12-2-12 mixed micelles were also determined to form through synergistic interactions.[110] In both cases, the mixed micelles were said to be enriched with the gemini component, but synergism was stronger for the F127 systems over P103.[110] Increased synergism was attributed to the larger PEO chains of F127 that would be expected to provide more effective reduction of electrostatic repulsion between cationic gemini headgroups by introducing more hydration into the stern layer.[110] (However, this theory conflicts with the fluorescence studies previously reported in the literature). Increasing the temperature from 21 to 40°C also induced greater synergism through dehydration of the Pluronic PPO blocks, thus enhancing hydrophobic interactions.[110]

Furthermore, notable differences in the mixing interactions of F127 and P103 polymers were highlighted due to the overall hydrophobicity of the Pluronic component when mixed with monomeric (dodecyl-, tetradecyl-, or hexadecyltrimethylammonium bromide) and dimeric (m-2-m, where m = 10, 12, 14, or 16) cationic surfactant series. All F127 mixtures showed synergistic mixing interactions and the calculated mixed micelle mole fractions indicated a greater amount of the cationic surfactant component over the F127 component in all cases.[134] Although all the interaction parameters were negative, the average parameter values pass through a broad maximum with increasing length of the hydrocarbon chain, which was seen for both types (monomeric and dimeric) of surfactants.[134] However, the synergism was stronger for the monomeric surfactant mixtures compared to those containing dimeric (gemini) surfactants.[134] While synergism was attributed to neutralization of the electrostatic repulsion between the surfactant polar head groups, it was suggested that replacement of a monomeric head group for a dimeric one introduces steric hindrance in the stern layer of the mixed micelle, causing a reduction in the synergism.[134] In contrast, the dimeric (gemini) surfactants resulted in greater synergism compared to the monomeric surfactants for P103 mixtures.[134] The difference in trends in comparing the interaction parameter of F127 versus P103 mixtures was expected to be due to the increased hydrophobicity of P103, where mixed micelle formation would be favourable due to hydrophobic interactions.[134] Accordingly, these hydrophobic interactions would be stronger for the dimeric surfactants compared to the monomeric counterparts.[134] In addition, synergism increased with increasing carbon tail lengths (on account of greater surfactant hydrophobicity), shifting from antagonism (positive interaction parameter values) for P103/10-2-10 and P103/12-2-/12 to synergism (negative values) for P103/14-2-14 and P103/16-2-16 mixtures.[134] Correspondingly, the monomeric surfactants show antagonistic mixing (positive interaction parameters) with Pluronic P103.[134] The calculated mixed micelle mole fractions (x) were close to the corresponding ideal values for the P103

mixtures with monomeric surfactants, indicating the mixed micelles are expected to be equally occupied by both components; meanwhile, the P103/dimeric surfactant mixtures produced surfactant-rich micelles.[134]

Chapter 2
Project Aims, Hypothesis, and Objectives

2.1 Combining Pluronics and Gemini Surfactants Builds on Rational Vector Design

The use of helper lipids can be expensive, and in the absence of significant energy input (such as from ultrasonication or high pressure homogenization) the liposomes are inconsistently sized, which can pose a problem for predicting the pharmacokinetics of the delivery system. Gemini/DOPE/DNA lipoplexes also show decreased membrane integrity leading to increased sensitivity to DNase degradation over time.[72] Furthermore, the presence of serum has been known to inhibit transfection of gemini/DOPE systems, which raises concerns for future applications in systemic delivery.[135] As an alternative, addition of biocompatible Pluronics to a gemini surfactant gene delivery formulation is expected to provide stealth for i.v. administration *in vivo*, colloidal stability for storage, and enhance transfection activity through biological membrane interactions and activation of signaling pathways that aid in cellular uptake, nuclear localization, and transcription (as discussed above in previous formulations). Incorporating Pluronics in the gene delivery formulation also provides an opportunity for tissue-targeted delivery, since the Pluronic terminal hydroxyl groups can be functionalized with targeting molecules that become part of the ethylene oxide corona. Meanwhile, use of a dicationic gemini surfactant can condense the DNA, provide an overall positive charge to the nanoparticle (depending on the ratios used) for electrostatic interaction with cells, and possibly endosomal membrane disruption.

The potential for improved transfection efficiencies by combining gemini surfactants and Pluronics motivated a preliminary investigation using national formulary-grade Pluronics (L44, F68, F87, F108, and F127) in combination with the 16-3-16 gemini surfactant, which was reported by Dr. Shawn Wettig's research group (School of Pharmacy, University of Waterloo, Canada). In this study, human ovarian adenocarcinoma (OVCAR-3) cells were transfected *in vitro* with nanoparticles consisting of varying Pluronic concentrations and N^+/P^- charge ratios; however, the transfection efficiency was lower than that of the commercial positive control, Lipofectamine 2000 but cell viability was higher for the novel formulations compared to the control.[73] Most nanoparticles showed appropriate particle sizes (hydrodynamic diameters of approximately 200 nm) and positive zeta potentials (for N^+/P^- charge ratios

5:1 and 10:1).[73] Despite the benefits that gemini surfactant and Pluronic block copolymers bring to pDNA transfection when used separately, the combination of these two materials together in a single formulation did not have a synergistic effect. However, these novel nanoparticle formulations showed the ability to transfect cells, which is a promising result, but further optimization is likely needed. Next steps could involve testing more charge ratios, Pluronic concentrations, order of mixing, surface functionalization, use of different gemini surfactant structures, different Pluronic block copolymers, and so on. Alternatively, a deeper understanding of the interactions between the components in these formulations that could be influencing the transfection efficiencies seen *in vitro* may be informative in helping to steer future optimization efforts.

2.2 Project Aims

The work presented here focuses on the influence of Pluronic block copolymer's molecular structure; specifically, how it influences the mixing behaviour when combined with the 16-3-16/pDNA complex, and whether these mixing behaviours are related to *in vitro* transfection efficiency to potentially identify a new set of criteria for screening these transfection systems and choose a more appropriate combination (e.g. a different Pluronic) if necessary. Additionally, the presence of DNA has the potential to alter these interactions; therefore, DNA was included in the characterizations reported in this work.

2.3 Hypothesis

The interaction between Pluronics and a pre-formed 16-3-16/pDNA complex are expected to be synergistic, which increases in strength with higher PO content and PEO chain lengths of the Pluronic structure. The interaction parameter values for the complete Pluronic/16-3-16/pDNA mixtures are hypothesized to correlate with transfection efficiency. In particular, as synergism within the nanoparticle increases, transfection efficiency will decrease due to insufficient pDNA release.

2.4 Objectives

1) Determine the micellization properties of the pre-formed 16-3-16/pDNA complex (N^+/P^- = 10:1) in aqueous solution

2) Investigate the interaction between Pluronics and the 16-3-16/pDNA complex, and the influence of the Pluronic composition (such as PPO length, PEO length, and hydrophobicity) on the mixing interaction

   (i) Determine the interaction parameters of Pluronic/16-3-16/pDNA mixtures with Pluronics F87 P84, L121, F127, P103, and L44

   (ii) Investigate the effect of each Pluronic on the condensed state of the 16-3-16/pDNA complex

3) Determine whether there is a relationship between these interactions and the *in vitro* transfection efficiency of these formulations

   (i) Characterize pDNA-loaded nanoparticles by size and zeta potential

   (ii) Determine the *in vitro* transfection efficiency and cytotoxicity of each Pluronic/16-3-16/pDNA mixture

Chapter 3
Cationic Gemini Surfactant – Plasmid Deoxyribonucleic Acid Condensates as a Single Amphiphilic Entity

3.1 Abstract

A critical aggregate concentration for the surfactant-DNA "complex" or "condensate" consisting of the 16-3-16 gemini surfactant and circular plasmid DNA was determined using surface tensiometry, dynamic light scattering and conductometry. This surfactant-DNA complex acts as an amphiphile itself, for example, decreasing the surface tension of water until a critical concentration is reached. The evidence presented here introduces a new way of thinking about these surfactant-DNA condensates – not simply as aggregates in solution, but as surface active agents in their own right. At concentrations below the critical aggregate concentration, there is some dissociation of surfactant molecules from the condensate, creating a more "loose" or "relaxed" complex; however, at and above the critical aggregate concentration, the surfactant-DNA system forms smaller and more uniformly distributed condensates once again. This behavior is analogous to the demicellization/micellization that occurs in typical surfactant systems.

3.2 Introduction

Use of various gemini surfactants in gene therapy applications continues as a topic of significant investigation. Of course, the interaction of deoxyribonucleic acid (DNA) with gemini surfactants is a complimentary topic of interest which has been the subject of many recent investigations and reviews over the past decade.[65,67,117,125,137–147] Gemini surfactants are known to complex with DNA, eventually collapsing and condensing the DNA into globules of smaller size that can enter cells more easily. In general, the interaction of cationic surfactants with DNA has been equated to that seen in systems of surfactants with oppositely charged polyelectrolytes.[117,118,121,148–150] Cationic gemini surfactants are thought to initially bind to the negatively charged DNA chains through electrostatic interaction.[125] Much like the interaction of cationic surfactants with anionic polymers, this binding is reported to occur well below the critical micelle concentration (CMC) of the surfactant.[118] Surfactants with sufficiently long aliphatic tails (12 carbons and greater) orient their tails away from the DNA groove.[121] The bound

surfactant molecules may then form micelle-like aggregates through hydrophobic interactions between their hydrocarbon tails, creating nucleation centres that DNA can wrap around to form a densely packed, or "bead-like", structure.[125] This compaction can be reversed to dissociate the DNA molecule from the surfactant (whether mono- or di-cationic) using a decrease in temperature or pH, or the addition of various reagents such as sodium dodecyl sulfate[125,151] or other anionic surfactants[151], cyclodextrin[125,152,153], nonionic surfactants[127], monovalent salts[120], synthetic polyacids[126], nucleotides.[120] Depending on the reagent used, varying levels of decompaction and different final DNA conformations are obtained.[125]

Unlike previous studies where DNA is titrated into a surfactant solution or vice versa, we treated the already formed surfactant-DNA complex as a single entity and titrated into a known volume of water. The gemini surfactant *N,N'*-bis(dimethylhexadecyl)-1,3-propanediammonium dibromide, commonly known as 16-3-16 (having 16-carbon tails and a 3-carbon spacer between two quaternary amine headgroups), was used to condense the pVGtel.RL plasmid DNA at a (N^+/P^-) charge ratio of 10:1. Here we introduce evidence that the final gemini surfactant-DNA complex or condensate (16-3-16/pDNA) acts as a single amphiphilic entity in physicochemical studies where an abrupt change in the physical properties of a solution is observed at a critical concentration (referred to here as the critical aggregate concentration, CAC).

3.3 Materials

The 16-3-16 gemini surfactant was synthesized in our lab as described in previous work.[154,155] The plasmid, pVG.telRL[156], was extracted from DH5α cells (a gift from Dr. Roderick Slavcev, School of Pharmacy, University of Waterloo, Canada) using an Omega Bio-tek E.Z.N.A. Plasmid DNA Maxi Kit and HyClone HyPure Molecular Biology Grade Water for elution. Ultrapure MilliQ water (Millipore) was used for all sample preparations and experiments. Purified plasmid DNA concentration was measured by UV-Visible light absorbance at 260 nm using a Thermo Scientific NanoDrop 2000 spectrophotometer, and the pDNA sample was accepted as "pure" for DNA (vs. RNA) for absorbance ratios at 260 nm and 280 nm (260/280) of ~ 1.8. Isolation of the pVG.telRL plasmid was confirmed by restriction enzyme digestion with *Hin*dIII followed by gel electrophoresis on 1.2% agarose gel to separate the products.

3.4 Methods

3.4.1 16-3-16/pDNA complex preparation

16-3-16/pDNA complexes were prepared in water by mixing a 0.1 mM aqueous solution of 16-3-16with an appropriate volume of the pDNA solution to achieve a charge ratio of 10:1 (N^+/P^-). These 2 components were allowed to incubate for 15 minutes in a water bath (Fisher Scientific Isotemp® GPD 10) set to 25°C. The 16-3-16 solution was filtered using a 0.22 µm polyethersulfone (PES) syringe filter (Sartorius) before use.

3.4.2 Critical concentration determination by tensiometry

Surface tension measurements were performed at room temperature using the Wilhelmy plate method with a KSV NIMA surface tension balance (KSV NIMA/Biolin Scientific, Finland). The plate was thoroughly cleaned and flame dried until glowing red before each experiment. The 16-3-16/pDNA condensate solution was titrated into 60 mL of Ultrapure MilliQ water (re-filtered using a 0.22 µm PES syringe filter before use). The solution was allowed to equilibrate (with magnetic stirring) for 5 minutes before measurement. All critical concentration determinations were carried out in triplicate.

In each CAC experiment, the surface tension was plotted against the logarithm of the total amphiphile concentration (moles of 16-3-16 + moles of pDNA per litre). The CAC of the mixture was identified by the point of intersection of the linear trendlines before and after the first breakpoint in these plots.

3.4.3 Critical concentration determination by dynamic light scattering

Size and intensity measurements were carried out using a Malvern Zetasizer Nano ZS equipped with an MPT-2 Autotitrator connected to a quartz flow cell (Malvern Instruments, UK). The sample container was prepared with an initial 10 mL of Ultrapure MilliQ water (re-filtered using a 0.22 µm PES syringe filter before use). 20 additions of the 16-3-16/pDNA complex (in a single titrant container) were made to reach a final concentration of 6 µM final surfactant concentration, with the sample recirculated between repeat measurements. Three measurements were taken per concentration at a measurement angle of 173°.

3.4.4 Critical concentration determination by conductivity

Conductivity measurements were performed in a double-walled glass cell (Fisher Scientific, USA) connected to an RE304 circulating water bath (Lauda, Germany) set to 25°C. The 16-3-16/pDNA complex was titrated into 30 mL Ultrapure water (re-filtered using a 0.22 µm PES syringe filter before use). The solution stirred for 5 minutes before conductivity was measured. For each concentration point, three measurements were taken by rinsing the electrode between each measurement. The average conductivity of the solution was plotted against the logarithm of the total amphiphile concentration of the solution. The data was then fit to Equation 3.4-1 following the method presented by Carpena et al.[157]:

$$\kappa = \kappa_0 + A_1 c + \Delta x (A_2 - A_1) ln\left(\frac{1+e^{(c-cmc)/\Delta x}}{1-e^{-cmc/\Delta x}}\right) \qquad \textbf{Equation 3.4-1}$$

where κ_0 is the conductivity at concentration = 0, and A_1 and A_2 are the slopes at low (pre-CAC) and high concentrations (post-CAC), respectively. Δx is a constant representing the width of the CAC transition region. The CAC was indicated by x_0.

The conductivity experiments were performed in triplicate.

3.5 Results

3.5.1 Tensiometry

As seen in Table 3.5-1 the CAC determined from surface tension studies was 4.5 ± 1.5 µM. Figure 3.5-1 shows a plot of surface tension vs. log concentration (of total amphiphile added) during titration of 16-3-16/pDNA condensates into water. There is a steep decrease in surface tension as the 16-3-16/pDNA mixture is added to water, followed by a clear breakpoint or transition region leading to a plateau where the surface tension is minimally affected by further addition of the 16-3-16/pDNA. From these plots, we are able to gather a critical concentration value, much like that of a pure surfactant sample. (Surface excess concentration and molecular area calculations from the tensiometry calculations were not attempted since the number of ionic species, n in the Gibb's equation, are unknown.)

Table 3.5-1 Average critical aggregate concentration values from triplicate measurements using each method – tensiometry, dynamic light scattering and conductometry

CAC (μM) ± SD (n = 3)	Method
4.5 ± 1.5	Tensiometry
1.7 ± 0.6	Dynamic Light Scattering
31 ± 1	Conductometry

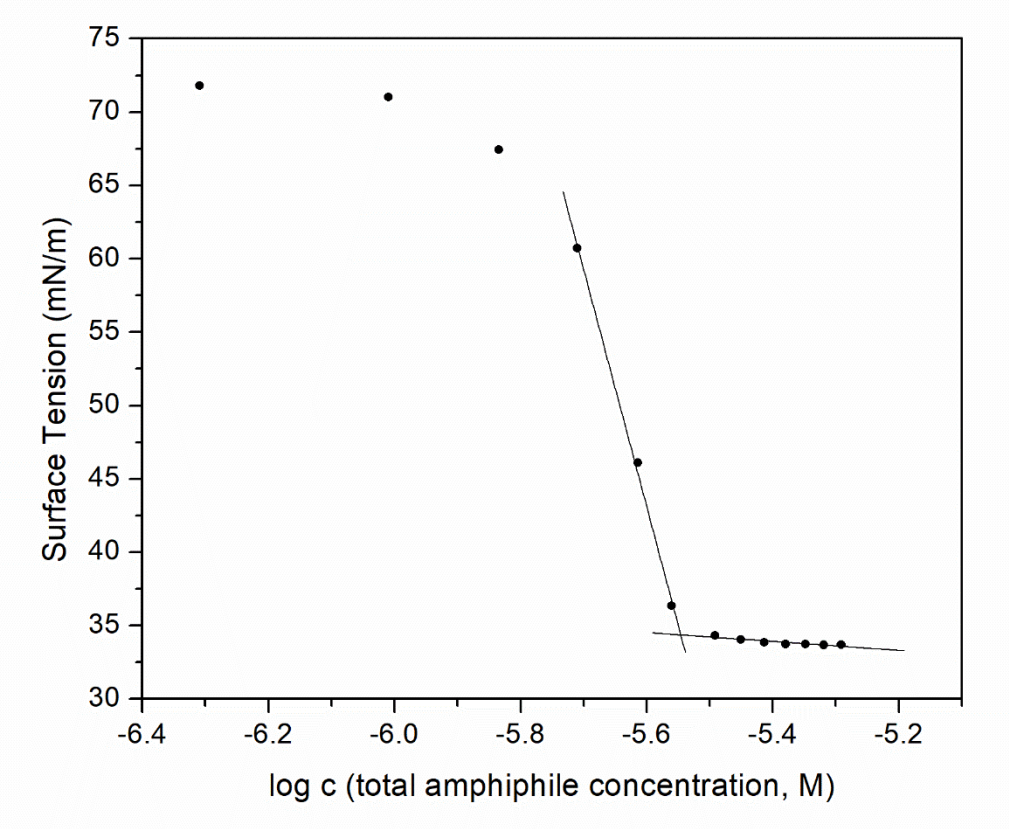

Figure 3.5-1 Surface tension vs. log 16-3-16/pDNA concentration plot

3.5.2 Dynamic Light Scattering

Likewise, in dynamic light scattering (DLS) measurements there is a sudden change (increase) in the intensity of the scattered light once the CAC is reached through titration of the condensate solution into water (Figure 3.5-2). At concentrations below the CAC the scattering intensities are approximately

constant and near that of the UltraPure water. After the CAC the intensity increases linearly with the addition of more condensate solution. Using DLS, the CAC of 16-3-16/pDNA was found at 1.7 ± 0.6 μM, which agrees well with that found through the tensiometry method.

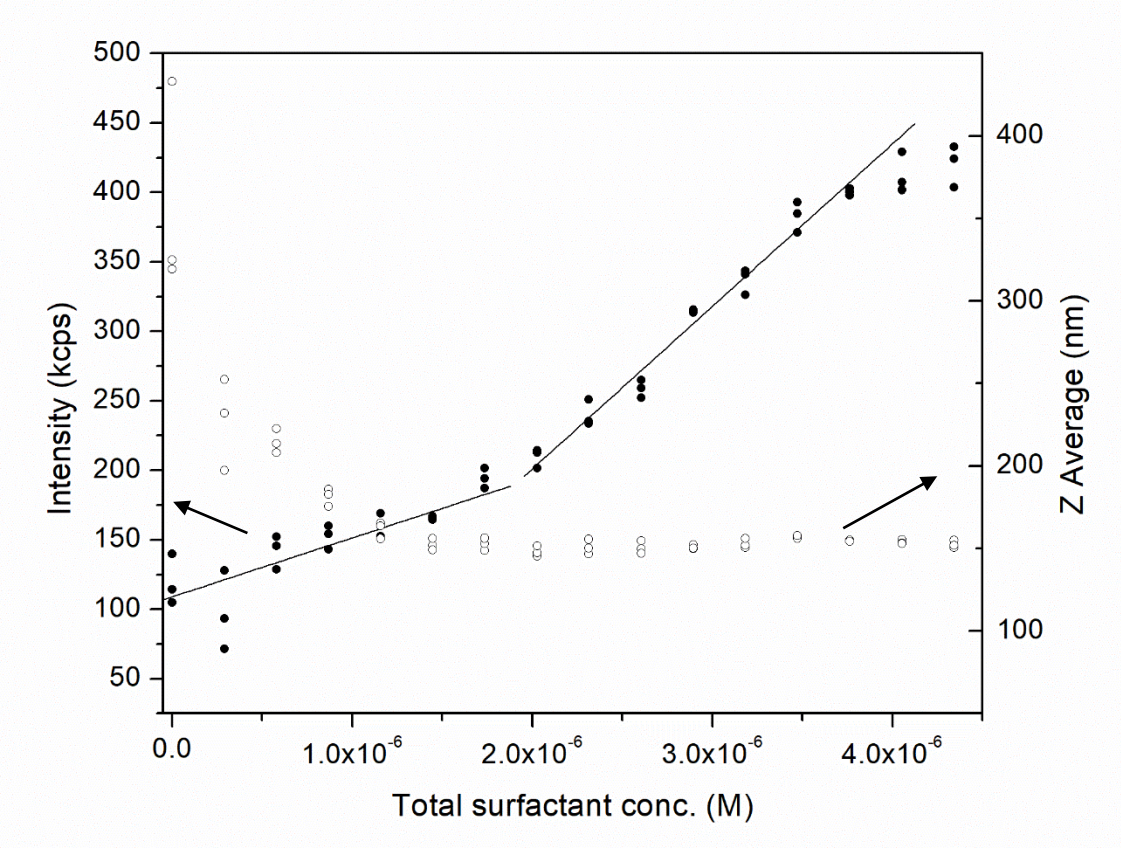

Figure 3.5-2 Scattered light intensity (left axis, ●) and Z-average hydrodynamic diameter (right axis, ○) as a function of 16-3-16/pDNA concentration.

Additionally, we see a sudden change in the hydrodynamic radius of the condensates around the CAC. Initially at low concentrations, the sizes are large and more heterogeneous (larger polydispersity index values), as seen in Figure 3.5-3. After the CAC, we see the size of the condensates is approximately 150nm, which remains constant with further addition of the condensate solution. Size measurements of the condensate stock solution reveal a hydrodynamic diameter of 150nm (data not shown).

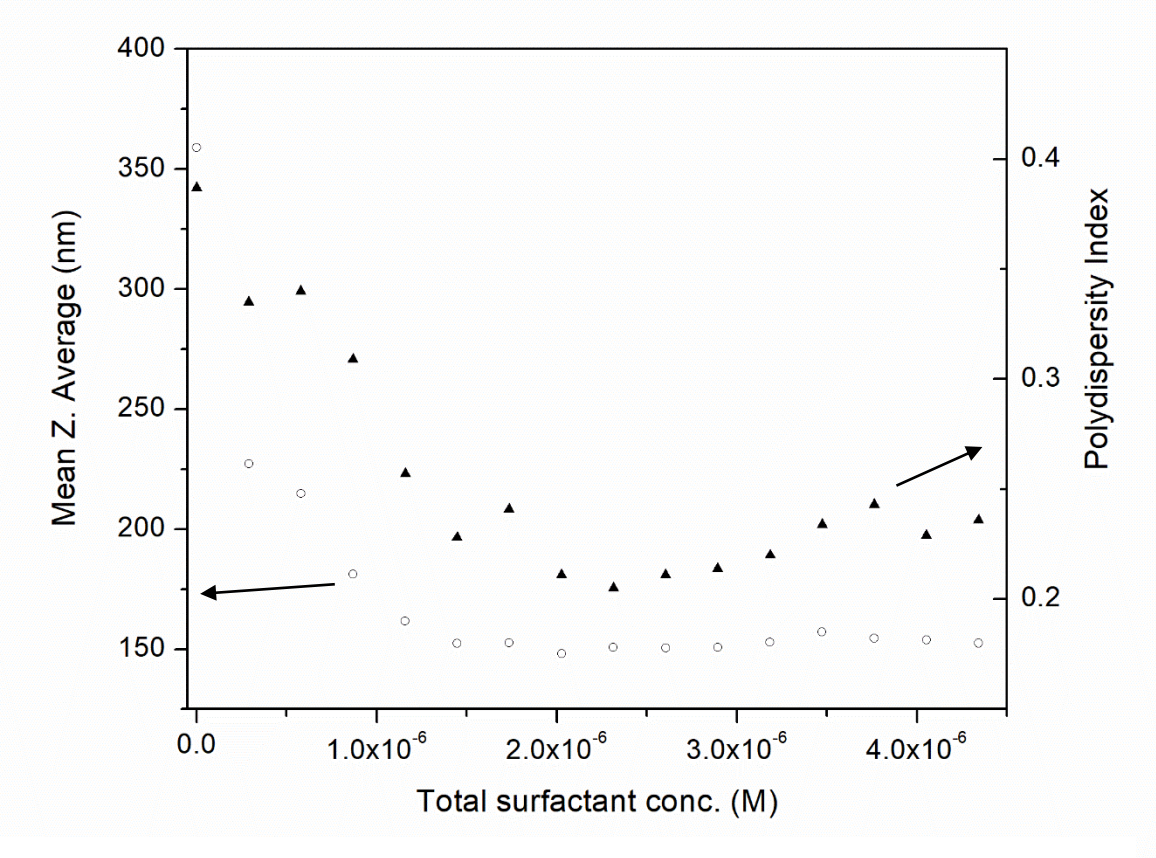

Figure 3.5-3 Mean Z-average hydrodynamic diameter (left axis, ○) and polydispersity index (right axis, ▲) throughout 16-3-16/pDNA titration into water.

The g1 correlation functions shown in Figure 3.5-4 start with an intercept of 0.35 following the first titration of the condensate solutions (red line), which trends upward approaching 1.0 with increasing concentration. At the start of titration, these correlation functions also have lower rates of decay (red, green and blue lines, corresponding to concentrations below the CAC) that increase as more 16-3-16/pDNA is added to the sample. This rate of decay is eventually unchanged by increasing concentration (black line and onward).

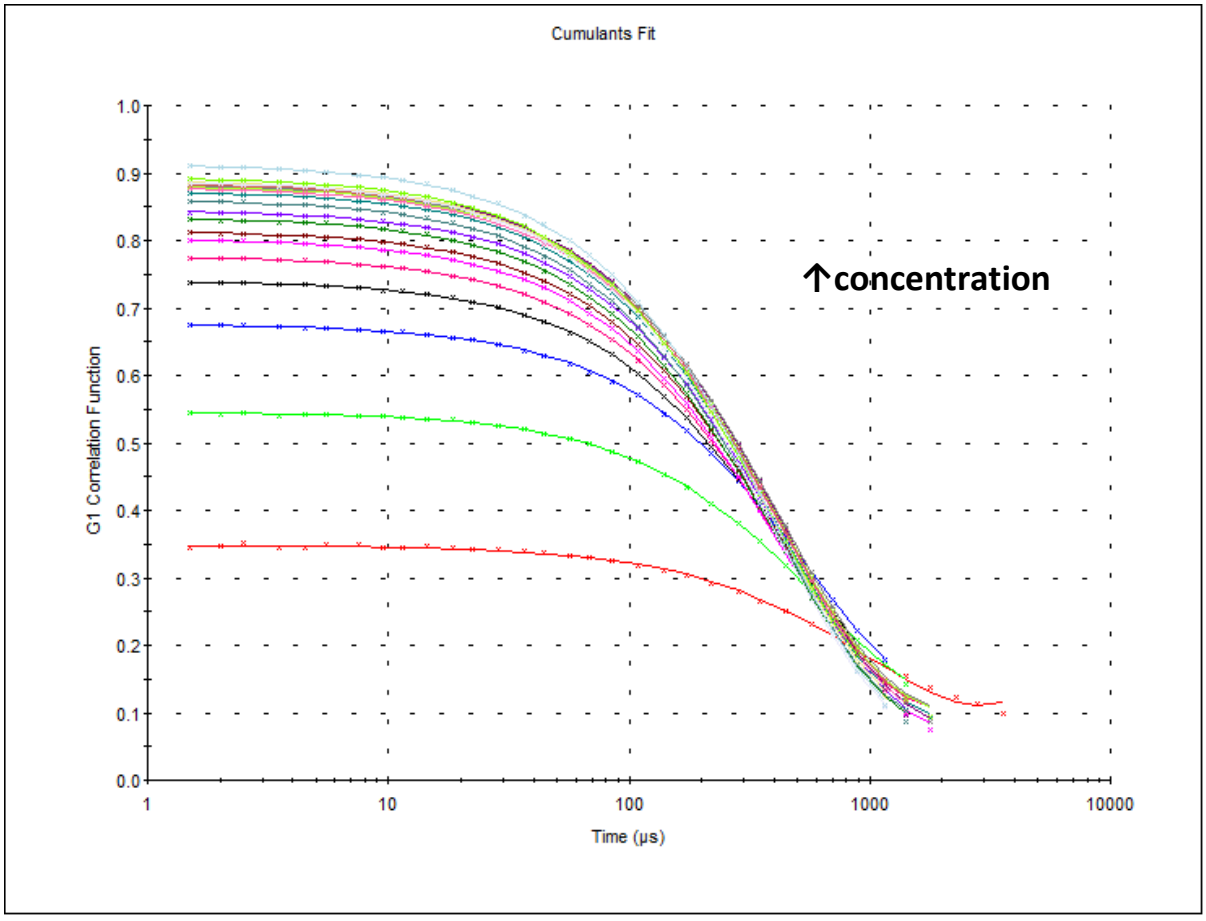

Figure 3.5-4 G1 Correlation function with increasing concentration

3.5.3 Conductometry

The titration of the 16-3-16/pDNA mixture into water results in a steady increase in the conductivity of the solution, eventually followed by a decrease in the slope of the conductivity vs. concentration curve (Figure 3.5-1). Again, the break in the conductivity plot, where the change of slope begins, represents the 16-3-16/pDNA CAC. Our conductivity studies indicate a CAC of 31 ± 1 µM.

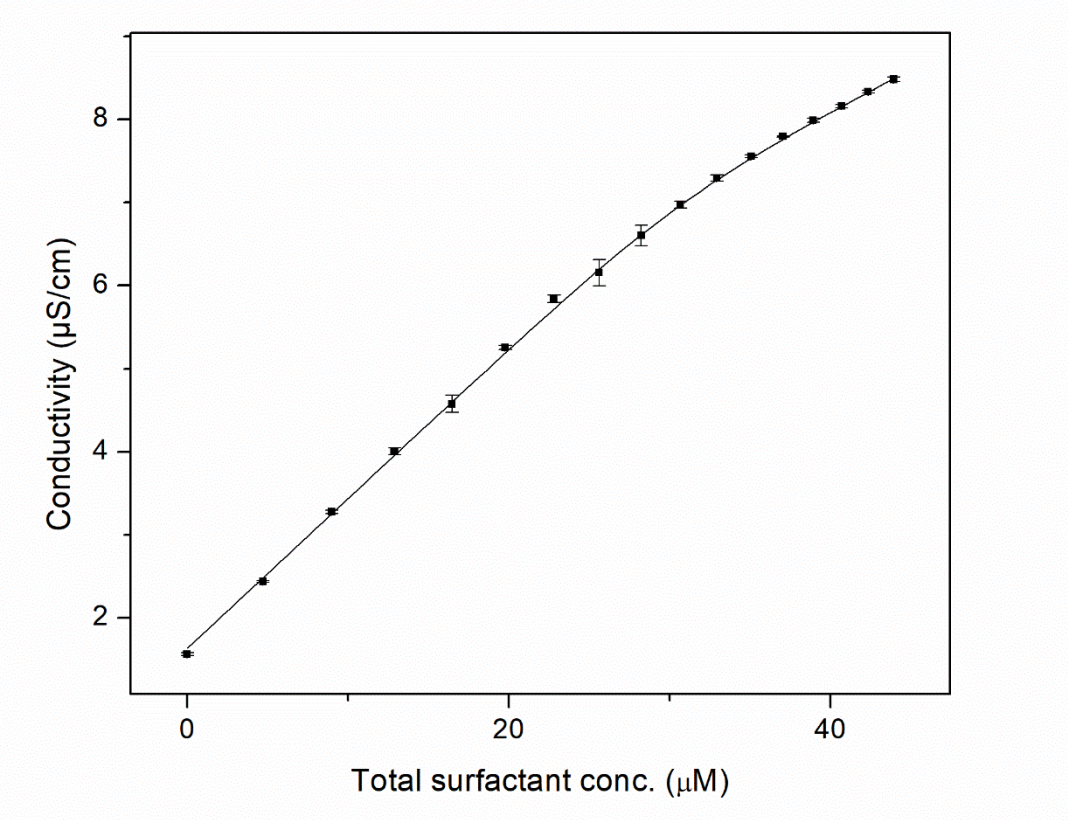

Figure 3.5-1 Conductivity as a function of 16-3-16/pDNA concentration

3.6 Discussion

CAC values from all three methods discussed here are reported in Table 3.5-1. The CACs obtained from all three methods reported here are in very good agreement. Of course, CMC or CAC values vary in numerical value depending on the method used, sometimes by an order of magnitude.[3] Even with pure surfactant systems, a precise CMC value can be somewhat arbitrary considering experimentally, micellization is observed as a transition over a concentration range.[3,158] Although the CACs determined from tensiometry and DLS are close in number, the conductivity results are within an order of magnitude and are considered to be at an acceptable level of agreement with the others.

In this study, we see typical plot shapes for each method (tensiometry, dynamic light scattering and conductometry) that would be expected in typical CMC determinations of a single amphiphile[3,157,159,160]

despite the use of surfactant/pDNA condensates. Typical CMC experiments start with a concentrated solution where the amphiphile is in micellar/aggregated form which then gets diluted to monomers upon titration into a volume of water. As more of the amphiphile is titrated in, the amphiphile monomers eventually aggregate again into micelles at a threshold concentration known as the critical micelle concentration, which is detected by a sudden physical change.

In this case, our amphiphile in question is the 16-3-16/pDNA condensate. It is unlikely that all 16-3-16 molecules completely dissociate from the plasmid DNA; however, there may be some dissociation or re-organization of the looser, hydrophobically-bound surfactant molecules (as depicted in Figure 3.6-1(A). Based on our dynamic light scattering results we expect that the condensates from our 16-3-16/pDNA stock solution become larger and have a more "relaxed" or dynamic structure upon titration into water (as suggested by the larger particle sizes at concentrations below the CAC). The g1 correlation function intercepts in Figure 3.5-4 show good signal to noise ratios (greater than 0.2)[160], which gives further confirmation that the hydrodynamic diameter measurements obtained, even at low concentrations below the CAC, correspond to the presence of aggregate structures such as surfactant-DNA condensates rather than free monomers in solution. Moreover, the slower rates of decay in the correlation functions for c < CAC indicate the presence of large particles in solution.[160,161] In this concentration range, we also see a steady increase in the conductivity of the solution (similar to typical micellization studies of a pure surfactant system). This is due to an increase in the number of charge carriers as the condensate solution is added to the sample. Again, we believe this is an indication of an initial incomplete dissociation of the condensates giving rise to some free surfactant molecules upon dilution (at the start of titration, c < CAC), which contributes to free surfactant ions (and counterions) in the bulk phase that increase the conductivity of the solution.

Once the CAC is reached, the condensates re-form into their tightly-bound state (Figure 3.6-1B) and any additional condensates added from our stock remain in their condensed form (as seen by the smaller and more uniform particle sizes at concentrations above the CAC). With increasing 16-3-16/pDNA concentration, the intercepts of the correlation functions increase, which indicates the growing presence of condensates in the solution as titration continues. The rates of decay also increase, which is consistent with a change from large, "relaxed" particles to smaller, "condensed" particles. Eventually the rates of decay remain constant near and post-CAC, perhaps confirming any additional condensates added after the CAC remain in their condensed form. (Similar trends were reported in the use of DLS for CMC

determinations of block copolymers, like that described by Topel, et al).[160] Typically, in conductivity studies of ionic surfactant micellization, addition of surfactant beyond the CMC increases the concentration of micelles which are larger and less efficient charge carriers (they diffuse through the solution slower), while the monomer concentration remains approximately unchanged. Hence, a decreased slope is observed in the conductivity vs. concentration plot. This change in slope is normally due to a decrease in either the number of or the mobility of the ions present. However, the DLS data for the 16-3-16/pDNA system does not provide evidence for the formation of larger aggregates beyond the CAC (in fact, it suggests a decrease in size, as discussed previously). Therefore, we hypothesize the trends observed through conductivity are solely due to a change in the number of free charge carriers (surfactant monomers and counterions) in solution rather than the size of the charged surfactant-DNA aggregates. When the 16-3-16/pDNA condensates reform into their condensed form at the CAC, this results in less charge carriers (surfactant ions) free in solution.

In the surface tension measurements for concentrations below the CAC, there is a steady decrease, which is due to the condensates and free surfactant molecules associating at the water surface. Above the CAC, there is no longer a change in surface tension, likely indicating the surface is saturated with condensates. Previous surface tension studies, by Zhao et al., involving the titration of gemini surfactant into a DNA solution, reported increased surface tensions compared to the pure surfactant and suggest this is due to the formation of surface-inactive complexes in the bulk phase.[138] However, our results clearly show the surfactant-pDNA complex is in fact surface-active. Furthermore, the condensates reduce the surface tension of water to a greater extent than the 16-3-16 surfactant alone[158], indicating synergism between the two components.[138,162] So, our observations are more consistent with those reported by Vongsetskul et al., who acknowledged decreases in surface tension for 12-6-12/DNA mixtures began at much lower concentrations than in the pure surfactant system.[150] In the same report, neutron reflectometry studies showed the presence of DNA enhanced the surface adsorption of the 12-6-12 surfactant and with higher concentrations of surfactant, thick structured layers were formed (which are thicker than the gemini surfactant monolayer on its own).[150] However, it should be noted that these earlier reports[150] (and others[88,113,114]) involve a fixed concentration of DNA with increasing concentration of surfactant, rather than titration of a pre-formed mixture into water like we have here.

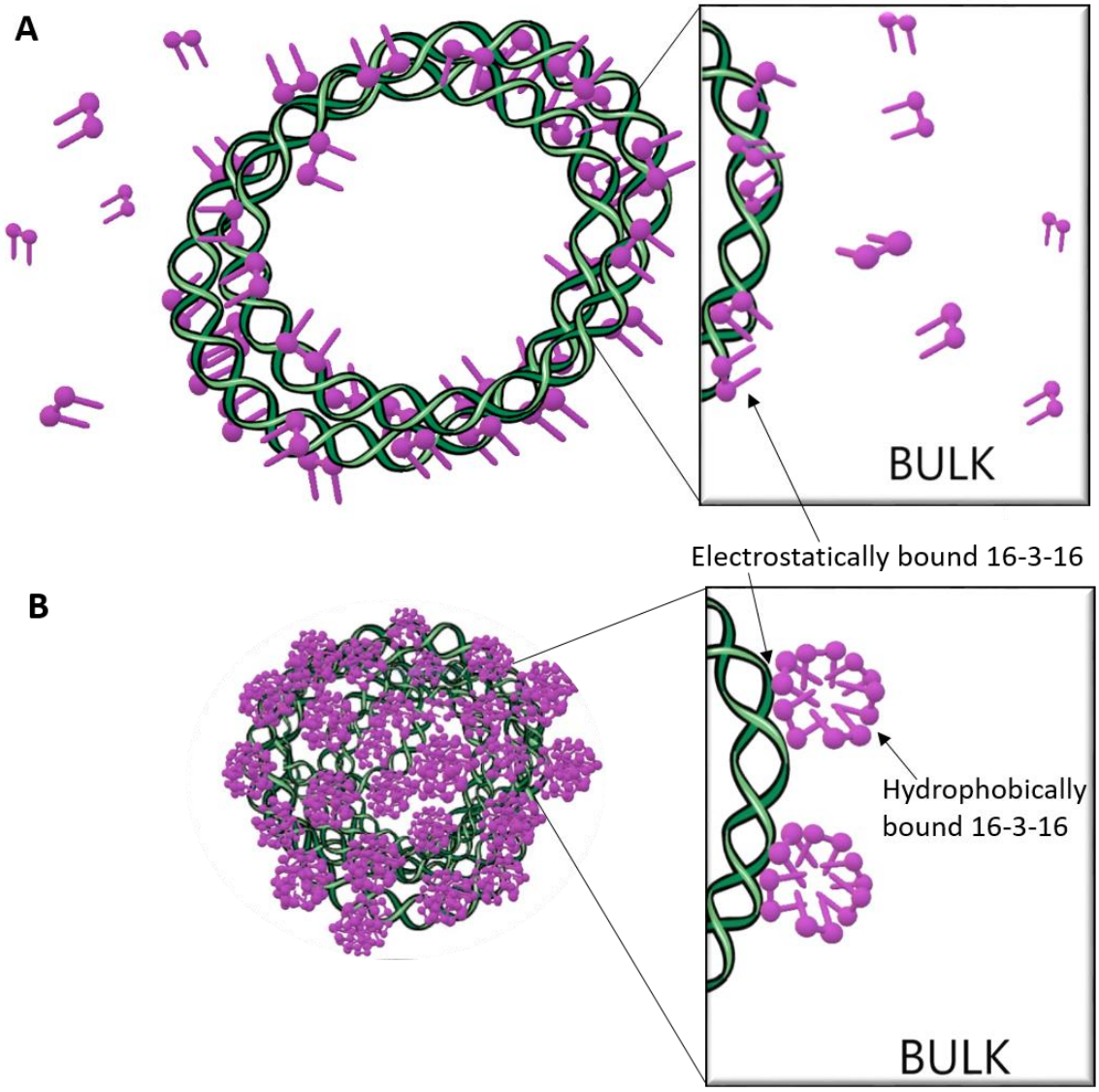

Figure 3.6-1 (A) "relaxed" condensate due to dilution (c < CAC). (B) Condensate at c ≥ CAC.

3.7 Conclusion

We propose that the pre-formed surfactant/pDNA condensates do not completely break up into their monomers upon dilution; rather, they become less compact below a threshold concentration (the CAC) determined here, and eventually re-form into their condensed state post-CAC. Despite this atypical behavior during titration of these condensates into water, significant changes in the physicochemical properties (surface tension, light scattering, and conductivity) of the solution occur at a critical

aggregate concentration - analogous to a single surfactant system. This proposed behavior of the condensates in solution may have valuable implications for the use of gemini surfactant-condensed DNA for applications such as gene therapy where there is a requirement for the DNA to remain condensed for part of the journey (followed by de-condensation later on for transcription to occur). This knowledge might also contribute to many other fields and applications, including: i) DNA purification methods where CTAB is often used for precipitation and other cationic surfactants are currently under investigated for selective precipitation of various isoforms of plasmid DNA[118,165]; ii) synthesis of functionalized DNA molecules, for example DNA-lipid conjugates, where the DNA-surfactant complex overcomes differences in solubility between the hydrophilic DNA and the hydrophobic moiety; iii) DNA-surfactant complex-based vehicles or depots for small molecule therapeutics such as chemotherapy or antimicrobial drugs that interact with DNA.[119]

Chapter 4
Mixing Behaviour of Pluronics with Gemini Surfactant/plasmid DNA Condensates: Effect of Pluronic Composition

This chapter is adapted from [166] with permission from the PCCP Owner Societies.

4.1 Abstract

Nanoparticles prepared from plasmid DNA (pDNA) and *N,N*-bis(dimethylhexadecyl)-1,3-propanediammonium bromide (16-3-16) have been mixed with various Pluronic block copolymers and investigated as binary surfactant systems in water using the previously demonstrated critical aggregate concentration of the surfactant-DNA complex. Surface tensiometry was used to determine critical micelle concentrations of mixed micelle formation within these Pluronic/16-3-16/pDNA mixtures. Use of mixed micelle theories reveal mixed micelle composition and the interaction parameter, β, are influenced by the structure, in particular hydrophobicity, of the Pluronic component. Ethidium bromide fluorescence studies demonstrate the ability of the Pluronics to de-condense the plasmid DNA from the cationic 16-3-16 gemini surfactant complex, and shows some relationship to the interaction parameter and Pluronic composition.

4.2 Introduction

Among the potential uses for dimeric surfactants (also known as gemini surfactants) throughout various fields, a significant one is their applicability in non-viral gene therapy formulations. Cationic gemini surfactants can be used to complex and condense nucleic acid cargo and, combined with other formulation components such as lipids or polymers, can achieve more favourable properties for successful delivery to cells. The reader is referred to the following publications and reviews of various in vitro and in vivo transfection studies utilizing gemini surfactant-based vehicles.[54,62,64,69,167–172]

Gemini surfactants have the structure of two amphiphilic monomers covalently linked at or near their polar head group by a spacer.[173] A commonly studied series of gemini surfactants is the *N,N'*-bis(dimethylalkyl)-alkane-diammonium dibromide series, or "*m-s-m*" type, where the *m* in this notation refers to the number of carbon atoms in the symmetric alkyl tails, while *s* refers to the number of atoms making up the spacer that connects two quaternary ammonium head groups.[174,175]

A popular additive in gene therapy formulations are the neutral block copolymers known as Pluronics (BASF Corp.), or under the non-proprietary name "poloxamers", which have been known to improve transfection efficiency in numerous gene delivery systems.[76] These polymers have amphiphilic/surface active properties themselves, owing to their general structure of a hydrophobic polypropylene oxide (PPO) block flanked by two hydrophilic polyethylene oxide (PEO) chains, PEO_x– PPO_y – PEO_x. Pluronic unimers adsorb to the air-water interface through the PPO block with the PEO chains extending into the aqueous solution.[75] Micelles are then formed with polymer concentrations beyond the critical micelle concentration (CMC), that consist of a hydrophilic PEO outer shell or corona and a weakly hydrated hydrophobic PPO core that can solubilize hydrophobic compounds.[76,128] The number of EO (ethylene oxide) and PO (propylene oxide) units, represented by *x* and *y*, respectively, can be varied to form a family of Pluronics with different molecular weights and water-solubility.

A system combining cationic gemini surfactant and Pluronic holds potential for a gene therapy formulation where (sufficient excess of) the gemini surfactant component condenses the nucleic acid cargo and provides a positive charge for colloidal stability as well as interaction with biological membranes. Meanwhile, the Pluronic component has the potential to increase internalization of the cargo and intracellular trafficking as a biological response modifier.[176] In vivo, the PEO corona of Pluronic micelles also helps to reduce non-specific interactions with blood components and clearance from the circulation by the immune system.[177]

The interactions between some gemini surfactants and Pluronic block copolymers in solution have been the subject of a number of studies reported in the literature. Early studies by Wettig and Verrall demonstrated a decrease in micelle polarity which suggested that the polymers interact at the palisade layer of the surfactant micelle, resulting in the replacement of hydration water by the polymer, and resulting in a release of counterions (supporting the increased specific conductance reported).[133] Furthermore, the surfactant headgroup size had little effect on the interactions in this case; however, the greatest interaction was observed for the most hydrophobic of the Pluronics (P103) in the study.[133] Bakshi et al. found unfavourable mixing behaviours between m-2-m (m = 12, 14, 16) gemini surfactants and Pluronic block copolymers of varying PEO/PPO ratio, which produced Pluronic-rich mixed micelles; however, antagonism was reduced with increased hydrophobicity of the gemini component.[129] In another study, the same group identified synergism within the binary mixtures of L64 with 10-2-10, 12-2-12, or 14-2-14 cationic gemini surfactants.[132] Again, synergism increased with an increase in the

surfactant hydrophobicity (alkyl tail length) and this favourable mixing was attributed to 1) greater hydrophobic effects due to increased hydrophobicity and 2) neutralization of the electrostatic repulsion between gemini headgroups by intercalation of the L64 PEO chains in the mixed micelles.[132] Increases in temperature have also been shown to increase synergism owing to dehydration of the PPO block which in turn enhances the hydrophobic interaction between Pluronics and gemini surfactants.[110] No significant differences in micropolarity and aggregation number among the F127 and P103 systems were observed due to the mixed micelles being relatively rich in the cationic surfactant component (and poor in Pluronic), and temperature having little effect on the electrostatic interactions.[110] More recently, Wang et al., exploited the critical micelle temperatures (CMT) of Pluronics F127 and P123 to differentiate between the interaction of copolymer monomers, micelles, or monomer and micelle mixtures with the cationic ammonium 12-6-12 surfactant.[131] Below the Pluronic CMT, 12-6-12 binds to single copolymer unimers and initiates micelle formation similar to conventional single-chain ionic surfactant/copolymer systems; meanwhile, above the CMT 12-6-12 binding to the Pluronic micelles forms mixed micelles of smaller size due to an equilibrium of the hydrophobic interactions between the two components and electrostatic repulsion between the gemini surfactant headgroups.[131] At the copolymer CMT, where both Pluronic unimers and micelles are present, addition of 12-6-12 leads to mixed 12-6-12/Pluronic micelle formation.[131] Further addition of 12-6-16 eventually breaks down the mixed micelles into smaller 12-6-12-rich mixed micelles and releases Pluronic unimers. 12-6-12 binds the free unimers until saturation, then free 12-6-12 micelles are formed.[131]

Given the interest in using these systems for gene therapy applications, here we report on the interactions of the 16-3-16 gemini surfactant with various Pluronic polymers in the presence of plasmid DNA (pDNA). It was recently demonstrated that the pre-formed complex of plasmid DNA condensed by the 16-3-16 gemini surfactant at a charge ratio of 10:1 (N^+/P^-) can be considered as a single amphiphile with its own critical aggregate concentration.[136] This assumption was then used to investigate the interaction of the 16-3-16/pDNA condensate with six different Pluronic block copolymers (F87, P84, L121, F127, P103, and L44) as binary systems using Clint's, Rubingh's, Motomura's, and Maeda's mixed micelle theories. As seen in the literature, Pluronic micellization and interactions with ionic surfactants can be influenced by the composition of the Pluronic component. Therefore, the interactions reported here were assessed based on the Pluronic propylene oxide (PO) and ethylene oxide (EO) content.

For the purpose of gene therapy, de-condensation of DNA from its cationic surfactant complex by the addition of salts, anionic or neutral surfactants is also an important consideration, especially with the addition of such materials to the delivery formulation. He et al. reported that DNA compaction by the 12-3-12·2Br gemini surfactant can be reversed by sufficient addition of Pluronic P123. This de-condensation is attributed to a disruption of the equilibrium between DNA-associated surfactant aggregates and free surfactants in the bulk phase due to hydrophobic interaction of the block copolymer with the free gemini surfactants.[127] Therefore, de-condensation of pDNA from the 16-3-16/pDNA complex upon the addition of Pluronic at fixed mole fractions was also included in an effort to further understand the mixed systems.

4.3 Materials

The Pluronic® block copolymers (F87, P84, L121, F127, P103, and L44) were provided as samples from BASF Corp. The 16-3-16 gemini surfactant was synthesized in the Wettig lab as described previously.[154,155] The pVG.telRL plasmid[156], was extracted from DH5α cells (provided as a gift from Dr. Roderick Slavcev, School of Pharmacy, University of Waterloo, Canada) using an E.Z.N.A. Plasmid DNA Maxi Kit (Omega Bio-tek) and HyPure Molecular Biology Grade Water (HyClone) for elution. Ultrapure MilliQ water (Millipore) was used for all sample preparations and experiments. Plasmid DNA concentrations and purity were measured by UV-Visible light absorbance at 260 nm, and the 260 nm/280 nm absorbance ratio using a Thermo Scientific NanoDrop 2000 spectrophotometer. Restriction enzyme digestion with HindIII and fragment separation by gel electrophoresis confirmed isolation of the pVG.telRL plasmid. The average molecular weight, composition and CMC of each Pluronic used in this study are listed in Table 4.3-1.

Table 4.3-1 Properties of Pluronic block copolymers used in this study

Pluronic	Average number of EO units[a]	Average number of PO units[a]	Average MW[b]	HLB	PO/EO wt. ratio	Approximate EO content (% wt.)	CMC (M)[c]
F87	122	40	7700	24	0.43	70	9.1×10^{-5}
P84	38	43	4200	14	1.5	40	7.1×10^{-5}
L121	10	68	4400	1	9.0	10	1.0×10^{-6}
F127	200	65	12600	22	0.43	70	2.8×10^{-6}
P103	34	60	4950	9	2.3	30	6.1×10^{-6}
L44	20	23	2200	16	1.5	40	3.6×10^{-3}

[a]Average number of EO and PO units calculated from the average molecular weights, as reported in [178], rounded to the nearest whole unit
[b]Average molecular weight (MW) provided by the manufacturer (BASF, Corp.)
[c]CMCs reported in [178], determined by the pyrene solubilisation technique

4.4 Methods

4.4.1 16-3-16/pDNA complex preparation

16-3-16/pDNA complexes prepared for CMC determination of the complex (without Pluronic) consisted of a 0.1 mM 16-3-16 aqueous solution mixed with pDNA (eluted in water) at a charge ratio of 10:1 (N^+/P^-). These 2 components were allowed to incubate for 15 minutes in a water bath set to 25°C (Isotemp GPD 10, Fisher Scientific). The 16-3-16 solution was filtered using a 0.22 µm PES syringe filter (Sartorius) before use.

4.4.2 Pluronic/16-3-16/pDNA complex preparation

The 16-3-16 stock solution, Pluronic stock solution, and water were first filtered through a 0.22 µm PES syringe filter (Sartorius) prior to use in preparation of the complexes. The pDNA and 16-3-16 components (along with an appropriate volume of water) were first mixed and allowed to incubate for 15 minutes in a 25°C water bath (Isotemp GPD 10, Fisher Scientific). The appropriate Pluronic was

then added to the 16-3-16/pDNA complex and allowed to incubate for 30 minutes in the 25°C water bath.

Pluronic/16-3-16/pDNA mixtures were prepared with 0.1 mM 16-3-16 and Pluronic stocks with concentrations equal to approximately 35 times the Pluronic CMC (with the exception of the L44 stock which was approximately 6 times the L44 CMC, see Table 4.3-1). Mixtures containing varying mole fractions ($\alpha_{Pluronic}$) of the Pluronic component were prepared while maintaining a total surfactant concentration of 8×10^{-6} M (using an appropriate amount of ultrapure water). For example, for a α_{F87} = 0.4 mixture, 1.7×10^{-7} moles 16-3-16 and 1.1×10^{-7} moles F87 were used, whereas for α_{F87} = 0.8, 5.6×10^{-8} moles 16-3-16 and 2.2×10^{-7} moles F87 were used. In each case, an appropriate amount of pDNA was added to provide a charge ratio of 10:1 (N^+/P^-), and an appropriate volume of ultrapure water was added to maintain a constant volume and total concentration. Although the moles of pDNA was also considered in the total moles of amphiphile during concentration calculations, it did not largely contribute to these values as most samples ranged from 10^{-14} – 10^{-12} moles of plasmid.

The F87/16-3-16/pDNA mixture was also prepared at a F87 mole fraction of 0.4 with a 16-3-16/pDNA charge ratio of 5:1 to briefly demonstrate the effect of pDNA content on the resulting interaction parameter.

4.4.3 CMC determination by Tensiometry

Surface tension measurements for the F87, F127, P103, and L44 systems were performed using the du Noüy ring method with a Lauda TE3 automated Tensiometer (Lauda, Germany). Temperature was maintained at 25°C (± 0.05°C) using an RE304 circulating water bath (Lauda, Germany) connected to the tensiometer. The ring was thoroughly cleaned with methanol and water then flame dried until glowing red before each experiment. A minimum of three successive measurements were performed per concentration until a maximum standard deviation of 0.1 mN/m was reached. Each surface tension value was corrected using the Harkins-Jordan correction factor.[179] Surface tension measurements for the P84 and L121 systems were performed at room temperature using the Wilhelmy plate method with a KSV NIMA surface tension balance (KSV NIMA/Biolin Scientific, Finland). The plate was thoroughly cleaned using ethanol and water and flame-dried until it was glowing red before each experiment. In all cases, the 16-3-16/pDNA or Pluronic/16-3-16/pDNA complex was titrated into 60 mL of Ultrapure MilliQ water (refiltered using a 0.22 μm PES syringe filter before use). The solution was allowed to equilibrate (with magnetic stirring) for 5 minutes before measurement.

All CMC measurements were carried out in triplicate. In each CMC experiment, the surface tension was plotted against the logarithm of the total amphiphile concentration (moles of 16-3-16 + moles of pDNA + moles of Pluronic per liter). The point of intersection of the linear trendlines before and after the first breakpoint in these plots was recorded as the critical micelle concentration of the mixture.

CMC values were also determined for the 16-3-16/pDNA complex and Pluronic alone and conducted in the same manner. Investigation of the individual components used 1% F87, 0.0077% L121, 8% P84, 1% F127, 0.01% P103, 5% and 10% L44 stock solutions, and the 16-3-16/pDNA 10:1 complex prepared as previously described. All solutions were used at room temperature during preparation and surface tension titration experiments with the exception of L121 solutions which were kept on ice due to the low cloud point.

4.4.4 DNA-Ethidium Bromide Fluorescence

Fluorescence was detected at 595 nm with an excitation wavelength of 535 nm using a SpectraMax M5 Multi-Mode Microplate Reader (Molecular Devices, California, USA). A 10 mg/mL ethidium bromide (EtBr) solution (Sigma-Aldrich) was diluted to 0.1 mg/mL and added to a 24-well plate (Sigma-Aldrich) in volumes appropriate for a 1:4 molar ratio of pDNA:EtBr. Each well contained a total volume of 0.5 mL and a final amphiphile (16-3-16 + Pluronic) concentration of 5×10^{-4} M, therefore, an appropriate volume of ultrapure water was added to keep volume and concentration consistent across all wells. Fluorescence from wells containing EtBr + pDNA + water was used as I_0. An appropriate volume of 1 mM aqueous 16-3-16 solution was added to achieve a charge ratio of 10:1 (N^+/P^-) between 16-3-16 and pDNA. The plates were incubated for 15 minutes at room temperature protected from light, followed by measurement of fluorescence (giving I_1). The Pluronic component was then added at desired mole fractions, followed by 30-minute incubation at room temperature in dark conditions and subsequent fluorescence reading (I_2). Plates containing L121 were incubated at 4°C only after addition of the Pluronic to avoid phase separation of L121. Each experiment was carried out in triplicate.

I_2/I_0 was normalized by first subtracting I_1/I_0 to account for remaining fluorescence after gemini surfactant condensation of the DNA.

4.4.5 Transmission Electron Microscopy

Mixtures were prepared as previously described, at a N+/P- charge ratio of 10:1 and a final amphiphile concentration of 5×10^{-4} M using a 1 mM 16-3-16 stock solution. A 10 µL aliquot of sample was added

to the centre of a carbon coated 300 mesh copper grid and incubated for 15 seconds before the liquid was removed by blotting with filter paper. The sample was then stained with 10 μL of 1% (w/v) phosphotungstic acid for 20 seconds, followed by blotting with filter paper to remove excess liquid. Prepared grids were air dried overnight and examined with a Philips CM10 transmission electron microscope (TEM) in the Department of Biology, University of Waterloo.

4.4.6 Statistical Analysis

All statistical analysis was performed using R Studio software. A multiple linear regression analysis was used to determine the effect and statistical significance of each of the main independent variables on the β interaction parameter value (namely number of PO units, number of EO units, and mole fraction). Given the small sample size, two-factor interaction terms were excluded from the regression model in order to avoid over-fitting the data. Values of $p < 0.05$ were considered statistically significant. The linear model was checked for conditional homoscedasticity, normality of residuals and multicollinearity.

4.5 Results

4.5.1 F87/16-3-16/pDNA systems

Sample plots of surface tension as a function of log concentration of F87/16-3-16/pDNA mixtures (with varying mole fractions, α, of F87) are shown in Figure 4.5-1. As concentration increases, each plot shows a steep decrease in surface tension followed by a plateau or change in the plot's slope. For some samples, this transition is abrupt and there is a clear breakpoint (e.g. the 16-3-16/pDNA complex without Pluronic, $\alpha = 0$) and for others the transition is more gradual and occurs over a small concentration range (e.g. $\alpha = 0.4$). The intersection of the slopes of the pre- and post-breakpoint regions are used to determine the critical micelle concentration of each, which is reported in Table 4.3-1 as CMC_{exp}.

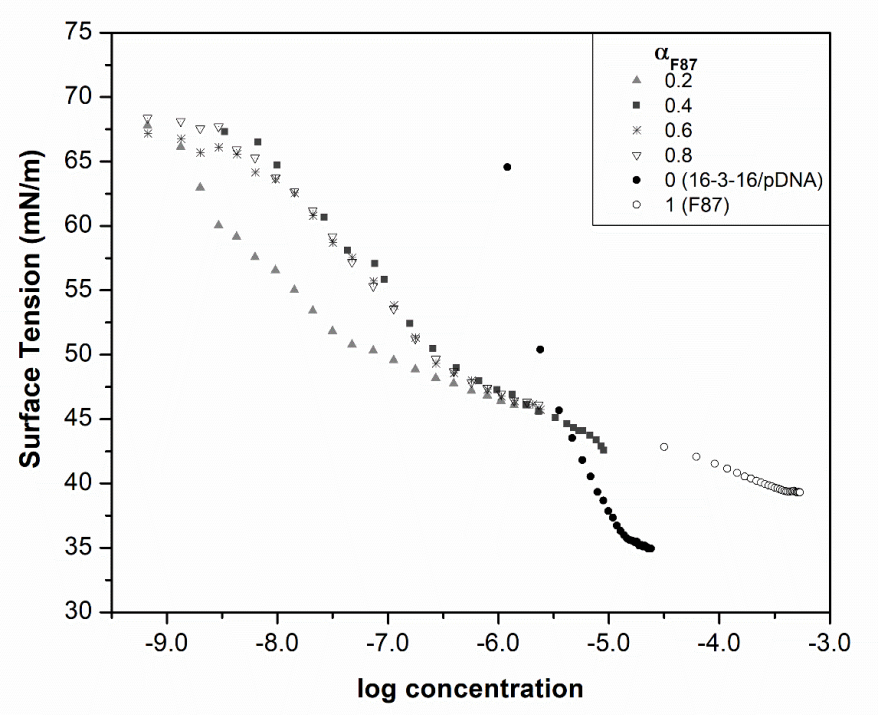

Figure 4.5-1 Plots of surface tension versus total amphiphile for F87/16-3-16/pDNA mixtures with varying mole fractions of F87. α = 1, and α = 0 represent pure F87 and 16-3-16/pDNA solutions, respectively.

Table 4.5-1 Average critical micelle concentrations ($CMC_{exp.}$) determined by tensiometry, and corresponding calculated parameters (CMC_{ideal}, X_{ideal}, X_1, β, f_1, f_2, ΔG_{ex}) for mixtures of Pluronic with 16-3-16/pDNA condensates at varying mole fractions of the Pluronic component.

System	Mole fraction Pluronic ($\alpha_{Pluronic}$)	CMC_{exp} ($\times 10^{-6}$ M)	CMC_{ideal} ($\times 10^{-6}$ M)	X_{ideal}	X_1	β	f_1	f_2	ΔG_{ex} (kJ/mol)
F87	0	14.5 ± 1.16	-	-	-	-	-	-	-
	0.2	0.83 ± 0.14	17.9	0.009	0.382	-17.8	1.11×10^{-3}	0.074	-10.4
	0.4	0.58 ± 0.10	23.6	0.024	0.412	-18.9	1.44×10^{-3}	0.041	-11.3
	0.6	0.61 ± 0.12	34.3	0.053	0.431	-18.9	2.18×10^{-3}	0.030	-11.5
	0.8	0.53 ± 0.15	63.1	0.129	0.458	-20.6	2.35×10^{-3}	0.013	-12.7
	1	391 ± 96.7	-	-	-	-	-	-	-
P84	0	4.47 ± 1.45	-	-	-	-	-	-	-
	0.2	0.43 ± 0.05	5.57	0.002	0.345	-18.1	4.34×10^{-4}	0.116	-10.1
	0.4	0.28 ± 0.10	7.41	0.005	0.378	-19.5	5.30×10^{-4}	0.061	-11.4
	0.6	0.17 ± 0.06	11.0	0.012	0.408	-22.1	4.38×10^{-4}	0.025	-13.2
	0.8	0.20 ± 0.03	21.7	0.031	0.429	-22.4	6.71×10^{-4}	0.016	-13.6
	1	567 ± 71.9	-	-	-	-	-	-	-
L121	0	4.47 ± 1.45	-	-	-	-	-	-	-
	0.2	1.56 ± 0.11	1.29	0.769	0.921	1.48	1.01	3.52	0.268
	0.4	0.50 ± 0.16	0.752	0.899	0.729	-2.61	0.826	0.250	-1.28
	0.6	0.29 ± 0.02	0.531	0.952	0.725	-4.52	0.710	0.093	-2.23
	0.8	0.08 ± 0.05	0.411	0.982	0.657	-10.6	0.289	0.010	-5.90
	1	0.34 ± 0.10	-	-	-	-	-	-	-
F127	0	14.5 ± 1.16	-	-	-	-	-	-	-
	0.2	1.81 ± 0.18	6.74	0.628	0.535	-5.37	0.314	0.215	-3.31
	0.4	1.41 ± 0.34	4.39	0.818	0.603	-5.28	0.435	0.147	-3.13
	0.6	0.81 ± 0.12	3.26	0.910	0.625	-7.21	0.363	0.060	-4.18
	0.8	0.76 ± 0.22	2.59	0.964	0.667	-7.77	0.423	0.031	-4.28
	1	2.15 ± 1.17	-	-	-	-	-	-	-
P103	0	14.5 ± 1.16	-	-	-	-	-	-	-
	0.2	0.65 ± 0.07	0.815	0.955	0.819	-2.42	0.924	0.198	-0.886
	0.4	0.33 ± 0.04	0.420	0.983	0.845	-3.40	0.921	0.089	-1.10
	0.6	0.27 ± 0.01	0.282	0.992	0.962	-1.75	0.997	0.199	-0.158
	0.8	0.17 ± 0.01	0.213	0.997	0.873	-5.22	0.920	0.019	-1.43
	1	0.17 ± 0.02	-	-	-	-	-	-	-
L44	0	14.5 ± 1.16	-	-	-	-	-	-	-
	0.2	0.34 ± 0.04	18.1	0.002	0.384	-24.2	1.01×10^{-4}	0.028	-14.2
	0.4	0.32 ± 0.04	24.0	0.006	0.399	-23.3	2.22×10^{-4}	0.024	-13.8
	0.6	0.31 ± 0.03	35.7	0.013	0.417	-24.0	2.92×10^{-4}	0.015	-14.4
	0.8	0.17 ± 0.00	69.9	0.035	0.444	-27.7	1.90×10^{-4}	0.004	-17.0
	1	1604.8 ± 194.3	-	-	-	-	-	-	-

Clint's model for ideal mixed micellar systems (Equation 4.5-1) is used to calculate the ideal CMC values of the mixtures (CMC_{ideal}), which are reported in Table 4.5-1. CMC_{ideal} assumes there is no net interaction between the two amphiphiles comprising the micelle/aggregate (i.e. ideal mixing) and its value is an intermediate between the CMC values of the pure components.

$$\frac{1}{CMC_{ideal}} = \frac{\alpha_1}{CMC_1} + \frac{(1-\alpha_1)}{CMC_2} \qquad \textbf{Equation 4.5-1}$$

Here, α_1 is the mole fraction of the Pluronic component in the total amphiphile mixture (bulk), and CMC_1 and CMC_2 are the CMC values of the pure Pluronic and pure 16-3-16/pDNA (10:1) condensate, respectively.

The deviation of $CMC_{exp.}$ from the ideal values can be further characterized using Rubingh's model, based on the regular solution approximation, (Equation 4.5-2) to determine the interaction parameter, β.

$$\beta = \frac{\ln\left(\frac{CMC_{exp.}\alpha_1}{CMC_1 X_1}\right)}{(1-X_1)^2} = \frac{\ln\left(\frac{CMC_{exp.}\alpha_2}{CMC_2 X_2}\right)}{(1-X_2)^2} \qquad \textbf{Equation 4.5-2}$$

X_1 and X_2 reflect the composition of the mixed micelle phase, representing the mole fractions of amphiphile 1 (in this case, Pluronic) and amphiphile 2 (16-3-16/pDNA condensate), respectively, in the mixed micelle. X_1 is calculated by an iterative process from Equation 4.5-3.

$$\frac{(X_1)^2 ln\left(\frac{CMC_{exp.}\alpha_1}{CMC_1 X_1}\right)}{(1-X_1)^2 ln\left[\frac{CMC_{exp.}(1-\alpha_1)}{CMC_2(1-X_1)}\right]} = 1 \qquad \textbf{Equation 4.5-3}$$

X_1 can then be compared to the micelle mole fraction of Pluronic for the ideal state (X_{ideal}), which is calculated using Motomura's equation (Equation 4.5-4).

$$X_{ideal} = \frac{(\alpha_1 CMC_2)}{[\alpha_1 CMC_2 + (1-\alpha_1) CMC_1]} \qquad \textbf{Equation 4.5-4}$$

The β and X_1 values then allow for the calculation of the activity coefficients of the Pluronic component (f_1) and the 16-3-16/pDNA component (f_2), as seen in Equation 4.5-5 and Equation 4.5-6, which indicate the contribution of each component in the mixed micelle.

$$ln f_1 = \beta(1 - X_1)^2 \qquad \textbf{Equation 4.5-5}$$

$$lnf_2 = \beta(X_1)^2 \qquad \textbf{Equation 4.5-6}$$

The excess free energy of micellization can be calculated using the activity coefficient for each component, as seen in Equation 4.5-7.

$$\Delta G_{ex} = RT[X_1 lnf_1 + (1 - X_1) lnf_2] \qquad \textbf{Equation 4.5-7}$$

For each mole fraction tested, the $CMC_{exp.}$ of the F87 mixtures are lower than the individual components (F87α=1, and α=0), and lower than the corresponding CMC_{ideal} (Table 4.5-1 and Figure 4.5-2A). Therefore, there is a net interaction between F87 and the pre-formed 16-3-16/pDNA condensate, which is synergistic in nature. The mixed micelle composition, X_1, remains relatively constant (0.38 – 0.46) throughout the range of F87 mole fractions (Table 4.5-1 and Figure 4.5-3A), suggesting the mixed micelle compositions are minimally influenced by the bulk solution composition. Comparing X_1 to X_{ideal}, there is a positive deviation from the ideal state, which indicates the mixed micelles are enriched in the F87 component and poorer in the 16-3-16/pDNA. The interaction parameters of all F87 mixtures are negative with large magnitudes (-17.8 to -20.6), indicating strong synergism in all cases (Table 4.5-1). The calculated synergistic interactions generally increase with increasing F87 mole fraction, however β is unchanged from 0.4 to 0.6 mole fractions.

All activity coefficients of the F87 mixtures reported in Table 4.5-1 are much less than unity, confirming there is non-ideal mixing behaviour of a strongly attractive nature. The negative excess free energies of mixing (ΔG_{ex}) values indicate the mixed micelles formed from the F87 and 16-3-16/pDNA components are more stable than micelles of the individual components in these systems.

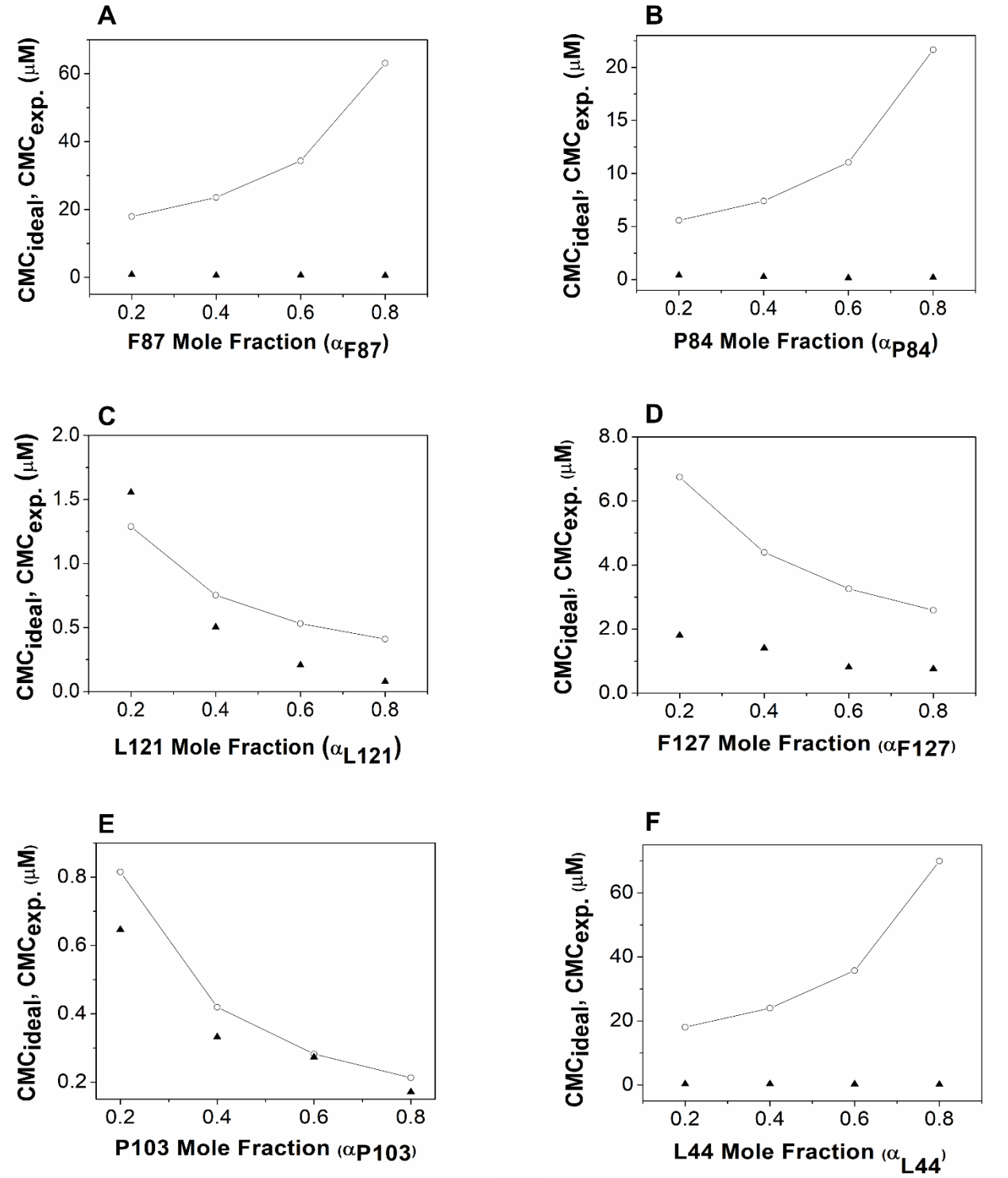

Figure 4.5-2 Calculated ideal CMC (○) and experimentally determined CMC values (▲) for each Pluronic/16-3-16/pDNA mixtures at varying Pluronic mole fractions. **A)** shows F87 mixtures, **B)** P84, **C)** L121, **D)** F127**, E)** P103, **F)** L44.

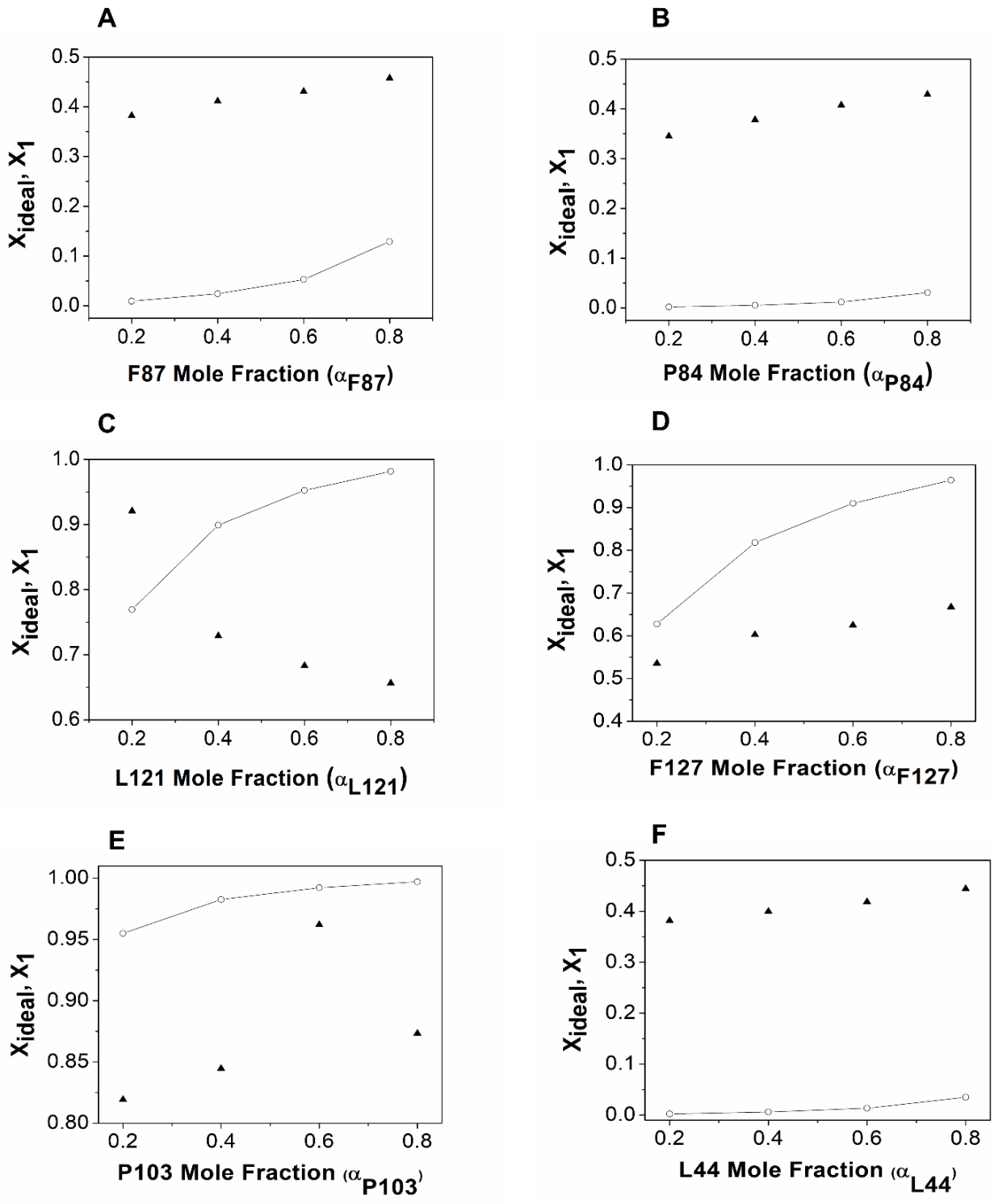

Figure 4.5-3 Calculated X_{ideal} (○) and X_1 values (▲) for Pluronic/16-3-16/pDNA mixtures at varying Pluronic mole fractions. **A)** shows F87 mixtures, **B)** P84, **C)** L121, **D)** F127, **E)** P103, **F)** L44.

4.5.2 P84/16-3-16/pDNA systems

Similar to the F87 system, there is a clear indication of synergistic interactions between P84 and the pre-formed 16-3-16/pDNA condensate within each mixture shown. The experimentally determined CMCs of the P84 mixtures were much lower than the expected ideal CMCs (for all mole fractions of P84 investigated), and much lower than the individual P84 and 16-3-16/pDNA components (as seen in Figure 4.5-2B, and Table 4.5-1). (Surface tension plots for the P84 mixtures are shown in Figure 4.5-4). The mole fraction of P84 in the bulk solution appears to have little effect on the composition of the mixed micelles, which lies within a narrow range (X_1 = 0.345 and X_1=0.429 for α_{P84}=0.2 and α_{P84}=0.8, respectively). There is also a much larger presence of the P84 component than the 16-3-16/pDNA component within the mixed micelles compared to the ideal state ($X_1 > X_{ideal}$) for all mole fractions (Figure 4.5-3B). Rubingh's interaction parameter, β, confirms there are synergistic interactions within the P84/16-3-16/pDNA mixtures for all mole fractions of P84. Furthermore, the large magnitudes (18.1-22.4) indicate not only is there synergism within the system, there is *strong* synergism, which grows with increasing mole fractions of P84.The activity coefficients of all P84 systems investigated are also less than 1, again indicative of a synergistic interaction between P84 and 16-3-16/pDNA. As with the F87 systems reported above, the ΔG_{ex} values are negative suggesting the P84/16-3-16/pDNA mixed micelles are more stable than the pure micelles.

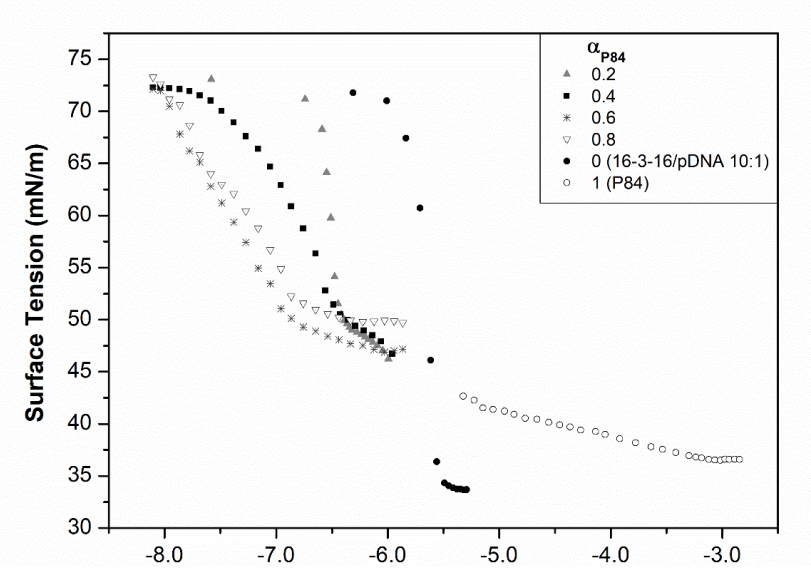

Figure 4.5-4 Plots of surface tension versus total amphiphile for P84/16-3-16/pDNA mixtures with varying mole fractions of P84. α = 1, and α = 0 represent pure P84 and 16-3-16/pDNA solutions, respectively.

4.5.3 L121/16-3-16/pDNA systems

The L121 mixtures follow a similar trend, where there is growing synergism with increasing mole fractions. Although interestingly, the 0.2 mole fraction L121 mixture is identified as having antagonistic interactions since the experimentally determined CMC of the mixture is slightly larger than Clint's ideal CMC. Conversely, for mixtures $\alpha_{L121} = 0.4 – 0.8$, the CMC_{exp} of each mixture is lower than the calculated CMC_{ideal} (as seen in Table 4.5-1 and illustrated in Figure 4.5-2C and Figure 4.5-5). For the case of the L121/16-3-16/pDNA mixture containing an L121 mole fraction of 0.2, the mixed micelles are assumed to be enriched with the L121 component and poor in 16-3-16/pDNA, as indicated by the positive deviation of X_1 from X_{ideal}. Observing the entire range of X_1 for the L121 systems, the bulk solution composition does appear to affect the composition of the mixed micelles; X_1 values range from 0.921 to 0.657 for $\alpha_{L121} = 0.2$ and 0.8, respectively. However, for the $\alpha_{L121} = 0.4 – 0.8$ mixtures only, X_1 lies in a much smaller range of 0.729 to 0.657, and a similar trend as seen previously with the F87 and P84 systems is observed; the composition of these mixed micelles is minimally influenced by the composition of the bulk solution. Furthermore, X_1 is much lower than X_{ideal} for the $\alpha_{L121} = 0.4$, 0.6, and 0.8 mixtures, implying that the resultant mixed micelles are poorer in L121 and richer in the 16-3-16/pDNA component.

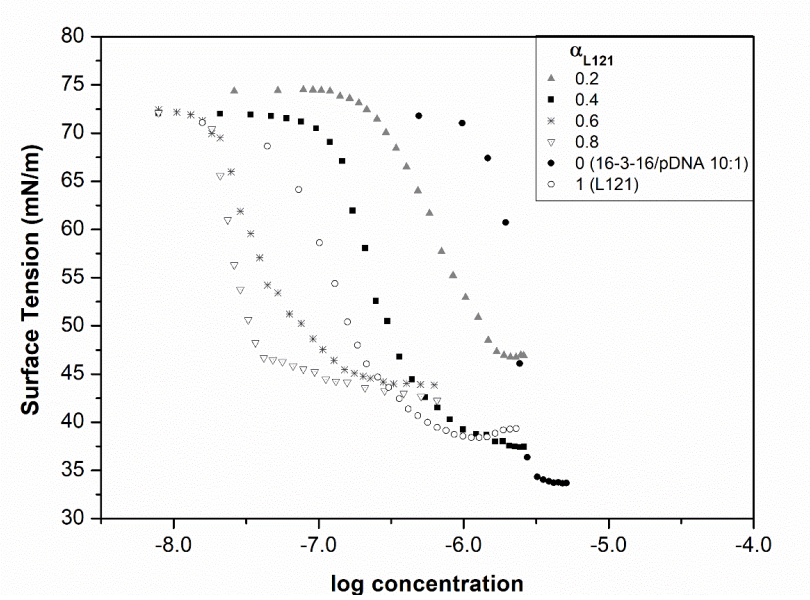

Figure 4.5-5 Plots of surface tension versus total amphiphile for L121/16-3-16/pDNA mixtures with varying mole fractions of L121. α = 1, and α = 0 represent pure L121 and 16-3-16/pDNA solutions, respectively.

Rubingh's interaction parameters reflect a slight antagonism for $\alpha_{L121} = 0.2$, as indicated by a positive β value, but with a small magnitude. Meanwhile. synergism is indicated for $\alpha_{L121} = 0.4$, 0.6, ad 0.8, given the negative interaction parameters (β), which increase in magnitude with increasing mole fractions of L121. The activity coefficients slightly above unity also indicate repulsion in the mixed $\alpha_{L121} = 0.2$ system, and attraction for $\alpha_{L121} = 0.4$ and greater (due to f_1 and f_2 values < 1). Correspondingly, the ΔG_{ex} imply more stability in the separate micelles of the individual components than in the mixed micelles of the $\alpha_{L121} = 0.2$ system. For $\alpha_{L121} = 0.4$, 0.6 and 0.8 systems the reverse is true; ΔG_{ex} indicates the L121/16-3-16/pDNA mixed micelles are more stable than the micelles of the individual components.

4.5.4 F127/16-3-16/pDNA systems

As seen in Table 4.5-1 and Figure 4.5-2D, the CMC_{exp}. values are lower than the CMC_{ideal} for all F127/16-3-16/pDNA mixtures tested, and lower than the individual components of the mixtures (as seen in Figure 4.5-6). This indicates there are synergistic interactions between the F127 polymer and the pre-formed 16-3-16/pDNA complex. Comparison of X_1 versus X_{ideal} for these F127 systems shows a negative deviation from the ideal scenario, so mixed micelles are expected to have a greater presence of the 16-3-16/pDNA component than the F127 component. The calculated X_1 value for $\alpha_{F127} = 0.2$ is 0.535, meanwhile that of $\alpha_{F127} = 0.8$ is 0.667. This range of X_1 values is fairly small, but larger than that seen with the F87 and P84 systems, implying the composition of the F127/16-3-16/pDNA mixed micelles may be ever so slightly influenced by the composition of the bulk solution.

The interaction parameters calculated for these F127 mixtures range from -5.37 to -7.77, for $\alpha_{F127} =$ 0.2 to 0.8, respectively. In all cases, F127 is said to have synergistic interactions with the 16-3-16/pDNA. Activity coefficients below 1 also give support for the presence of synergistic, non-ideal mixing within the F127 systems. Negative excess free energies of mixing for all F127/16-3-16/pDNA mixtures give evidence of more stability in the mixed micelles than the individual micelles.

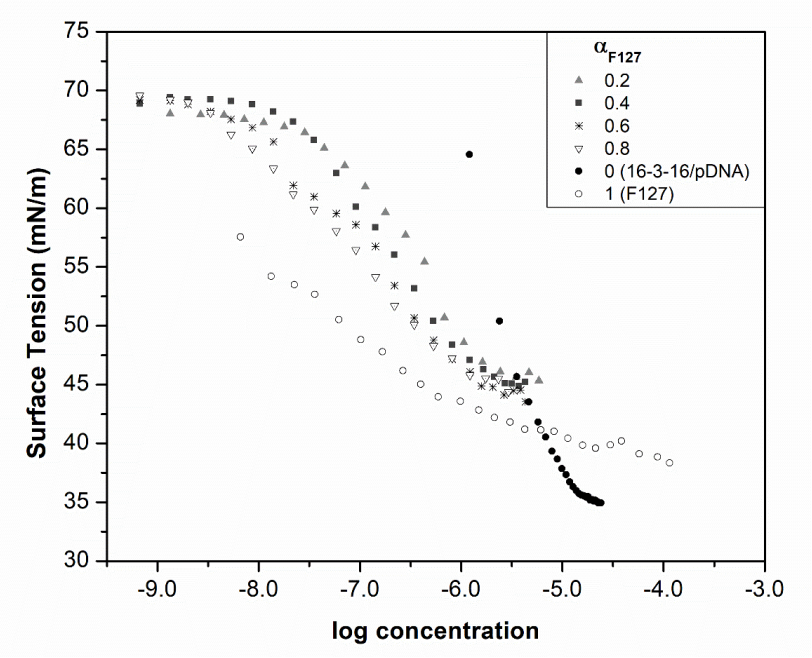

Figure 4.5-6 Plots of surface tension versus total amphiphile for F127/16-3-16/pDNA mixtures with varying mole fractions of F127. $\alpha = 1$, and $\alpha = 0$ represent pure F127 and 16-3-16/pDNA solutions, respectively

4.5.5 P103/16-3-16/pDNA systems

The P103/16-3-16/pDNA mixtures also show synergism at all mole fractions ($CMC_{exp} < CMC_{ideal}$, and negative β values), although there is no clear pattern corresponding to the Pluronic mole fraction like that seen in the other systems reported. Increasing the mole fraction of P103 from 0.2 to 0.4 results in an increase in synergism (-2.42 to -3.40, respectively); however, further increase to 0.6 mole fraction of P103 results in a $CMC_{exp.}$ very close to the CMC_{ideal}, and subsequently reduces the magnitude of the interaction parameter ($\beta = -1.75$). At $\alpha_{P103} = 0.8$, the magnitude of β increases once again. The activity coefficients are below 1, which confirm the non-ideal mixing behaviours are synergistic. The negative ΔG_{ex} values also suggest mixed micelles of P103/16-3-16/pDNA are more stable than the component micelles. (Surface tension plots of the P103 mixtures are shown in Figure 4.5-7)

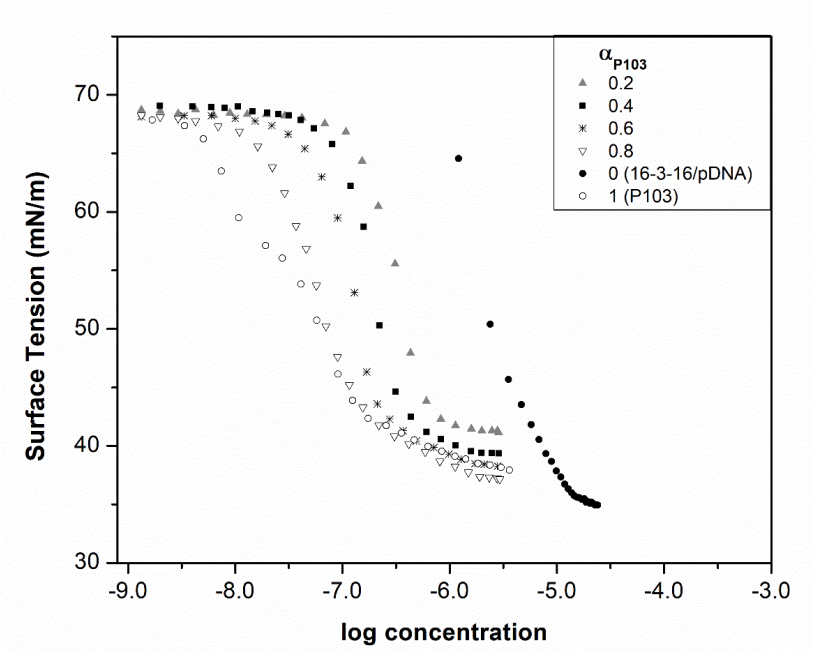

Figure 4.5-7 Plots of surface tension versus total amphiphile for P103/16-3-16/pDNA mixtures with varying mole fractions of P103. $\alpha = 1$, and $\alpha = 0$ represent pure P103 and 16-3-16/pDNA solutions, respectively.

For all mole fractions of P103, X_1 is less than X_{ideal}, indicating the mixed micelles are poor in the P103 component of the mixture. Considering the variability in X_1 values of the P103 systems, the mixed micelle compositions appear to be dependent on the composition of the bulk.

4.5.6 L44/16-3-16/pDNA systems

L44 mixtures with the 16-3-16/pDNA complex also show synergistic mixing behaviour at all mole fractions used, as indicated by experimental CMC values below the calculated ideal CMCs and negative interaction parameter values (surface tension plots shown in Figure 4.5-8). The interaction parameter fluctuates slightly with values of -24.2, -23.3, and -24.0 for $\alpha_{L44} = 0.2$, 0.4, and 0.6, respectively. However, for $\alpha_{L44} = 0.8$ there is a greater increase in β to -27.7 with the increased L44 content. Again, the activity coefficients are below 1, which also suggest non-ideal mixing due to synergistic interaction between the components of the mixture. Excess free energies of mixing (ΔG_{ex}) for each of the L44 mixtures are large and negative which also suggests the formation of mixed micelles is favourable and the mixed micelles are more stable than aggregation of the individual components separately in the mixture.

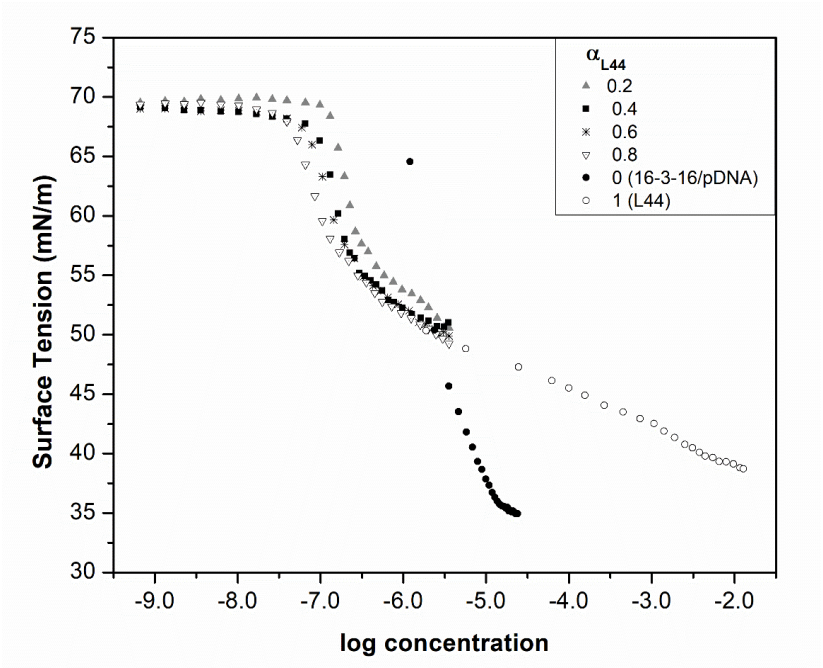

Figure 4.5-8 Plots of surface tension versus total amphiphile for L44/16-3-16/pDNA mixtures with varying mole fractions of L44. $\alpha = 1$, and $\alpha = 0$ represent pure L44 and 16-3-16/pDNA solutions, respectively.

The calculated values of X_1 for each of the L44 mixtures are greater than their respective X_{ideal} values, which suggests the formation of L44-rich mixed micelles. X_1 exists in a small range of 0.384 to 0.444 for L44 mole fractions from 0.2 to 0.8, suggesting the composition of the bulk mixture has little effect on the composition of the mixed micelles.

In all of the Pluronic/16-3-16/pDNA systems investigated here, there is generally an increase in the extent of synergism with increasing mole fraction of Pluronic in the mixtures (with the exception of the P103 systems and F87 at 0.4 and 0.6 moles fractions), based on the calculated Rubingh's interaction parameter. As seen in Figure 4.5-9, the L44 mixtures show the largest magnitudes, and greatest synergism across all mole fractions tested. For low Pluronic mole fractions ($\alpha = 0.2 – 0.4$), synergistic interactions increase in the order: L121 < P103 < F127 < F87 < P84 < L44, with 0.2 L121 showing weak antagonism (β is small in magnitude, but positive). However, for $\alpha = 0.6$ and 0.8, this order changes slightly to: P103 < L121 < F127 < F87 < P84 < L44, and P103 < F127 < L121 < F87 < P84 < L44, respectively.

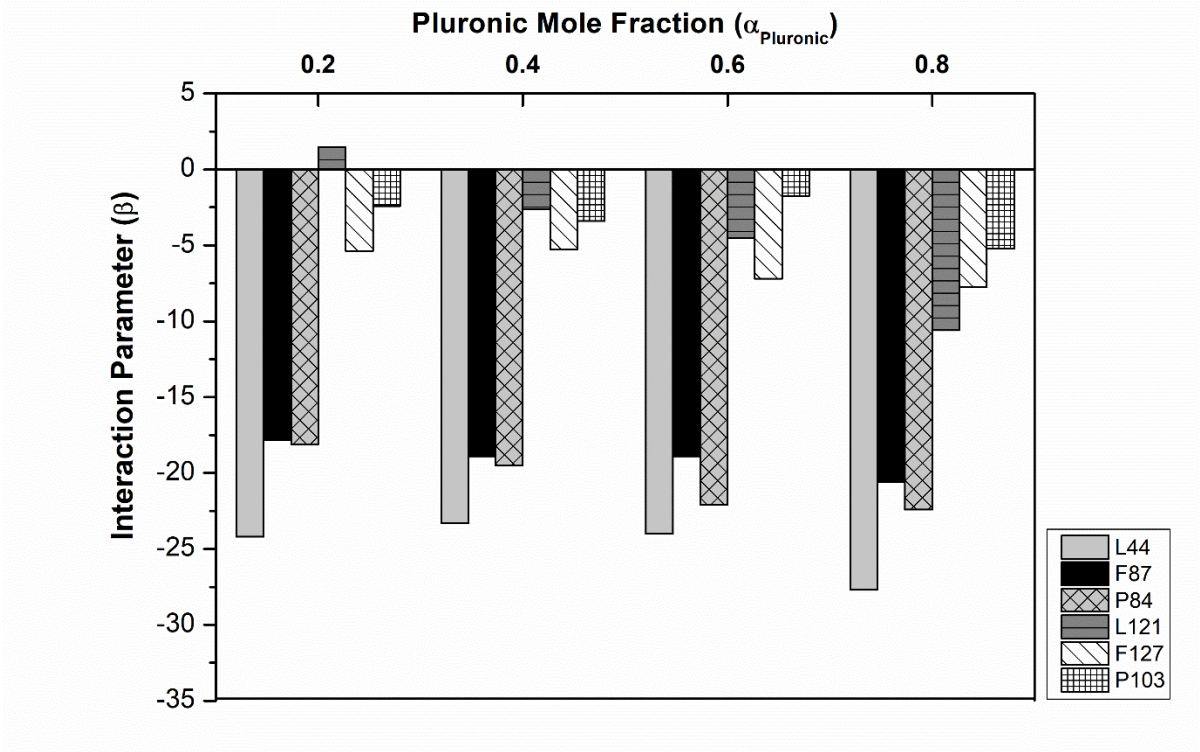

Figure 4.5-9 Average interaction parameters of Pluronic/16-3-16/pDNA mixtures of varying Pluronic mole fraction calculated from experimental CMC determinations shown above. Each bar represents the mean value (n=3)

4.5.7 Maeda's Interaction Parameters

According to Maeda, Rubingh's approach based on the regular solution theory takes the long-range electrostatic interactions that are important in mixed micelle formation into account[116]. However, Maeda proposes a measure of the mixed micelle stability (ΔG_{Maeda}) as a function of the ionic surfactant mole fraction within the mixed micelle (x_2) and takes both hydrophobic chain-chain and electrostatic interactions into account (Equation 4.5-8) [116]. B_1, in Equation 4.5-8, is related to the free energy change associated with replacing a non-ionic monomer within a non-ionic micelle with an ionic monomer [116]. This transfer process involves short-range interactions between the head groups and between the hydrophobic chains [116]. Negative values of B_1 indicate an important contribution by the hydrophobic chain interactions.

$$\Delta G_{Maeda} = RT(B_0 + B_1 x_2 + B_2 x_2^2) \qquad \textbf{Equation 4.5-8}$$

In this case, x_2, the mole fraction of ionic component in the mixed micelle is the 16-3-16/pDNA complex.

$B_0 = ln\ CMC_{16-3-16/pDNA\ complex}$

$B_2 = -\beta$, where β is the interaction parameter from Rubingh's theory

B_1 can then be determined according to $B_1 = ln\left(\frac{CMC_{Pluronic}}{CMC_{16-3-16/pDNA}}\right) + B_2$

The calculated Maeda parameters reported in Table 4.5-2 show negative free energy values, indicating mixed micelle stability (with the exception of α_{F127} = 0.2 and 0.4 mixtures). However, the magnitudes of ΔG_{Maeda} are smaller than that of ΔG_{ex} calculated from the regular solution theory. Negative B_1 values suggest hydrophobic interactions are involved in mixed micelle stability, with the exception of the α_{L121} = 0.2 and α_{P103} = 0.2 – 0.6 mixture, which are positive. The B_1 values of the F87, P84 and L44 mixtures are the most negative.

Table 4.5-2 Interaction parameters and free energy of micellization (ΔG_{Maeda}) calculated according to the Maeda approach

System	Mole fraction Pluronic ($\alpha_{Pluronic}$)	X_2	B_0	B_1	B_2	ΔG_{Maeda} (kJ/mol)
F87	0.2	0.618	5.97	-21.100	17.805	-0.67
	0.4	0.588	5.97	-22.185	18.890	-1.35
	0.6	0.569	5.97	-22.232	18.937	-1.36
	0.8	0.542	5.97	-23.884	20.589	-2.30
P84	0.2	0.655	6.34	-22.906	18.062	-2.27
	0.4	0.622	6.34	-24.355	19.512	-3.12
	0.6	0.592	6.34	-26.901	22.058	-4.60
	0.8	0.571	6.34	-27.276	22.432	-4.76
L121	0.2	0.079	-1.09	4.076	-1.485	-1.94
	0.4	0.289	-1.09	-0.460	3.051	-2.41
	0.6	0.275	-1.09	-1.924	4.516	-3.18
	0.8	0.343	-1.09	-7.986	10.578	-6.42
F127	0.2	0.465	0.76	-3.458	5.367	0.78
	0.4	0.397	0.76	-3.366	5.275	0.64
	0.6	0.375	0.76	-5.297	7.206	-0.52
	0.8	0.333	0.76	-5.863	7.772	-0.81
P103	0.2	0.181	-1.77	2.025	2.416	-3.28
	0.4	0.155	-1.77	1.043	3.398	-3.78
	0.6	0.038	-1.77	2.695	1.746	-4.12
	0.8	0.127	-1.77	-0.778	5.218	-4.42
L44	0.2	0.616	7.38	-28.948	24.240	-3.11
	0.4	0.601	7.38	-28.001	23.294	-2.56
	0.6	0.583	7.38	-28.671	23.964	-2.95
	0.8	0.556	7.38	-32.451	27.744	-5.17

4.5.8 F87/16-3-16/pDNA with charge ratio 5:1

The $\alpha_{F87} = 0.4$ mixture was also tested with a 16-3-16/pDNA charge ratio of 5:1 (N^+/P^-) to confirm the presence of pDNA influences the interaction parameter of the mixtures. From CMC measurements (by tensiometry, as previously described) obtained in duplicate, the interaction parameter (β) is calculated to be -28.9, and the resulting mixed micelles are expected to be enriched with the Pluronic component, as indicated by an X_1 value greater than the expected X_{ideal}. Further confirmation of synergism is seen in activity coefficients below 1, and a free energy of micellization (according the Rubingh's theory) of -17.4 kJ/mole indicating an energetically favourable process. All CMC and calculated parameters for the $\alpha_{F87} = 0.4$ mixtures with charge ratio 5:1 are reported in Table 4.5-3.

Table 4.5-3 Average critical micelle concentrations ($CMC_{exp.}$) determined by tensiometry, and corresponding calculated parameters (CMC_{ideal}, X_{ideal}, X_1, β, f_1, f_2, ΔG_{ex}) for a 0.4 F87 mole fraction mixture with a 16-3-16/pDNA condensate of charge ratio 5:1.

System	Mole fraction F87 (α_{F87})	CMC_{exp} ($\times 10^{-6}$ M)	CMC_{ideal} ($\times 10^{-6}$ M)	X_{ideal}	X_1	β	f_1	f_2	ΔG_{ex} (kJ/mol)
F87 (N^+/P^- = 5:1)	0	2.75 ± 1.70 (n=3)	-	-	-	-	-	-	-
	0.4	0.019 (n=2)	4.55	4.66×10^{-3}	0.413	-28.9	4.78×10^{-5}	7.20×10^{-3}	-17.4
	1	391 ± 96.7 (n=3)	-	-	-	-	-	-	-

4.5.9 Ethidium Bromide Relative Fluorescence Intensity

Figure 4.5-10 shows the normalized relative ethidium bromide (EtBr) fluorescence after addition of the Pluronic component (at specified mole fractions) to the 16-3-16/pDNA complex. At the concentration and charge ratio used, there is only partial loss of EtBr binding after formation of the 16-3-16/pDNA complex (data not shown); however, the addition of Pluronic, any Pluronic present at any mole fraction shown, recovers at least a small amount of EtBr fluorescence. As the mole fraction of Pluronic present in the mixtures increases, there is a general decrease in the relative fluorescence. The greatest recovery of ethidium bromide fluorescence is observed with the addition of L121 across all mole fractions and Pluronics tested. Meanwhile, the least recovery occurs with the addition of L44.

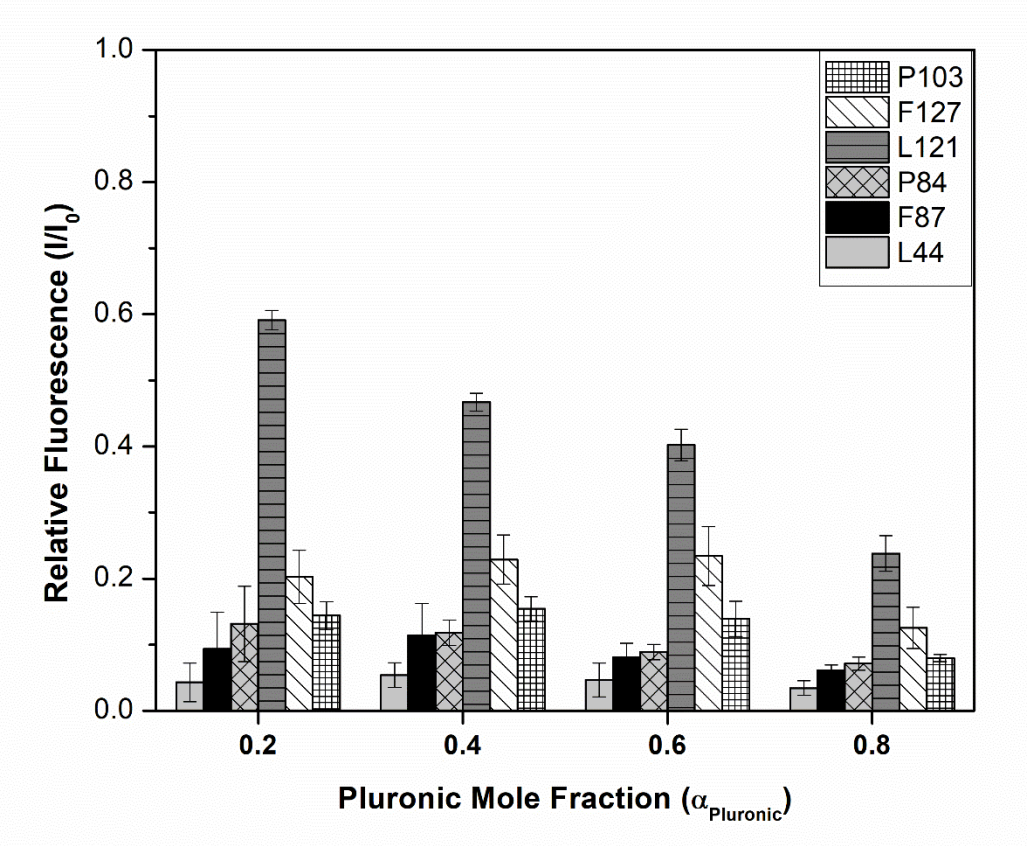

Figure 4.5-10 Relative fluorescence of ethidium bromide (595 nm excitation/535 nm emission) binding to 16-3-16-complexed pDNA followed by 30-minute incubation with Pluronic. Each bar represents the mean value ± standard deviation indicated by error bars (n=3).

4.5.10 Mixed micelle morphology

TEM imaging of the 16-3-16/pDNA complex alone (without Pluronic) shows a rosette morphology that is consistent with previous reports of similar complexes analyzed by atomic force microscopy [180]. Micrographs of the mixtures show spherical micelle structures after the addition of various Pluronics (Figure 4.5-11). Particle diameters for each mixture appear to be approximately 100 – 200 nm, which is consistent with the results of our dynamic light scattering measurements (Chapter 5).

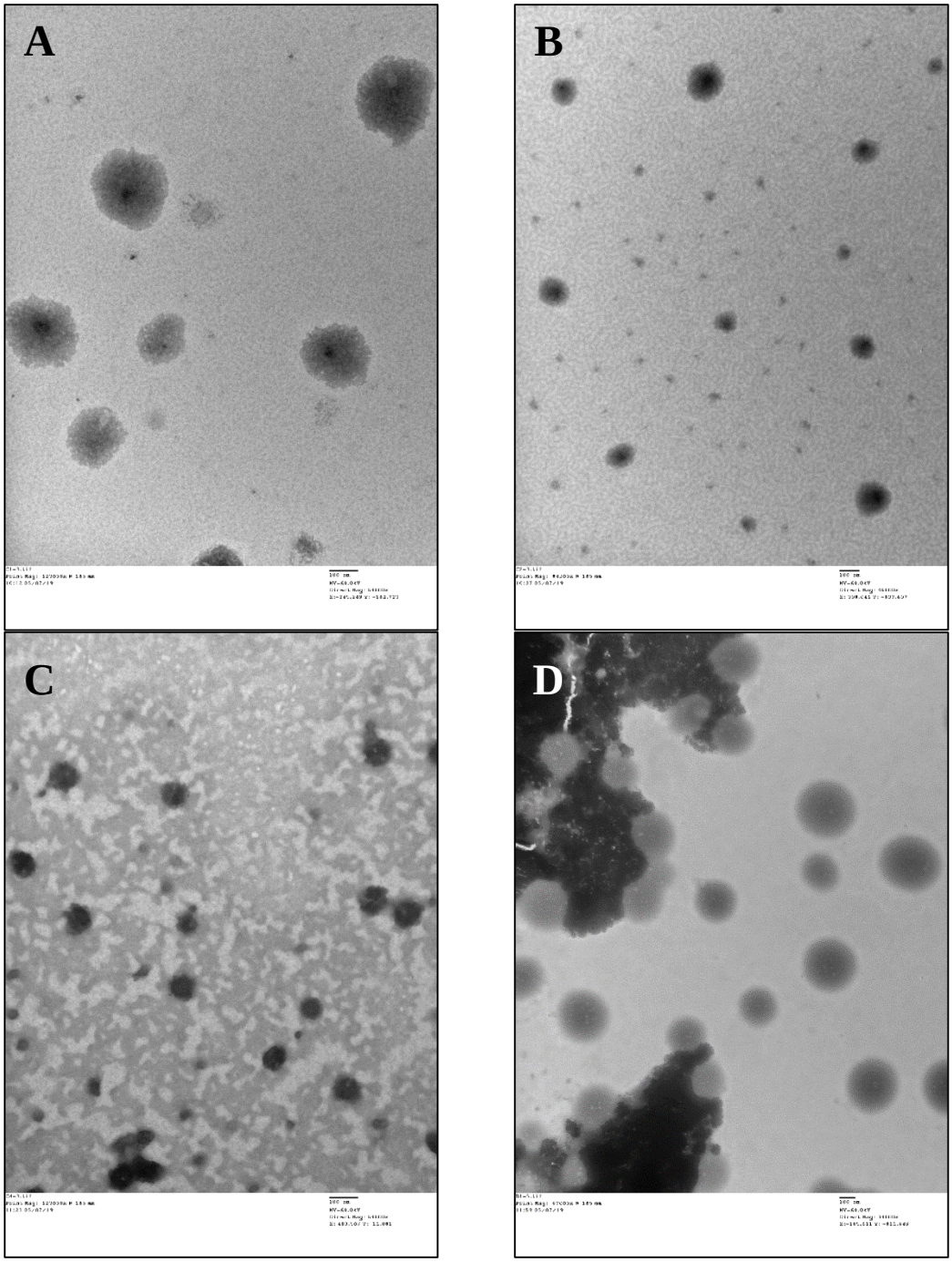

Figure 4.5-11 Transmission electron micrographs of A) 16-3-16/pDNA 10:1 complex (without Pluronic) at 64000x magnification, B) 0.2 P84 at 46000x, C) 0.6 F127 at 64000x magnification, and D) 0.8 L121 at 34000x magnification. All size bars represent 100 nm.

4.6 Discussion

The CMCs of each Pluronic copolymer determined through tensiometry are considered to be in agreement with previously reported literature values (generally within one order of magnitude) [181]. Differences between our findings and those previously reported are attributed to the use of different methods. As seen in the surface tension plot of F127 (Figure 4.5-6), there is a gradual transition region rather than a sharp breakpoint typically seen with conventional surfactants, which has been attributed to composition polydispersity [75]. As expected, the CMC of the 16-3-16/pDNA complex (presented as $\alpha = 0$ in Table 4.5-1 above) is slightly below that of pure 16-3-16 (discussed in [136]). As previously mentioned, the surface tension measurements of the F87, F127, P103, and L44 systems were completed on a different instrument than the L121 and P84 systems, therefore the CMC of 16-3-16/pDNA was measured with both instruments to account for any discrepancies due to instrumentation. As expected, there are slight differences in the 16-3-16/pDNA CMC due to the instruments used; however, the values are within an order of magnitude, which was considered acceptable.

Although the mixing behaviour remains synergistic whether F87 is combined with 16-3-16/pDNA condensates of charge ratio 10:1 or 5:1, there is a marked increase in this synergism when the pDNA is doubled (to ratio 5:1) while the 16-3-16 and F87 components are kept constant. As the ratio between the two charged species (cationic gemini surfactant and anionic plasmid DNA) approaches 0.50, the pre-formed 16-3-16/pDNA condensate may have more hydrophobicity due to charge neutralization. In turn, interactions between the condensate and F87 might be more favourable due to the hydrophobic effect. It is worth noting the CMC plot and interaction parameter appear unchanged when comparing the F87/16-3-16/pDNA charge ratio 10:1 mixture to F87/16-3-16 without pDNA (data not shown); however, this may be due to the small presence of pDNA in 10:1 mixture. Once the pDNA content is at least doubled, a difference is observed.

4.6.1 Effect of PPO length on Interaction Parameter

The mixed micellization is clearly influenced by the composition of the Pluronic component. Upon comparison of L121 vs. P84 or P103 vs. P84 systems, where there are similar molecular weights but less propylene oxide units in P84, the synergism within the mixed systems appears to increase with decreasing propylene oxide content. There is a similar observation for F87 vs. F127 and L44 vs. P84; although their % wt. EO are the same, the synergism reflected by the interaction parameter (β) shows a decrease (β becomes more positive) with increased average propylene oxide units. Therefore, it

appears there is a strong positive correlation between average PPO chain lengths in these Pluronics and the interaction parameter value. A multiple linear regression analysis estimates that the value of the interaction parameter increases by 0.53 with 1-unit increase in PPO length (p-value < 0.001) while PEO and mole fraction are held constant. Figure 4.6-1A clearly illustrates the trend between the size of the Pluronic PPO block and the interaction parameter. This result was unexpected considering increased hydrophobicity of either component is expected to strengthen the hydrophobic effect and onset of aggregation.

Upon further analysis of the results, one may notice the L121, F127 and P103 mixtures' X_1 values are less than their respective X_{ideal} (with the exception of $\alpha_{L121} = 0.2$); therefore, although mixed micelles are formed with the 16-3-16/pDNA complex, they are poor in the Pluronic component of these systems. In contrast, the L44, F87, and P84 mixtures resulted in mixed micelles enriched with the Pluronic component, as indicated by X_1 values greater than their respective X_{ideal}. It is interesting to note that the different micelle compositions generally correspond to the size of the Pluronic PPO block, with the larger blocks (approximately 60-68 PO units) resulting in Pluronic-poor micelles (as shown in Figure 4.6-2A). The decreased propensity of these Pluronics to form mixed micelles may be due to greater steric hindrance opposing the incorporation of a larger PO block into a mixed micelle with the 16-3-16/pDNA complex.

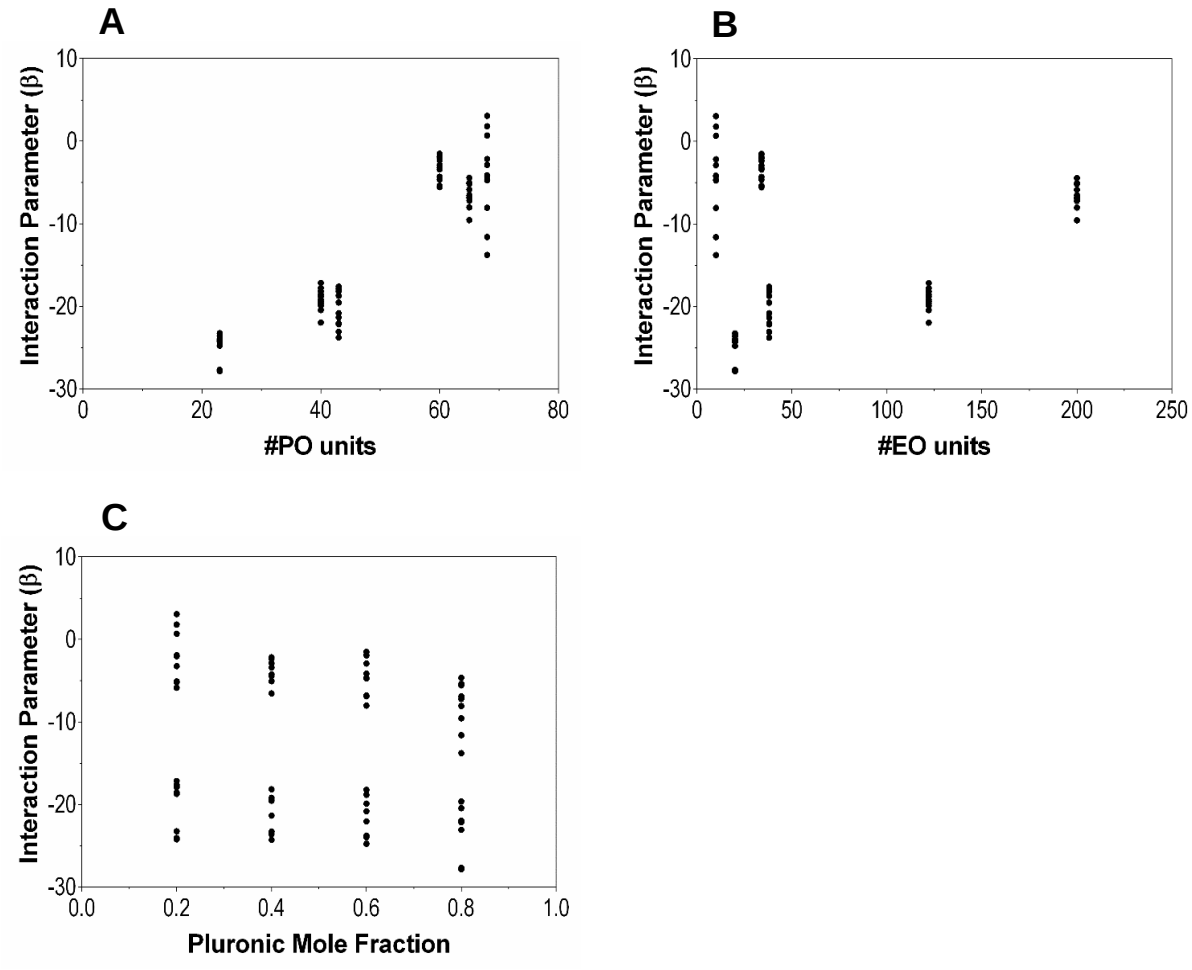

Figure 4.6-1 Scatter plots illustrating relationships between the interaction parameters and **A)** the number of PO units in the Pluronic component, **B)** the number of EO units in the Pluronic component, and **C)** the mole fraction of Pluronic in the mixture, for all Pluronic/16-3-16/pDNA (charge ratio 10:1) mixtures

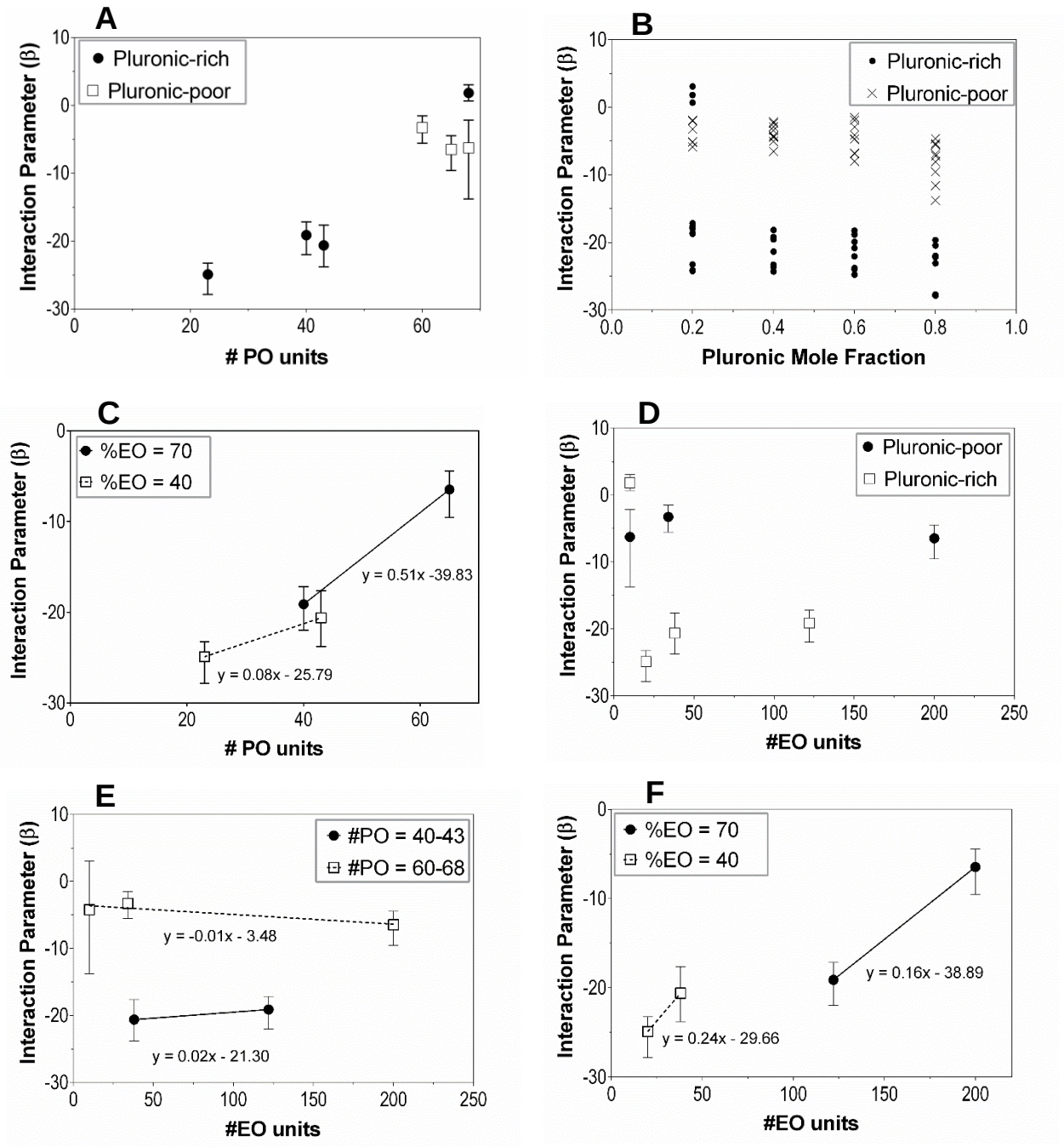

Figure 4.6-2 Scatter plots illustrating relationships between Rubingh's interaction parameter and **A)** the number of PO units in the Pluronic component and the mixed micelle composition, **B)** the mole fraction of Pluronic in the mixture and the mixed micelle composition, **C)** Pluronic % wt. EO and # of PO units, **D)** the number of EO units in the Pluronic component and mixed micelle composition, **E)** the number of EO units and Pluronic PO content, and **F)** Pluronic % wt. EO and # of EO units, for all Pluronic/16-3-16/pDNA (charge ratio 10:1) mixtures. In all plots except panel B, the mean is shown with error bars representing the data range.

Ethidium bromide fluorescence emission at 595 nm (with 535 nm excitation) is detected due to its intercalation with DNA. Similar to previous reports, there is a loss of EtBr fluorescence which accompanies condensation of pDNA by the gemini surfactant. Initially, the cationic ethidium bromide dye intercalates in the DNA strands and emits fluorescence, I_0.[127,182] This fluorescence decreases when the dye is competitively displaced from the DNA chains by complexation with the cationic 16-3-16 surfactant (data not shown). Some of the fluorescence returns after Pluronic is added, indicating some reversal of the 16-3-16-induced condensation. Less de-condensation of the plasmid DNA appears in mixed micelles that are enriched in the Pluronic component and show the greatest level of synergism. This may be a case of solubilisation of the 16-3-16/pDNA complex by the Pluronic component, which show greater participation in the mixed micelle formation. The exact orientation of the components within a Pluronic-rich mixed micelle is unknown; however, it is reasonable to assume the 16-3-16/pDNA complex could reside at any location within the micelle (i.e. PPO core, PEO corona, or the palisade layer) depending on the relative magnitudes of hydrophobic or ion-dipole interactions, where ion-dipole interactions could occur between the 16-3-16 headgroups and the oxygens of the EO or PO groups.

There also appears to be an inverse relationship between synergism and de-condensation, where systems with lower synergism (more positive interaction parameter, β, values) correspond with greater pDNA de-condensation. Accordingly, the greatest return of EtBr fluorescence was in the $\alpha_{L121} = 0.2$ condition. Moreover, mixed micelles poor in the Pluronic component compared to the ideal state (α_{L121} = 0.4-0.8 and all F127 and P103 mixtures) show greater ability to de-condense the pDNA from the pre-formed 16-3-16/pDNA complex compared to the Pluronic-rich mixed micelles of the F87, P84, and L44 systems. In other words, the 16-3-16/pDNA complex stays more intact when F87, P84, or L44 is added. Recall, the Pluronic-poor micelles are observed in the mixed systems involving Pluronics with relatively larger PPO blocks (approximately 60 PO units, compared to approximately 40 units in F87 and P84 and 23 units in L44). From the negative interaction parameter and excess free energy values, we see that mixed micelle formation does occur; however, it is less energetically favourable than for those Pluronics with a smaller PPO block. It is hypothesized that the larger PPO blocks encounter more steric hindrance and perhaps their incorporation results in partial de-complexation of the 16-3-16/pDNA, possibly due to displacement of some 16-3-16 molecules, in order to accommodate the longer PPO block.

Alternatively, the de-condensation of DNA from the pre-formed gemini surfactant complex is typically attributed to Pluronic binding to free gemini surfactant in the bulk phase, which disrupts the thermodynamic equilibrium between DNA-associated surfactant aggregates and free surfactants in the bulk phase, as proposed by He et al. [127]. In this case, the gemini surfactant may have the greatest interaction with the larger or more hydrophobic Pluronics, as previously reported [133], leading to greater change in the surfactant-induced DNA condensation. However, the current data shown does not allow us to discern whether the mixed aggregates/micelles strictly consist of all 3 components present (Pluronic, gemini surfactant, and pDNA) or a mixture of 3-component and smaller Pluronic/16-3-16 aggregates (without pDNA) formed from Pluronic binding to free gemini surfactant in the bulk phase. Further analysis, perhaps using equilibrium dialysis, may provide confirmation. For now, the discussion has been limited to the formation of a 3-component mixed aggregate. Nonetheless, we acknowledge that interpretation of the EtBr fluorescence results is complicated by the possibility of entrapment of the fluorescent probe in the hydrophobic regions of the mixed micelles, or free gemini surfactant or Pluronic micelles reducing the opportunity to re-bind to the pDNA. Furthermore, multiple interactions may be responsible for the results observed, and cannot be separately identified through the experimentation presented here.

Analysis according to Maeda's theory suggests that hydrophobic interactions stabilize the mixed micelles of 16-3-16/pDNA with L44, F87 and P84, as evidenced by the large negative B_1 values in the ΔG_{Maeda} calculation (Table 4.5-2), which supports our hypothesis of 16-3-16/pDNA being solubilized by the L44, F87 and P84 of Pluronic-rich micelles. On the other hand, hydrophobic interactions do not appear to play a major role in the micellization involving P103 and $\alpha_{L121} = 0.2$, as seen with positive or small negative B_1 values, which is possibly due to steric effects; however, the mixed micelles may be stabilized by electrostatic contributions instead. Micellar hydration has been associated with greater mixed micelle stability, which occurs with increased participation of the ionic component in octaoxyethylene monododecyl ether ($C_{12}E_8$) – cetyltrimethylammonium bromide (CTAB) mixtures [183]. Similarly, the mixed micelles mainly consisting of the 16-3-16/pDNA component, may be stabilized by greater micelle hydration (although further investigation is required to confirm this). The presence of hydrated PEO chains may also introduce more water molecules in the Stern layer, also contributing some stability through reduction of head group repulsions.[110] Interestingly, there does appear to be a hydrophobic contribution in the $\alpha_{L121} = 0.4$-0.8 and all F127 systems, but the ΔG_{Maeda} values indicate the mixed micelles of $\alpha_{F127} = 0.2$-0.4 mixtures are not stable. Taking the Maeda and X_1 values for the

F127 and α_{L121} = 0.4-0.8 systems into account, we might also propose that the limited participation of these Pluronics in mixed micelle formation potentially leaves electrostatic repulsion between the cationic components, which leads to a breakdown of the mixed micelles, as reported previously for 12-6-12/Pluronic systems.[131] This may also support the EtBr fluorescence results which suggest a high level of pDNA de-condensation by Pluronics L121 and F127.

The antagonism and low levels of synergism observed for the L121 mixtures may be a reflection of the poor solubility and phase separation of the L121 polymer in aqueous solutions above its cloud point (14°C for a 1% solution).[76] Also, the increasing synergism in the L121 system at higher mole fractions may be a reflection of dehydration of the PPO block as CMC experiments were carried out above the L121 cloud point, therefore increasing the hydrophobic interactions, similar to that reported by Bakshi in investigating the influence of temperature on the interaction of F127 or P103 with the 12-2-12 gemini surfactant.[110] Furthermore, L121 is reported to have multiple phases present even at low concentrations (and ambient temperatures) such as that used to prepare the L121 stock prior to addition to the 16-3-16/pDNA complex. The presence of more ordered aggregates such as cubic [81] or lamellar structures [184] may contribute to the antagonism observed and pDNA de-condensation from the 16-3-16 complex. The Pluronic mesophases might have a greater capacity for disrupting the equilibrium between free gemini surfactants and surfactants bound to the pDNA complex;however, further investigation is required to better understand the potential effect of higher order Pluronic structures on the interaction with the pre-formed 16-3-16/pDNA complexes.

4.6.2 Effect of PEO length on Interaction Parameter

Previous discussions of gemini surfactant and Pluronic block copolymer interactions also include the role of the polymer PEO chains in mixed micelle formation. It was suggested the EO chains intercalate between the cationic headgroups of the gemini surfactants in the mixed micelle and consequently neutralize their repulsion, which favours mixed micelle growth.[128,132] Furthermore, greater synergism was reported for mixtures of 12-2-12 with F127 versus the P103 system owing to the greater number of EO units in F127, while the PO content was similar between the polymers.[110] Therefore, the effect of PEO chain lengths were also considered here.

In general, PEO length appears to have only a small but significant effect on the interaction parameter values in the current study (Figure 4.6-1B). Overall, β is estimated to decrease by 0.02 (p-value < 0.05)

with a 2-unit increase in EO number (1 EO unit added to each chain) while PPO length and mole fraction are held constant.

Looking specifically at the F87 and P84 systems, the interaction parameters are very similar despite having notably different PEO chain lengths (seen in Figure 4.5-9 and Figure 4.6-2E, slope = 0.02). This suggests the effect of PPO length primarily dictates the strength of the interactions and changes to the PEO chain lengths have a small impact on Rubingh's interaction parameter. Maeda's B_1 parameters for the F87 and P84 systems are also similar. Assuming similar PPO blocks result in comparable hydrophobic interactions, the small change in B_1 values might suggest there is also a similar level of charge neutralization between neighbouring cationic surfactant headgroups despite very different PEO chain lengths. Likewise, the β interaction parameter is minimally impacted by the PEO chain length among the 60-unit PPO group of L121, F127 and P103 (Figure 4.6-2E, slope = -0.01). Similar trends are observed in β vs. % wt. EO plots (data not shown). There is however more variability in Maeda's B_1 values for these systems. Although these findings are not consistent with previous investigations of gemini surfactant/Pluronic mixtures, Marangoni and Kwak reported the CMC of dodecyltrimethylammonium bromide (DTAB) was insensitive to the addition of ethoxylated alcohols as the number of EO groups in the alcohol increased from 0 to 3.[185] This indicated that EO groups did not contribute to the interactions between cationic DTAB and ethoxylated alcohols.[185] Moreover, Din, et al. also observed a reduction in the interaction parameter magnitude and suggested it may be due to the PEO chain of Brij56 imposing steric constraints that restrict effective interactions between the non-ionic surfactant and gemini surfactant headgroup.[186] In addition, the longer alkyl tails of 16-3-16 and the presence of pDNA may also account for this deviation from previous literature on gemini surfactant/Pluronic mixing behaviours.

Based on the above discussion, some trends between Pluronic composition and interaction parameter are clear but we also acknowledge there may be additional factors that are yet to be investigated (for example, micropolarity of the pure components) or combinations of multiple factors together should also be considered. As previously mentioned, β becomes more negative with increasing mole fraction of Pluronic in the mixture. Figure 4.6-1C shows two almost parallel groups (with the exception of the positive β values reflecting the L121 mixtures at mole fraction 0.2) showing an inverse correlation between mole fraction and the interaction parameter. When the results are sorted by Pluronic-rich and Pluronic-poor mixed micelles (as in Figure 4.6-2B), a similar inverse relationship is observed regardless

of the mixed micelle composition. Granted, the interaction parameter is notably more positive for the Pluronic-poor group, which is linked to the length of the Pluronic PPO block. Therefore, it can be said that both PPO and mole fraction influence the interaction parameter but independent of one another. (Overall, the interaction parameter value is estimated to change by -0.78 for every increase in mole fraction by 0.1, p-value < 0.001, at constant PPO and PEO chain lengths). What's more, although an increase in PO content of the Pluronic component results in an increase in the interaction parameter value, even with consistent % wt. EO, Figure 4.6-2C illustrates PPO length has a greater impact on β at the higher EO content of 70% (F87 vs. F127) than at % wt. EO = 40% (P84 vs. L44) (slopes = 0.51 and 0.08, respectively). The impact of PPO length on β in comparing F87 to F127 may be a reflection of reaching a threshold PPO length for favourable incorporation of the Pluronic component into a mixed micelle with 16-3-16/pDNA due to hindrance. Meanwhile, PEO chain length may have a greater impact on β for the more hydrophobic Pluronics with % wt. EO = 40% compared to the effect of PPO in this case (Figure 4.6-2F vs. Figure 4.6-2C, slopes = 0.24 vs. 0.08, respectively). Thus, the interaction parameter is primarily dictated by the length of the PPO block, however, other factors (e.g. bulk mixture composition) or in some cases an interaction between two factors (e.g. length of PEO at constant % wt. EO) may also play a role. As previously mentioned, 2-factor or higher order interaction terms were not included in the statistical analysis due to the sample size; accordingly, the conclusions made here may change if such terms were added to the linear regression.

A full understanding of how the Pluronic structure influences the net interactions observed between the 16-3-16/pDNA and Pluronic components may require a wider range of methods and Pluronic compositions; however, here we have demonstrated that Pluronic composition and mole fraction can influence the mixed micelle composition, interaction parameters, and the ability of the Pluronic to decondense plasmid DNA from pre-formed 16-3-16 gemini surfactant condensates.

4.7 Conclusion

Overall, this study has shown synergistic interactions exist between pre-formed 16-3-16/pDNA complexes (with an N^+/P^- 10:1) and the Pluronic block copolymers in this study. However, one exception was observed; mixtures containing a 0.2 mole fraction of L121 demonstrated weak antagonism, which may be due to phase separation of the Pluronic at room temperature or the presence of L121 mesophases.

The strength of the interaction is dependent on the PO content of the polymers, PEO chain lengths, and the mole fraction of Pluronic present in the bulk mixture. These relationships also appear to be influenced by the overall percentage of EO in the Pluronic.

An inverse relationship between synergism and pDNA de-condensation (shown through ethidium bromide fluorescence) has also been demonstrated here. The ethidium bromide fluorescence studies show a marked difference in the block copolymers' ability to de-condense the plasmid DNA from the cationic gemini surfactant complex, which appears greater for those systems that form Pluronic-poor mixed micelles.

Favourable mixing between the cationic 16-3-16 gemini surfactant/plasmid DNA complex and these Pluronic block copolymers is promising for gene therapy applications; not only are mixed micelles formed, but only low surfactant/polymer concentrations are required. However, as reported in the literature and also demonstrated here, the addition of Pluronics can reduce the level of pDNA condensation in surfactant-DNA complexes, which may influence the performance of these mixed micelles as gene delivery vectors. Therefore, a balance between synergism and plasmid de-condensation should be considered.

Lastly, when studied with other concentrations of plasmid DNA, the interaction between the gemini surfactant and Pluronic block copolymer may differ from what is reported here. We have demonstrated that the interactions between the surface active components of this gene delivery formulation can be studied in the presence of its nucleic acid cargo, which allows for a more accurate determination of the mixing behaviours that can be expected in gene therapy applications.

Chapter 5
In Vitro Transfection Efficiency of Self-Assembled Gemini Surfactant/Pluronic-Based Nanoparticles and a Relationship to Mixing Behaviours

5.1 Abstract

Transfection efficiency remains a primary drawback in the utilization of non-viral gene delivery carriers, including self-assembled nanoparticles. Although gemini surfactants and Pluronic block copolymers are both promising families of molecules for building mixed micelle gene delivery formulations, vectors combining these two materials have only recently been investigated. In this work, nanoparticles combining the 16-3-16 gemini surfactant with various Pluronic block copolymers were used for *in vitro* transfection of COS-7 cells. In the past, factors such as nanoparticle size, surface potential, and stability have been shown to influence cellular uptake and transfection efficiency. However, there is less known about the significance of the mixing interactions between the amphiphilic molecules that form these nanocarriers.

The transfection efficiencies of the Pluronic/16-3-16/pDNA presented here displayed poor correlation to the size and zeta potential of the nanoparticles, but there was a significant correlation to the mixing behaviour (characterized in Chapter 4) involved in the formation of these mixed micelle carriers. This relationship holds value for future mixed micelle gene delivery formulation development as it demonstrates the potential benefit of simultaneous investigation of these interactions in order to identify important criteria for physical characteristics needed for increased transfection efficiency.

5.2 Introduction

Gene therapy using recombinant viral vectors has seen many recent successes in clinical trials, including recent licensing by European and North American agencies; however, despite these success, cargo capacity and immunogenicity continue to limit viral use.[13] Non-viral gene therapy provides an alternative solution in order to overcome these limitations, but remains impeded by poor transfection efficiency.

Traditionally, non-viral gene therapy formulation development relies on a rational design approach, where vector components are selected based on their individual characteristics known to favour

transfection. However, despite this rational design, optimization still tends to rely on an experiment-heavy trial and error approach that may not be feasible long-term.[2] It was recently proposed that the formulation development of drug delivery nanocarriers using polymer/surfactant mixed micelles would benefit from a comprehensive and predictive theory, in order to understand the interactions involved in mixing and support optimization of new mixtures.[2] At the same time, non-viral gene therapy formulations using self-assembling materials, such as mixed micelles of polymers, lipids, and/or surfactants, could similarly benefit from a predictive theory to aid in the screening and optimization of these mixtures and potentially reduce the need for trial and error. Previous work in this field has demonstrated that cellular uptake mechanisms and transfection activity can be influenced by particle size, shape, charge, and supramolecular structure,[187,188] which are typically characterized during development; however, in some cases these characteristics do not reliably account for all differences in transfection (as demonstrated in this current work). Consideration for the self-assembly phenomena involved in the formation of these mixed carriers may provide another piece to the puzzle.

Recently, self-assembling nanoparticles consisting of dicationic 16-3-16 gemini surfactant, plasmid DNA (pDNA), and various non-ionic polyoxyethylene-polyoxypropylene-polyoxyethylene (PEO-PPO-PEO) triblock copolymers (widely known as Pluronics (BASF Corp.) or by the non-proprietary name poloxamers), successfully transfected human ovarian adenocarcinoma (OVCAR-3) cells *in vitro*; however, the transfection efficiencies were lower than that of the commercial standard, Lipofectamine 2000.[73]

The 16-3-16 gemini surfactant consists of two lipophilic 16-carbon tails, and a 3-carbon spacer connecting two cationic quaternary amine headgroups, and belongs to the family of m-s-m gemini surfactants which are known to form condensed surfactant-DNA structures capable of cellular entry. While these complexes can transfect cells, the addition of helper lipids has been known to improve their transfection efficiency, or is even a requirement in some cases.[54,62,189,190] For example, early investigations of the 12-s-12 gemini surfactant series did not show any transfection in the absence of the DOPE helper lipid.[68] Correspondingly, the 16-3-16, and 18:1-s-18:1 formulations showed a large increase in transfection following the incorporation of DOPE.[68]

Further, the addition of Pluronic block copolymers to non-viral transfection formulations has improved the transfection efficiencies of numerous materials by enhancing internalization and intracellular trafficking through its interactions with cellular membranes and proven adjuvant

activity.[57,76,91,100–103,107] Moreover, Pluronics are non-cytotoxic and their PEO chains reduce interactions with blood components and clearance by the immune system, allowing for prolonged circulation in intravenous administration.[33,76,96–98] Although the addition of Pluronic block copolymers has enhanced pDNA transfection in previously reported systems, the combination of 16-3-16 with Pluronic did not necessarily enhance the transfection efficiency of 16-3-16 (as shown here). This work aimed to study the effect of the Pluronic component (namely the Pluronic composition) in the Pluronic/16-3-16/pDNA formulation on i) nanoparticle physicochemical characteristics in solution, and ii) *in vitro* transfection, as well as explore a potential link between the in vitro transfection efficiency and our previously reported mixing behaviours for these formulations (Chapter 4), which may inform the development and optimization of these (and similar) formulations.

5.3 Materials

The 16-3-16 gemini surfactant used in this study was synthesized in the Wettig lab according to methods previously described in the literature.[191] Pluronic® block copolymers were provided as samples from BASF Corp, and used as is without further purification or modification.

The pVG.telRL plasmid (depicted in Figure A-1) coding for enhanced green fluorescence protein (eGFP) downstream of a cytomegalovirus (CMV) immediate early promoter[156], was extracted from DH5α cells (provided as a gift from Dr. Roderick Slavcev, School of Pharmacy, University of Waterloo, Canada). E.Z.N.A. Endo-Free Plasmid DNA Maxi Kit (Omega Bio-tek) was used for extraction of the plasmid from cells grown in lysogeny broth (Fisher Scientific) supplemented with kanamycin (Sigma-Aldrich). HyPure Molecular Biology Grade Water (HyClone, GE Healthcare) was used for elution of the pDNA from the columns. Plasmid DNA concentrations and purity were measured by UV-Visible light absorbance at 260 nm using a Thermo Scientific NanoDrop 2000 spectrophotometer. Purity was assessed by the 260/280 nm absorbance ratio and gel electrophoresis following *Hin*dIII digestion.

Ultrapure MilliQ water (Millipore) was used for all stock solution preparations and characterization experiments. Transfection experiments used HyPure water. Dimethyl sulfoxide (DMSO) and Canadian-origin fetal bovine serum (FBS) were obtained from Sigma-Aldrich (Oakville, ON, Canada). 1X Dulbecco's phosphate-buffered saline without magnesium and calcium (DPBS), Dulbecco's Modified Eagle Medium (DMEM) formulated with high glucose and pyruvate (Gibco), DMEM/F-12 without phenol red (Gibco), 0.25% Trypsin-EDTA with phenol red, 75cm^2 and 175cm^2 Nunc

EasYFlask cell culture flasks, cell culture coated 96-well plates (Nunc, Thermo Scientific), cell culture coated 6-well plates (Nunc, Thermo Scientific), Opti-MEM I Reduced Serum Medium (Gibco), and Lipofectamine 2000 (Invitrogen) were purchased from Thermo Fisher Scientific (Burlington, ON, Canada). COS-7 African Green monkey kidney fibroblast cells (ATCC CRL-1651) were purchased from American Type Culture Collection, ATCC (Manassas, VA, USA).

5.4 Methods

5.4.1 Preparation of transfection nanoparticles

Transfection nanoparticles were made from mixtures containing varying mole fractions ($\alpha_{Pluronic}$) of the Pluronic block copolymer while maintaining a total surfactant concentration of 0.5 mM. All mixtures contained a 16-3-16 to pDNA charge ratio of 10:1 (N^+/P^-).

The 16-3-16 and Pluronic stock solutions were prepared at 1 mM and approximately 35 times the Pluronic CMC (with the exception of the L44 stock which was approximately 6 times the L44 CMC), respectively. Prior to use, all stock solutions and water were filtered through a sterile 0.22 μm polyethersulfone (PES) syringe filter (Sartorius). An aqueous mixture of pDNA and 16-3-16 (with N^+/P^- charge ratio 10:1) was allowed to incubate for 15 minutes at room temperature. Next, the Pluronic was added to the 16-3-16/pDNA complex, and an appropriate volume of molecular biology grade water was added to achieve the desired total amphiphile concentration. The solution was mixed gently and allowed to incubate for 30 minutes.

5.4.2 Physical characterization of nanoparticles

Hydrodynamic diameter and zeta potential analyses were performed on all Pluronic/16-3-16/pDNA mixtures and the 16-3-16/pDNA complex using a Zetasizer NanoZS set to 25°C (or 4°C for L121 systems) (Malvern Instruments). Particle sizes were determined using the scattered light intensity distribution from dynamic light scattering with a measurement angle of 173° and three measurements completed per sample. Zeta potential was determined from laser Doppler electrophoresis taking three measurements per sample. Disposable folded capillary cells (Malvern Instruments) used for zeta potential were primed with the sample before loading. All samples were prepared as described immediately prior to measurement. The results are expressed as the average of three independent experiments.

L44 nanoparticles were also diluted in either water or DMEM/F-12 (warmed to 37°C) to a final pDNA concentration of 0.5 µg/mL (equal to 7.6 µM 16-3-16), as used in transfection, and incubated for 3 hours in a water bath set to 37°C (Isotemp GPD 10, Fisher Scientific), followed by particle size determination at 37°C.

5.4.3 Cell culturing and 16-3-16 half maximal inhibitory concentration (IC_{50}) determination

COS-7 cells were cultured in DMEM (with pyruvate and high glucose) supplemented with 10% (v/v) FBS. Cells were incubated at 37°C with 5% carbon dioxide in a tissue culture incubator (Thermo Scientific). No antibiotics were used throughout the culturing and transfection of these cells. Cells were sub-cultured at least once before use in any transfection and viability experiments. Experiments were carried out with cultures having passage numbers 4 to 14.

Cells were harvested, suspended in complete medium (DMEM with 10% FBS) and plated into cell culture-coated 96-well plates with 5,000 cells per well in 100 µL/well. All peripheral and blank wells were filled with DPBS. Cells were incubated overnight. The next day, the cells were rinsed with DPBS and incubated with 100 µL of serum-free DMEM one hour before treatment. To maintain consistent volumes across all wells, 10 µL of medium was removed from each treatment well and replaced with either 10 µL of a 16-3-16 stock (concentrations ranging from 5 µM to 1 mM), HyPure molecular biology grade water as a solvent control, or DMSO for a cell death control. All conditions were repeated in triplicate wells. Cells were incubated for five hours in a cell culture incubator, after which point the cells were rinsed with DPBS and 100 µL of complete medium was added to each well. The cells were incubated overnight and analyzed approximately 18 hours later. To prepare cells for analysis, the medium in all wells was refreshed with complete medium. Three blank wells (previously containing DPBS and no cells) were also filled with complete medium as “no cell” controls to be used for background absorbance correction. The plate was returned to the incubator for one hour. 20 µL of CellTiter 96Aqueous One Solution Reagent (Promega, Madison, WI, USA) was added to each well containing medium. Plates were returned to the cell culture incubator and incubated for four hours protected from light. Absorbance at 490 nm was measured using a SpectraMax M5 Multi-Mode Microplate Reader (Molecular Devices, California, USA).

Average absorbance values (corrected by subtracting background absorbance) from triplicate wells were plotted against the logarithm of the final 16-3-16 dose (0.5 µM – 0.1 mM) in OriginPro 8.5. Data

was analyzed using a dose-response fitting function and the IC_{50} was determined from the centre of the curve (the dose resulting in half the maximal response). The IC_{50} assay was repeated in three independent experiments.

5.4.4 In vitro transfection assay

To initiate a transfection experiment, cells were harvested at approximately 90% confluence and suspended in complete medium and plated into 6-well plates at a density of 500,000 cells/well and volume of 2 mL/well. Plated cells were incubated overnight until treatment the next day. One hour prior to treatment, cells were washed with 1X DPBS and incubated with 2 mL DMEM without FBS. Meanwhile, all transfection treatments and controls were prepared fresh under aseptic conditions. All Pluronic and gemini surfactant stock solutions and HyPure water, were filtered through a sterile 0.22 µm PES syringe filter (Sartorius) before use. 300 µL of the transfection complexes were prepared as described. An appropriate volume of the transfection nanoparticles was added to each well to achieve a plasmid dose of 1 µg/well (which corresponds to $1.5x10^{-8}$ moles/well of 16-3-16). To keep a consistent concentration of plasmid and gemini surfactant throughout all wells, first a volume of medium was removed from each well equal to the volume of treatment to be added. Treatments were then added to the wells dropwise, and the plates were gently rocked to ensure even distribution in the wells before being returned to the incubator. Following 5-hour incubation, the medium was aspirated from each well, the cells were rinsed with DPBS, and 2 mL of complete medium was added per well. Plates were incubated for an additional 40 hours until the cells were harvested for flow cytometry analysis to assess transgene (eGFP) expression and cell viability. Prior to harvesting, the medium was collected from each well and combined with the corresponding harvested cells.

Lipofectamine 2000 was used as a positive transfection control, which was completed simultaneously with each transfection experiment. Lipofectamine-pDNA complexes were prepared in Opti-MEM Medium and optimized according to the manufacturer recommendations. Optimization revealed a ratio of 1 µg pDNA to 4 µL of Lipofectamine 2000 achieved the greatest transgene expression (data not shown). The final plasmid dose per well for Lipofectamine treatments was kept consistent with the test treatments at 1 µg/well.

All transfection conditions were repeated in three independent experiments with freshly made nanoparticle solutions.

5.4.5 Flow cytometry analysis

Cells were harvested 40 hours after removal of the treatments. First, the supernatant medium was collected from each well, cells were rinsed with DPBS and detached with 1 mL 0.25% Trypsin-EDTA for 5 minutes in the cell culture incubator followed by neutralization with 2 mL of complete medium. The contents of each well was combined with its corresponding supernatant in 5 mL round-bottom polystyrene tubes (Falcon, Corning Life Sciences). All collected samples were then centrifuged for 10 minutes at 125xg (Sorvall Legend RT, Thermo Scientific), the supernatant was aspirated, and cells were washed twice with 2 mL DPBS followed by centrifugation. The final cell pellet was re-suspended in 700 µL of DPBS, and stored on ice, protected from light until analysis. Five to ten minutes before flow cytometry analysis, 3 µL of a 0.1 µg/mL propidium iodide (PI) solution (Sigma Aldrich) was added to each tube, with the exception of the unstained and eGFP-only control samples.

Samples were analyzed using a BD FACSAria Fusion (BD Biosciences, San Jose, CA, USA) operated by the FACS Facility Manager (Department of Biology, University of Waterloo). Samples were excited with a 488 nm laser, and 10,000 events analyzed per sample. Cells that did not receive any additional treatment/transfection reagent, and were not stained with PI, were used as an unstained cell control to set initial parameters for voltage and gating. Cells treated with Lipofectamine/pDNA complexes without PI staining, and cells treated with a final 16-3-16 concentration of 23 µM ($4.5x10^{-8}$ moles/well of 16-3-16) and stained with PI were used as single colour controls, (+ GFP, − PI) and (−GFP, + PI), respectively. Single-colour samples were used for setting the fluorescence compensation to minimize spectral overlap prior to data collection.

Data files were subsequently analyzed using FlowJo V10 software. Polygonal gating was used in a side scatter vs. forward scatter dot plot to distinguish cells of interest from debris. This population of interest was then plotted in a PI fluorescence intensity vs. GFP fluorescence intensity dot plot. Quadrant gating was then used to quantify subpopulations based on fluorescence.

5.4.6 Statistical Analysis

All statistical analyses were performed using R Studio software. Statistical comparison between groups (e.g. Pluronic-rich vs. Pluronic-poor in Figure 5.6-1) were made using Student's t-test. Statistical analysis comparing treatment results to a control group were determined by one-way analysis of

variance (ANOVA) and Dunnet's post-test (Figure 5.5-6 and Figure 5.5-7). Values of $p < 0.05$ were considered statistically significant.

A predictive multiple linear regression model (Equation 5.6-1 and Equation 5.6-2) was developed through the validation set approach using random selection of 62 observations to make a training dataset (leaving the remaining 10 observations for the test set).[192] Using a bootstrap method, each transfection result (1 replicate) was randomly assigned to an interaction parameter value (1 replicate) since these measurements were acquired separately (using different samples). Then the training data set was used to build multiple linear regression models using the following factors: PO units, EO units, mole fraction, interaction parameter value, Pluronic-rich vs. Pluronic-poor mixed micelles, zeta potential, and particle size. Each model was then used to predict the GFP value for the 10 test conditions, and these predicted values were used to calculate the mean squared error (MSE) for each model. This process was repeated 10,000 times through a loop (including random assignment of the transfection replicates), all predicted GFP values and MSEs were recorded and then averaged. The final model presented here was chosen based on having the lowest average MSE, since a lower MSE is an indication that the prediction values are closer to the actual value obtained experimentally. The MSE for a single data set was calculated according to Equation 5.4-1:

$$\mathrm{MSE_d} = \frac{1}{10}\sum_{i=1}^{10}\left(\mathrm{GFP_i^*}\text{-}\mathrm{GFP_i}\right)^2 \qquad \textbf{Equation 5.4-1}$$

Where GFP_i^* is the predicted value from the model for observation *i* of the test data set, and GFP_i is the actual value obtained experimentally. Since the bootstrap was repeated 10,000 times the average MSE was calculated according to Equation 5.4-2:

$$Average\ MSE = \frac{1}{N}\sum_{d=1}^{N} MSE_d = \frac{1}{10{,}000}\sum_{d=1}^{10{,}000} MSE_d \qquad \textbf{Equation 5.4-2}$$

Sample GFP prediction values from the model with the lowest average MSE are presented in Figure 5.6-7, along with 2 other models prepared for comparison and discussed later on.

5.5 Results

5.5.1 Physical characterization of nanoparticles

TEM images of some nanoparticle mixtures reported in Chapter 4 showed spherical particles with sizes of 100-200 nm, which is in good agreement with our findings from dynamic light scattering shown below. For a given Pluronic, the mean hydrodynamic diameters of the Pluronic/16-3-16/pDNA nanoparticles varied only within a small range with varying mole fraction of Pluronic. However, variations in the Pluronic structure appeared to have a greater influence on the particle sizes, particularly at a Pluronic mole fraction of 0.2. With the exception of F87, P84, and L44 at mole fraction 0.2, all nanoparticle formulations showed a unimodal size distribution based on intensity and low polydispersity index (PDI) values (reported in Table 5.5-1).

Table 5.5-1 Particle size and zeta potential of Pluronic/16-3-16/pDNA nanoparticles with varying mole fraction of each Pluronic measured at 25°C (L121 sample measured at 4°C). Mean values ± standard deviation for triplicate measurements (n=3) are reported. In the case of 16-3-16/pDNA without Pluronic, the mean ± standard deviation of 14 replicates are reported (n = 14).

Pluronic added	**Mole Fraction of Pluronic**	**Mean hydrodynamic diameter (nm)**	**Mean PDI**	**Mean Zeta Potential (mV)**
16-3-16/pDNA (10:1) (no Pluronic added) (n = 14)	0	198.7 ± 35.6	0.21 ± 0.03	48 ± 7
F87	0.2	See Table 5.5-2		31 ± 2
	0.4	164.6 ± 11.0	0.18 ± 0.01	26 ± 3
	0.6	155.5 ± 20.4	0.20 ± 0.02	26 ± 3
	0.8	153.2 ± 12.8	0.28 ± 0.05	25 ± 1
P84	0.2	See Table 5.5-2		42 ± 5
	0.4	202.5 ± 27.3	0.21 ± 0.03	44 ± 4
	0.6	173.7 ± 16.3	0.21 ± 0.02	39 ± 4
	0.8	166.9 ± 6.5	0.22 ± 0.01	37 ± 4
L121 (4°C)	0.2	164.5 ± 10.3	0.12 ± 0.03	51 ± 1
	0.4	160.9 ± 8.6	0.14 ± 0.02	52 ± 1
	0.6	147.0 ± 10.6	0.11 ± 0.02	51 ± 2
	0.8	139.3 ± 9.4	0.11 ± 0.04	48 ± 2
F127	0.2	181.2 ± 9.2	0.18 ± 0.02	20 ± 1
	0.4	178.8 ± 19.5	0.18 ± 0.02	15 ± 1
	0.6	181.9 ± 15.2	0.20 ± 0.01	13 ± 1
	0.8	173.8 ± 16.0	0.29 ± 0.01	11 ± 1
P103	0.2	229.5 ± 64.0	0.24 ± 0.03	38 ± 2
	0.4	185.4 ± 17.5	0.22 ± 0.01	33 ± 1
	0.6	180.2 ± 9.7	0.23 ± 0.02	33 ± 2
	0.8	173.6 ± 30.0	0.33 ± 0.05	31 ± 2
L44	0.2	See Table 5.5-2		44 ± 1
	0.4	159.2 ± 12.1	0.19 ± 0.01	45 ± 2
	0.6	153.1 ± 24.5	0.19 ± 0.02	43 ± 2
	0.8	148.2 ± 17.7	0.24 ± 0.06	40 ± 3

The nanoparticle formulations shown in Table 5.5-2 (0.2 mole fraction of F87, P84 or L44) show high polydispersity and overall increased hydrodynamic diameters suggesting aggregation occurs within these samples. Granted, there is some polydispersity expected in the molecular weight distribution of these Pluronic samples which may further complicate this DLS data and contribute to different sizes. Figure 5.5-1 provides a graphical representation of all particle sizes from Table 5.5-1 and Table 5.5-2.

Table 5.5-2 Particle size distribution for polydisperse samples. Mean peak values for triplicate measurements (n=3) are reported.

Pluronic mole fraction	**Peak 1**		**Peak 2**		**Peak 3**	
	Mean diameter (nm)	**% Intensity**	**Mean diameter (nm)**	**% Intensity**	**Mean diameter (nm)**	**% Intensity**
0.2 F87	644	53.1	176	46.6	5561	0.3
0.2 P84	531	60.7	190	34.6	5136	4.7
0.2 L44	440	78.6	119	18.9	5348	2.4

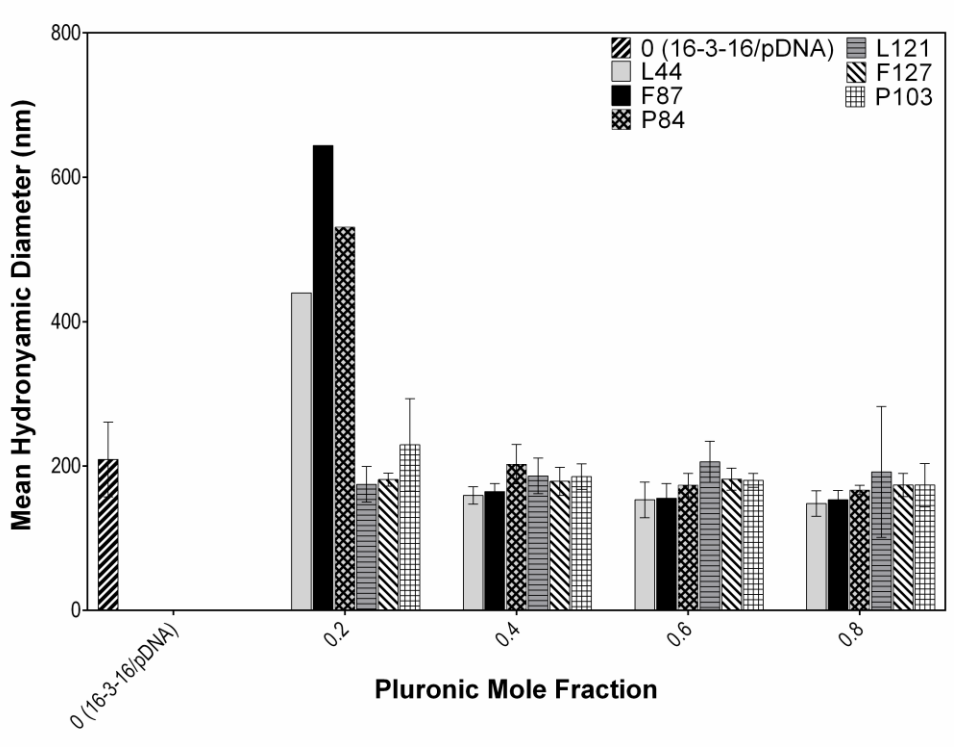

Figure 5.5-1 Mean hydrodynamic diameter of 16-3-16/pDNA (n = 14) and Pluronic/16-3-16/pDNA (n = 3) nanoparticles with varying mole fractions of each Pluronic. Error bars represent standard deviation. The major peak from the size distribution by intensity is shown for F87, P84, and L44 mixtures with 0.2 Pluronic mole fraction. Average size taken from the major peak of the intensity distribution is shown.

In contrast, the zeta potential measurements appear uniform for all samples. In addition, all nanoparticle formulations except that of F127 show zeta potentials around +30 mV or greater which is generally associated with high colloidal stability based on electrostatic repulsive forces; whereas F127 nanoparticles might be classified as relatively stable based on zeta potentials between +10 to +20 mV[193] (Table 5.5-1, Figure 5.5-2). Compared to the initial 16-3-16/pDNA complex, the addition of Pluronic results in a decrease in the zeta potential, presumably due to shielding by the PEO chains, with the greatest reduction occurring upon the addition of F127 which possesses the longest PEO chains. However, PEGylation is also known to facilitate colloidal stability despite decreasing the zeta potential; therefore, the zeta potentials reported here may not reflect the entire picture of stability for these nanoparticles.[193] Interestingly, the zeta potential tends to decrease linearly with the length of the Pluronic PEO chain lengths (Figure 5.5-3), which may be evidence that the PEO chains are fully extended in solution. Therefore, we can conclude that the zeta potentials are influenced by the Pluronic

structure; however, there are no notable changes in the zeta potential magnitudes as the mole fraction of Pluronic in the mixture is increased.

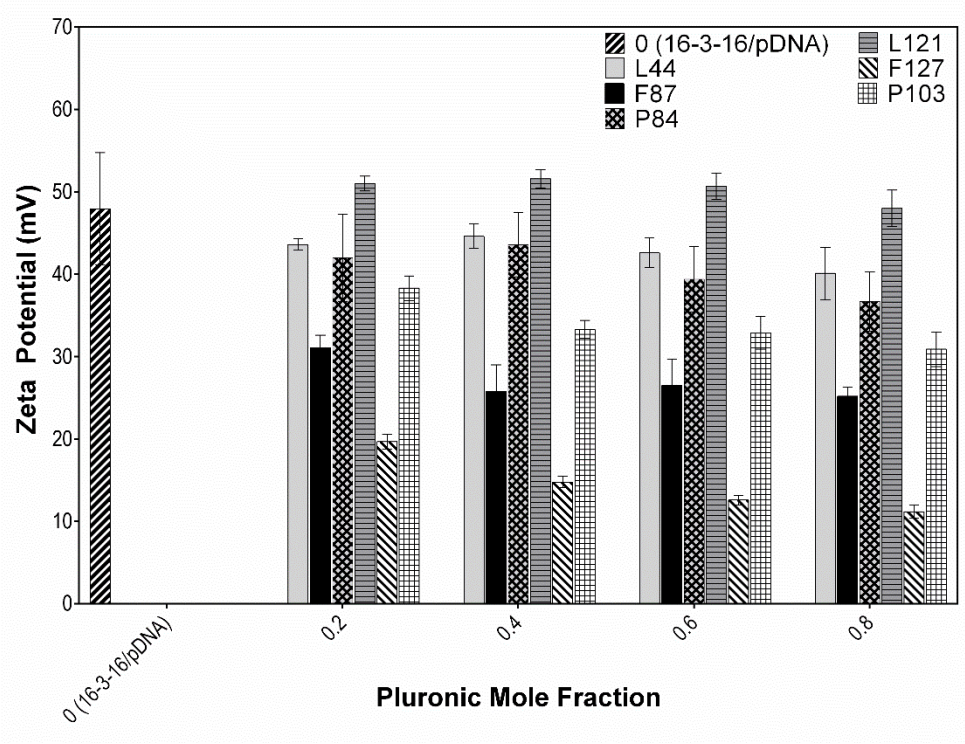

Figure 5.5-2 Mean zeta potential of 16-3-16/pDNA (n = 14) and Pluronic/16-3-16/pDNA (n = 3) nanoparticles with varying mole fractions of each Pluronic. Error bars represent standard deviation.

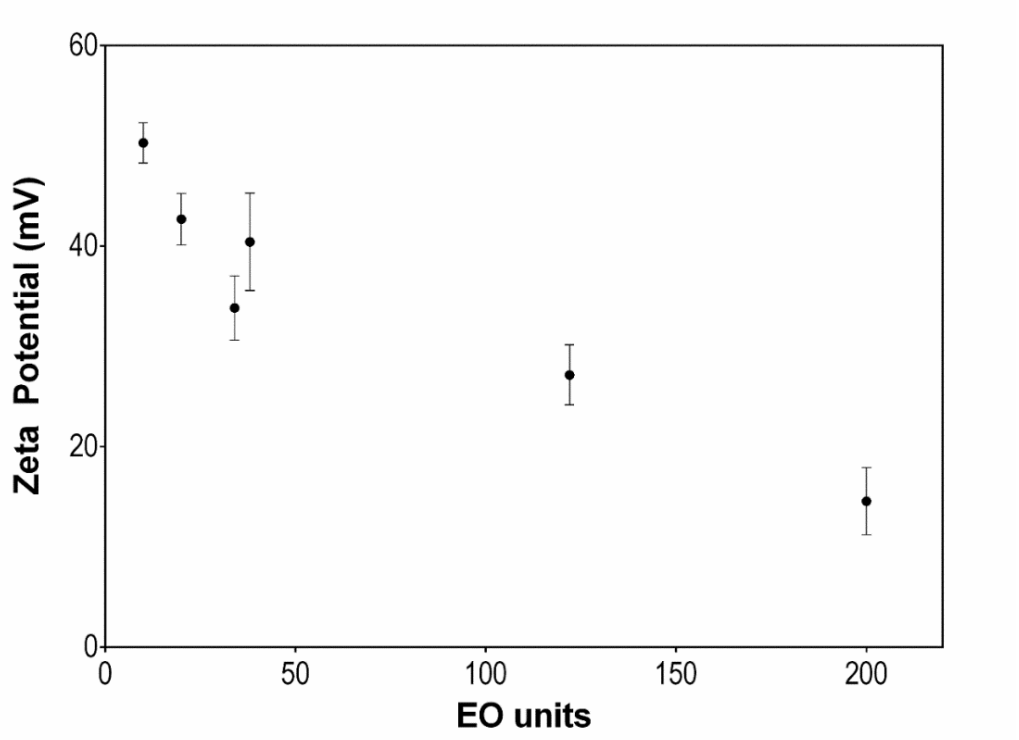

Figure 5.5-3 Mean zeta potential of Pluronic/16-3-16/pDNA nanoparticles as a function of the number of EO units in the Pluronic structure.

To briefly assess the impact of temperature and dilution, the L44 formulations were diluted to the concentrations used for transfection in either water or DMEM/F12 medium (without serum or phenol red), and incubated for 3 hours at 37°C. Aside from the 0.2 L44 mole fraction mixtures, the hydrodynamic diameters under these conditions were not considered significantly different from the measurements obtained in water at 25°C (as shown in Figure 5.5-4). Interestingly, the 0.2 mole fraction formulation showed a unimodal distribution and large decrease in size after dilution and incubation at 37°C (regardless of medium).

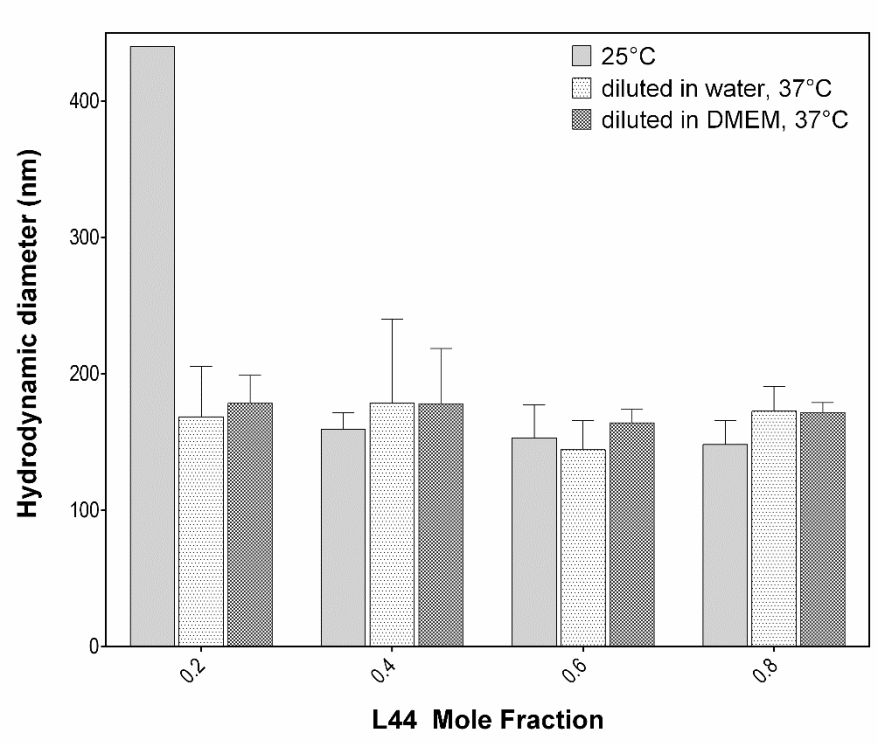

Figure 5.5-4 Mean hydrodynamic diameter of L44/16-3-16/pDNA nanoparticles with varying mole fractions of each L44 measured under different conditions: 1) 0.5mM mixtures in water, measured at 25°C (same as shown in Figure 5.5-1), 2) mixtures diluted in 37°C water to a final 16-3-16 concentration of 7.6 µM, measured at 37°C, and 3) mixtures diluted in 37°C DMEM/F12 to a final 16-3-16 concentration of 7.6 µM, measured at 37°C. Error bars represent standard deviation (n = 3). Average size taken from the major peak of the intensity distribution is shown.

5.5.2 In vitro transfection of COS-7 cells

The COS-7 cell viability showed a dose-dependent response following treatment with varying concentrations of 16-3-16. Measurements of formazan production as an indicator of cell viability (measured by absorbance at 490 nm, shown in Figure 5.5-5) showed that a concentration of 18 µM ± 2.6 resulted in a 50% reduction in formazan. Using this half maximal inhibitory concentration as a guide, transfection efficiency assays were then completed with a final 16-3-16 concentration of 7.6 µM per well (approximately 0.4x the half maximal inhibitory concentration). Considering the 16-3-16 concentration is likely the determining factor for cell viability following treatment with the Pluronic/16-

3-16/pDNA nanoparticles, the final concentration of 16-3-16 (and pDNA) was kept constant across all treatment conditions. This was a key step in optimizing the transfection protocol, in order to reduce the possibility of transfection to be influenced by variations in cell death by 16-3-16.

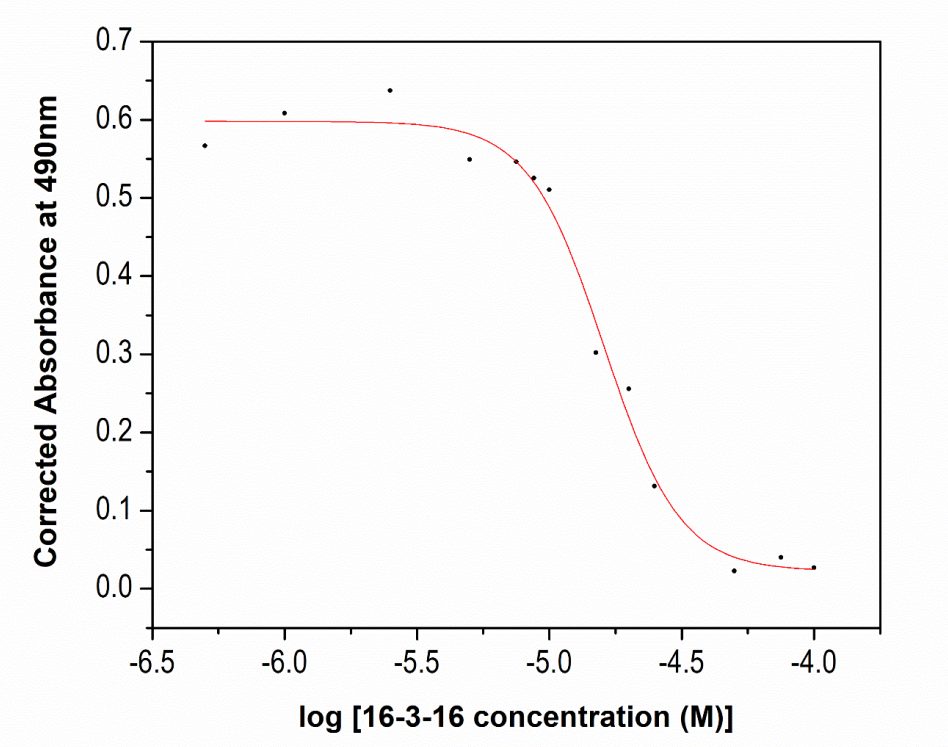

Figure 5.5-5 Formazan absorbance in COS-7 cells at 490 nm measured 18h after treatment with varying concentrations of 16-3-16.

Transfection efficiency determined by eGFP expression in viable COS-7 cells was dependent on the Pluronic component of the nanoparticles, as well as the mole fraction of Pluronic present in the nanoparticle formulation (Figure 5.5-6). However, the effect of mole fraction on transfection was not consistent for all nanoparticles. For example, an increasing Pluronic mole fraction in the formulation mixture resulted in a downward trend in transfection for F87 and P84 nanoparticles, whereas L44 and L121 nanoparticles generally increased in transfection efficiency with increasing mole fraction. F127 and P103 nanoparticles produced the least (in effect, negligible) eGFP expression; while the greatest transfection was achieved with L44/16-3-16/pDNA nanoparticles from a 0.8 L44 mole fraction mixture (α_{L44} = 0.8). Addition of Pluronic to the 16-3-16/pDNA complex did not necessarily improve the *in vitro* transfection. In fact, only addition of L44 showed increases in transfection efficiency compared to the 16-3-16/pDNA alone; however, no statistically significant improvement was achieved. In comparison to the average transfection efficiency obtained with the Lipofectamine 2000 positive control, the average transfection efficiency of α_{L44} = 0.8 nanoparticles was equal to approximately 61% of that of Lipofectamine. These results are consistent with a previous study using NF-grade Pluronics with 16-3-16/pDNA at varying charge ratios and Pluronic concentrations in the OVCAR-3 cell line, which also showed a dependence on the composition and concentration of the Pluronic component.[73]

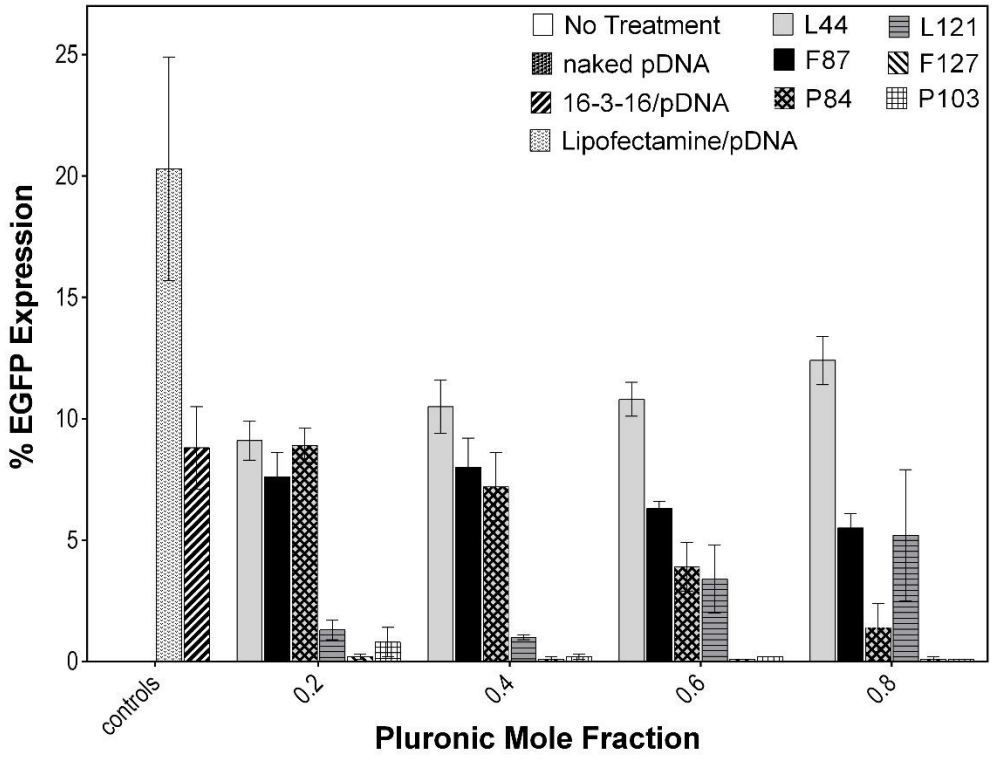

Figure 5.5-6 Transfection efficiency in COS-7 cells treated with Pluronic/16-3-16/pDNA nanoparticles consisting of varying Pluronic mole fraction represented by the number of live cells expressing eGFP (as a percentage of total cells analyzed). Mean values are plotted with error bars representing standard deviation. Control conditions consisting of untreated cells (labelled "no treatment"), cells treated with Lipofectamine/pDNA complexes, and 16-3-16/pDNA complexes were replicated 12 times (n = 12). Treatment with naked pDNA was replicated 5 times (n = 5), while all Pluronic/16-3-16/pDNA nanoparticle treatments were repeated in triplicate (n = 3).

Cell viability, shown in Figure 5.5-7, was not significantly reduced by any of the transfection treatments when compared to the negative control (untreated cells). However, a "positive death control" using 23 μM 16-3-16 confirms our findings that higher doses of 16-3-16 can significantly impact cell viability. Similar cell viability results were also obtained for the F87 formulations in a smaller assay detecting the cellular metabolic capacity to reduce resazurin to resorufin (using the Promega CellTiter Blue reagent). A comparison of viability results from both methods are shown in Table C-4 of the Appendix. It is also interesting to note there was a large improvement in cell viability when the cells were harvested and analyzed two days following transfection as compared to the results obtained the

day after treatment (data not shown). This is likely due to recovery of the cell membrane following permeabilization.

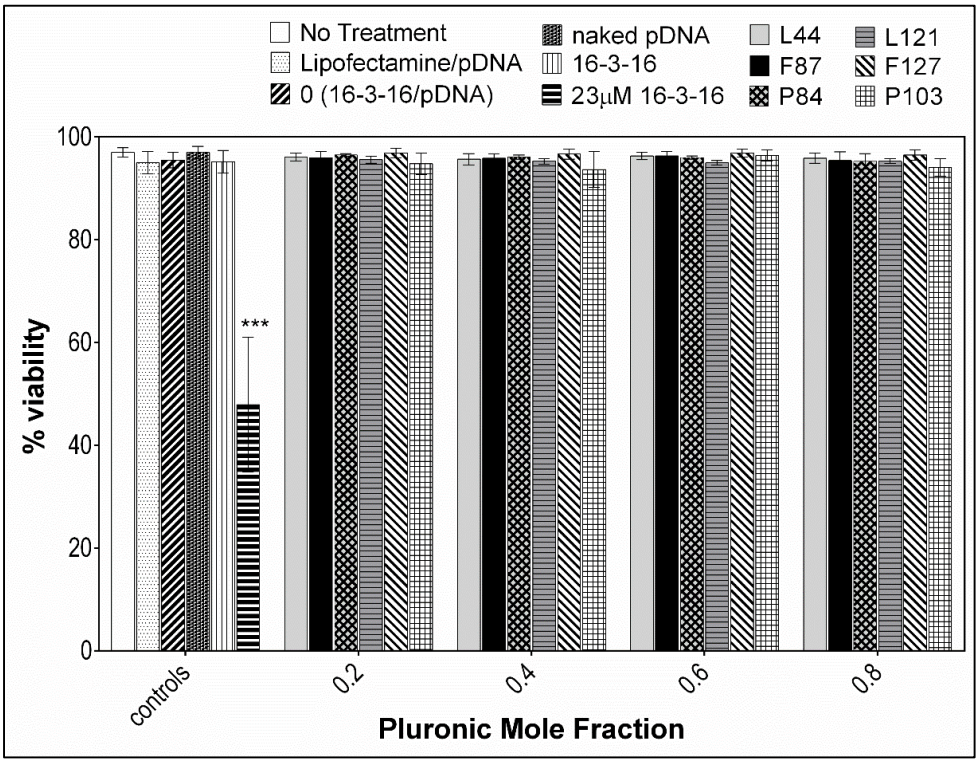

Figure 5.5-7 Cell viability of COS-7 cells treated with Pluronic/16-3-16/pDNA nanoparticles with varying Pluronic mole fraction indicated by positive propidium iodide staining (shown as a percentage of total cells analyzed). Control conditions consisting of untreated cells (labelled "no treatment"), cells treated with Lipofectamine/pDNA complexes, 16-3-16/pDNA complexes, and 23 μM of 16-3-16 were replicated 12 times (n = 12). Treatment with 7.6 μM 16-3-16 was replicated 9 times (n = 9), and treatment with naked pDNA was replicated 5 times (n = 5). All Pluronic/16-3-16/pDNA nanoparticle treatments were repeated in triplicate (n = 3). Mean values are plotted with error bars representing standard deviation. ***p-value < 0.001

5.6 Discussion

The DLS and zeta potential measurements presented in Table 5.5-1, Figure 5.5-1 and Figure 5.5-2 give a preliminary illustration of these nanoparticle formulations in aqueous medium prior to use, which show promising characteristics for gene therapy applications. Particles above 30 nm are also likely able to by-pass clearance through glomerular filtration *in vivo*, which contributes to longer circulation

times.[35] For cancer gene therapy in particular, the particle sizes generated by these formulations are also typically promising for passive targeting to tumor tissue *in vivo* since they are expected to extravasate through the discontinuous epithelium of tumor vasculature (10 – 500 nm) but not through the tight junctions of normal vasculature (2 – 4 nm).[36,37] Although the EPR effect may not be an appropriate approach for all tumors, as previously discussed in Chapter 1, there are some tissues that demonstrate a strong EPR effect that these nanoparticle sizes may be suitable for.

Furthermore, the positive zeta potentials are generally desirable in order to facilitate interactions with cell membranes.[35] Additionally, a particle size of 100-150 nm is generally optimal for endocytosis.[69] Most nanoparticle sizes reported here are within this range or are only slightly above 150 nm (aside from the polymodal samples identified above). It is also interesting to note the samples showing polymodal size distributions achieve some of the highest transfection efficiencies seen in this investigation (mixtures with 0.2 mole fractions of F87, P84 or L44). Previously, it was proposed that the enhanced transfection efficiencies achieved with RGD-conjugated gemini surfactant-based lipoplexes may be due in part to their polymodal size distribution, which may heighten the use of multiple endocytotic pathways.[187] Likewise, the transfection achieved with the $\alpha = 0.2$ F87, P84 and L44 formulations might similarly be due in part to their size distributions. However, it is also worth noting that a polymodal size distribution is not observed in the diluted L44 samples incubated and measured at 37°C (Figure 5.5-4). Further investigation of cellular uptake and intracellular distribution could shed more light on the differences in transfection between the various formulations.

Despite having promising particle size and zeta potential characteristics for future use *in vivo*, these results cannot account for many of the differences in the *in vitro* transfection efficiency for these systems since the size and zeta potential of most mixtures are within a similar range (with the exception of the polydisperse samples shown in Table 5.5-2). Therefore, consideration of the physical interactions involved in the self-assembly of these materials might be useful in explaining the observed differences.

The work presented in Chapter 4 used phenomenological mixed micelle theories to characterize the tendency of the 16-3-16/pDNA complex to assemble into mixed nanoparticles with these Pluronics (at varying mole fractions of Pluronic). An interaction parameter, β, which quantifies the nature (synergism vs. antagonism) and strength of the interactions within these mixed amphiphile systems, and X_1, an estimate of the mole fraction of the Pluronic component within the resulting nanoparticles (at a particular concentration above the CMC), were calculated. Combining the findings of our previously

reported characterizations and the transfection efficiencies shown here, a number of relationships were identified that may give further insight into key aspects of these self-assembled nanoparticles that impact transfection. Firstly, in terms of the X_1 parameter, the concentrated mixtures (0.5 mM total surfactant concentration) used for the *in vitro* transfection experiments are estimated to produce transfection nanoparticles with a Pluronic mole fraction that is equal to the mole fraction of Pluronic in the mixture (denoted X_1^{stock} in Table B-4). Even following dilution with medium when added to the transfection well, this value remained roughly constant for all formulations except the L121 mole fraction 0.2 mixture, which indicates a large increase in X_1 to 0.711 upon dilution (denoted X_1^{stock} in Table C-5), and is close to but slightly under the calculated X_{ideal} value (0.769) expected for an ideal mixture with no net interaction between the Pluronic and 16-3-16/pDNA components. Although it is interesting to note the effect of dilution on these X_1 values, this dilution occurred in cell culture medium, not simply water. Even considering the particle size data for L44 remained relatively unchanged upon dilution in medium and heating to 37°C, the impact that the medium components would have on the self-assembly behaviour and subsequent nanoparticle composition remain unknown; therefore, the X_1^{well} values were not used for further analysis or discussion.

A significant increase in transfection efficiency was achieved with nanoparticles estimated to be enriched with the Pluronic component ("Pluronic-rich") versus those mixtures that produce "Pluronic-poor" nanoparticles (Figure 5.6-1). This finding suggests greater involvement of the Pluronic component in the transfection nanoparticles may be important for transfection. Considering the reported ability of Pluronics to improve the transfection efficiency of numerous non-viral formulations through interaction with lipid membranes or activation of cell signaling pathways that can enhance nuclear transport[57,76,91,100–103,107], we speculate that a greater presence of Pluronic may provide more opportunity for these critical events to occur. Alternatively, Pluronic-poor nanoparticles may leave excess Pluronic in solution, which is then free to interact with cell membranes and potentially inhibits internalization, as previously demonstrated by treatment of cells with L64 prior to introduction of PEI/pDNA transfection complexes.[51]

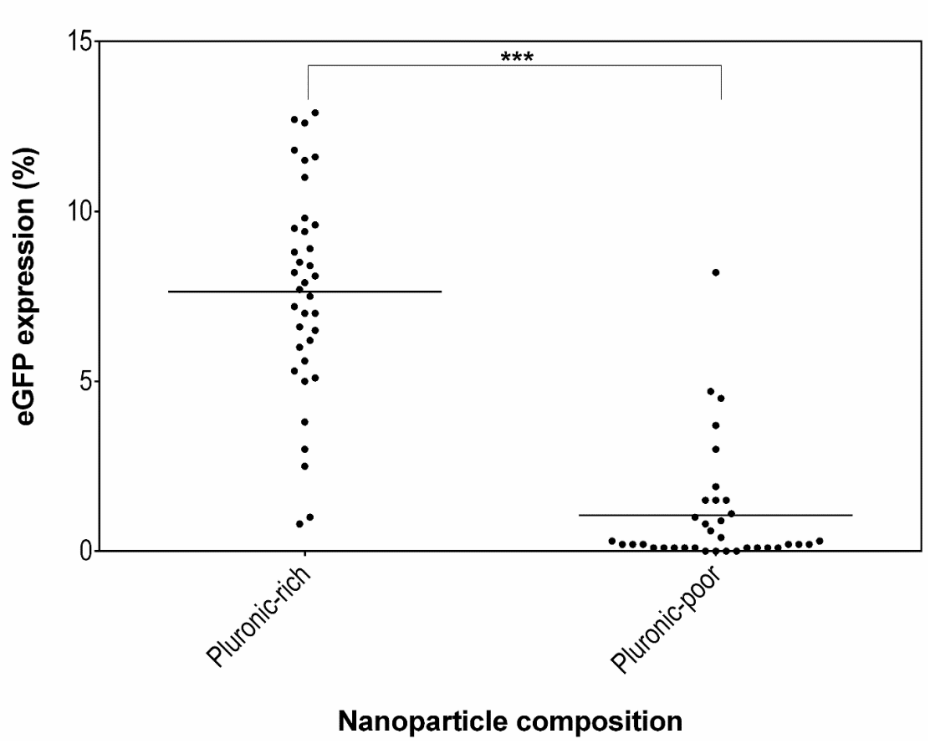

Figure 5.6-1 Transfection efficiency according to mixed nanoparticle composition (Pluronic-rich vs. Pluronic-poor nanoparticles) in the 0.5 mM stock mixture. ***p-value < 0.001

Moreover, the nature of the interaction between the components in these mixed micellar transfection formulations may also influence the transfection efficiencies. More specifically, the strength (represented by the magnitude of β) of the synergism in this formulation may be important. A linear trend is clearly seen in Figure 5.6-2, which shows there is a negative correlation between the interaction parameter value of the mixture and the transfection efficiency (or keeping in mind negative β values indicate synergistic interactions, transfection efficiency rises with increasing/stronger synergism). This trend may correspond to the nanoparticle's stability during delivery.

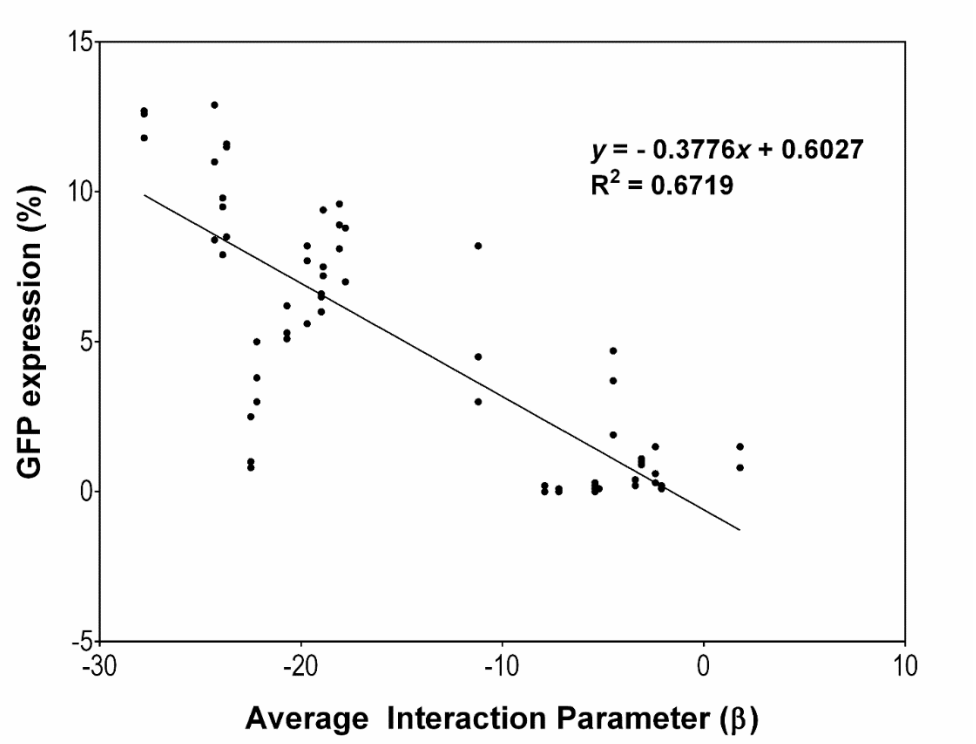

Figure 5.6-2 Relationship between transfection efficiency and the calculated Rubingh's interaction parameter (from Chapter 4)

While the relationships between transfection efficiency and interaction parameter or nanoparticle composition are apparent, it is also important to consider the impact of the Pluronic structure. For example, the length of the Pluronic PPO block is unmistakably related to transfection efficiency, with a steady decline in transfection efficiency occurring while hydrophobic PPO block lengths increase (Figure 5.6-3). After all, not only was the Pluronic structure (most notably the PPO block length) found to clearly influence mixing behaviours and nanoparticle composition (Chapter 4), previous reports also show a relationship between Pluronic composition and their effect on cells and model membranes that are in agreement with some of the structure-based differences in transfection efficiency shown here.

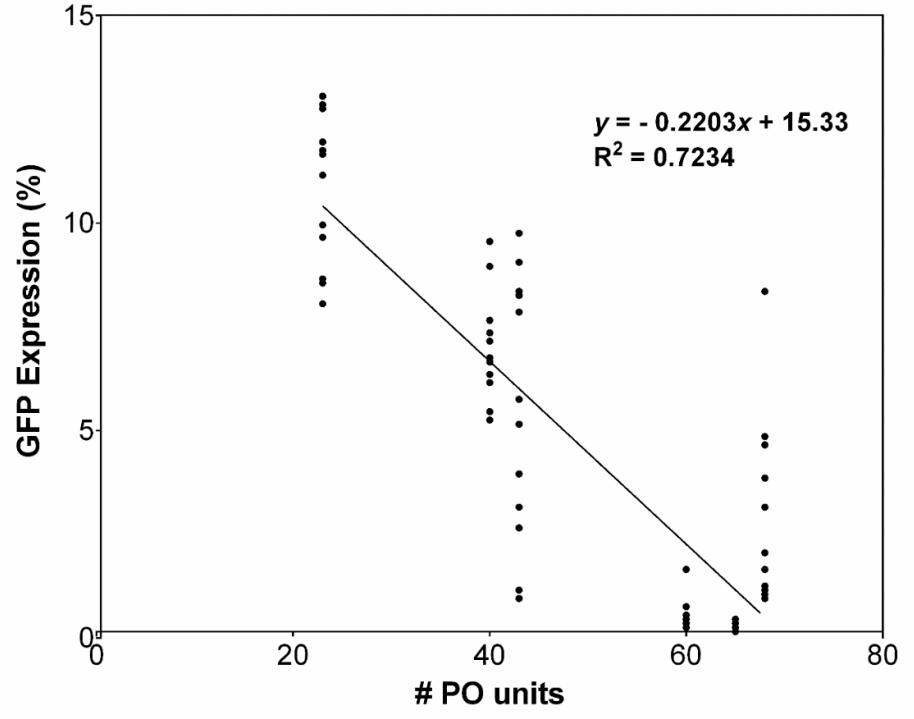

Figure 5.6-3 Relationship between transfection efficiency and number of PO units in the Pluronic component

For instance, previous work has demonstrated that both Pluronic PO and EO content influence the polymer's effect on cell membranes. Molecular dynamics simulations of Pluronic chain penetration in dipalmitoylphosphatidylcholine (DPPC) model membranes suggest that long PEO chains tend to adsorb just beneath the polar headgroup region of the lipid bilayer, interact with several lipid molecules and provide temporary stabilization to the membrane structure.[102] Conversely, short PEO chains are more likely localized in a small region of the membrane and pull the lipid headgroups internally, causing bending of the membrane[102] or formation of ion traversable pores.[105] Also, decreases in the PEO chain length (of Pluronics with an equal PPO length) have been associated with a slight increase in lipid flip-flop activity between the inner and outer leaflets of liposomes.[103] Further, in a systematic characterization of the optimal Pluronic structure for drug efflux modification in bovine brain microvessel endothelial cells, Group I polymers, consisting of hydrophilic Pluronics (similar to F87 and F127 in our case), were found to adhere to the plasma membrane but typically showed poor internalization, and intracellular accumulation was presumably limited to endocytic compartments.[104]

Conversely, hydrophobic Pluronics (HLB < 20) with intermediate-length PPO blocks (referred to as Group II), like that of P84 and P103, incorporated into and fluidized the cell membranes, spread throughout the cytoplasm (even reaching the nucleus to some extent), and were also associated with inhibiting ATP synthesis via changes to the electron transport in mitochondrial membranes.[104] Meanwhile, Group IIIa polymers similar to L44 that are classified as hydrophobic with a short PO block, showed a tendency to adhere to cell membranes, spread easily throughout the cytoplasm and reach the nucleus, similar to the behaviour of the intermediate hydrophobic Pluronic group.[104] However, in spite of their intracellular distribution, this group of polymers did not impact ATP levels.[104] On the other hand, Group IIIb consisting of hydrophobic polymers with a long PPO block (e.g. L121) showed significant fluidization of the plasma membrane due to its large hydrophobic PPO block and short PEO chains.[104,105] However, L121 was also found to anchor into the membrane and remain localized in endocytic compartments, suggesting an ability to decrease the microviscocity of plasma membranes but not intracellular membranes.[104] Moreover, the ability of Pluronics to bind cell membranes not only influences cellular uptake and distribution, but has also been shown to improve transfection by activating cell signaling pathways that enhance cellular uptake and nuclear transport of pDNA with a CMV promoter (recall, the pVG.telRL plasmid used in this study also contains a CMV promoter).[57]

In summary, the transfection achieved by these Pluronic/16-3-16/pDNA nanoparticles may be due to the Pluronic's ability to bind cell membranes, but in some cases these properties may also create limitations. For example, an initial expectation may be that greater membrane permeabilization by the Pluronic ultimately results in greater transfection efficiency. However, high levels of plasma membrane disruption by Pluronic L64 was previously associated with decreased cellular uptake and transfection efficiency of PEI/pDNA complexes due to inhibition of endocytosis in vitro.[51] Taken together, it can be hypothesized that differences in transfection by the Pluronic-rich F87, P84, and L44 nanoparticles may be due to loss of membrane integrity or energy depletion in cells treated by P84 nanoparticles compared to those with F87 or L44. Similarly, although transfection was achieved with the L121 systems, it may have been limited by poor endosomal escape, as previously reported with this particular Pluronic.

It is interesting to note Pluronics with similar hydrophobicity and membrane interaction classified by Batrakova et al.[104] do not necessarily show similar transfection efficiencies here. For example, despite both being hydrophilic polymers (Group I) which typically show poor cellular internalization

according to previous reports[104], F87-containing nanoparticles have significantly greater transfection efficiency over F127 nanoparticles. Similarly, both P84 and P103 should fluidize cell membranes and easily distribute throughout the cytoplasm based on their intermediate hydrophobicity[104]; however, P84 nanoparticles greatly out-perform the P103 nanoparticles. Admittedly, the current data does not allow us to distinguish whether enhanced transfection efficiency is due to an increased ability to overcome particular barrier(s); for example, increased cellular entry, endosomal escape, nuclear entry, or plasmid transcription. Even so, given the relationships shown in Figure 5.6-1 and Figure 5.6-4, these differences may be a reflection of the nanoparticle compositions and mixing behaviours that were determined in our previous work. The F87 and P84 mixtures show strong synergism between the 16-3-16/pDNA complex and the Pluronic component, and a greater Pluronic presence in the mixed nanoparticles. Perhaps more Pluronic content may create more opportunity for the Pluronics to act as biological response modifiers and improve transfection, compared to those nanoparticles that are considered Pluronic-poor (such as F127 and P103).

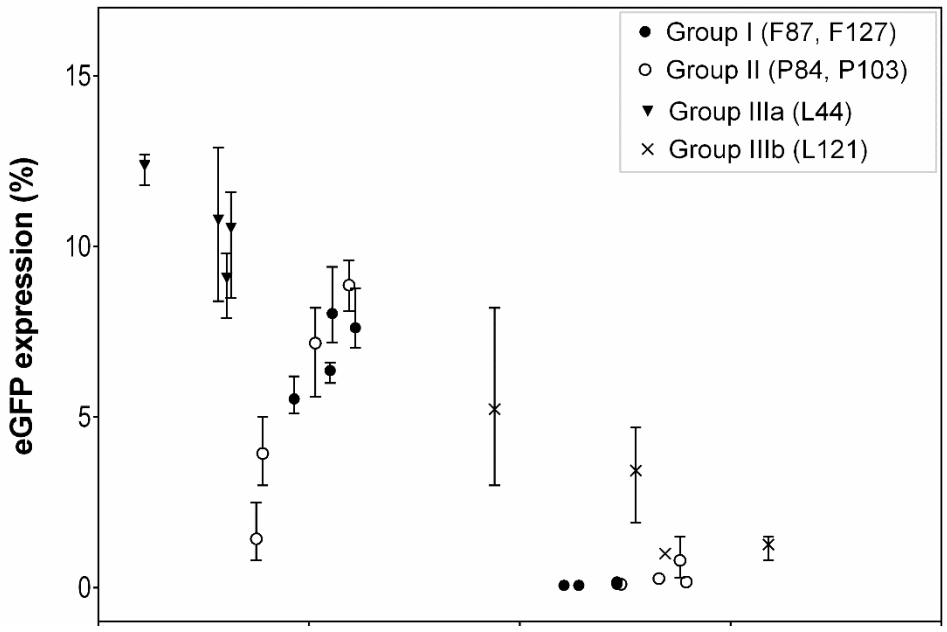

Figure 5.6-4 Effect of interaction parameter on transfection efficiency for different Pluronic categories previously described by Batrakova et al.[104] Mean values are represented by the symbols while error bars indicate the data range.

Although the L121 nanoparticles are considered Pluronic-poor, there is a measurable amount of transgene expression (compared to the negligible expression achieved by F127 and P103 nanoparticles), which increases with the synergistic interaction parameter values. The greatest level of GFP expression achieved from L121 nanoparticles was achieved from a Pluronic mole fraction of 0.8, which showed an intermediate level of synergism in our previous characterizations. Thus, in addition to nanoparticle composition, stronger attraction (synergism), represented by negative interaction parameter values, is likely also important (Figure 5.6-5). Although more investigation is needed, synergism may be related to the nanoparticles' ability to stay intact and protect the pDNA cargo while overcoming the many barriers to transfection. In fact, our previous work showed stronger synergism was associated with lower levels of ethidium bromide – DNA binding due to less dissociation of gemini molecules from the pDNA complex when Pluronic is added, which supposedly maintains the condensed pDNA form. While this may turn out to be an important feature for successful delivery *in vivo*, it is also worth noting that our previous characterization of the 16-3-16/pDNA complex (without Pluronic) suggests the cationic gemini surfactant does not completely dissociate from the plasmid DNA even when diluted below its critical aggregate concentration.[136] This might limit the transfection efficiency due to incomplete unpacking of the pDNA cargo for transcription.[24] Nonetheless, further research is required to confirm these hypotheses.

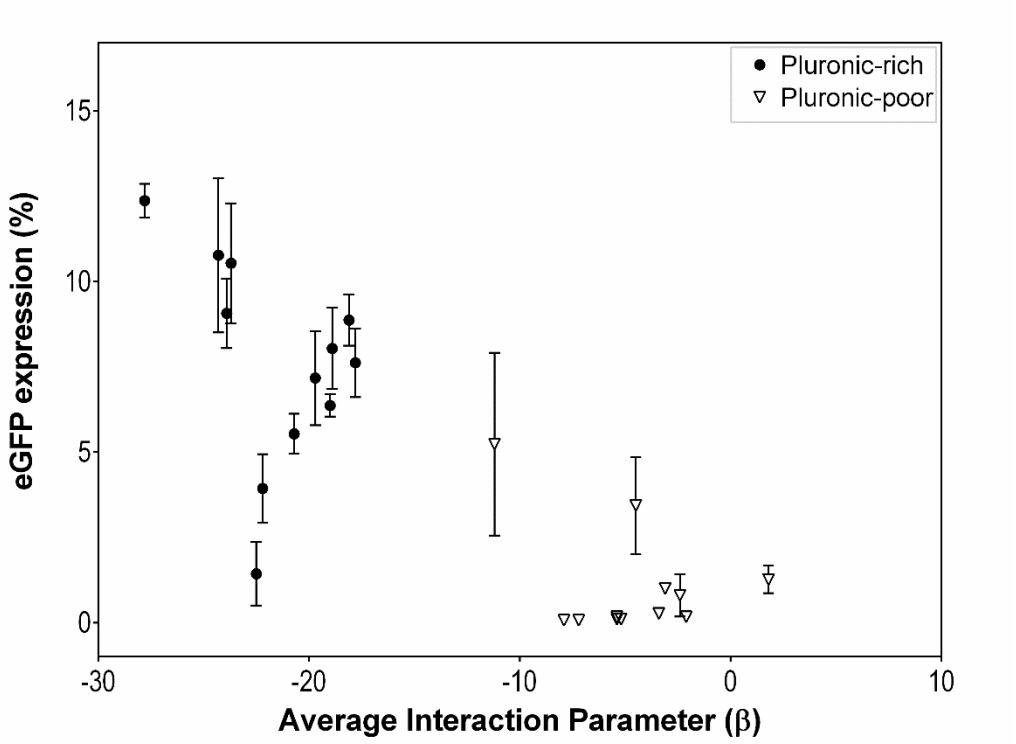

Figure 5.6-5 Simultaneous effect of interaction parameter and nanoparticle composition on transfection efficiency. Mean values are plotted with error bars representing standard deviation.

Unfortunately, data from the L121 series is also complicated by poor solubility of L121 in aqueous solution at room temperature and above, which may impact the stability of the nanoparticles under the *in vitro* transfection conditions. (Note the cloud point of 1% aqueous solution of L121 is 14°C.[76]) The increased variability observed in the L121 transfection efficiencies, especially for the 0.8 L121 mole fraction (depicted by larger error bars in Figure 5.5-6) may be due to possible phase separation. Additionally, the L121 nanoparticle sizes and zeta potentials reported here were collected at 4°C to avoid phase separation during the measurement and also reflect the incubation conditions of these mixtures prior to use for *in vitro* transfection. However, size data collected at 25°C (Table C-2) generally show larger PDI values, most notably in the 0.8 mole fraction mixture, which may also reasonably occur at 37°C and under the conditions used for the *in vitro* transfection assays. This may be an indication of reduced stability for these systems but it is interesting to note that these changes are associated with greater transfection efficiency. Although multi-modal size distributions are not present,

this might be related to what was observed with the polydispersed samples of 0.2 mole fraction F87, P84 and L44 mixtures, and may be worth exploring further.

5.6.1 Cross-validation model for transfection efficiency prediction

With our current data, a preliminary cross-validation model using the interaction parameter (β), nanoparticle composition (X_1^{stock} vs. X_{ideal}), and Pluronic structure, represented by

Equation 5.6-1 and Equation 5.6-2 (depending on nanoparticle composition), was able to predict the transfection efficiency (% eGFP expression) with an average mean standard error of 1.95.

$$\text{eGFP}_{Pluronic-rich} = 11.69 - 2.22(\text{R}) + 20.33(\alpha_1) - 0.06(\beta) - 0.68(\text{PO} \times \alpha_1) + 0.04(\text{PO} \times \text{R})$$

Equation 5.6-1

$$eGFP_{Pluronic-poor} = -1.81 - 2.22(R) + 40.79(\alpha_1) - 0.49(\beta) - 0.68(PO \times \alpha_1) + 0.04(PO \times R)$$

Equation 5.6-2

Where R is the PO/EO weight ratio, α_1 is the mole fraction of Pluronic present in the mixture, PO is the number of PO units in the Pluronic structure, and β is the interaction parameter (from Chapter 4). For formulations where a Pluronic-rich nanoparticle expected ($X_1^{stock} > X_{ideal}$), the eGFP prediction is represented by Equation 5.6-1; whereas the eGFP expression prediction for Pluronic-poor nanoparticle formulations ($X_1^{stock} > X_{ideal}$) is represented by Equation 5.6-2. From the above equations, we see that in addition to the effect of the interaction parameter, and nanoparticle composition, the mole fraction of Pluronic in the overall mixture, and the Pluronic's PO/EO ratio also have an influence on the eGFP prediction. For the purpose of improving the model's predictions, the number of PO units was excluded as a main effect (because it increased the MSE value), but the 2-factor interactions in the above equations demonstrate that PO content influences the effects that the PO/EO ratio and Pluronic mole fraction have on the eGFP expression. As seen in Figure 5.6-6A, for a given PO/EO ratio a smaller PPO block results in greater transfection efficiency. Similarly, lower PO content generally increases transfection efficiency at a given Pluronic mole fraction in the formulation mixture (Figure 5.6-6B). Considering the strong correlation between PO and β, previously identified in Figure 4.6-1, the effect of PO is already accounted for by the presence of β in the model and the addition of a PO term as a main effect would likely cause over-fitting of the current data and worsen the prediction. However, the

replacing the β terms with PO will also increase the MSE and compromise the prediction. Likewise, PO was also shown to have a strong influence on nanoparticle composition (Pluronic-rich vs. Pluronic-poor), which is already reflected in Equation 5.6-1 and Equation 5.6-2.

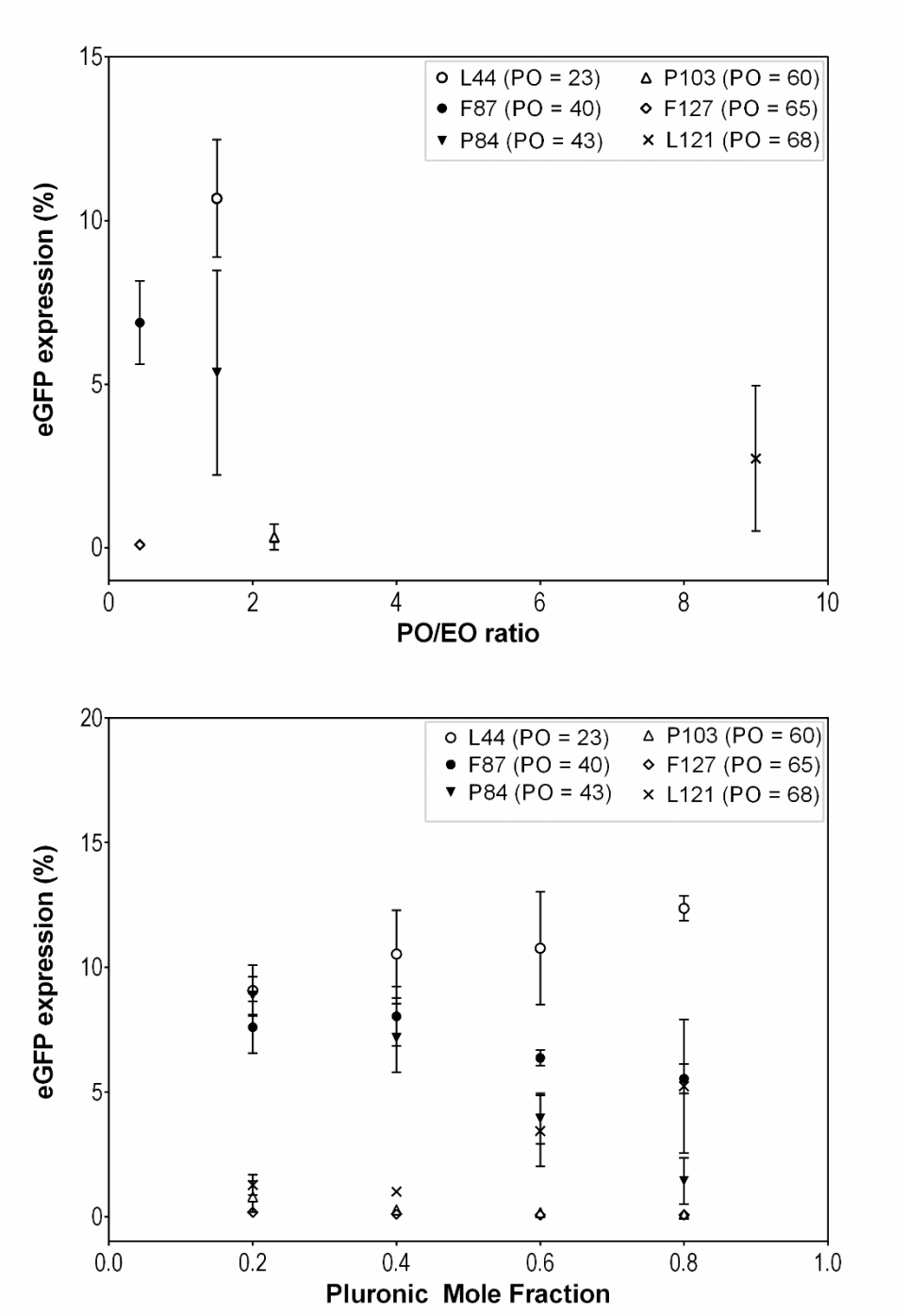

Figure 5.6-6 A) Influence of PO content on the effect of Pluronic PO/EO weight ratio on transfection efficiency. **B)** Influence of PO content on the effect of Pluronic mole fraction on transfection efficiency.

For comparison, a linear regression model without any of the β or X_1^{stock} terms had an MSE of 7.43, which indicates a large improvement in the prediction with the addition of the mixed micellization parameters (Equation 5.6-3).

$$\text{eGFP} = 3.03 + 3.76(\text{R}) + 13.10(\alpha_1) - 0.28(PO \times \alpha_1) - 0.05(PO \times R)$$

Equation 5.6-3

In this case, without the use of mixed micellization parameters, the average MSE can be improved to a value of 3.86 by simply adding the number of PO units as a main effect (Equation 5.6-4).

$$eGFP = 23.00 - 0.37(PO) - 2.96(R) - 4.60(\alpha_1) + 0.07(PO \times \alpha_1) + 0.05(PO \times R)$$

Equation 5.6-4

As seen in Figure 5.6-7 , the predictions from Equation 5.6-4 do not appear very different from those of Equation 5.6-1 and Equation 5.6-2; however, interaction studies may still have a place in helping to explain differences in transfection efficiency between systems that are seemingly similar based on the Pluronic molecular structure and formulation composition.

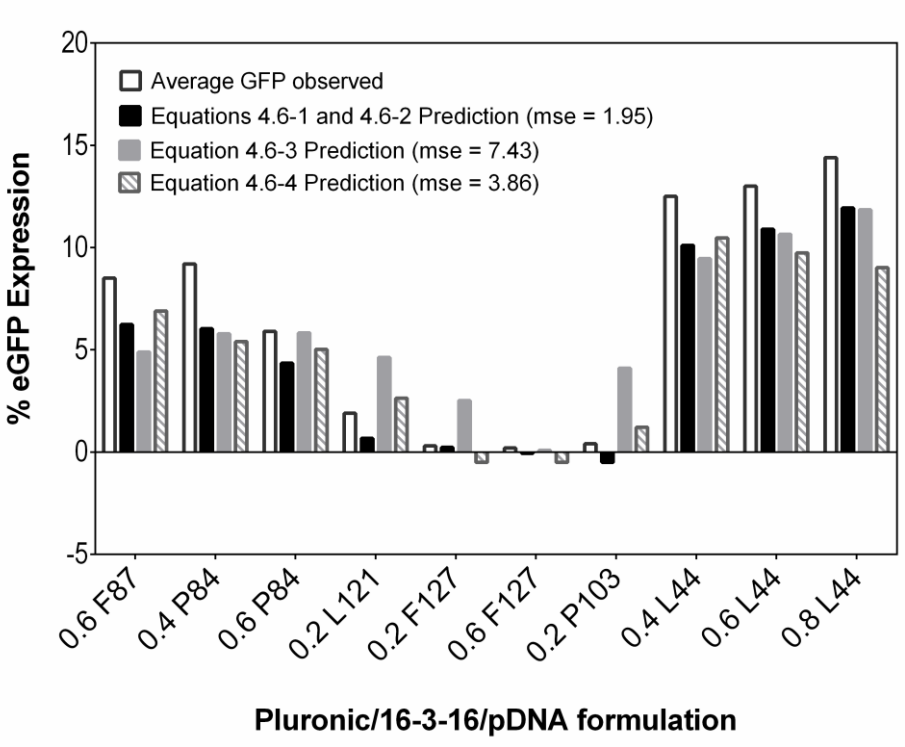

Figure 5.6-7 Comparison of experimentally observed transfection efficiencies for randomly selected Pluronic/16-3-16/pDNA formulations versus predicted values from the cross-validation models discussed above.

The above analysis demonstrates the utility of interaction studies, such as that used in our previous work (Chapter 4), within the development process of formulations that involve mixed micelles. With the relationships currently identified, one could likely exclude Pluronic/16-3-16/pDNA combinations that demonstrate antagonism or weak synergism. Perhaps by establishing a basic relationship between mixing behaviours and transfection efficiency, like that shown here, similar interaction studies might be useful in predicting the success of future formulations of a similar nature or as an additional screening tool during the optimization process

5.7 Conclusion

In vitro transfection efficiency in COS-7 cells were clearly dependent on the Pluronic composition of the Pluronic/16-3-16/pDNA transfection complexes; meanwhile, cell viability was not significantly impacted by the treatments/concentrations used. To our knowledge, this is the first report showing a

clear relationship between transfection efficiency and parameters determined from phenomenological mixed micelle theories. Of note, nanoparticles enriched with the Pluronic component, and those with strong synergistic interactions and mixed micelle stability were associated with greater *in vitro* transfection efficiency. The trends revealed here may lead to greater understanding of the physicochemical properties involved in the transfection success or failure of these systems *in vitro*, and in the future, may inspire the use of such interaction studies as an additional tool for formulation assessment or screening.

Chapter 6
Conclusions and Future Directions

With recent successes in improving the safety of recombinant viral vectors and increasing efficiency of liposomal formulations for gene delivery to treat genetic diseases, the potential of gene therapy has finally reached the market. However, many synthetic gene therapy carriers in development continue to suffer from poor transfection efficiency. One such example, is the combination of the 16-3-16 gemini surfactant and National Formulary-grade Pluronic block copolymers, which was previously tested in the Wettig lab for *in vitro* delivery of pDNA to OVCAR-3 cells but showed limited transfection efficiencies. In this work, the pDNA/16-3-16/Pluronic formulation was revisited by expanding to other Pluronic compositions and evaluating the self-assembly tendencies involved in the formation of these nanoparticles.

In Chapter 3, a critical aggregate concentration was reported for the 16-3-16/pDNA condensate (also referred to as a "complex") prepared at a (N^+/P^-) charge ratio of 10:1. Based on the physical changes detected by tensiometry, conductivity, and light scattering methods as the pre-formed complex was titrated into water, it is suggested that the 16-3-16/pDNA complex only partially dissociates upon dilution in water. This is thought to result in a "loose" aggregate structure as some of the surfactant monomers likely dissociate from the complex, as evidenced by larger particle sizes and a steep slope in the conductivity curve that decreases to a slower rate of change as the concentration of 16-3-16/pDNA added to the system increases. Once the CAC is reached (indicated by a breakpoint in each of these characterizations), a more condensed complex re-forms. Surface activity was also detected for this complex, which allowed for: 1) CAC determination through tensiometry, 2) treatment of 16-3-16/pDNA as a single amphiphilic component in the pDNA/16-3-16/Pluronic mixtures, and 3) mixing behaviour characterizations in the presence of the intended pDNA cargo.

Addition of the various Pluronic block copolymers to the 16-3-16/pDNA complex generally showed mixing of these two components is energetically favourable, with the exception of L121 at a mole fraction of 0.2, which showed antagonistic mixing. More importantly, the magnitude of the synergistic interactions responsible for the mixed micelle stability is influenced by the Pluronic molecular structure, and the composition of the mixture. Contrary to the initial hypothesis, longer Pluronic PPO blocks are associated with decreased synergism, which is thought to be due to greater steric hindrance

that opposes mixed micelle formation. Depending on the PO content, the deviations from ideal mixed micellization are attributed to different micelle compositions; for PPO block lengths of approximately 20 – 43 units (like that of L44, F87, and P84), the mixed aggregates are rich in the Pluronic component, whereas larger PO blocks result in 16-3-16/pDNA-rich mixed aggregates. While the PO content is the primary factor that dictates the interaction parameter value, there is generally a small but statistically significant decrease in β with increasing PEO chain lengths, which might be attributed to favourable charge neutralization between adjacent gemini surfactant headgroups by intercalation of PEO chains. Nevertheless, the effect of PO on the interaction parameter was also found to be influenced by the number of EO units (and vice versa), and the overall percentage of EO. In addition, increasing the mole fraction of Pluronic in the mixture also increased the synergism, but this effect appears to be independent of the effect(s) of PO content. Finally, reducing the N^+/P^- charge ratio to 5:1 increased the synergism of the F87 system, indicating that the presence of pDNA also plays a role in the mixed aggregate formation and should be explored further.

Similar to previous literature reports, ethidium bromide-DNA binding studies indicate that addition of Pluronic to the 16-3-16/pDNA complex results in some de-condensation of the complex. In general, the level of dye binding (DNA de-condensation) is inversely related to the synergism present in the mixture. Although the exact mechanism of mixed micelle formation is unknown for these systems, these results may indicate encapsulation of the pDNA/16-3-16 complex in Pluronic-rich nanoparticles versus - de-mixing that allows for greater ethidium bromide binding in the Pluronic-poor nanoparticles.

Most of the formulations tested produce nanoparticles with sizes below 250 nm, which is desirable for future *in vivo* applications to reduce clearance by glomerular filtration and potentially for passive targeting of tumors with a strong EPR effect (although the existence of an EPR effect is debatable). The different polymers and mole fractions used generally show no effect on the nanoparticle sizes (only the F87, P84 and L44 samples with Pluronic mole fractions of 0.2 showed size polydispersity), but longer PEO chain lengths appear to introduce shielding effects that generally decreased the zeta potential of the nanoparticles. In terms of *in vitro* transfection efficiency in COS-7 cells, reporter gene expression (eGFP) varies significantly depending on the Pluronic and the mole fraction in the formulation. In general, Pluronics with smaller PPO blocks, such as L44, F87 and P84, show greater transfection, but only the formulation containing L44 at mole fraction 0.8 produces a statistically significant increase in transfection compared to the 16-3-16/pDNA complex (without Pluronic). The

Pluronic mole fraction also influences the transfection efficiencies, but this effect varies for different Pluronics. No significant reduction in cell viability was detected, which is partly attributed to restricting the 16-3-16 concentration to well below the IC_{50} of the gemini surfactant.

The differences in transfection efficiencies observed in these systems reflect some of the trends previously reported in the literature between cell membrane interactions and Pluronic structure and hydrophobicity. In particular, hydrophobic polymers with short PPO blocks are known to bind cellular membranes and spread throughout the cytoplasm, which may have contributed to the L44 formulations showing the highest transfections throughout. In addition to PPO block length, the PO/EO ratio, and mole fraction of Pluronic in the formulation mixture appeared to influence the transfection efficiencies that were observed for these systems. In contrast, the hydrodynamic diameter of the various nanoparticles did not assist in understanding the differences in transfection efficiencies between the systems since the majority of the particles were so similar in size. Furthermore, transfection showed a general increase with more positive zeta potentials, but the results were still quite variable even at high magnitudes.

Taking all findings reported in this work into account, some important relationships between transfection efficiency and the estimated mixing behaviours involved in the Pluronic/16-3-16/pDNA nanoparticle self-assembly have come to light. Most notably, transfection increased with stronger synergistic interactions in the mixed systems, which is thought to be an indication of a sufficient level of nanoparticle stability necessary for protection of the pDNA. The ethidium bromide binding studies are also generally consistent with this theory since those mixtures with stronger synergism appear to maintain a condensed pDNA state more than those with medium or weak synergism. Synergism resulting from a greater presence of the Pluronic component in the nanoparticles is also associated with higher transfection efficiency (as opposed to the nanoparticles that are considered “Pluronic-poor”), which might be attributed to the Pluronics’ cell membrane interactions and activity as biological response modifiers.

As seen with the Pluronic/16-3-16/pDNA system, the rational design approach for non-viral gene therapy formulation development does not guarantee improvements to transfection efficiency; however, the influence of interaction parameter and mixed micelle composition on transfection efficiency can be used for guiding the optimization of these systems in future work. Furthermore, few methods exist for screening the formulations early on, but the work presented in Chapter 5 demonstrates

that predictions of *in vitro* transfection efficiencies can be improved by taking these mixed micellization parameters into account. This points to the importance of considering *and quantifying* the interactions within self-assembled gene delivery carriers, especially for systems like the Pluronic/16-3-16/pDNA nanoparticles that cannot be distinguished by parameters such as particle size or zeta potential.

Based on the results of this work, for a Pluronic mixture with 16-3-16/pDNA complexes having a charge ratio of 10:1 it is recommended to pursue mixtures that have strong synergism (indicated by a negative interaction parameter with a large magnitude) and a mixed aggregation composition that is rich in the Pluronic component (as opposed to the 16-3-16/pDNA component), as these mixtures should have the greatest potential for maximizing transfection efficiency. According to the findings of Chapter 4, this would likely require a Pluronic with a small PPO block (less than 60 units), at larger Pluronic mole fraction. Although % PEO showed some influence on synergism, its effect is also influenced by the PPO length (and vice versa). Based on the small sample size of this study, a lower % PEO is recommended for increasing synergism with small PPO block Pluronic mixtures, but more work to confirm these trends is still needed.

6.1 Future Directions

6.1.1 Further Characterization of Mixed Micelle Formation

A number of additional mixtures and techniques have been identified as potential extensions of this work in order to build a deeper understanding of the Pluronic/16-3-16/pDNA systems, and potentially confirm some of the more speculative points made during the interpretation of the non-ideal mixing interactions that are presented.

The relationships between the Pluronic molecular structure and interaction parameter could be strengthened by testing other Pluronic block copolymers. For example, expansion of the 40% PEO group to include Pluronic P104, which consists of approximately 61 PO units, would add a third data set to the series to help confirm the effect of PPO length across the entire range of PO for the 40% PEO. Similarly, to investigate whether other highly lipophilic Pluronics would also show any antagonistic mixing with the 16-3-16/pDNA complex, it would be interesting to test polymers such as L81 and L62, which have only 10% and 20% PEO, respectively, but much smaller PPO blocks compared to L121 (43 and 31 PO units, respectively). Furthermore, the current study only included 2 polymers with PEO

chains longer than 50 EO units – future work should also include Pluronics with PEO chains greater than 50 units.

Isothermal titration calorimetry studies would be a valuable addition to the physical characterization of these mixtures, as deviations from ideal mixing conditions may be confirmed through calorimetrically determined enthalpies of mixed micelle formation (and subsequent calculation of excess enthalpies of mixing). Similar to previous literature reports, some additional characterization may also include DLS measurements to monitor changes in hydrodynamic diameter over a range of Pluronic concentrations as the polymer is titrated into a solution of 16-3-16/pDNA complexes. Smaller aggregates resulting from aggregation of pure gemini surfactant or polymer could potentially be detected as a result of dissociation from the pDNA complex (using DLS or nanoparticle tracking analysis). If these results can be observed, it may offer confirmation of antagonistic mixing, for example in the 0.2 mole fraction L121 sample where the Pluronic is expected to form aggregates separate from the mixed micelle, or may even support the ethidium bromide study results presented here. Appearance of aggregates of a size consistent with that of a Pluronic/16-3-16 aggregate might be evidence that the 16-3-16 dissociates from the gemini/pDNA complex to bind to the Pluronic component, leading to de-condensation of the pDNA. Alternatively, equilibrium dialysis could also be useful in determining whether gemini surfactant binding to the Pluronic block copolymers in solution is responsible for the pDNA de-condensation results that are observed.

Two-dimensional nuclear magnetic resonance (NMR) spectra, specifically nuclear Overhauser effect spectroscopy (NOESY), have also been helpful additions to mixed micelle studies since the intermolecular cross-peaks help identify atoms that are in close proximity (<0.5 nm) to each other. Admittedly, the presence of pDNA in these particular systems, may make the spectra too complex to interpret.

The ratio of the first and third vibronic peaks of the pyrene fluorescence emission spectrum provides a measure of the polarity of the medium that the pyrene is dissolved in (i.e. the micelle core). As seen in previous literature reports, antagonistic mixing behaviour can be attributed to differences in the micropolarity of the pure components. Therefore, it would be worthwhile to measure the micropolarity of the pure Pluronic micelles, and the 16-3-16/pDNA complex as another means of understanding the differences in mixed aggregate stabilities. Similarly, the micropolarities of the 16-3-16/pDNA complexes with different charge ratios (for example, N^+/P^- 5:1 versus 10:1) should be compared, as this

might provide an explanation for the stronger synergism observed in the F87 mixtures with the 5:1 complex.

6.1.2 Improvements for Transfection Efficiency

As previously discussed, the gene delivery vector and pDNA cargo need to overcome several barriers prior to transgene expression. Seeing as the level of cellular entry can account for variations in transfection efficiency, cellular uptake studies are a recommended addition to this work. Cellular uptake is often determined by fluorescently tagging the pDNA to be delivered, followed by quantification of the fluorescent probe within the cells by techniques such as flow cytometry. Similarly, co-localization of fluorescently-labelled pDNA or nanoparticle components and various cellular compartments visualized by live cell confocal microscopy is typically used to learn more about the vector's distribution throughout the cell. For example, co-localization of the pDNA and lysosome fluorescent signals would qualitatively indicate poor endosomal escape. Alternatively, localization at the nucleus is usually observed for nanoparticles that achieve high transfection. However, it is important to acknowledge that the presence of a fluorescent probe may alter the self-assembly of the system (through increased hydrophobic effect), or cleavage of the dye from the nanoparticle within biological systems can produce fluorescent metabolites that cannot be distinguished from the labelled molecule of interest. Some more recent cellular uptake and distribution studies of gemini surfactant-based vectors have used label-free methods such as differential centrifugation (to isolate organelles/subcellular fractions of interest, such as the nuclei, cytosol, plasma membranes, and endosomes), followed by quantification of the gemini surfactant component within each fraction using mass spectrometry.[71]

Efforts to improve the transfection efficiency of a non-viral system often include the use of targeting ligands to increase uptake in the cells of interest. This approach also has potential to improve the Pluronic/16-3-16/pDNA systems proposed here, where the terminal hydroxyl groups of the Pluronic would most likely be exploited for functionalizing the nanoparticle. However, these modifications may only be practical for formulations with synergistic interactions, since de-mixing of the nanoparticle components might negate the effects of a targeting moiety if the functionalized component (e.g. labelled Pluronic) dissociates and is internalized by the cells separate from the pDNA component.

Due to high transfectability, the COS-7 cells are often used as a standard cell line for non-viral transfection studies in general, and especially utilized in the evaluation of numerous gemini surfactant-based formulations.[194] Hence, the use of COS-7 cells was the most appropriate starting point for the

stage of exploration in this work. However, in order to assess the potential of these formulations as cancer treatments, transfection studies should also be conducted in a cancer cell line *in vitro* as well as an *in vivo* model appropriate for the disease of interest. For example, this research project was initiated with a particular focus on gene therapy of ovarian epithelial cell cancer; thus the OVCAR-3 or OVCAR-8 cell lines would be suggested for use as *in vitro* models which can also be used for aggressive tumor formation in xenograft mouse models.[195] Still, factors such as gene mutations of interest, formation of ascites fluid, and chemotherapy sensitivity will also influence the choice of cell line. More recent improvements to *in vitro* models such as three-dimensional spheroids derived from either primary patient cells or cell lines also provide an opportunity to gather transfection data that is more reflective of the cellular responses *in vivo*.[196,197] Typically, *in vitro* transfection efficiencies have poor translation *in vivo*; however, this will depend on the disease of interest, the models used, and the formulation. In fact, the *in vivo* results of the amino acid substituted gemini surfactant-based systems for vaginal genetic vaccination reflected those seen *in vitro*.[94] Even so, the *in vitro-in vivo* correlation for the Pluronic/gemini surfactant systems need to be determined.

The transfection achieved with all of the formulations explored in this work were still significantly below the commercially available reagent, Lipofectamine 2000. Despite the comparatively low transfection efficiencies seen to date with these Pluronic/16-3-16/pDNA systems, the previous studies conducted in OVCAR-3 cells used higher concentrations of the transfection reagents than were used in this work, and showed greater cell viability than Lipofectamine 2000. Therefore, a gemini surfactant and Pluronic combo remains of interest. Although more characterization is needed, based on the solution behaviour of the 16-3-16/pDNA complex described in Chapter 3 and the ethidium bromide fluorescence studies reported in Chapter 4, it is conceivable that the low transfection efficiencies of the mixtures may be related to strong binding between the pDNA and gemini surfactant which may be hindering efficient endosomal escape, nuclear import and/or transcription of the pDNA on account of incomplete de-condensation and dissociation from the 16-3-16 molecules. Granted, those mixtures showing greater synergism (suggesting greater nanoparticle stability during delivery) and greater pDNA condensation (estimated by lower EtBr binding) produced the highest transgene expression, but it may be a matter of striking a balance between the two to achieve sufficient pDNA release at the correct moment. Thus, in addition to testing other Pluronic copolymers (as previously discussed), efforts to improve the transfection efficiency of the Pluronic/gemini/pDNA system could include

changes to the charge ratio of the 16-3-16/pDNA complex, the order of mixing, use of different gemini surfactants, or nanoparticle preparation in the presence of added salt.

Although many of these suggested changes to the formulation would likely alter the strength and possibly the nature of the interactions within the mixtures, the work in this thesis clearly demonstrates that researchers in the field of self-assembled gene therapy formulation *must* consider and continue to systematically study the interactions within these multi-component systems in the presence of the genetic cargo as much as possible. Uncovering conditions that contribute to higher (or lower) transfection efficiency could be valuable in designing and optimizing more successful non-viral gene therapy systems.

References

1 M. Donkuru, I. Badea, S. Wettig, R. Verrall, M. Elsabahy and M. Foldvari, Advancing nonviral gene delivery: Lipid- and surfactant-based nanoparticle design strategies, *Nanomedicine*, 2010, **5**, 1103–1127.

2 J. Sobczyński and B. Chudzik-Rząd, *Mixed micelles as drug delivery nanocarriers*, 2018.

3 D. Myers, *Surfactant Science and Technology*, John Wiley & Sons, Inc., Hoboken, Third., 2006.

4 K. C. Tam and E. Wyn-Jones, Insights on polymer surfactant complex structures during the binding of surfactants to polymers as measured by equilibrium and structural techniques, *Chem. Soc. Rev.*, 2006, **35**, 693.

5 M. J. Rosen, in *Surfactants and Interfacial Phenomena*, John Wiley & Sons, Inc., Hoboken, NJ, USA, 2004, pp. 105–177.

6 S. D. Wettig, University of Saskatchewan, 2000.

7 A. M. S. Cardoso, S. G. Silva, M. Luísa do Vale, E. F. Marques, M. C. Pedroso De Lima and A. S. Jurado, in *Engineering of Nanobiomaterials*, 2016, pp. 227–256.

8 A. E. Hargreaves, *Chemical Formulation: An Overview of Surfactant Based Chemical Preparations Used in Everyday Life*, Royal Society of Chemistry, Cambridge, 2003.

9 T. F. Tadros, *Applied Surfactants: Principles and Applications*, Wiley, 2005.

10 M. J. Rosen, *Surfactants and Interfacial Phenomena*, John Wiley & Sons, Inc., Hoboken, NJ, USA, 2004.

11 X. B. Zhao and R. J. Lee, Tumor-selective targeted delivery of genes and antisense oligodeoxyribonucleotides via the folate receptor, *Adv. Drug Deliv. Rev.*, 2004, **56**, 1193–1204.

12 D. Wang and G. Gao, State-of-the-art human gene therapy: Part II. gene therapy strategies and clinical applications, *Discov. Med.*, 2014, **18**, 151–161.

13 S. L. Ginn, A. K. Amaya, I. E. Alexander, M. Edelstein and M. R. Abedi, Gene therapy clinical trials worldwide to 2017: An update, *J. Gene Med.*, 2018, **20**, 1–16.

14 M. L. Edelstein, M. R. Abedi and J. Wixon, Gene therapy clinical trials worldwide to 2007—an update, *J. Gene Med.*, 2007, **9**, 833–842.

15 S. D. Patil, D. G. Rhodes and D. J. Burgess, DNA-based therapeutics and DNA delivery systems: a comprehensive review., *AAPS J.*, 2005, **7**, E61–E77.

16 D. V Schaffer, J. T. J. T. Koerber and K. Lim, Molecular engineering of viral gene delivery vehicles, *Annu. Rev. Biomed. Eng.*, 2008, **10**, 169.

17 R. Gardlík, R. Pálffy, J. Hodosy, J. Lukács, J. Turna and P. Celec, Vectors and delivery systems in gene therapy., *Med. Sci. Monit.*, 2005, **11**, RA110-A121.

18 C. S. Lee, E. S. Bishop, R. Zhang, X. Yu, E. M. Farina, S. Yan, C. Zhao, Z. Zeng, Y. Shu, X. Wu, J. Lei, Y. Li, W. Zhang, C. Yang, K. Wu, Y. Wu, S. Ho, A. Athiviraham, M. J. Lee, J. M. Wolf, R. R. Reid and T. C. He, Adenovirus-mediated gene delivery: Potential applications for gene and cell-based therapies in the new era of personalized medicine, *Genes Dis.*, 2017, **4**, 43–63.

19 Gene Therapy Clinical Trials Worldwide, http://www.abedia.com/wiley/vectors.php, (accessed 4 April 2020).

20 D. Gomes-Silva and C. A. Ramos, Cancer Immunotherapy Using CAR-T Cells: From the Research Bench to the Assembly Line, *Biotechnol. J.*, 2018, **13**, 1–8.

21 Z. Zhou, X. Liu, D. Zhu, Y. Wang, Z. Zhang, X. Zhou, N. Qiu, X. Chen and Y. Shen, Nonviral cancer gene therapy: Delivery cascade and vector nanoproperty integration, *Adv. Drug Deliv. Rev.*, 2017, **115**, 115–154.

22 A. Akinc, M. A. Maier, M. Manoharan, K. Fitzgerald, M. Jayaraman, S. Barros, S. Ansell, X. Du, M. J. Hope, T. D. Madden, B. L. Mui, S. C. Semple, Y. K. Tam, M. Ciufolini, D. Witzigmann, J. A. Kulkarni, R. van der Meel and P. R. Cullis, The Onpattro story and the clinical translation of nanomedicines containing nucleic acid-based drugs, *Nat. Nanotechnol.*, 2019, **14**, 1084–1087.
23 R. Rai, S. Alwani and I. Badea, Polymeric nanoparticles in gene therapy: New avenues of design and optimization for delivery applications, *Polymers (Basel).*, 2019, **11**, 745.
24 X.-X. Zhang, T. J. McIntosh and M. W. Grinstaff, Functional lipids and lipoplexes for improved gene delivery, *Biochimie*, 2012, **94**, 42–58.
25 J. Chen, Z. Guo, H. Tian and X. Chen, Production and clinical development of nanoparticles for gene delivery, *Mol. Ther. - Methods Clin. Dev.*, 2016, **3**, 16023.
26 A. Pathak, S. Patnaik and K. C. Gupta, Recent trends in non-viral vector-mediated gene delivery, *Biotechnol. J.*, 2009, **4**, 1559–1572.
27 C. Pichon, L. Billiet and P. Midoux, Chemical vectors for gene delivery: uptake and intracellular trafficking, *Curr. Opin. Biotechnol.*, 2010, **21**, 640–645.
28 S. Y. Wong, J. M. Pelet and D. Putnam, Polymer systems for gene delivery—Past, present, and future, *Prog. Polym. Sci.*, 2007, **32**, 799–837.
29 B. S. Pattni, V. V. Chupin and V. P. Torchilin, New Developments in Liposomal Drug Delivery, *Chem. Rev.*, 2015, **115**, 10938–10966.
30 M. Yousefpour Marzbali and A. Yari Khosroushahi, Polymeric micelles as mighty nanocarriers for cancer gene therapy: a review, *Cancer Chemother. Pharmacol.*, 2017, **79**, 637–649.
31 A. V. Kabanov, P. Lemieux, S. Vinogradov and V. Alakhov, Pluronic® block copolymers: Novel functional molecules for gene therapy, *Adv. Drug Deliv. Rev.*, 2002, **54**, 223–233.
32 D. E. Owens and N. A. Peppas, Opsonization, biodistribution, and pharmacokinetics of polymeric nanoparticles, *Int. J. Pharm.*, 2006, **307**, 93–102.
33 H. Hatakeyama, H. Akita and H. Harashima, A multifunctional envelope type nano device (MEND) for gene delivery to tumours based on the EPR effect: A strategy for overcoming the PEG dilemma, *Adv. Drug Deliv. Rev.*, 2011, **63**, 152–160.
34 F. Danhier, To exploit the tumor microenvironment: Since the EPR effect fails in the clinic, what is the future of nanomedicine?, *J. Control. Release*, 2016, **244**, 108–121.
35 J. A. Roacho-Perez, H. L. Gallardo-Blanco, M. Sanchez-Dominguez, P. Garcia-Casillas, C. Chapa-Gonzalez and C. N. Sanchez-Dominguez, Nanoparticles for death-induced gene therapy in cancer (Review), *Mol. Med. Rep.*, 2018, **17**, 1413–1420.
36 X. Xu, W. Ho, X. Zhang, N. Bertrand and O. Farokhzad, Cancer nanomedicine: From targeted delivery to combination therapy, *Trends Mol. Med.*, 2015, **21**, 223–232.
37 N. Bertrand, J. Wu, X. Xu, N. Kamaly and O. C. Farokhzad, Cancer nanotechnology: The impact of passive and active targeting in the era of modern cancer biology, *Adv. Drug Deliv. Rev.*, 2014, **66**, 2–25.
38 N. Kamaly, Z. Xiao, P. M. Valencia, A. F. Radovic-Moreno and O. C. Farokhzad, *Chem. Soc. Rev.*, 2012, 41, 2971–3010.
39 C. J. H. Porter, S. M. Moghimi, L. Illum and S. S. Davis, The polyoxyethylene/polyoxypropylene block co-polymer Poloxamer-407 selectively redirects intravenously injected microspheres to sinusoidal endothelial cells of rabbit bone marrow, *FEBS Lett.*, 1992, **305**, 62–66.
40 S. D. Conner and S. L. Schmid, Regulated portals of entry into the cell, *Nature*, 2003, **422**, 37.

41 I. A. Khalil, K. Kogure, H. Akita and H. Harashima, Uptake Pathways and Subsequent Intracellular Trafficking in Nonviral Gene Delivery, *Pharmacol. Rev.*, 2006, **58**, 32–45.
42 J. Singh, D. Michel, J. M. Chitanda, R. E. Verrall and I. Badea, Evaluation of cellular uptake and intracellular trafficking as determining factors of gene expression for amino acid-substituted gemini surfactant-based DNA nanoparticles, *J. Nanobiotechnology*, 2012, **10**, 7.
43 I. Canton and G. Battaglia, Endocytosis at the nanoscale, *Chem. Soc. Rev.*, 2012, **41**, 2718–2739.
44 S. Xiang, H. Tong, Q. Shi, J. C. Fernandes, T. Jin, K. Dai and X. Zhang, Uptake mechanisms of non-viral gene delivery, *J. Control. Release*, 2012, **158**, 371–378.
45 A. Elouahabi and J. M. Ruysschaert, Formation and intracellular trafficking of lipoplexes and polyplexes, *Mol. Ther.*, 2005, **11**, 336–347.
46 B. M. Tandia, M. Vandenbranden, R. Wattiez, Z. Lakhdar, J. M. Ruysschaert and A. Elouahabi, Identification of human plasma proteins that bind to cationic lipid/DNA complex and analysis of their effects on transfection efficiency: Implications for intravenous gene transfer, *Mol. Ther.*, 2003, **8**, 264–273.
47 T. Kaur, R. A. Slavcev and S. D. Wettig, Addressing the challenge: current and future directions in ovarian cancer therapy, *Curr. Gene Ther.*, 2009, **9**, 434–58.
48 S. M. Farkhani, A. Valizadeh, H. Karami, S. Mohammadi, N. Sohrabi and F. Badrzadeh, Cell penetrating peptides: Efficient vectors for delivery of nanoparticles, nanocarriers, therapeutic and diagnostic molecules, *Peptides*, 2014, **57**, 78–94.
49 H. Eliyahu, Y. Barenholz and A. J. Domb, *Polymers for DNA Delivery*, 2005, vol. 10.
50 M. a Mintzer and E. E. Simanek, Nonviral Vectors for Gene Delivery, *Chem. Rev.*, 2009, **109**, 259–302.
51 J. Chen, J. Luo, Y. Zhao, L. Pu, X. Lu, R. Gao, G. Wang and Z. Gu, Increase in transgene expression by pluronic L64-mediated endosomal/lysosomal escape through its membrane-disturbing action, *ACS Appl. Mater. Interfaces*, 2015, **7**, 7282–7293.
52 Y. Xu and F. C. Szoka, Mechanism of DNA release from cationic liposome/DNA complexes used in cell transfection, *Biochemistry*, 1996, **35**, 5616–5623.
53 R. Koynova, L. Wang, Y. Tarahovsky and R. C. MacDonald, Lipid Phase Control of DNA Delivery, *Bioconjug. Chem.*, 2005, **16**, 1335–1339.
54 S. D. Wettig, I. Badea, M. Donkuru, R. E. Verrall and M. Foldvari, Structural and transfection properties of amine-substituted gemini surfactant-based nanoparticles, *J. Gene Med.*, 2007, **9**, 649–658.
55 E. Wagner, K. Zatloukal, M. Cotten, H. Kirlappos, K. Mechtler, D. T. Curiel and M. L. Birnstiel, Coupling of adenovirus to transferrin-polylysine/DNA complexes greatly enhances receptor-mediated gene delivery and expression of transfected genes, *Proc. Natl. Acad. Sci. U. S. A.*, 1992, **89**, 6099–6103.
56 L. J. Brandén, A. J. Mohamed and C. I. E. Smith, A peptide nucleic acid-nuclear localization signal fusion that mediates nuclear transport of DNA, *Nat. Biotechnol.*, 1999, **17**, 784–787.
57 Z. Yang, G. Sahay, S. Sriadibhatla and A. V Kabanov, Amphiphilic block copolymers enhance cellular uptake and nuclear entry of polyplex-delivered DNA., *Bioconjug. Chem.*, 2008, **19**, 1987–94.
58 M. Schleef, Ed., *Plasmids for Therapy and Vaccination*, Wiley, 2001.
59 R. W. Herzog and S. Zolotukhin, Eds., *A Guide to Human Gene Therapy*, World Scientific, 2010.
60 H. Lv, S. Zhang, B. Wang, S. Cui and J. Yan, Toxicity of cationic lipids and cationic polymers

in gene delivery, *J. Control. Release*, 2006, **114**, 100–109.
61 Z. Zhou, Y. Shen, J. Tang, E. Jin, X. Ma, Q. Sun, B. Zhang, E. A. Van Kirk and W. J. Murdoch, Linear polyethyleneimine-based charge-reversal nanoparticles for nuclear-targeted drug delivery, *J. Mater. Chem.*, 2011, **21**, 19114–19123.
62 S. D. Wettig, R. E. Verrall and M. Foldvari, Gemini surfactants: a new family of building blocks for non-viral gene delivery systems, *Curr. Gene Ther.*, 2008, **8**, 9–23.
63 I. Badea, R. Verrall, M. Baca-Estrada, S. Tikoo, A. Rosenberg, P. Kumar and M. Foldvari, In vivo cutaneous interferon-gamma gene delivery using novel dicationic (gemini) surfactant-plasmid complexes, *J. Gene Med.*, 2005, **7**, 1200–14.
64 M. Foldvari, I. Badea, S. Wettig, R. Verrall and M. Bagonluri, Structural characterization of novel gemini non-viral DNA delivery systems for cutaneous gene therapy, *J. Exp. Nanosci.*, 2006, **1**, 165–176.
65 N. Jiang, P. Li, Y. Wang, J. Wang, Y. Haike, R. K. Thomas, H. Yan, R. K. Thomas, Y. Haike and R. K. Thomas, Micellization of cationic gemini surfactants with various counterions and their interaction with DNA in aqueous solution, *J. Phys. Chem. B*, 2004, **108**, 15385–15391.
66 M. S. Islam, Characterization of Counterion Effects of Gemini Surfactants and In vitro Studies of Transfection Efficiency for Gene Therapy in Epithelial Ovarian Cancer.
67 C. Wang, X. Li, S. D. Wettig, I. Badea, M. Foldvari and R. E. Verrall, Investigation of complexes formed by interaction of cationic gemini surfactants with deoxyribonucleic acid, *Phys. Chem. Chem. Phys.*, 2007, **9**, 1616–28.
68 I. Badea, University of Saskatchewan, 2006.
69 P. Yang, J. Singh, S. Wettig, M. Foldvari, R. E. Verrall and I. Badea, Enhanced gene expression in epithelial cells transfected with amino acid-substituted gemini nanoparticles, *Eur. J. Pharm. Biopharm.*, 2010, **75**, 311–320.
70 J. Singh, P. Yang, D. Michel, R. E. Verrall, M. Foldvari and I. Badea, Amino acid-substituted gemini surfactant-based nanoparticles as safe and versatile gene delivery agents, *Curr. Drug Deliv.*, 2011, **8**, 299–306.
71 W. Jin, M. Al-Dulaymi, I. Badea, S. C. Leary, J. Rehman and A. El-Aneed, Cellular Uptake and Distribution of Gemini Surfactant Nanoparticles Used as Gene Delivery Agents, *AAPS J.*, 2019, **21**, 98.
72 J. R. Akbar, University of Waterloo, 2010.
73 O. Madkhali, University of Waterloo, 2013.
74 D. Cosco, C. Federico, J. Maiuolo, S. Bulotta, R. Molinaro, D. Paolino, P. Tassone and M. Fresta, Physicochemical features and transfection properties of chitosan/poloxamer 188/poly(D,L-lactide-co-glycolide) nanoplexes, *Int. J. Nanomedicine*, 2014, **9**, 2359.
75 P. Alexandridis and T. Alan Hatton, Poly(ethylene oxide)-poly(propylene oxide)-poly(ethylene oxide) block copolymer surfactants in aqueous solutions and at interfaces: thermodynamics, structure, dynamics, and modeling, *Colloids Surfaces A Physicochem. Eng. Asp.*, 1995, **96**, 1–46.
76 A. Kabanov, J. Zhu and V. Alakhov, in *Non-Viral Vectors for Gene Therapy*, Academic Press, 2005, vol. 53, pp. 231–261.
77 P. Alexandridis, J. F. Holzwarth and T. A. Hatton, Micellization of Poly(ethylene oxide)-Poly(propylene oxide)-Poly(ethylene oxide) Triblock Copolymers in Aqueous Solutions: Thermodynamics of Copolymer Association, *Macromolecules*, 1994, **27**, 2414–2425.
78 A. V Kabanov, E. V Batrakova and V. Y. Alakhov, Pluronic block copolymers as novel polymer therapeutics for drug and gene delivery, *J. Control. Release*, 2002, **82**, 189–212.

79 Y. Li, R. Xu, S. Couderc, D. M. Bloor, J. F. Holzwarth and E. Wyn-Jones, Binding of Tetradecyltrimethylammonium Bromide to the ABA Block Copolymer Pluronic F127 (EO_{97} PO_{69} EO_{97}): Electromotive Force, Microcalorimetry, and Light Scattering Studies, *Langmuir*, 2001, **17**, 5742–5747.
80 B. Chu and Z. Zhou, in *Nonionic Surfactants Polyoxyalkylene Block Copolymers*, 1996, pp. 67–143.
81 G. Wanka, H. Hoffmann and W. Ulbricht, Phase diagrams and aggregation behavior of poly(oxyethylene)-poly(oxypropylene)-poly(oxyethylene) triblock copolymers in aqueous solutions, *Macromolecules*, 1994, **27**, 4145–4159.
82 R. Nagarajan, Solubilization of hydrocarbons and resulting aggregate shape transitions in aqueous solutions of Pluronic® (PEO-PPO-PEO) block copolymers, *Colloids Surfaces B Biointerfaces*, 1999, **16**, 55–72.
83 D. A. Chiappetta and A. Sosnik, Poly(ethylene oxide)–poly(propylene oxide) block copolymer micelles as drug delivery agents: Improved hydrosolubility, stability and bioavailability of drugs, *Eur. J. Pharm. Biopharm.*, 2007, **66**, 303–317.
84 A. M. Bodratti and P. Alexandridis, Amphiphilic block copolymers in drug delivery: advances in formulation structure and performance, *Expert Opin. Drug Deliv.*, 2018, **15**, 1085–1104.
85 A. M. Bodratti and P. Alexandridis, Formulation of poloxamers for drug delivery, *J. Funct. Biomater.*, 2018, **9**, 11.
86 US FDA, Inactive Ingredient Search for Approved Drug Products, https://www.accessdata.fda.gov/scripts/cder/iig/index.cfm, (accessed 10 September 2019).
87 S. C. Rodriguez and E. J. Singer, in *Nonionic Surfactants Polyoxyalkylene Block Copolymers*, 1996, pp. 211–241.
88 Z.-Y. J. O. Wang and I. J. Stern, Disposition in rats of a polyoxypropylene-polyoxyethylene copolymer used in plasma fractionation, *Drug Metab. Dispos.*, 1975, **3**, 536–542.
89 Alexander V. Kabanov and Valery Yu. Alakhov, in *Amphiphilic Block Copolymers: Self-Assembly and Applications*, 2000, pp. 347–376.
90 J. Gau-Racine, J. Lal, M. Zeghal and L. Auvray, PEO-PPO block copolymer vectors do not interact directly with DNA but with lipid membranes, *J. Phys. Chem. B*, 2007, **111**, 9900–9907.
91 Z. Yang, J. Zhu, S. Sriadibhatla, C. Gebhart, V. Alakhov and A. Kabanov, Promoter- and strain-selective enhancement of gene expression in a mouse skeletal muscle by a polymer excipient Pluronic P85, *J. Control. Release*, 2005, **108**, 496–512.
92 I. Hauber, N. Beschorner, S. Schrödel, J. Chemnitz, N. Kröger, J. Hauber and C. Thirion, Improving lentiviral transduction of CD34+ hematopoietic stem and progenitor cells, *Hum. Gene Ther. Methods*, 2018, **29**, 104–113.
93 K. L. March, J. E. Madison and B. C. Trapnell, Pharmacokinetics of adenoviral vector-mediated gene delivery to vascular smooth muscle cells: modulation by poloxamer 407 and implications for cardiovascular gene therapy, *Hum. Gene Ther.*, 1995, **6**, 41–53.
94 J. Singh, D. Michel, H. M. Getson, J. M. Chitanda, R. E. Verrall and I. Badea, Development of amino acid substituted gemini surfactant-based mucoadhesive gene delivery systems for potential use as noninvasive vaginal genetic vaccination, *Nanomedicine (Lond).*, 2015, **10**, 405–417.
95 T. C. Lai, K. Kataoka and G. S. Kwon, Pluronic-based cationic block copolymer for forming pDNA polyplexes with enhanced cellular uptake and improved transfection efficiency, *Biomaterials*, 2011, **32**, 4594–4603.

96 J.-H. S. Kuo, Effect of Pluronic-block copolymers on the reduction of serum-mediated inhibition of gene transfer of polyethyleneimine - DNA complexes, *Biotechnol. Appl. Biochem.*, 2003, **37**, 267–271.
97 L. Bromberg, S. Deshmukh, M. Temchenko, L. Iourtchenko, V. Alakhov, C. Alvarez-Lorenzo, R. Barreiro-Iglesias, A. Concheiro and T. A. Hatton, Polycationic block copolymers of poly(ethylene oxide) and poly(propylene oxide) for cell transfection, *Bioconjug. Chem.*, 2005, **16**, 626–633.
98 T. Liu, X. Zhang, B. Ke, Y. Wang, X. Wu, G. Jiang, T. Wu and G. Nie, F-127-PEI co-delivering docetaxel and TFPI-2 plasmid for nasopharyngeal cancer therapy, *Mater. Sci. Eng. C*, 2016, **61**, 269–277.
99 A. Rey-Rico, J. Frisch, J. K. Venkatesan, G. Schmitt, I. Rial-Hermida, P. Taboada, A. Concheiro, H. Madry, C. Alvarez-Lorenzo and M. Cucchiarini, PEO-PPO-PEO Carriers for rAAV-Mediated Transduction of Human Articular Chondrocytes in Vitro and in a Human Osteochondral Defect Model, *ACS Appl. Mater. Interfaces*, 2016, **8**, 20600–20613.
100 M. A. Firestone, A. C. Wolf and S. Seifert, Small-angle X-ray scattering study of the interaction of poly(ethylene oxide)-b-poly(propylene oxide)-b-poly(ethylene oxide) triblock copolymers with lipid bilayers, *Biomacromolecules*, 2003, **4**, 1539–1549.
101 N. S. Melik-Nubarov, O. O. Pomaz, Dorodnych, G. A. Badun, A. L. Ksenofontov, O. B. Schemchukova and S. A. Arzhakov, Interaction of tumor and normal blood cells with ethylene oxide and propylene oxide block copolymers, *FEBS Lett.*, 1999, **446**, 194–198.
102 S. Nawaz, M. Redhead, G. Mantovani, C. Alexander, C. Bosquillon and P. Carbone, Interactions of PEO-PPO-PEO block copolymers with lipid membranes: A computational and experimental study linking membrane lysis with polymer structure, *Soft Matter*, 2012, **8**, 6744–6754.
103 T. Demina, I. Grozdova, O. Krylova, A. Zhirnov, V. Istratov, H. Frey, H. Kautz and N. Melik-Nubarov, Relationship between the structure of amphiphilic copolymers and their ability to disturb lipid bilayers, *Biochemistry*, 2005, **44**, 4042–4054.
104 E. V. Batrakova, Optimal structure requirements for Pluronic block copolymers in modifying P-glycoprotein drug efflux transporter activity in bovine brain microvessel endothelial cells, *J. Pharmacol. Exp. Ther.*, 2003, **304**, 845–854.
105 M. Redhead, G. Mantovani, S. Nawaz, P. Carbone, D. C. Gorecki and C. Alexander, Relationship between the affinity of PEO-PPO-PEO block copolymers for biological membranes and their cellular effects, 2012, 1908–1918.
106 A. E. Zhirnov, T. V. Demina, O. O. Krylova, I. D. Grozdova and N. S. Melik-Nubarov, Lipid composition determines interaction of liposome membranes with Pluronic L61, *Biochim. Biophys. Acta - Biomembr.*, 2005, **1720**, 73–83.
107 S. Sriadibhatla, Z. Yang, C. Gebhart, V. Alakhov and A. Kabanov, Transcriptional activation of gene expression by Pluronic block copolymers in stably and transiently transfected cells, *Mol. Ther.*, 2006, **13**, 804–813.
108 S. Tas, M. Vervoordeldonk and P. Tak, Gene therapy targeting nuclear factor-kB: towards clinical application in inflammatory diseases and cancer, *Curr. Gene Ther.*, 2009, **9**, 160–170.
109 J. Hiscott, H. Kwon and P. Génin, Hostile takeovers: viral appropriation of the NF-kB pathway, *J. Clin. Invest.*, 2001, **107**, 143–151.
110 M. S. Bakshi and S. Sachar, Influence of temperature on the mixed micelles of Pluronic F127 and P103 with dimethylene-bis-(dodecyldimethylammonium bromide), *J. Colloid Interface Sci.*, 2006, **296**, 309–315.

111 V. Peyre, Determination of activities of mixed micelles involving neutral surfactants, *Langmuir*, 2002, **18**, 1014–1023.
112 N. Nishikido, in *Mixed Surfactant Systems*, eds. K. Ogino and M. Abe, MARCEL DEKKER INC, 1993, pp. 23–61.
113 D. N. Rubingh, in *Solution Chemistry of Surfactants: Volume 1*, ed. K. L. Mittal, Springer New York, Boston, MA, 1979, pp. 337–354.
114 M. Bergström and J. C. Eriksson, A theoretical analysis of synergistic effects in mixed surfactant systems, *Langmuir*, 2000, **16**, 7173–7181.
115 H. Maeda, Electrostatic contribution to the stability and the synergism of ionic/nonionic mixed micelles in salt solutions, *J. Phys. Chem. B*, 2004, **108**, 6043–6051.
116 H. Maeda, *J. Colloid Interface Sci.*, 1995, 172, 98–105.
117 Y. Han and Y. Wang, Aggregation behavior of gemini surfactants and their interaction with macromolecules in aqueous solution, *Phys. Chem. Chem. Phys.*, 2011, **13**, 1939–1956.
118 R. S. Dias, K. Dawson and M. G. Miguel, in *DNA Interactions with Polymers and Surfactants*, eds. R. Dias and Bjorn Lindman, 2008, pp. 89–117.
119 K. Liu, L. Zheng, C. Ma, R. Göstl and A. Herrmann, DNA-surfactant complexes: Self-assembly properties and applications, *Chem. Soc. Rev.*, 2017, **46**, 5147–5172.
120 A. A. Zinchenko, O. A. Pyshkina, A. V. Lezov, V. G. Sergeyev and K. Yoshikawa, in *DNA Interactions with Polymers and Surfactants*, John Wiley & Sons, Inc., Hoboken, NJ, USA, 2008, pp. 59–88.
121 S. Husale, W. Grange, M. Karle, S. Bürgi and M. Hegner, Interaction of cationic surfactants with DNA: A single-molecule study, *Nucleic Acids Res.*, 2008, **36**, 1443–1449.
122 L. Karlsson, M. C. P. van Eijk and O. Söderman, Compaction of DNA by gemini surfactants: effects of surfactant architecture, *J. Colloid Interface Sci.*, 2002, **252**, 290–296.
123 C. Leal, D. Topgaard, Rachel W. Martin and H. Wennerström, NMR Studies of Molecular Mobility in a DNA−Amphiphile Complex, *J. Phys. Chem. B*, 2004, **108**, 15392–15397.
124 Kai K. Ewert, H. M. Evans, Alexandra Zidovska, Nathan F. Bouxsein, A. Ahmad and C. R. Safinya, A olumnar phase of dendritic lipid−based cationic liposome−DNA complexes for gene delivery: hexagonally ordered cylindrical micelles embedded in a DNA honeycomb lattice, *J. Am. Chem. Soc.*, 2006, **128**, 3998–4006.
125 M. Cao, M. Deng, X. L. Wang and Y. Wang, Decompaction of cationic gemini surfactant-induced DNA condensates by β-cyclodextrin or anionic surfactant, *J. Phys. Chem. B*, 2008, **112**, 13648–13654.
126 S. M. Mel'nikov, V. G. Sergeyev and K. Yoshikawa, Transition of double-stranded DNA chains between random coil and compact globule states induced by cooperative binding of cationic surfactant, *J. Am. Chem. Soc.*, 1995, **117**, 9951–9956.
127 Y. He, S. Xu, D. Sun, Y. Shang, X. Zhao and H. Liu, Decondensation of cationic gemini surfactant-induced DNA aggregates using triblock copolymer (PEO)20-(PPO)70-(PEO)20, *Colloid Polym. Sci.*, 2013, **291**, 2139–2146.
128 M. S. Bakshi, S. Sachar, T. Yoshimura and K. Esumi, Association behavior of poly(ethylene oxide)-poly(propylene oxide)-poly(ethylene oxide) block copolymers with cationic surfactants in aqueous solution, *J. Colloid Interface Sci.*, 2004, **278**, 224–233.
129 M. S. Bakshi, J. Singh and G. Kaur, Antagonistic mixing behavior of cationic gemini surfactants and triblock polymers in mixed micelles., *J. Colloid Interface Sci.*, 2005, **285**, 403–12.
130 X. F. Li, S. D. Wettig and R. E. Verrall, Isothermal titration calorimetry and dynamic light

scattering studies of interactions between gemini surfactants of different structure and Pluronic block copolymers, *J. Colloid Interface Sci.*, 2005, **282**, 466–477.
131 R. Wang, Y. Tang and Y. Wang, Effects of cationic ammonium gemini surfactant on micellization of PEO-PPO-PEO triblock copolymers in aqueous solution, *Langmuir*, 2014, **30**, 1957–1968.
132 M. S. Bakshi, S. Sachar, K. Singh and A. Shaheen, Mixed micelle behavior of Pluronic L64 and Triton X-100 with conventional and dimeric cationic surfactants, *J. Colloid Interface Sci.*, 2005, **286**, 369–377.
133 S. D. Wettig and R. E. Verrall, Studies of the interaction of cationic gemini surfactants with polymers and triblock copolymers in aqueous solution, *J. Colloid Interface Sci.*, 2001, **244**, 377–385.
134 M. S. Bakshi and S. Sachar, Influence of hydrophobicity on the mixed micelles of Pluronic F127 and P103 plus cationic surfactant mixtures, *Colloids Surfaces A Physicochem. Eng. Asp.*, 2006, **276**, 146–154.
135 Howard S. Rosenzweig, A. Vera A. Rakhmanova and R. C. MacDonald, Diquaternary ammonium compounds as transfection agents, *Bioconjug. Chem.*, 2001, **12**, 258–263.
136 S. M. Shortall and S. D. S. D. Wettig, Cationic gemini surfactant-plasmid deoxyribonucleic acid condensates as a single amphiphilic entity, *J. Phys. Chem. B*, 2018, **122**, 194–199.
137 A. Bhadani and S. Singh, Novel gemini pyridinium surfactants: synthesis and study of their surface activity, DNA binding, and cytotoxicity, *Langmuir*, 2009, **25**, 11703–11712.
138 X. Zhao, Y. Shang, J. Hu, H. Liu and Y. Hu, Biophysical characterization of complexation of DNA with oppositely charged Gemini surfactant 12-3-12, *Biophys. Chem.*, 2008, **138**, 144–149.
139 T. Ahmed, Langmuir-Blodgett monolayer studies of mixed gemini surfactant-phospholipid monolayers system for gene therapy applications.
140 D. A. Faizullin, Y. F. Zuev, L. Y. Zakharova, A. G. Pokrovsky, V. A. Korobeinikov, T. A. Mukhametzyanov and A. I. Konovalov, Lipoplexes of dicationic gemini surfactants with DNA: Structural features of DNA compaction and transfection efficiency, *Dokl. Biochem. Biophys.*, 2015, **465**, 432–435.
141 T. Zhou, A. Llizo, C. Wang, G. Xu and Y. Yang, Nanostructure-induced DNA condensation, *Nanoscale*, 2013, **5**, 8288–8306.
142 T. Ahmed, A. O. Kamel and S. D. Wettig, Interactions between DNA and Gemini surfactant: impact on gene therapy: part II, *Nanomedicine*, 2016, **11**, 289–306.
143 X. Chen, J. Wang, N. Shen, Y. Luo, L. Li, M. Liu and R. K. Thomas, Gemini surfactant/DNA complex monolayers at the air-water interface: Effect of surfactant structure on the assembly, stability, and topography of monolayers, *Langmuir*, 2002, **18**, 6222–6228.
144 Martin Pisárčik and F. Devínsky, Surface tension study of cationic gemini surfactants binding to DNA, *Cent. Eur. J. Chem.*, 2014, **12**, 577–585.
145 X. Chen, J. Wang and M. Liu, Influence of surfactant molecular structure on two-dimensional surfactant?DNA complexes: Langmuir balance study, *J. Colloid Interface Sci.*, 2005, **287**, 185–190.
146 Q. Chen, X. Kang, R. Li, X. Du, Y. Shang, H. Liu and Y. Hu, Structure of the complex monolayer of gemini surfactant and DNA at the air/water Interface, *Langmuir*, 2012, **28**, 3429–3438.
147 T. Zhou, G. Xu, M. Ao, Y. Yang and C. Wang, DNA compaction to multi-molecular DNA condensation induced by cationic imidazolium gemini surfactants, *Colloids Surfaces A*

Physicochem. Eng. Asp., 2012, **414**, 33–40.
148 D. Langevin, 2008, pp. 253–289.
149 R. S. Dias, M. G. Miguel and B. Lindman, in *DNA Interactions with Polymers and Surfactants*, 2008, pp. 367–376.
150 T. Vongsetskul, D. J. F. Taylor, J. Zhang, P. X. Li, R. K. Thomas and J. Penfold, Interaction of a cationic gemini surfactant with DNA and with sodium poly(styrene sulphonate) at the air/water interface: A neutron reflectometry study, *Langmuir*, 2009, **25**, 4027–4035.
151 R. S. Dias, B. Lindman and M. G. Miguel, Compaction and decompaction of DNA in the presence of catanionic amphiphile mixtures, *J. Phys. Chem. B*, 2002, **106**, 12608–12612.
152 A. González-Pérez, R. S. Dias, T. Nylander and B. Lindman, Cyclodextrin−Surfactant Complex: A New Route in DNA Decompaction, *Biomacromolecules*, 2008, **9**, 772–775.
153 J. Carlstedt, D. Lundberg, R. S. Dias and B. Lindman, Condensation and decondensation of DNA by cationic surfactant, spermine, or cationic surfactant-cyclodextrin mixtures: Macroscopic phase behavior, aggregate properties, and dissolution mechanisms, *Langmuir*, 2012, **28**, 7976–7989.
154 S. D. Wettig and R. E. Verrall, Thermodynamic studies of aqueous m–s–m gemini surfactant systems, *J. Colloid Interface Sci.*, 2001, **235**, 310–316.
155 H. Wang and S. D. Wettig, Synthesis and aggregation properties of dissymmetric phytanyl-gemini surfactants for use as improved DNA transfection vectors, *Phys. Chem. Chem. Phys.*, 2011, **13**, 637–642.
156 J. Heinrich, J. Schultz, M. Bosse, G. Ziegelin, E. Lanka and K. Moelling, Linear closed mini DNA generated by the prokaryotic cleaving-joining enzyme TelN is functional in mammalian cells, *J. Mol. Med.*, 2002, **80**, 648–654.
157 P. Carpena, J. Aguiar, P. Bernaola-Galván and C. Carnero Ruiz, Problems associated with the treatment of conductivity-concentration data in surfactant solutions: Simulations and experiments, *Langmuir*, 2002, **18**, 6054–6058.
158 K. M. Jenkins, University of Saskatchewan, 2000.
159 M. J. Rosen and D. J. Tracy, Gemini surfactants, *J. Surfactants Deterg.*, 1998, **1**, 547–554.
160 Ö. Topel, B. A. Çakır, L. Budama and N. Hoda, Determination of critical micelle concentration of polybutadiene-block-poly(ethyleneoxide) diblock copolymer by fluorescence spectroscopy and dynamic light scattering, *J. Mol. Liq.*, 2013, **177**, 40–43.
161 Malvern, Malvern Zetasizer SZ User Manual, 2013, 2–15.
162 E. D. Goddard, Polymer-surfactant interaction part II. Polymer and surfactant of opposite charge, *Colloids and Surfaces*, 1986, **19**, 301–329.
163 N. Jain, S. Trabelsi, S. Guillot, D. McLoughlin, D. Langevin, P. Letellier and M. Turmine, Critical Aggregation Concentration in Mixed Solutions of Anionic Polyelectrolytes and Cationic Surfactants, *Langmuir*, 2004, **20**, 8496–8503.
164 D. J. F. Taylor, R. K. Thomas and J. Penfold, The adsorption of oppositely charged polyelectrolyte/surfactant mixtures: Neutron reflection from dodecyl trimethylammonium bromide and sodium poly(styrene sulfonate) at the air/water interface, *Langmuir*, 2002, **18**, 4748–4757.
165 P. Tomanee and J. T. Hsu, Selective precipitation of RNA, supercoiled plasmid DNA, and open-circular plasmid DNA with different cationic surfactants, *J. Liq. Chromatogr. Relat. Technol.*, 2006, **29**, 1531–1540.
166 S. M. Shortall, G. Marangoni and S. Wettig, Mixing Behaviour of Pluronics with Gemini Surfactant/plasmid DNA Condensates: Effect of Pluronic Composition, *Phys. Chem. Chem.*

Phys., , DOI:10.1039/D0CP00309C.
167 A. J. Kirby, P. Camilleri, J. B. F. N. Engberts, M. C. Feiters, R. J. M. Nolte, O. Söderman, M. Bergsma, P. C. Bell, M. L. Fielden, C. L. García Rodríguez, P. Guédat, A. Kremer, C. McGregor, C. Perrin, G. Ronsin and M. C. P. van Eijk, Gemini surfactants: new synthetic vectors for gene transfection, *Angew. Chem. Int. Ed. Engl.*, 2003, **42**, 1448–57.
168 A. M. Cardoso, C. M. Morais, S. G. Silva, E. F. Marques, M. C. P. De Lima and M. A. S. Jurado, Bis-quaternary gemini surfactants as components of nonviral gene delivery systems: A comprehensive study from physicochemical properties to membrane interactions, *Int. J. Pharm.*, 2014, **474**, 57–69.
169 A. M. S. Cardoso, H. Faneca, J. A. S. Almeida, A. A. C. C. Pais, E. F. Marques, M. C. P. De Lima and A. S. Jurado, Gemini surfactant dimethylene-1,2-bis(tetradecyldimethylammonium bromide)-based gene vectors: A biophysical approach to transfection efficiency, *Biochim. Biophys. Acta - Biomembr.*, 2011, **1808**, 341–351.
170 A. M. Cardoso, C. M. Morais, A. R. Cruz, A. L. Cardoso, S. G. Silva, M. L. Do Vale, E. F. Marques, M. C. Pedroso De Lima and A. S. Jurado, Gemini Surfactants Mediate Efficient Mitochondrial Gene Delivery and Expression, *Mol. Pharm.*, 2015, **12**, 716–730.
171 C. Bombelli, L. Giansanti, P. Luciani and G. Mancini, Gemini surfactant based carriers in gene and drug delivery, *Curr. Med. Chem.*, 2009, **16**, 171–183.
172 A. M. S. Cardoso, S. G. Silva, M. Luísa do Vale, E. F. Marques, M. C. Pedroso de Lima and A. S. Jurado, in *Engineering of Nanobiomaterials*, Elsevier, 2016, pp. 227–256.
173 R. Zana and J. Xia, Eds., *Gemini Surfactants: Synthesis, Interfacial and Solution-Phase Behavior, and Applicalions*, 2004.
174 F. Menger and C. Littau, Gemini Surfactants: Synthesis and Properties, *J. Am. Chem. Soc.*, 1991, **113**, 1451–1452.
175 R. Zana, Dimeric and oligomeric surfactants. Behavior at interfaces and in aqueous solution: a review, *Adv. Colloid Interface Sci.*, 2002, **97**, 205–253.
176 E. V. Batrakova and A. V. Kabanov, Pluronic block copolymers: Evolution of drug delivery concept from inert nanocarriers to biological response modifiers, *J. Control. Release*, 2008, **130**, 98–106.
177 E. Wagner, C. Culmsee and S. Boeckle, Targeting of Polyplexes: Toward Synthetic Virus Vector Systems, *Adv. Genet.*, 2005, **53**, 333–354.
178 E. Batrakova, S. Lee, S. Li, A. Venne, V. Alakhov and A. Kabanov, Fundamental relationship between the composition of Pluronic block copolymers and their hypersensitization effect in MDR cancer cells, *Pharm. Res.*, 1999, **16**, 1373–1379.
179 W. D. Harkins and H. F. Jordan, A method for the determination of surface and interfacial tension from the maximum pull on a ring, *J. Am. Chem. Soc.*, 1930, **52**, 1751–1772.
180 C. Dong, I. Badea, M. Poorghorban, R. Verrall and M. Foldvari, Impact of phospholipids on plasmid packaging and toxicity of gemini nanoparticles, *J. Mater. Chem. B*, 2015, **3**, 8806–8822.
181 A. Kabanov, J. Zhu and V. Alakhov, in *Advances in Genetics*, eds. L. Huang, M.-C. Hung and E. Wagner, Elsevier, Second., 2005, vol. 53, pp. 119–155.
182 V. A. Izumrudov, M. V. Zhiryakova and A. A. Goulko, Ethidium bromide as a promising probe for studying DNA interaction with cationic amphiphiles and stability of the resulting complexes, *Langmuir*, 2002, **18**, 10348–10356.
183 C. Carnero Ruiz and J. Aguiar, Mixed micellization of octaoxyethylene monododecyl ether and n-alkyltrimethylammonium bromides, *Colloids Surfaces A Physicochem. Eng. Asp.*, 2003,

224, 221–230.
184 K. Schulén, K. Bryskhe and Y. S. Mel'Nikova, Vesicles formed from a poly(ethylene oxide)-poly(propylene oxide)-poly(ethylene oxide) triblock copolymer in dilute aqueous solution, *Macromolecules*, 1999, **32**, 6885–6888.
185 D. Gerrard Marangoni and J. C. T. Kwak, Solubilization of alcohols and ethoxylated alcohols in anionic and cationic micelles, *Langmuir*, 1991, **7**, 2083–2088.
186 K. U. Din, M. S. Sheikh and A. A. Dar, Analysis of mixed micellar and interfacial behavior of cationic gemini hexanediyl-1,6-bis(dimethylcetylammonium bromide) with conventional ionic and nonionic surfactants in aqueous medium, *J. Phys. Chem. B*, 2010, **114**, 6023–6032.
187 W. Mohammed-Saeid, J. Chitanda, M. Al-Dulaymi, R. Verrall and I. Badea, Design and evaluation of RGD-modified gemini surfactant-based lipoplexes for targeted gene therapy in melanoma model, *Pharm. Res.*, 2017, **34**, 1886–1896.
188 S. E. A. Gratton, P. A. Ropp, P. D. Pohlhaus, J. C. Luft, V. J. Madden, M. E. Nappier and J. M. DeSimone, The effect of particle design on cellular internalization pathways, *Proc. Natl. Acad. Sci.*, 2008, **105**, 11613–11618.
189 M. Muñoz-Úbeda, S. K. Misra, A. L. Barrán-Berdón, S. Datta, C. Aicart-Ramos, P. Castro-Hartmann, P. Kondaiah, E. Junquera, S. Bhattacharya and E. Aicart, How does the spacer length of cationic gemini lipids influence the lipoplex formation with plasmid DNA? physicochemical and biochemical characterizations and their relevance in gene therapy, *Biomacromolecules*, 2012, **13**, 3926–3937.
190 M. Muñoz-Úbeda, S. K. Misra, A. L. Barrán-Berdón, C. Aicart-Ramos, M. B. Sierra, J. Biswas, P. Kondaiah, E. Junquera, S. Bhattacharya and E. Aicart, Why is less cationic lipid required to prepare lipoplexes from plasmid DNA than linear DNA in gene therapy?, *J. Am. Chem. Soc.*, 2011, **133**, 18014–18017.
191 S. D. Wettig and R. E. Verrall, Thermodynamic studies of aqueous m – s – m gemini surfactant systems, *J. Colloid Interface Sci.*, 2001, **235**, 310–316.
192 G. Casella, S. Fienberg and I. Olkin, *An Introduction to Statistical Learning*, 2013.
193 S. Bhattacharjee, DLS and zeta potential - What they are and what they are not?, *J. Control. Release*, 2016, **235**, 337–351.
194 M. Donkuru, S. D. Wettig, R. E. Verrall, I. Badea and M. Foldvari, Designing pH-sensitive gemini nanoparticles for non-viral gene delivery into keratinocytes, *J. Mater. Chem.*, 2012, **22**, 6232–6244.
195 A. K. Mitra, D. A. Davis, S. Tomar, L. Roy, H. Gurler, J. Xie, D. D. Lantvit, H. Cardenas, F. Fang, Y. Liu, E. Loughran, J. Yang, M. Sharon Stack, R. E. Emerson, K. D. Cowden Dahl, M. V. Barbolina, K. P. Nephew, D. Matei and J. E. Burdette, In vivo tumor growth of high-grade serous ovarian cancer cell lines, *Gynecol. Oncol.*, 2015, **138**, 372–377.
196 E. Lengyel, J. E. Burdette, H. A. Kenny, D. Matei, J. Pilrose, P. Haluska, K. P. Nephew, D. B. Hales and M. S. Stack, Epithelial ovarian cancer experimental models, *Oncogene*, 2014, **33**, 3619–3633.
197 N. Maenhoudt, C. Defraye, M. Boretto, Z. Jan, R. Heremans, B. Boeckx, F. Hermans, I. Arijs, B. Cox, E. Van Nieuwenhuysen, I. Vergote, A.-S. Van Rompuy, D. Lambrechts, D. Timmerman and H. Vankelecom, Developing organoids from ovarian cancer as experimental and preclinical models, *Stem cell reports*, 2020, **14**, 717–729.

Appendices

Appendix A

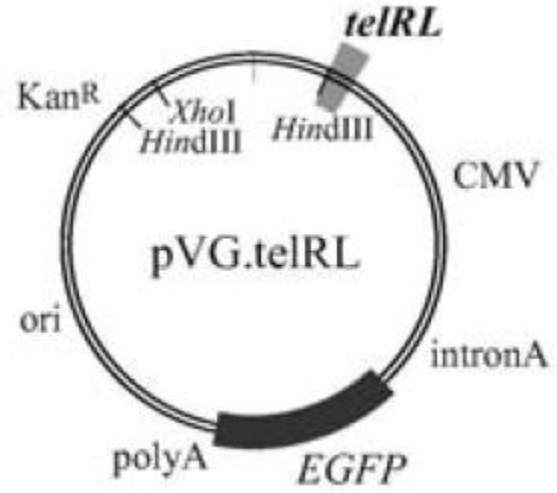

Figure A-1 pVG.telRL plasmid encoding enhanced green fluorescence protein (eGFP).[156]

Conductivity

Table A-1 Conductivity of 16-3-16/pDNA (10:1) complex in water

Trial 1			Trial 2			Trial 3		
Concentration (μM)	**Average Specific Conductance (μS/cm)**	**Standard Deviation**	**Concentration (μM)**	**Average Specific Conductance (μS/cm)**	**Standard Deviation**	**Concentration (μM)**	**Average Specific Conductance (μS/cm)**	**Standard Deviation**
0.00	1.67	0.02	0.00	1.24	0.03	0.00	1.56	0.02
4.70	3.10	0.04	4.70	2.13	0.02	4.70	2.44	0.01
8.98	4.16	0.18	8.98	2.82	0.08	8.98	3.28	0.02
12.89	5.25	0.09	12.89	3.54	0.04	12.89	4.00	0.04
16.47	5.82	0.68	16.47	4.18	0.04	16.47	4.57	0.10
19.76	6.95	0.04	19.76	4.73	0.04	19.76	5.26	0.03
22.80	7.26	0.45	22.80	5.11	0.14	22.80	5.84	0.05
25.62	8.04	0.34	25.62	5.50	0.19	25.62	6.15	0.16
28.23	8.65	0.34	28.23	6.01	0.02	28.23	6.60	0.12
30.66	9.30	0.12	30.66	6.34	0.06	30.66	6.97	0.04
32.93	9.55	0.25	32.93	6.64	0.08	32.93	7.29	0.04
35.06	9.98	0.11	35.06	6.87	0.02	35.06	7.55	0.02
37.05	10.24	0.31	37.05	7.04	0.01	37.05	7.79	0.01
38.92	10.64	0.34	38.92	7.25	0.01	38.92	7.99	0.03
40.68	10.90	0.28	40.68	7.43	0.03	40.68	8.16	0.02
			42.34	7.59	0.04	42.34	8.33	0.02
			43.91	7.71	0.03	43.91	8.48	0.03

Dynamic Light Scattering

Table A-2 Scattered light intensity, Z-average, and polydispersity index of 16-3-16/pDNA complex titrated into water

Concentration (M)	Intensity (kcps)	Z-Average (nm)	Polydisperisty Index
0.00	104.90	319.40	0.31
0.00	114.30	325.00	0.42
0.00	139.60	433.00	0.43
2.89×10^{-7}	93.40	231.80	0.35
2.89×10^{-7}	71.40	197.40	0.33
2.89×10^{-7}	128.00	252.50	0.33
5.79×10^{-7}	152.00	207.90	0.32
5.79×10^{-7}	128.70	222.70	0.40
5.79×10^{-7}	145.50	213.40	0.31
8.69×10^{-7}	160.00	185.80	0.33
8.69×10^{-7}	154.10	182.70	0.31
8.69×10^{-7}	143.10	175.50	0.30
1.16×10^{-6}	169.20	165.50	0.28
1.16×10^{-6}	152.40	155.80	0.24
1.16×10^{-6}	161.20	163.60	0.25
1.45×10^{-6}	165.40	151.80	0.23
1.45×10^{-6}	164.30	149.20	0.24
1.45×10^{-6}	166.70	156.10	0.22
1.74×10^{-6}	187.30	148.70	0.23
1.74×10^{-6}	194.00	152.80	0.23
1.74×10^{-6}	201.70	156.20	0.26
2.03×10^{-6}	201.40	145.30	0.21
2.03×10^{-6}	214.40	147.30	0.22
2.03×10^{-6}	212.90	151.40	0.21
2.31×10^{-6}	233.50	146.80	0.19
2.31×10^{-6}	235.40	150.10	0.21
2.31×10^{-6}	250.80	155.50	0.22
2.60×10^{-6}	265.00	154.50	0.23
2.60×10^{-6}	259.00	150.00	0.19
2.60×10^{-6}	252.30	147.00	0.22
2.89×10^{-6}	313.60	152.20	0.21
2.89×10^{-6}	313.50	149.70	0.21
2.89×10^{-6}	315.70	150.30	0.23
3.18×10^{-6}	326.20	150.60	0.22
3.18×10^{-6}	341.30	151.80	0.22
3.18×10^{-6}	343.50	156.00	0.21
3.47×10^{-6}	371.20	157.40	0.23
3.47×10^{-6}	384.80	156.00	0.23
3.47×10^{-6}	392.80	157.90	0.24

Table A-2 Scattered light intensity, Z-average, and polydispersity index of 16-3-16/pDNA complex titrated into water

Concentration (M)	Intensity (kcps)	Z-Average (nm)	Polydisperisty Index
3.76×10^{-6}	402.70	155.10	0.22
3.76×10^{-6}	398.00	154.10	0.27
3.76×10^{-6}	400.40	154.10	0.24
4.05×10^{-6}	429.30	155.40	0.24
4.05×10^{-6}	401.80	153.10	0.23
4.05×10^{-6}	407.50	153.00	0.22
4.34×10^{-6}	432.70	150.60	0.24
4.34×10^{-6}	424.30	154.90	0.23
4.34×10^{-6}	403.60	151.90	0.24
4.63×10^{-6}	423.00	149.10	0.23
4.63×10^{-6}	415.70	145.40	0.21
4.63×10^{-6}	414.20	145.60	0.22
4.92×10^{-6}	419.70	144.10	0.18
4.92×10^{-6}	396.80	141.40	0.17
4.92×10^{-6}	417.70	142.10	0.19
5.22×10^{-6}	443.40	154.60	0.25
5.22×10^{-6}	434.90	150.10	0.26
5.22×10^{-6}	421.90	143.50	0.24
5.50×10^{-6}	442.90	141.60	0.19
5.50×10^{-6}	457.10	144.50	0.21
5.50×10^{-6}	434.70	143.30	0.19

Appendix B

Tensiometry Data

Table B-1 Surface tension of 16-3-16/pDNA (10:1) complexes in water at 25°C

Trial 1		Trial 2		Trial 3	
Concentration (mol/L)	**γ (mN/m)**	**Concentration (mol/L)**	**γ (mN/m)**	**Concentration (mol/L)**	**γ (mN/m)**
0.00	71.0	0.00	71.0	0.00	70.8
1.21×10^{-6}	64.6	1.21×10^{-6}	66.3	1.21×10^{-6}	63.4
2.39×10^{-6}	50.4	2.39×10^{-6}	58.7	2.39×10^{-6}	48.3
3.54×10^{-6}	45.7	3.54×10^{-6}	53.5	3.54×10^{-6}	44.5
4.67×10^{-6}	43.5	4.67×10^{-6}	49.5	4.67×10^{-6}	42.4
5.76×10^{-6}	41.8	5.76×10^{-6}	46.7	5.76×10^{-6}	40.3
6.84×10^{-6}	40.5	6.84×10^{-6}	44.8	6.84×10^{-6}	39.2
7.89×10^{-6}	39.3	7.89×10^{-6}	43.4	7.89×10^{-6}	38.4
8.91×10^{-6}	38.7	8.91×10^{-6}	42.1	8.91×10^{-6}	37.7
9.91×10^{-6}	37.9	9.91×10^{-6}	41.1	9.91×10^{-6}	36.8
1.09×10^{-5}	37.3	1.09×10^{-5}	40.2	1.09×10^{-5}	36.5
1.18×10^{-5}	36.7	1.18×10^{-5}	39.2	1.18×10^{-5}	36.1
1.28×10^{-5}	36.3	1.28×10^{-5}	38.5	1.28×10^{-5}	35.6
1.37×10^{-5}	36.0	1.37×10^{-5}	37.9	1.37×10^{-5}	35.3
1.46×10^{-5}	35.7	1.46×10^{-5}	37.5	1.46×10^{-5}	35.3
1.55×10^{-5}	35.6	1.55×10^{-5}	37.2	1.55×10^{-5}	34.8
1.63×10^{-5}	35.6	1.63×10^{-5}	36.9	1.63×10^{-5}	34.6
1.72×10^{-5}	35.4	1.72×10^{-5}	36.6	1.72×10^{-5}	34.5
1.80×10^{-5}	35.5	1.80×10^{-5}	36.4	1.80×10^{-5}	34.3
1.88×10^{-5}	35.2	1.88×10^{-5}	36.2	1.88×10^{-5}	34.2
1.96×10^{-5}	35.2	1.96×10^{-5}	36.0	1.96×10^{-5}	34.1
2.04×10^{-5}	35.1	2.04×10^{-5}	36.0	2.04×10^{-5}	34.1
2.11×10^{-5}	35.2	2.11×10^{-5}	35.9	2.11×10^{-5}	34.1
2.19×10^{-5}	35.1	2.19×10^{-5}	35.7	2.19×10^{-5}	34.2
2.26×10^{-5}	34.9	2.26×10^{-5}	35.7	2.26×10^{-5}	34.1
2.33×10^{-5}	35.0	2.33×10^{-5}	35.5	2.33×10^{-5}	34.0
2.40×10^{-5}	35.0	2.40×10^{-5}	35.5	2.40×10^{-5}	34.0
		2.47×10^{-5}	35.3	2.47×10^{-5}	33.9
		2.54×10^{-5}	35.3	2.54×10^{-5}	33.9
		2.61×10^{-5}	35.2	2.61×10^{-5}	33.9
		2.67×10^{-5}	35.1	2.67×10^{-5}	34.0
		2.74×10^{-5}	35.1	2.74×10^{-5}	34.0
		2.80×10^{-5}	35.1	2.80×10^{-5}	33.9

Table B-2 Surface tension of F87/16-3-16/pDNA mixtures of varying F87 mole fraction in water at 25°C

Trial 1							
α = 0.2 F87		**α = 0.4 F87**		**α = 0.6 F87**		**α = 0.8 F87**	
Concentration (mol/L)	**γ (mN/m)**	**Concentration (mol/L)**	**γ (mN/m)**	**Concentration (mol/L)**	**γ (mN/m)**	**Concentration (mol/L)**	**γ (mN/m)**
0.00	69.1	0.00	68.8	0.00	69.1	0.00	69.3
6.67×10^{-10}	68.0	6.67×10^{-10}	67.8	6.72×10^{-10}	67.2	6.67×10^{-10}	68.4
1.33×10^{-9}	68.1	1.33×10^{-9}	67.7	1.34×10^{-9}	66.8	1.33×10^{-9}	68.1
2.00×10^{-9}	68.1	2.00×10^{-9}	67.6	2.01×10^{-9}	65.7	2.00×10^{-9}	67.6
2.93×10^{-9}	68.0	2.93×10^{-9}	67.5	2.95×10^{-9}	66.1	2.93×10^{-9}	67.7
4.26×10^{-9}	67.7	4.26×10^{-9}	66.0	4.30×10^{-9}	65.6	4.26×10^{-9}	65.9
6.26×10^{-9}	67.6	6.26×10^{-9}	65.2	6.31×10^{-9}	64.2	6.26×10^{-9}	65.3
9.59×10^{-9}	67.5	9.59×10^{-9}	62.5	9.66×10^{-9}	63.6	9.59×10^{-9}	63.7
1.42×10^{-8}	66.5	1.42×10^{-8}	60.0	1.43×10^{-8}	62.6	1.42×10^{-8}	62.7
2.09×10^{-8}	66.1	2.09×10^{-8}	58.9	2.10×10^{-8}	60.8	2.09×10^{-8}	61.2
3.15×10^{-8}	65.1	3.15×10^{-8}	58.0	3.17×10^{-8}	58.7	3.15×10^{-8}	59.2
4.73×10^{-8}	63.6	4.73×10^{-8}	56.7	4.77×10^{-8}	57.5	4.73×10^{-8}	57.2
7.36×10^{-8}	62.1	7.36×10^{-8}	55.5	7.41×10^{-8}	55.7	7.36×10^{-8}	55.3
1.13×10^{-7}	60.3	1.13×10^{-7}	53.7	1.14×10^{-7}	53.8	1.13×10^{-7}	53.6
1.77×10^{-7}	58.5	1.77×10^{-7}	50.4	1.78×10^{-7}	51.3	1.77×10^{-7}	51.3
2.71×10^{-7}	55.6	2.71×10^{-7}	49.4	2.73×10^{-7}	49.3	2.71×10^{-7}	49.7
3.94×10^{-7}	52.3	3.94×10^{-7}	48.5	3.97×10^{-7}	48.8	3.94×10^{-7}	48.7
5.70×10^{-7}	50.5	5.70×10^{-7}	47.5	5.75×10^{-7}	48.0	5.70×10^{-7}	47.9
7.94×10^{-7}	49.5	7.94×10^{-7}	46.9	8.00×10^{-7}	47.3	7.94×10^{-7}	47.4
1.05×10^{-6}	48.9	1.05×10^{-6}	46.4	1.06×10^{-6}	46.8	1.05×10^{-6}	47.0
1.34×10^{-6}	48.7	1.39×10^{-6}	46.4	1.40×10^{-6}	46.4	1.39×10^{-6}	46.4
1.61×10^{-6}	48.4	1.73×10^{-6}	46.2	2.06×10^{-6}	46.2	1.82×10^{-6}	46.3
1.85×10^{-6}	48.0	2.05×10^{-6}	46.1	2.41×10^{-6}	45.7	2.32×10^{-6}	46.1
2.08×10^{-6}	47.8						
2.29×10^{-6}	47.7						
2.49×10^{-6}	47.5						
2.67×10^{-6}	47.5						
2.84×10^{-6}	47.0						

Table B-2 (cont'd) Surface tension of F87/16-3-16/pDNA mixtures of varying F87 mole fraction in water at 25°C

Trial 2							
α = 0.2 F87		**α = 0.4 F87**		**α = 0.6 F87**		**α = 0.8 F87**	
Concentration (mol/L)	**γ (mN/m)**	**Concentration (mol/L)**	**γ (mN/m)**	**Concentration (mol/L)**	**γ (mN/m)**	**Concentration (mol/L)**	**γ (mN/m)**
0.00	68.3	0.00	68.8	0.00	68.9	0.00	69.1
6.67×10^{-10}	67.2	6.67×10^{-10}	67.7	6.67×10^{-10}	67.4	6.67×10^{-10}	67.7
1.33×10^{-9}	67.4	1.33×10^{-9}	67.9	1.33×10^{-9}	67.0	1.33×10^{-9}	67.6
2.00×10^{-9}	67.4	2.00×10^{-9}	67.5	2.00×10^{-9}	65.9	2.00×10^{-9}	66.9
2.93×10^{-9}	67.6	2.93×10^{-9}	67.4	2.93×10^{-9}	65.1	2.93×10^{-9}	65.4
4.26×10^{-9}	67.5	4.26×10^{-9}	67.3	4.26×10^{-9}	64.7	4.26×10^{-9}	64.1
6.26×10^{-9}	67.6	6.26×10^{-9}	66.9	6.26×10^{-9}	64.0	6.26×10^{-9}	62.8
9.59×10^{-9}	67.7	9.59×10^{-9}	65.8	9.59×10^{-9}	62.4	9.59×10^{-9}	60.9
1.42×10^{-8}	67.7	1.42×10^{-8}	64.9	1.42×10^{-8}	60.8	1.42×10^{-8}	59.3
2.09×10^{-8}	67.7	2.09×10^{-8}	62.6	2.09×10^{-8}	59.3	2.09×10^{-8}	57.5
3.15×10^{-8}	67.3	3.15×10^{-8}	61.0	3.15×10^{-8}	58.1	3.15×10^{-8}	55.9
4.73×10^{-8}	66.9	4.73×10^{-8}	58.8	4.73×10^{-8}	56.7	4.73×10^{-8}	54.1
7.36×10^{-8}	65.6	7.36×10^{-8}	57.0	7.36×10^{-8}	55.2	7.36×10^{-8}	52.0
1.13×10^{-7}	63.3	1.13×10^{-7}	55.4	1.13×10^{-7}	52.8	1.13×10^{-7}	49.6
1.77×10^{-7}	59.1	1.77×10^{-7}	52.4	1.77×10^{-7}	50.6	1.77×10^{-7}	48.6
2.71×10^{-7}	56.6	2.71×10^{-7}	49.7	2.71×10^{-7}	49.5	2.71×10^{-7}	47.6
3.94×10^{-7}	54.0	3.94×10^{-7}	49.0	3.94×10^{-7}	48.7	3.94×10^{-7}	46.9
5.70×10^{-7}	50.7	5.70×10^{-7}	48.1	5.70×10^{-7}	48.3	5.70×10^{-7}	46.4
7.94×10^{-7}	49.3	7.94×10^{-7}	47.1	7.94×10^{-7}	47.9	7.94×10^{-7}	46.0
1.05×10^{-6}	48.4	1.05×10^{-6}	46.6	1.39×10^{-6}	47.4	1.05×10^{-6}	45.8
1.34×10^{-6}	48.0	1.30×10^{-6}	46.5	1.73×10^{-6}	47.2	1.39×10^{-6}	45.7
1.61×10^{-6}	47.3	1.52×10^{-6}	46.3	2.05×10^{-6}	46.8	1.73×10^{-6}	45.7
1.85×10^{-6}	47.0	1.73×10^{-6}	46.2	2.31×10^{-6}	46.7	2.05×10^{-6}	45.8
2.08×10^{-6}	46.7	1.93×10^{-6}	46.2			2.33×10^{-6}	45.4
2.29×10^{-6}	46.4	2.12×10^{-6}	46.1				
2.49×10^{-6}	46.3	2.29×10^{-6}	45.8				
2.67×10^{-6}	46.2						
2.84×10^{-6}	46.1						

Table B-2 (cont'd) Surface tension of F87/16-3-16/pDNA mixtures of varying F87 mole fraction in water at 25°C

Trial 3							
α = 0.2 F87		**α = 0.4 F87**		**α = 0.6 F87**		**α = 0.8 F87**	
Concentration (mol/L)	**γ (mN/m)**	**Concentration (mol/L)**	**γ (mN/m)**	**Concentration (mol/L)**	**γ (mN/m)**	**Concentration (mol/L)**	**γ (mN/m)**
0.00	69.0	0.00	68.1	0.00	67.3	0.00	68.2
6.67×10^{-10}	67.6	6.72×10^{-10}	66.7	6.67×10^{-10}	66.1	6.67×10^{-10}	67.0
1.33×10^{-9}	67.5	1.34×10^{-9}	67.0	1.33×10^{-9}	66.1	1.33×10^{-9}	66.9
2.00×10^{-9}	67.5	2.00×10^{-9}	66.9	2.00×10^{-9}	66.1	2.00×10^{-9}	66.4
2.93×10^{-9}	67.5	2.93×10^{-9}	66.9	2.93×10^{-9}	65.9	2.93×10^{-9}	66.1
4.26×10^{-9}	67.5	4.26×10^{-9}	66.8	4.26×10^{-9}	65.1	4.26×10^{-9}	65.4
6.26×10^{-9}	67.4	6.26×10^{-9}	66.68	6.26×10^{-9}	64.7	6.26×10^{-9}	64.3
9.59×10^{-9}	67.6	9.59×10^{-9}	66.7	9.59×10^{-9}	64.3	9.59×10^{-9}	63.0
1.42×10^{-8}	67.6	1.42×10^{-8}	66.4	1.42×10^{-8}	63.8	1.42×10^{-8}	61.0
2.09×10^{-8}	67.4	2.09×10^{-8}	65.8	2.09×10^{-8}	62.4	2.09×10^{-8}	59.8
3.15×10^{-8}	66.9	3.15×10^{-8}	65.4	3.15×10^{-8}	61.2	3.15×10^{-8}	58.4
4.73×10^{-8}	66.6	4.73×10^{-8}	64.2	4.73×10^{-8}	59.7	4.73×10^{-8}	57.0
7.36×10^{-8}	65.7	7.36×10^{-8}	61.5	7.36×10^{-8}	58.2	7.36×10^{-8}	55.2
1.13×10^{-7}	63.6	1.13×10^{-7}	58.8	1.13×10^{-7}	56.7	1.13×10^{-7}	53.4
1.77×10^{-7}	60.8	1.77×10^{-7}	56.9	1.77×10^{-7}	53.9	1.77×10^{-7}	51.3
2.71×10^{-7}	58.1	2.71×10^{-7}	53.5	2.71×10^{-7}	51.4	2.71×10^{-7}	49.6
3.94×10^{-7}	55.7	3.94×10^{-7}	50.3	3.94×10^{-7}	49.8	3.94×10^{-7}	48.5
5.70×10^{-7}	51.9	5.70×10^{-7}	49.0	5.70×10^{-7}	48.7	5.70×10^{-7}	47.7
7.94×10^{-7}	50.2	7.94×10^{-7}	48.2	7.94×10^{-7}	47.9	7.94×10^{-7}	47.1
1.05×10^{-6}	49.1	1.05×10^{-6}	48.4	1.05×10^{-6}	47.2	1.05×10^{-6}	46.9
1.34×10^{-6}	48.5	1.34×10^{-6}	47.4	1.34×10^{-6}	46.8	1.34×10^{-6}	46.4
1.61×10^{-6}	48.3	1.61×10^{-6}	46.9	1.61×10^{-6}	46.4	1.61×10^{-6}	46.3
1.85×10^{-6}	47.7	1.85×10^{-6}	46.8	1.85×10^{-6}	46.4	1.85×10^{-6}	46.0
2.08×10^{-6}	47.3	2.08×10^{-6}	46.5	2.08×10^{-6}	45.9	2.08×10^{-6}	45.9
2.29×10^{-6}	47.4	2.29×10^{-6}	46.4	2.29×10^{-6}	45.7	2.29×10^{-6}	45.9
2.49×10^{-6}	47.0	2.49×10^{-6}	46.0	2.49×10^{-6}	45.5	2.49×10^{-6}	45.7
2.67×10^{-6}	46.8	2.67×10^{-6}	45.9	2.67×10^{-6}	45.4	2.67×10^{-6}	45.7
2.84×10^{-6}	46.8	2.84×10^{-6}	45.9	2.84×10^{-6}	45.3	2.84×10^{-6}	45.8

Table B-3 Surface tension of P84/16-3-16/pDNA mixtures of varying P84 mole fraction in water at 25°C

Trial 1							
α = 0.2 P84		**α = 0.4 P84**		**α = 0.6 P84**		**α = 0.8 P84**	
Concentration (mol/L)	**γ (mN/m)**	**Concentration (mol/L)**	**γ (mN/m)**	**Concentration (mol/L)**	**γ (mN/m)**	**Concentration (mol/L)**	**γ (mN/m)**
0.00	73.1	0.00	72.0	0.00	72.4	0.00	72.5
7.87×10^{-9}	73.2	7.87×10^{-9}	71.6	7.87×10^{-9}	72.1	7.87×10^{-9}	71.4
9.18×10^{-9}	73.0	9.18×10^{-9}	70.8	9.18×10^{-9}	72.0	9.18×10^{-9}	70.2
1.10×10^{-8}	72.6	1.10×10^{-8}	69.2	1.10×10^{-8}	70.5	1.10×10^{-8}	69.2
1.36×10^{-8}	72.5	1.36×10^{-8}	67.7	1.36×10^{-8}	67.8	1.36×10^{-8}	68.6
1.68×10^{-8}	72.5	1.68×10^{-8}	65.3	1.68×10^{-8}	66.2	1.68×10^{-8}	66.3
2.07×10^{-8}	71.6	2.07×10^{-8}	63.0	2.07×10^{-8}	65.1	2.07×10^{-8}	64.5
2.59×10^{-8}	70.7	2.59×10^{-8}	61.4	2.59×10^{-8}	62.8	2.59×10^{-8}	62.3
3.25×10^{-8}	69.9	3.25×10^{-8}	60.4	3.25×10^{-8}	61.2	3.25×10^{-8}	61.2
4.16×10^{-8}	69.4	4.16×10^{-8}	58.6	4.16×10^{-8}	59.4	4.16×10^{-8}	59.5
5.33×10^{-8}	68.7	5.33×10^{-8}	57.3	5.33×10^{-8}	57.4	5.33×10^{-8}	58.3
6.89×10^{-8}	68.0	6.89×10^{-8}	56.2	6.89×10^{-8}	54.9	2.26×10^{-7}	49.3
8.84×10^{-8}	66.9	8.84×10^{-8}	55.0	8.84×10^{-8}	53.5	2.89×10^{-7}	48.7
1.10×10^{-7}	65.6	1.10×10^{-7}	53.5	1.10×10^{-7}	51.1	3.65×10^{-7}	48.2
1.36×10^{-7}	63.4	1.36×10^{-7}	52.7	1.36×10^{-7}	50.1	4.65×10^{-7}	47.7
1.75×10^{-7}	61.9	1.75×10^{-7}	51.8	1.75×10^{-7}	49.3	5.99×10^{-7}	47.1
2.26×10^{-7}	60.0	2.26×10^{-7}	51.6	2.26×10^{-7}	48.9	7.56×10^{-7}	46.6
2.89×10^{-7}	56.7	2.89×10^{-7}	51.4	2.89×10^{-7}	48.4	9.38×10^{-7}	46.3
3.65×10^{-7}	54.2	3.65×10^{-7}	51.1	3.65×10^{-7}	48.1	1.14×10^{-6}	45.6
4.65×10^{-7}	51.8	4.65×10^{-7}	51.1	4.65×10^{-7}	47.7	1.37×10^{-6}	45.2
5.99×10^{-7}	50.4	5.99×10^{-7}	51.2	5.99×10^{-7}	47.5	1.58×10^{-6}	45.1
7.56×10^{-7}	49.4	7.56×10^{-7}	51.2	7.56×10^{-7}	47.1	1.79×10^{-6}	44.8
9.38×10^{-7}	48.6	9.38×10^{-7}	51.0	9.38×10^{-7}	46.9	2.00×10^{-6}	44.4
1.14×10^{-6}	47.5	1.14×10^{-6}	50.8	1.14×10^{-6}	47.0	2.23×10^{-6}	44.2
1.37×10^{-6}	46.6	1.37×10^{-6}	50.1	1.37×10^{-6}	47.2		
1.58×10^{-6}	44.4	1.58×10^{-6}	49.4				

Table B-3 (cont'd) Surface tension of P84/16-3-16/pDNA mixtures of varying P84 mole fraction in water at 25°C

Trial 2							
α = 0.2 P84		**α = 0.4 P84**		**α = 0.6 P84**		**α = 0.8 P84**	
Concentration (mol/L)	**γ (mN/m)**	**Concentration (mol/L)**	**γ (mN/m)**	**Concentration (mol/L)**	**γ (mN/m)**	**Concentration (mol/L)**	**γ (mN/m)**
0.00	73.1	0.00	73.3	0.00	73.5	0.00	73.6
2.62×10^{-8}	73.1	7.87×10^{-9}	73.2	7.87×10^{-9}	73.3	7.87×10^{-9}	73.3
1.82×10^{-7}	71.2	9.18×10^{-9}	73.3	9.18×10^{-9}	72.6	9.18×10^{-9}	72.6
2.58×10^{-7}	68.3	1.10×10^{-8}	73.0	1.10×10^{-8}	71.6	1.10×10^{-8}	71.2
2.83×10^{-7}	64.2	1.36×10^{-8}	72.9	1.36×10^{-8}	70.1	1.36×10^{-8}	70.6
3.09×10^{-7}	59.8	1.68×10^{-8}	71.7	1.68×10^{-8}	68.4	1.68×10^{-8}	68.6
3.34×10^{-7}	54.1	2.07×10^{-8}	69.9	2.07×10^{-8}	65.7	2.07×10^{-8}	65.8
3.59×10^{-7}	51.5	2.59×10^{-8}	68.5	2.59×10^{-8}	63.4	2.59×10^{-8}	64.0
3.84×10^{-7}	50.5	3.25×10^{-8}	67.7	3.25×10^{-8}	61.1	3.25×10^{-8}	63.0
4.06×10^{-7}	49.9	4.16×10^{-8}	65.7	4.16×10^{-8}	59.0	4.16×10^{-8}	62.1
4.31×10^{-7}	49.6	5.33×10^{-8}	63.3	5.33×10^{-8}	56.7	5.33×10^{-8}	60.4
4.56×10^{-7}	49.3	6.89×10^{-8}	61.5	6.89×10^{-8}	55.3	6.89×10^{-8}	58.8
4.81×10^{-7}	49.0	8.84×10^{-8}	60.4	8.84×10^{-8}	53.6	8.84×10^{-8}	56.7
5.30×10^{-7}	48.8	1.10×10^{-7}	52.5	1.10×10^{-7}	52.1	1.10×10^{-7}	54.9
5.79×10^{-7}	48.6	1.36×10^{-7}	51.7	1.36×10^{-7}	51.2	1.36×10^{-7}	52.2
6.28×10^{-7}	48.3	1.75×10^{-7}	50.6	1.75×10^{-7}	50.1	1.75×10^{-7}	51.6
6.76×10^{-7}	48.1	2.26×10^{-7}	50.0	2.26×10^{-7}	49.5	2.26×10^{-7}	51.0
7.36×10^{-7}	47.8	2.77×10^{-7}	49.7	2.89×10^{-7}	48.9	2.89×10^{-7}	50.6
8.07×10^{-7}	47.5	3.27×10^{-7}	49.2	3.65×10^{-7}	48.5	3.65×10^{-7}	50.2
9.01×10^{-7}	47.0	3.78×10^{-7}	48.9	4.65×10^{-7}	47.9	4.65×10^{-7}	49.9
1.02×10^{-6}	46.2	4.40×10^{-7}	48.7	5.99×10^{-7}	47.2	5.99×10^{-7}	49.8
1.15×10^{-6}	45.2	5.14×10^{-7}	48.3	7.56×10^{-7}	46.3	7.56×10^{-7}	49.8
1.31×10^{-6}	43.4	6.12×10^{-7}	48.0	9.38×10^{-7}	45.6	9.38×10^{-7}	49.9
1.51×10^{-6}	41.3	7.32×10^{-7}	47.5	1.14×10^{-6}	44.3	1.14×10^{-6}	49.9
1.72×10^{-6}	40.7	8.74×10^{-7}	46.7	1.37×10^{-6}	43.1		
1.92×10^{-6}	38.2	1.10×10^{-6}	45.9	1.58×10^{-6}	42.4		
2.12×10^{-6}	36.8	1.55×10^{-6}	44.3	1.79×10^{-6}	42.8		

Table B-3 (cont'd) Surface tension of P84/16-3-16/pDNA mixtures of varying P84 mole fraction in water at 25°C

Trial 3							
α = 0.2 P84		**α = 0.4 P84**		**α = 0.6 P84**		**α = 0.8 P84**	
Concentration (mol/L)	**γ (mN/m)**	**Concentration (mol/L)**	**γ (mN/m)**	**Concentration (mol/L)**	**γ (mN/m)**	**Concentration (mol/L)**	**γ (mN/m)**
0.00	72.5	0.00	72.4	0.00	73.9	0.00	74.1
2.62×10^{-8}	72.5	7.87×10^{-9}	72.3	7.87×10^{-9}	73.7	7.87×10^{-9}	73.8
1.82×10^{-7}	71.9	9.18×10^{-9}	72.3	9.18×10^{-9}	73.4	9.18×10^{-9}	73.2
2.58×10^{-7}	70.2	1.10×10^{-8}	72.2	1.10×10^{-8}	73.0	1.10×10^{-8}	72.8
2.83×10^{-7}	66.4	1.36×10^{-8}	72.1	1.36×10^{-8}	72.5	1.36×10^{-8}	71.5
3.09×10^{-7}	64.5	1.68×10^{-8}	71.9	1.68×10^{-8}	71.2	1.68×10^{-8}	69.2
3.34×10^{-7}	61.6	2.07×10^{-8}	71.5	2.07×10^{-8}	69.1	2.07×10^{-8}	67.8
3.59×10^{-7}	59.3	2.59×10^{-8}	71.0	2.59×10^{-8}	67.3	2.59×10^{-8}	65.9
3.84×10^{-7}	57.1	3.25×10^{-8}	70.0	3.25×10^{-8}	65.9	3.25×10^{-8}	64.5
4.09×10^{-7}	54.2	4.16×10^{-8}	68.9	4.16×10^{-8}	64.9	4.16×10^{-8}	63.4
4.34×10^{-7}	52.5	5.33×10^{-8}	67.6	5.33×10^{-8}	63.8	5.33×10^{-8}	61.2
4.59×10^{-7}	50.7	6.89×10^{-8}	66.4	6.89×10^{-8}	61.8	6.89×10^{-8}	59.6
4.83×10^{-7}	49.7	8.84×10^{-8}	64.7	8.84×10^{-8}	60.4	8.84×10^{-8}	58.1
5.32×10^{-7}	49.1	1.10×10^{-7}	62.9	1.10×10^{-7}	58.3	1.10×10^{-7}	56.0
5.81×10^{-7}	48.6	1.36×10^{-7}	60.9	1.36×10^{-7}	56.2	1.36×10^{-7}	53.8
6.30×10^{-7}	48.2	1.75×10^{-7}	58.8	1.75×10^{-7}	53.7	1.75×10^{-7}	52.1
6.78×10^{-7}	47.6	2.26×10^{-7}	56.4	2.26×10^{-7}	51.8	2.26×10^{-7}	50.9
7.38×10^{-7}	47.3	2.77×10^{-7}	52.8	2.89×10^{-7}	50.7	2.89×10^{-7}	50.2
8.09×10^{-7}	46.8	3.27×10^{-7}	51.4	3.65×10^{-7}	49.9	3.65×10^{-7}	49.8
9.03×10^{-7}	46.2	3.77×10^{-7}	50.5	4.65×10^{-7}	49.4	4.65×10^{-7}	49.3
1.02×10^{-6}	45.3	4.39×10^{-7}	50.0	5.99×10^{-7}	48.8	5.99×10^{-7}	49.1
1.16×10^{-6}	44.2	5.13×10^{-7}	49.4	7.56×10^{-7}	48.5	7.56×10^{-7}	48.7
1.31×10^{-6}	42.5	6.12×10^{-7}	49.0	9.38×10^{-7}	48.0	9.38×10^{-7}	48.4
1.51×10^{-6}	40.8	7.32×10^{-7}	48.5	1.14×10^{-6}	47.3	6.89×10^{-8}	73.8
1.72×10^{-6}	39.2	8.74×10^{-7}	47.9	1.37×10^{-6}	46.9		
1.93×10^{-6}	36.3	1.10×10^{-6}	46.7	1.58×10^{-6}	46.6		
2.20×10^{-6}	33.8	1.55×10^{-6}	45.1	1.79×10^{-6}	46.6		

Table B-4 Surface tension of L121/16-3-16/pDNA mixtures of varying L121 mole fraction in water at 25°C

Trial 1							
α = 0.2 L121		**α = 0.4 L121**		**α = 0.6 L121**		**α = 0.8 L121**	
Concentration (mol/L)	**γ (mN/m)**	**Concentration (mol/L)**	**γ (mN/m)**	**Concentration (mol/L)**	**γ (mN/m)**	**Concentration (mol/L)**	**γ (mN/m)**
1.31×10^{-9}	71.0	7.87×10^{-9}	73.0	7.87×10^{-9}	72.2	7.87×10^{-9}	72.3
2.62×10^{-9}	71.1	9.18×10^{-9}	73.0	2.10×10^{-8}	71.5	1.83×10^{-8}	71.4
3.93×10^{-9}	71.2	1.18×10^{-8}	72.8	3.40×10^{-8}	69.9	2.49×10^{-8}	70.8
5.77×10^{-9}	71.2	1.57×10^{-8}	72.7	4.71×10^{-8}	67.5	3.14×10^{-8}	69.2
8.39×10^{-9}	71.2	2.10×10^{-8}	72.7	5.75×10^{-8}	66.0	3.92×10^{-8}	62.9
1.23×10^{-8}	71.2	2.75×10^{-8}	72.5	7.05×10^{-8}	60.5	4.71×10^{-8}	60.8
1.89×10^{-8}	71.2	3.66×10^{-8}	72.2	8.74×10^{-8}	56.1	5.75×10^{-8}	58.6
2.80×10^{-8}	71.2	4.84×10^{-8}	71.6	1.07×10^{-7}	54.8	7.05×10^{-8}	56.3
4.24×10^{-8}	71.1	6.14×10^{-8}	71.3	1.33×10^{-7}	53.0	8.61×10^{-8}	51.4
6.58×10^{-8}	70.6	7.83×10^{-8}	70.4	1.58×10^{-7}	51.3	1.06×10^{-7}	47.3
9.70×10^{-8}	70.2	9.78×10^{-8}	67.7	1.84×10^{-7}	47.9	1.28×10^{-7}	46.3
1.36×10^{-7}	68.7	1.21×10^{-7}	65.5	2.22×10^{-7}	45.4	1.53×10^{-7}	45.3
1.87×10^{-7}	67.2	1.60×10^{-7}	62.4	2.73×10^{-7}	43.4	1.92×10^{-7}	44.1
2.64×10^{-7}	65.1	1.98×10^{-7}	59.1	3.36×10^{-7}	43.1	2.43×10^{-7}	43.1
3.64×10^{-7}	60.4	2.49×10^{-7}	53.3	4.16×10^{-7}	42.6	3.06×10^{-7}	42.5
4.89×10^{-7}	55.8	3.38×10^{-7}	49.3	5.15×10^{-7}	41.9	3.82×10^{-7}	41.9
6.35×10^{-7}	51.3	4.38×10^{-7}	47.2	6.37×10^{-7}	41.4	5.05×10^{-7}	41.2
8.03×10^{-7}	48.2	5.73×10^{-7}	44.2	7.81×10^{-7}	40.9	6.52×10^{-7}	40.7
9.67×10^{-7}	44.9	7.18×10^{-7}	42.2	9.68×10^{-7}	40.6	8.42×10^{-7}	40.2
1.13×10^{-6}	42.0	9.07×10^{-7}	40.8	1.20×10^{-6}	40.5	1.07×10^{-6}	39.6
1.28×10^{-6}	40.1	1.14×10^{-6}	39.4	1.42×10^{-6}	40.9	1.30×10^{-6}	39.4
1.44×10^{-6}	38.8	1.36×10^{-6}	38.4	1.63×10^{-6}	40.7	1.52×10^{-6}	39.0
1.63×10^{-6}	37.4	1.58×10^{-6}	37.5	1.84×10^{-6}	40.7	1.73×10^{-6}	38.8
1.84×10^{-6}	37.5	1.79×10^{-6}	36.8	2.04×10^{-6}	40.9	1.93×10^{-6}	38.7
2.04×10^{-6}	38.2	1.99×10^{-6}	36.0	2.24×10^{-6}	41.5	2.13×10^{-6}	38.6
2.18×10^{-6}	36.6	2.19×10^{-6}	35.2	2.43×10^{-6}	41.9	2.33×10^{-6}	38.5
		2.38×10^{-6}	34.5	2.62×10^{-6}	41.6		

Table B-4 (cont'd) Surface tension of L121/16-3-16/pDNA mixtures of varying L121 mole fraction in water at 25°C

Trial 2							
α = 0.2 L121		**α = 0.4 L121**		**α = 0.6 L121**		**α = 0.8 L121**	
Concentration (mol/L)	**γ (mN/m)**	**Concentration (mol/L)**	**γ (mN/m)**	**Concentration (mol/L)**	**γ (mN/m)**	**Concentration (mol/L)**	**γ (mN/m)**
2.62×10^{-8}	74.4	5.23×10^{-8}	71.9	7.87×10^{-9}	72.4	7.87×10^{-9}	71.6
5.23×10^{-8}	74.4	6.53×10^{-8}	70.6	1.05×10^{-8}	72.2	1.83×10^{-8}	70.9
7.83×10^{-8}	74.5	7.83×10^{-8}	69.6	1.31×10^{-8}	71.9	2.10×10^{-8}	69.5
9.13×10^{-8}	74.5	9.13×10^{-8}	67.2	1.57×10^{-8}	71.3	2.36×10^{-8}	67.7
1.04×10^{-7}	74.4	1.07×10^{-7}	65.1	1.83×10^{-8}	70.0	2.75×10^{-8}	64.4
1.20×10^{-7}	74.4	1.22×10^{-7}	61.4	2.10×10^{-8}	69.5	3.19×10^{-8}	59.2
1.40×10^{-7}	73.8	1.43×10^{-7}	60.1	2.49×10^{-8}	66.0	3.64×10^{-8}	56.2
1.64×10^{-7}	73.6	1.66×10^{-7}	56.4	2.88×10^{-8}	61.9	4.16×10^{-8}	52.7
1.89×10^{-7}	73.1	1.89×10^{-7}	55.4	3.40×10^{-8}	59.6	4.81×10^{-8}	50.9
2.15×10^{-7}	72.4	2.12×10^{-7}	54.0	3.92×10^{-8}	57.1	5.46×10^{-8}	49.5
2.53×10^{-7}	71.5	2.38×10^{-7}	52.8	4.45×10^{-8}	54.2	6.24×10^{-8}	50.3
2.91×10^{-7}	70.1	2.63×10^{-7}	51.8	5.23×10^{-8}	53.4	7.28×10^{-8}	49.8
3.41×10^{-7}	68.4	2.88×10^{-7}	49.2	6.27×10^{-8}	51.2	8.45×10^{-8}	47.9
4.04×10^{-7}	66.5	3.26×10^{-7}	48.5	7.57×10^{-8}	50.2	1.00×10^{-7}	46.5
4.83×10^{-7}	64.0	3.77×10^{-7}	47.4	9.13×10^{-8}	48.7	1.18×10^{-7}	45.6
5.81×10^{-7}	61.7	4.26×10^{-7}	46.5	1.07×10^{-7}	47.5	1.38×10^{-7}	44.9
7.02×10^{-7}	57.7	5.01×10^{-7}	45.5	1.27×10^{-7}	46.4	1.63×10^{-7}	44.7
8.45×10^{-7}	55.2	5.98×10^{-7}	44.4	1.51×10^{-7}	45.5	2.15×10^{-7}	44.4
1.03×10^{-6}	52.9	7.19×10^{-7}	42.2	1.76×10^{-7}	45.1	2.91×10^{-7}	44.2
1.26×10^{-6}	50.9	8.85×10^{-7}	40.8	2.02×10^{-7}	44.8	3.91×10^{-7}	44.4
1.48×10^{-6}	48.5	1.09×10^{-6}	39.6	2.28×10^{-7}	44.6		
1.69×10^{-6}	47.3	1.32×10^{-6}	38.9	2.78×10^{-7}	44.2		
1.90×10^{-6}	46.9	1.53×10^{-6}	38.9	3.29×10^{-7}	44.0		
2.10×10^{-6}	46.8	1.75×10^{-6}	38.6	4.04×10^{-7}	44.1		
2.29×10^{-6}	46.7	1.95×10^{-6}	38.5	5.03×10^{-7}	43.9		
2.48×10^{-6}	47.0	2.15×10^{-6}	38.8	6.25×10^{-7}	43.9		

Table B-4 (cont'd) Surface tension of L121/16-3-16/pDNA mixtures of varying L121 mole fraction in water at 25°C

Trial 3							
α = 0.2 L121		**α = 0.4 L121**		**α = 0.6 L121**		**α = 0.8 L121**	
Concentration (mol/L)	**γ (mN/m)**	**Concentration (mol/L)**	**γ (mN/m)**	**Concentration (mol/L)**	**γ (mN/m)**	**Concentration (mol/L)**	**γ (mN/m)**
7.87×10^{-9}	72.4	7.87×10^{-9}	72.0	7.87×10^{-9}	72.2	7.87×10^{-9}	72.1
2.09×10^{-8}	72.3	2.09×10^{-8}	72.0	1.05×10^{-8}	72.2	1.83×10^{-8}	70.4
3.40×10^{-8}	72.3	3.40×10^{-8}	71.9	1.31×10^{-8}	72.0	2.10×10^{-8}	65.6
4.71×10^{-8}	72.3	4.71×10^{-8}	71.8	1.57×10^{-8}	71.9	2.36×10^{-8}	61.0
6.27×10^{-8}	72.3	6.01×10^{-8}	71.5	1.83×10^{-8}	71.7	2.62×10^{-8}	56.3
7.83×10^{-8}	72.2	7.57×10^{-8}	71.2	2.10×10^{-8}	71.3	2.88×10^{-8}	53.8
9.91×10^{-8}	72.0	9.65×10^{-8}	70.5	2.49×10^{-8}	70.9	3.27×10^{-8}	50.6
1.22×10^{-7}	71.8	1.20×10^{-7}	69.1	3.01×10^{-8}	69.7	3.66×10^{-8}	48.3
1.48×10^{-7}	71.5	1.46×10^{-7}	67.1	3.53×10^{-8}	68.5	4.19×10^{-8}	46.7
1.74×10^{-7}	70.9	1.71×10^{-7}	61.9	4.06×10^{-8}	62.8	4.84×10^{-8}	46.5
2.12×10^{-7}	69.8	2.10×10^{-7}	58.1	4.58×10^{-8}	61.8	5.62×10^{-8}	46.3
2.50×10^{-7}	68.1	2.48×10^{-7}	52.6	5.10×10^{-8}	60.9	6.66×10^{-8}	45.8
3.01×10^{-7}	65.8	2.99×10^{-7}	50.5	5.88×10^{-8}	59.7	7.83×10^{-8}	45.5
3.64×10^{-7}	61.4	3.61×10^{-7}	46.8	6.66×10^{-8}	58.5	9.38×10^{-8}	45.2
4.44×10^{-7}	58.1	4.41×10^{-7}	44.4	7.96×10^{-8}	57.3	1.12×10^{-7}	44.5
5.42×10^{-7}	55.2	5.40×10^{-7}	42.6	9.51×10^{-8}	53.8	1.31×10^{-7}	44.2
6.64×10^{-7}	51.5	6.61×10^{-7}	41.5	1.16×10^{-7}	51.7	1.57×10^{-7}	44.1
8.07×10^{-7}	48.2	8.05×10^{-7}	40.3	1.39×10^{-7}	49.9	2.08×10^{-7}	43.6
9.94×10^{-7}	44.5	9.92×10^{-7}	39.3	1.65×10^{-7}	48.3	2.85×10^{-7}	43.3
1.22×10^{-6}	41.8	1.22×10^{-6}	38.8	1.90×10^{-7}	46.6	3.85×10^{-7}	43.0
1.44×10^{-6}	39.7	1.44×10^{-6}	38.7	2.16×10^{-7}	45.1	5.09×10^{-7}	42.7
1.66×10^{-6}	38.8	1.65×10^{-6}	38.0	2.67×10^{-7}	43.7	6.55×10^{-7}	42.3
1.86×10^{-6}	38.5	1.86×10^{-6}	38.0	3.18×10^{-7}	42.7		
2.07×10^{-6}	37.7	2.06×10^{-6}	37.6	3.93×10^{-7}	41.8		
2.26×10^{-6}	37.5	2.26×10^{-6}	37.5	4.92×10^{-7}	40.8		
2.45×10^{-6}	72.4	2.45×10^{-6}	37.4	6.02×10^{-7}	40.3		

Table B-3 Surface tension of F127/16-3-16/pDNA mixtures of varying F127 mole fraction in water at 25°C

Trial 1							
α = 0.2 F127		**α = 0.4 F127**		**α = 0.6 F127**		**α = 0.8 F127**	
Concentration (mol/L)	**γ (mN/m)**	**Concentration (mol/L)**	**γ (mN/m)**	**Concentration (mol/L)**	**γ (mN/m)**	**Concentration (mol/L)**	**γ (mN/m)**
0.00	69.8	0.00	69.8	0.00	69.5	0.00	70.2
6.67×10^{-10}	68.8	6.67×10^{-10}	68.8	6.67×10^{-10}	69.1	6.67×10^{-10}	69.6
1.33×10^{-9}	68.7	1.33×10^{-9}	69.4	1.33×10^{-9}	69.2	1.33×10^{-9}	69.2
2.67×10^{-9}	68.7	2.00×10^{-9}	69.2	2.00×10^{-9}	68.8	2.00×10^{-9}	69.0
5.33×10^{-9}	68.7	3.33×10^{-9}	69.3	3.33×10^{-9}	68.2	3.33×10^{-9}	68.1
9.32×10^{-9}	68.7	5.33×10^{-9}	69.1	5.33×10^{-9}	67.6	5.33×10^{-9}	66.3
1.46×10^{-8}	68.5	8.66×10^{-9}	68.8	8.66×10^{-9}	66.9	8.66×10^{-9}	65.1
2.26×10^{-8}	68.5	1.40×10^{-8}	68.2	1.40×10^{-8}	65.6	1.40×10^{-8}	63.4
3.58×10^{-8}	68.3	2.19×10^{-8}	67.4	2.19×10^{-8}	61.9	2.19×10^{-8}	61.2
5.56×10^{-8}	66.8	3.52×10^{-8}	65.8	3.52×10^{-8}	61.0	3.52×10^{-8}	59.9
8.83×10^{-8}	64.6	5.82×10^{-8}	63.0	5.82×10^{-8}	59.5	5.82×10^{-8}	58.1
1.40×10^{-7}	61.8	9.10×10^{-8}	60.1	9.10×10^{-8}	58.6	9.10×10^{-8}	56.4
2.17×10^{-7}	59.7	1.43×10^{-7}	58.4	1.43×10^{-7}	56.8	1.43×10^{-7}	54.2
3.29×10^{-7}	58.1	2.19×10^{-7}	56.0	2.19×10^{-7}	53.4	2.19×10^{-7}	51.7
4.73×10^{-7}	55.6	3.43×10^{-7}	53.2	3.43×10^{-7}	50.7	3.43×10^{-7}	50.1
9.48×10^{-7}	50.5	5.34×10^{-7}	50.4	5.34×10^{-7}	48.8	5.34×10^{-7}	48.3
1.39×10^{-6}	49.6	8.13×10^{-7}	48.4	8.13×10^{-7}	47.2	8.13×10^{-7}	47.2
1.81×10^{-6}	48.4	1.22×10^{-6}	47.1	1.22×10^{-6}	46.1	1.22×10^{-6}	45.8
2.26×10^{-6}	48.1	1.67×10^{-6}	46.3	1.58×10^{-6}	44.9	1.75×10^{-6}	45.5
2.76×10^{-6}	47.6	2.13×10^{-6}	45.7	2.06×10^{-6}	44.8	2.34×10^{-6}	45.5
3.27×10^{-6}	47.7	2.71×10^{-6}	45.1	2.65×10^{-6}	44.1	2.94×10^{-6}	44.4
3.70×10^{-6}	47.7	3.19×10^{-6}	45.1	3.28×10^{-6}	44.5		
4.31×10^{-6}	45.9	3.71×10^{-6}	44.9	3.85×10^{-6}	44.5		
		4.30×10^{-6}	45.2	4.30×10^{-6}	43.5		

Table B-5 (cont'd) Surface tension of F127/16-3-16/pDNA mixtures of varying F127 mole fraction in water at 25°C

Trial 2							
α = 0.2 F127		**α = 0.4 F127**		**α = 0.6 F127**		**α = 0.8 F127**	
Concentration (mol/L)	**γ (mN/m)**	**Concentration (mol/L)**	**γ (mN/m)**	**Concentration (mol/L)**	**γ (mN/m)**	**Concentration (mol/L)**	**γ (mN/m)**
0.00	68.5	0.00	69.8	0.00	69.4	0.00	69.7
1.33×10^{-9}	68.0	1.33×10^{-9}	68.6	1.33×10^{-9}	68.0	1.67×10^{-9}	67.9
2.67×10^{-9}	67.9	2.67×10^{-9}	68.3	2.67×10^{-9}	64.8	3.33×10^{-9}	64.1
4.53×10^{-9}	67.9	4.53×10^{-9}	66.8	4.53×10^{-9}	60.0	5.00×10^{-9}	61.5
7.20×10^{-9}	67.5	7.20×10^{-9}	65.1	7.20×10^{-9}	58.5	8.34×10^{-9}	59.8
1.12×10^{-8}	67.3	1.12×10^{-8}	63.2	1.12×10^{-8}	58.2	1.33×10^{-8}	58.7
1.78×10^{-8}	66.9	1.78×10^{-8}	61.9	1.78×10^{-8}	57.2	2.16×10^{-8}	58.4
2.85×10^{-8}	66.4	2.85×10^{-8}	60.7	2.85×10^{-8}	57.0	3.49×10^{-8}	57.6
4.44×10^{-8}	65.1	5.50×10^{-8}	60.0	4.44×10^{-8}	55.7	5.48×10^{-8}	56.9
7.09×10^{-8}	63.6	8.41×10^{-8}	59.0	7.09×10^{-8}	54.7	8.79×10^{-8}	55.1
1.13×10^{-7}	61.8	1.26×10^{-7}	58.4	1.13×10^{-7}	53.0	1.44×10^{-7}	52.8
1.79×10^{-7}	59.7	1.92×10^{-7}	56.8	1.79×10^{-7}	51.7	2.26×10^{-7}	51.1
2.82×10^{-7}	57.7	2.95×10^{-7}	54.5	2.82×10^{-7}	50.1	3.55×10^{-7}	49.0
4.35×10^{-7}	55.4	4.48×10^{-7}	51.9	4.35×10^{-7}	48.3	5.46×10^{-7}	47.3
6.83×10^{-7}	50.7	6.96×10^{-7}	49.4	6.83×10^{-7}	47.4	8.57×10^{-7}	46.1
1.06×10^{-6}	48.6	1.08×10^{-6}	47.4	1.06×10^{-6}	46.2	1.33×10^{-6}	45.7
1.62×10^{-6}	46.9	1.63×10^{-6}	46.7	1.62×10^{-6}	45.4	2.03×10^{-6}	44.9
2.44×10^{-6}	46.1	2.45×10^{-6}	46.5	2.44×10^{-6}	45.0	3.05×10^{-6}	44.3
3.50×10^{-6}	45.6	3.50×10^{-6}	46.2	3.50×10^{-6}	44.6	4.77×10^{-6}	43.4
4.68×10^{-6}	46.0	4.68×10^{-6}	45.6	4.68×10^{-6}	44.2	7.60×10^{-6}	40.6
5.71×10^{-6}	45.3	5.88×10^{-6}	45.7	5.87×10^{-6}	44.2		
				6.84×10^{-6}	44.0		
				7.78×10^{-6}	43.3		
				8.60×10^{-6}	42.7		

Table B-4 (cont'd) Surface tension of F127/16-3-16/pDNA mixtures of varying F127 mole fraction in water at 25°C

Trial 3							
α = 0.2 F127		**α = 0.4 F127**		**α = 0.6 F127**		**α = 0.8 F127**	
Concentration (mol/L)	**γ (mN/m)**	**Concentration (mol/L)**	**γ (mN/m)**	**Concentration (mol/L)**	**γ (mN/m)**	**Concentration (mol/L)**	**γ (mN/m)**
0.00	69.1	0.00	69.6	0.00	68.5	0.00	69.2
1.33×10^{-9}	68.3	1.33×10^{-9}	68.7	1.33×10^{-9}	67.5	1.33×10^{-9}	67.7
2.67×10^{-9}	68.2	2.67×10^{-9}	68.4	2.67×10^{-9}	66.0	2.67×10^{-9}	64.5
4.53×10^{-9}	67.8	4.53×10^{-9}	67.3	4.53×10^{-9}	64.6	4.00×10^{-9}	62.2
7.20×10^{-9}	67.2	7.20×10^{-9}	63.8	7.20×10^{-9}	63.7	6.66×10^{-9}	60.4
1.12×10^{-8}	66.7	1.12×10^{-8}	62.4	1.12×10^{-8}	60.8	1.07×10^{-8}	59.6
1.78×10^{-8}	65.0	1.78×10^{-8}	60.3	1.78×10^{-8}	59.7	1.73×10^{-8}	58.9
2.85×10^{-8}	63.1	2.85×10^{-8}	59.6	2.85×10^{-8}	59.0	2.80×10^{-8}	58.7
4.44×10^{-8}	61.4	4.44×10^{-8}	59.1	4.44×10^{-8}	57.6	4.39×10^{-8}	57.9
7.09×10^{-8}	59.4	7.09×10^{-8}	58.6	7.09×10^{-8}	56.8	7.04×10^{-8}	56.9
1.13×10^{-7}	58.7	1.13×10^{-7}	57.4	1.13×10^{-7}	55.1	1.13×10^{-7}	55.7
1.79×10^{-7}	58.1	1.79×10^{-7}	56.3	1.79×10^{-7}	51.3	1.78×10^{-7}	53.3
2.82×10^{-7}	57.0	2.82×10^{-7}	53.9	2.82×10^{-7}	48.7	2.82×10^{-7}	51.0
4.35×10^{-7}	54.7	4.35×10^{-7}	51.5	4.35×10^{-7}	47.4	4.35×10^{-7}	49.6
6.83×10^{-7}	50.7	6.83×10^{-7}	49.8	6.83×10^{-7}	46.1	6.83×10^{-7}	47.6
1.06×10^{-6}	48.4	1.06×10^{-6}	48.1	1.06×10^{-6}	45.4	1.06×10^{-6}	46.4
1.62×10^{-6}	47.1	1.62×10^{-6}	47.0	1.62×10^{-6}	45.1	1.62×10^{-6}	45.5
2.44×10^{-6}	46.1	2.44×10^{-6}	45.7	2.44×10^{-6}	44.2	2.44×10^{-6}	45.2
3.50×10^{-6}	45.5	3.50×10^{-6}	45.1	3.50×10^{-6}	43.2	3.50×10^{-6}	44.7
4.68×10^{-6}	45.9	4.68×10^{-6}	44.9	4.68×10^{-6}	42.8	4.68×10^{-6}	44.0
5.87×10^{-6}	45.6	5.87×10^{-6}	44.9	5.87×10^{-6}	42.7	5.87×10^{-6}	43.1

Table B-6 Surface tension of P103/16-3-16/pDNA mixtures of varying P103 mole fraction in water at 25°C

Trial 1							
α = 0.2 P103		**α = 0.4 P103**		**α = 0.6 P103**		**α = 0.8 P103**	
Concentration (mol/L)	**γ (mN/m)**	**Concentration (mol/L)**	**γ (mN/m)**	**Concentration (mol/L)**	**γ (mN/m)**	**Concentration (mol/L)**	**γ (mN/m)**
0.00	68.8			0.00	69.6	0.00	69.3
6.67×10^{-10}	68.5	6.67×10^{-10}	69.2	6.67×10^{-10}	68.0	1.33×10^{-9}	68.1
1.33×10^{-9}	68.5	1.33×10^{-9}	69.2	1.33×10^{-9}	67.9	2.00×10^{-9}	68.1
2.00×10^{-9}	68.4	2.00×10^{-9}	69.0	2.00×10^{-9}	68.1	2.93×10^{-9}	68.0
2.93×10^{-9}	68.2	2.93×10^{-9}	68.9	2.93×10^{-9}	68.1	4.26×10^{-9}	68.0
4.26×10^{-9}	68.1	4.26×10^{-9}	68.7	4.26×10^{-9}	68.0	6.93×10^{-9}	67.7
6.26×10^{-9}	68.1	6.26×10^{-9}	68.6	6.26×10^{-9}	67.7	1.09×10^{-8}	67.3
8.92×10^{-9}	68.1	8.92×10^{-9}	68.4	8.92×10^{-9}	67.6	1.62×10^{-8}	66.2
1.29×10^{-8}	67.9	1.29×10^{-8}	68.1	1.29×10^{-8}	67.2	2.22×10^{-8}	65.0
1.96×10^{-8}	67.6	1.96×10^{-8}	67.9	1.96×10^{-8}	66.6	2.88×10^{-8}	60.6
2.88×10^{-8}	67.3	2.88×10^{-8}	67.6	2.88×10^{-8}	65.1	3.68×10^{-8}	59.0
4.20×10^{-8}	66.9	4.20×10^{-8}	66.6	4.20×10^{-8}	63.8	4.60×10^{-8}	57.5
6.83×10^{-8}	66.2	6.83×10^{-8}	64.6	6.83×10^{-8}	61.5	5.72×10^{-8}	55.3
1.07×10^{-7}	64.9	1.07×10^{-7}	61.6	1.07×10^{-7}	58.3	7.03×10^{-8}	50.1
1.53×10^{-7}	63.0	1.53×10^{-7}	56.4	1.53×10^{-7}	52.9	8.99×10^{-8}	46.9
2.16×10^{-7}	60.6	2.16×10^{-7}	47.3	2.16×10^{-7}	44.9	1.16×10^{-7}	44.1
3.10×10^{-7}	58.0	3.10×10^{-7}	43.9	3.10×10^{-7}	42.7	1.55×10^{-7}	43.1
4.31×10^{-7}	51.3	4.31×10^{-7}	42.5	4.31×10^{-7}	41.5	2.18×10^{-7}	42.0
6.06×10^{-7}	44.6	6.06×10^{-7}	41.6	6.62×10^{-7}	40.6	3.05×10^{-7}	41.2
8.27×10^{-7}	42.5	8.27×10^{-7}	40.1	9.33×10^{-7}	40.0	4.15×10^{-7}	40.5
1.13×10^{-6}	41.5	1.13×10^{-6}	40.5	1.28×10^{-6}	39.7	5.91×10^{-7}	39.7
1.59×10^{-6}	41.2	1.59×10^{-6}	40.1	1.72×10^{-6}	39.0	8.12×10^{-7}	39.2
1.99×10^{-6}	41.2	1.99×10^{-6}	39.8	2.10×10^{-6}	38.9	1.12×10^{-6}	38.7
2.48×10^{-6}	40.9	2.48×10^{-6}	39.6	2.45×10^{-6}	38.8	1.58×10^{-6}	38.3
2.78×10^{-6}	40.7	2.89×10^{-6}	39.9	2.75×10^{-6}	38.6	1.98×10^{-6}	38.0
				2.86×10^{-6}	38.5	2.40×10^{-6}	37.9

Table B-6 (cont'd) Surface tension of P103/16-3-16/pDNA mixtures of varying P103 mole fraction in water at 25°C

Trial 2							
α = 0.2 P103		**α = 0.4 P103**		**α = 0.6 P103**		**α = 0.8 P103**	
Concentration (mol/L)	**γ (mN/m)**	**Concentration (mol/L)**	**γ (mN/m)**	**Concentration (mol/L)**	**γ (mN/m)**	**Concentration (mol/L)**	**γ (mN/m)**
0.00	69.5	0.00	69.4	0.00	70.3	0.00	69.6
6.67×10^{-10}	68.8	2.00×10^{-9}	66.3	2.00×10^{-9}	68.9	1.33×10^{-9}	67.6
1.33×10^{-9}	68.7	4.00×10^{-9}	69.1	4.00×10^{-9}	68.8	2.00×10^{-9}	68.0
2.00×10^{-9}	68.6	6.00×10^{-9}	69.1	6.00×10^{-9}	68.6	2.93×10^{-9}	67.8
2.93×10^{-9}	68.4	7.99×10^{-9}	69.0	8.66×10^{-9}	68.3	4.26×10^{-9}	67.6
4.26×10^{-9}	68.7	1.07×10^{-8}	68.8	1.26×10^{-8}	68.0	6.93×10^{-9}	67.2
6.26×10^{-9}	68.3	1.46×10^{-8}	68.4	1.80×10^{-8}	67.8	1.09×10^{-8}	66.7
8.92×10^{-9}	68.5	2.00×10^{-8}	68.1	2.46×10^{-8}	66.9	1.62×10^{-8}	65.6
1.29×10^{-8}	68.4	2.52×10^{-8}	67.6	3.39×10^{-8}	66.4	2.22×10^{-8}	63.8
1.96×10^{-8}	68.3	3.19×10^{-8}	66.9	4.70×10^{-8}	64.8	2.88×10^{-8}	62.4
2.88×10^{-8}	68.2	4.11×10^{-8}	65.8	6.68×10^{-8}	62.9	3.67×10^{-8}	60.5
4.20×10^{-8}	68.0	5.43×10^{-8}	63.7	9.29×10^{-8}	58.0	4.60×10^{-8}	58.6
6.83×10^{-8}	67.5	8.05×10^{-8}	60.8	1.32×10^{-7}	53.5	5.72×10^{-8}	56.9
1.07×10^{-7}	66.8	1.20×10^{-7}	56.5	1.70×10^{-7}	48.2	7.03×10^{-8}	54.3
1.53×10^{-7}	64.3	1.58×10^{-7}	52.2	2.15×10^{-7}	44.8	8.99×10^{-8}	50.9
2.16×10^{-7}	60.5	2.22×10^{-7}	47.1	2.77×10^{-7}	42.3	1.16×10^{-7}	46.5
3.10×10^{-7}	55.6	3.15×10^{-7}	43.9	3.69×10^{-7}	41.6	1.55×10^{-7}	43.9
4.31×10^{-7}	47.9	4.36×10^{-7}	42.4	4.89×10^{-7}	41.0	2.18×10^{-7}	42.5
6.06×10^{-7}	43.8	6.11×10^{-7}	41.7	7.17×10^{-7}	40.2	3.05×10^{-7}	41.6
8.27×10^{-7}	42.3	8.32×10^{-7}	40.9	9.83×10^{-7}	39.6	4.15×10^{-7}	40.5
1.13×10^{-6}	41.7	1.14×10^{-6}	40.1	1.28×10^{-6}	39.0	5.91×10^{-7}	39.8
1.59×10^{-6}	41.4	1.60×10^{-6}	39.3	1.72×10^{-6}	38.8	8.12×10^{-7}	39.2
1.99×10^{-6}	41.3	2.00×10^{-6}	39.0	2.10×10^{-6}	38.4	1.12×10^{-6}	38.7
2.48×10^{-6}	41.3	2.48×10^{-6}	38.6	2.44×10^{-6}	38.2	1.58×10^{-6}	38.0
2.78×10^{-6}	41.3	2.89×10^{-6}	38.4	2.75×10^{-6}	38.2	1.98×10^{-6}	37.6
2.86×10^{-6}	41.1			2.86×10^{-6}	38.2	2.40×10^{-6}	37.5
						2.88×10^{-6}	37.3

Table B-5 (cont'd) Surface tension of P103/16-3-16/pDNA mixtures of varying P103 mole fraction in water at 25°C

Trial 3							
α = 0.2 P103		**α = 0.4 P103**		**α = 0.6 P103**		**α = 0.8 P103**	
Concentration (mol/L)	**γ (mN/m)**	**Concentration (mol/L)**	**γ (mN/m)**	**Concentration (mol/L)**	**γ (mN/m)**	**Concentration (mol/L)**	**γ (mN/m)**
0.00	69.5	0.00	70.2	0.00	69.5	0.00	68.9
1.33×10^{-9}	68.5	2.00×10^{-9}	69.0	6.67×10^{-10}	68.3	1.33×10^{-9}	68.3
2.67×10^{-9}	68.8	4.00×10^{-9}	69.0	1.33×10^{-9}	68.2	2.00×10^{-9}	68.1
4.00×10^{-9}	68.7	6.00×10^{-9}	68.9	3.33×10^{-9}	68.2	2.93×10^{-9}	68.0
5.33×10^{-9}	68.6	7.99×10^{-9}	68.9	6.00×10^{-9}	68.2	4.26×10^{-9}	67.8
7.33×10^{-9}	68.8	1.07×10^{-8}	69.0	9.99×10^{-9}	68.0	6.93×10^{-9}	67.3
9.99×10^{-9}	68.7	1.46×10^{-8}	68.6	1.53×10^{-8}	67.8	1.09×10^{-8}	66.9
1.53×10^{-8}	68.6	2.00×10^{-8}	68.5	2.19×10^{-8}	67.4	1.62×10^{-8}	65.6
2.33×10^{-8}	68.6	2.52×10^{-8}	68.4	3.12×10^{-8}	66.6	2.22×10^{-8}	63.8
3.39×10^{-8}	68.6	3.19×10^{-8}	68.2	4.44×10^{-8}	65.4	2.88×10^{-8}	61.6
4.71×10^{-8}	68.5	4.11×10^{-8}	67.8	6.41×10^{-8}	63.0	3.68×10^{-8}	58.8
6.68×10^{-8}	68.4	5.43×10^{-8}	67.1	9.03×10^{-8}	59.5	4.60×10^{-8}	56.9
9.29×10^{-8}	67.8	8.05×10^{-8}	65.8	1.29×10^{-7}	53.1	5.72×10^{-8}	53.7
1.32×10^{-7}	67.3	1.20×10^{-7}	62.2	1.68×10^{-7}	46.3	7.03×10^{-8}	50.2
1.83×10^{-7}	65.5	1.58×10^{-7}	58.7	2.12×10^{-7}	43.6	8.99×10^{-8}	47.6
2.46×10^{-7}	59.9	2.22×10^{-7}	50.3	2.75×10^{-7}	42.3	1.16×10^{-7}	45.2
3.39×10^{-7}	51.7	3.15×10^{-7}	44.6	3.67×10^{-7}	41.3	1.55×10^{-7}	43.3
4.59×10^{-7}	45.8	4.36×10^{-7}	42.5	4.87×10^{-7}	40.4	2.18×10^{-7}	41.8
6.33×10^{-7}	42.9	6.11×10^{-7}	41.2	7.15×10^{-7}	39.9	3.05×10^{-7}	40.8
8.52×10^{-7}	41.8	8.32×10^{-7}	40.6	9.81×10^{-7}	39.3	4.15×10^{-7}	40.2
1.16×10^{-6}	41.2	1.14×10^{-6}	40.0	1.28×10^{-6}	38.9	5.91×10^{-7}	39.5
1.61×10^{-6}	41.1	1.60×10^{-6}	39.5	1.72×10^{-6}	38.5	8.12×10^{-7}	38.7
2.01×10^{-6}	41.1	2.00×10^{-6}	39.4	2.10×10^{-6}	38.4	1.12×10^{-6}	38.2
2.49×10^{-6}	41.0	2.48×10^{-6}	39.4	2.80×10^{-6}	38.3	1.49×10^{-6}	37.7
2.90×10^{-6}	41.2	2.89×10^{-6}	39.4			1.91×10^{-6}	37.4
						2.34×10^{-6}	37.3

Table B-7 Surface tension of L44/16-3-16/pDNA mixtures of varying L44 mole fraction in water at 25°C

Trial 1							
α = 0.2 L44		**α = 0.4 L44**		**α = 0.6 L44**		**α = 0.8 L44**	
Concentration (mol/L)	**γ (mN/m)**	**Concentration (mol/L)**	**γ (mN/m)**	**Concentration (mol/L)**	**γ (mN/m)**	**Concentration (mol/L)**	**γ (mN/m)**
6.67×10^{-10}	68.6	6.67×10^{-10}	69.2	6.67×10^{-10}	68.2	6.67×10^{-10}	68.8
1.33×10^{-9}	68.5	1.33×10^{-9}	69.0	1.33×10^{-9}	67.9	1.33×10^{-9}	68.7
2.27×10^{-9}	68.6	2.27×10^{-9}	69.3	2.27×10^{-9}	67.7	2.27×10^{-9}	68.5
3.60×10^{-9}	68.6	3.60×10^{-9}	69.2	3.60×10^{-9}	67.6	3.60×10^{-9}	68.4
6.26×10^{-9}	68.7	6.26×10^{-9}	69.3	6.26×10^{-9}	67.4	6.26×10^{-9}	68.2
1.03×10^{-8}	68.7	1.03×10^{-8}	69.2	1.03×10^{-8}	67.0	1.03×10^{-8}	67.5
1.69×10^{-8}	68.6	1.69×10^{-8}	69.1	1.69×10^{-8}	66.5	1.69×10^{-8}	67.3
2.62×10^{-8}	68.6	2.62×10^{-8}	69.1	2.62×10^{-8}	65.8	2.62×10^{-8}	66.6
3.94×10^{-8}	68.5	3.94×10^{-8}	69.1	3.94×10^{-8}	64.9	3.94×10^{-8}	65.2
6.57×10^{-8}	68.7	6.57×10^{-8}	69.1	6.57×10^{-8}	63.8	6.57×10^{-8}	63.1
9.84×10^{-8}	68.1	1.05×10^{-7}	68.5	1.05×10^{-7}	61.3	1.05×10^{-7}	60.4
1.31×10^{-7}	66.8	1.56×10^{-7}	66.2	1.56×10^{-7}	58.9	1.56×10^{-7}	57.1
1.63×10^{-7}	64.5	2.20×10^{-7}	61.2	2.20×10^{-7}	56.8	2.20×10^{-7}	55.7
1.95×10^{-7}	61.8	3.07×10^{-7}	57.2	3.07×10^{-7}	56.0	3.07×10^{-7}	54.5
2.26×10^{-7}	59.4	4.17×10^{-7}	56.5	4.17×10^{-7}	55.0	4.17×10^{-7}	53.8
2.64×10^{-7}	58.4	5.35×10^{-7}	55.1	5.35×10^{-7}	54.4	5.35×10^{-7}	53.1
3.13×10^{-7}	57.0	7.05×10^{-7}	54.3	7.05×10^{-7}	53.6	7.05×10^{-7}	52.8
3.75×10^{-7}	56.5	1.02×10^{-6}	53.6	1.02×10^{-6}	52.6	1.02×10^{-6}	52.1
4.70×10^{-7}	55.9	1.36×10^{-6}	52.6	1.50×10^{-6}	51.9	1.36×10^{-6}	51.6
5.87×10^{-7}	55.0	1.71×10^{-6}	52.1	1.98×10^{-6}	51.4	1.71×10^{-6}	51.1
7.54×10^{-7}	54.4	2.10×10^{-6}	51.7	2.53×10^{-6}	50.5	2.10×10^{-6}	50.9
9.67×10^{-7}	53.8	2.50×10^{-6}	51.1	2.77×10^{-6}	49.5	2.50×10^{-6}	50.3
1.26×10^{-6}	53.1	2.71×10^{-6}	50.7			2.96×10^{-6}	50.1
1.62×10^{-6}	52.3	2.91×10^{-6}	50.5			3.44×10^{-6}	49.9
2.02×10^{-6}	52.2					3.65×10^{-6}	49.6

Table B-7 (cont'd) Surface tension of L44/16-3-16/pDNA mixtures of varying L44 mole fraction in water at 25°C

Trial 2							
α = 0.2 L44		**α = 0.4 L44**		**α = 0.6 L44**		**α = 0.8 L44**	
Concentration (mol/L)	**γ (mN/m)**	**Concentration (mol/L)**	**γ (mN/m)**	**Concentration (mol/L)**	**γ (mN/m)**	**Concentration (mol/L)**	**γ (mN/m)**
1.00×10^{-10}	69.01	6.67×10^{-10}	68.8	6.67×10^{-10}	69.6	6.67×10^{-10}	69.4
2.00×10^{-9}	69.1	1.33×10^{-9}	68.8	1.33×10^{-9}	69.5	1.33×10^{-9}	69.5
3.40×10^{-9}	69.2	2.27×10^{-9}	68.7	2.27×10^{-9}	69.5	2.27×10^{-9}	69.4
5.40×10^{-9}	69.1	3.60×10^{-9}	68.7	3.60×10^{-9}	69.7	3.60×10^{-9}	69.5
9.39×10^{-9}	69.1	6.26×10^{-9}	68.6	6.26×10^{-9}	69.5	6.26×10^{-9}	69.4
1.54×10^{-8}	69.0	1.03×10^{-8}	68.7	1.03×10^{-8}	69.3	1.03×10^{-8}	69.3
2.53×10^{-8}	68.9	1.69×10^{-8}	68.6	1.69×10^{-8}	69.4	1.69×10^{-8}	69.0
3.92×10^{-8}	68.9	2.62×10^{-8}	68.6	2.62×10^{-8}	68.7	2.62×10^{-8}	68.7
5.90×10^{-8}	68.8	3.94×10^{-8}	68.7	3.94×10^{-8}	67.9	3.94×10^{-8}	67.9
9.82×10^{-8}	68.5	6.57×10^{-8}	67.9	5.92×10^{-8}	67.1	5.26×10^{-8}	66.4
1.47×10^{-7}	68.0	9.84×10^{-8}	66.8	7.88×10^{-8}	65.2	6.57×10^{-8}	64.3
1.95×10^{-7}	65.8	1.31×10^{-7}	63.7	1.05×10^{-7}	62.6	8.53×10^{-8}	61.7
2.51×10^{-7}	63.0	1.63×10^{-7}	60.7	1.44×10^{-7}	59.8	1.05×10^{-7}	59.6
3.26×10^{-7}	59.3	1.95×10^{-7}	58.6	1.95×10^{-7}	57.8	1.31×10^{-7}	58.1
4.17×10^{-7}	57.7	2.26×10^{-7}	57.5	2.58×10^{-7}	56.6	1.69×10^{-7}	56.9
5.23×10^{-7}	56.3	2.58×10^{-7}	56.9	3.32×10^{-7}	55.4	2.20×10^{-7}	56.2
6.43×10^{-7}	55.4	2.95×10^{-7}	55.7	4.29×10^{-7}	54.7	2.83×10^{-7}	55.0
7.92×10^{-7}	54.8	3.44×10^{-7}	55.3	5.35×10^{-7}	54.2	3.56×10^{-7}	54.4
9.51×10^{-7}	54.1	4.05×10^{-7}	54.7	6.49×10^{-7}	53.5	4.52×10^{-7}	53.5
1.25×10^{-6}	53.4	4.76×10^{-7}	54.7	8.67×10^{-7}	53.2	5.58×10^{-7}	52.8
1.65×10^{-6}	52.3	5.58×10^{-7}	54.1	1.17×10^{-6}	52.4	7.27×10^{-7}	52.4
2.12×10^{-6}	50.8	6.60×10^{-7}	54.0	1.54×10^{-6}	51.9	9.41×10^{-7}	51.8
2.61×10^{-6}	49.4	7.71×10^{-7}	53.2	1.87×10^{-6}	51.0	1.24×10^{-6}	51.4
3.11×10^{-6}	48.0	9.82×10^{-7}	52.7	2.24×10^{-6}	50.0	1.60×10^{-6}	50.8
3.58×10^{-6}	46.8	1.28×10^{-6}	51.0	2.62×10^{-6}	49.1	2.00×10^{-6}	50.5
4.02×10^{-6}	46.7	1.63×10^{-6}	50.0	3.07×10^{-6}	48.0	2.48×10^{-6}	50.0
4.38×10^{-6}	46.7	2.03×10^{-6}	48.7	3.53×10^{-6}	47.6	3.00×10^{-6}	49.7
		2.57×10^{-6}	50.1			3.56×10^{-6}	49.2
		3.07×10^{-6}	49.3				

Table B-76 (cont'd) Surface tension of L44/16-3-16/pDNA mixtures of varying L44 mole fraction in water at 25°C

Trial 3							
α = 0.2 L44		**α = 0.4 L44**		**α = 0.6 L44**		**α = 0.8 L44**	
Concentration (mol/L)	**γ (mN/m)**	**Concentration (mol/L)**	**γ (mN/m)**	**Concentration (mol/L)**	**γ (mN/m)**	**Concentration (mol/L)**	**γ (mN/m)**
6.67×10^{-10}	69.5	6.67×10^{-10}	69.1	6.67×10^{-10}	69.0	6.67×10^{-10}	69.1
1.33×10^{-9}	69.7	1.33×10^{-9}	69.1	1.33×10^{-9}	69.0	1.33×10^{-9}	69.0
2.27×10^{-9}	69.6	2.27×10^{-9}	68.9	2.27×10^{-9}	69.0	2.27×10^{-9}	69.0
3.60×10^{-9}	69.8	3.60×10^{-9}	68.9	3.60×10^{-9}	68.8	3.60×10^{-9}	68.9
6.26×10^{-9}	69.7	6.26×10^{-9}	68.8	6.26×10^{-9}	68.9	6.26×10^{-9}	68.8
1.03×10^{-8}	69.9	1.03×10^{-8}	68.7	1.03×10^{-8}	68.9	1.03×10^{-8}	69.0
1.69×10^{-8}	69.9	1.69×10^{-8}	68.5	1.69×10^{-8}	68.8	1.69×10^{-8}	68.5
2.62×10^{-8}	69.8	2.62×10^{-8}	68.3	2.62×10^{-8}	68.5	2.62×10^{-8}	68.2
3.94×10^{-8}	69.7	3.94×10^{-8}	68.2	3.94×10^{-8}	68.2	3.94×10^{-8}	67.5
6.57×10^{-8}	69.5	6.57×10^{-8}	67.8	5.92×10^{-8}	67.4	5.26×10^{-8}	65.9
9.84×10^{-8}	69.3	9.84×10^{-8}	66.3	7.88×10^{-8}	66.0	6.57×10^{-8}	63.9
1.31×10^{-7}	68.4	1.31×10^{-7}	63.5	1.05×10^{-7}	63.3	8.53×10^{-8}	60.9
1.63×10^{-7}	65.7	1.63×10^{-7}	60.2	1.44×10^{-7}	59.7	1.05×10^{-7}	58.7
1.95×10^{-7}	63.3	1.95×10^{-7}	58.0	1.95×10^{-7}	57.6	1.31×10^{-7}	57.6
2.26×10^{-7}	60.9	2.26×10^{-7}	56.9	2.58×10^{-7}	56.4	1.69×10^{-7}	56.6
2.64×10^{-7}	58.7	2.58×10^{-7}	56.4	3.32×10^{-7}	54.9	2.20×10^{-7}	55.9
3.13×10^{-7}	57.7	2.95×10^{-7}	55.2	4.29×10^{-7}	54.1	2.83×10^{-7}	54.6
3.75×10^{-7}	57.0	3.44×10^{-7}	54.9	5.35×10^{-7}	53.7	3.56×10^{-7}	54.3
4.70×10^{-7}	55.7	4.05×10^{-7}	54.6	6.49×10^{-7}	53.2	4.52×10^{-7}	53.6
5.87×10^{-7}	55.0	4.76×10^{-7}	54.2	8.67×10^{-7}	52.6	5.58×10^{-7}	53.2
7.54×10^{-7}	54.5	5.58×10^{-7}	53.7	1.17×10^{-6}	52.0	7.27×10^{-7}	52.3
9.67×10^{-7}	53.8	6.60×10^{-7}	52.9	1.54×10^{-6}	51.1	9.41×10^{-7}	51.9
1.26×10^{-6}	53.5	7.71×10^{-7}	52.7	1.87×10^{-6}	50.9	1.24×10^{-6}	51.3
1.62×10^{-6}	52.9	9.82×10^{-7}	52.2	2.24×10^{-6}	50.5	1.60×10^{-6}	50.8
2.02×10^{-6}	52.3	1.28×10^{-6}	51.7	2.62×10^{-6}	50.1	2.00×10^{-6}	50.3
2.56×10^{-6}	51.4	1.63×10^{-6}	51.4	3.07×10^{-6}	50.2	2.48×10^{-6}	49.9
3.11×10^{-6}	50.7	2.03×10^{-6}	51.2	3.57×10^{-6}	49.9	3.00×10^{-6}	49.6
		2.57×10^{-6}	50.7			3.56×10^{-6}	49.0
		3.12×10^{-6}	50.7				

Table B-8 Surface tension of F87 in water at 25°C

Trial 1		Trial 2		Trial 3	
Concentration (mol/L)	**γ (mN/m)**	**Concentration (mol/L)**	**γ (mN/m)**	**Concentration (mol/L)**	**γ (mN/m)**
0.00	70.6	0.00	70.4	0.00	70.3
3.17×10^{-5}	43.2	3.17×10^{-5}	42.73	3.17×10^{-5}	42.8
6.18×10^{-5}	42.2	6.18×10^{-5}	41.9	6.18×10^{-5}	42.1
9.06×10^{-5}	41.7	9.06×10^{-5}	41.4	9.06×10^{-5}	41.5
1.18×10^{-4}	41.3	1.18×10^{-4}	41.0	1.18×10^{-4}	41.2
1.44×10^{-4}	40.9	1.44×10^{-4}	40.7	1.44×10^{-4}	40.8
1.69×10^{-4}	40.6	1.69×10^{-4}	40.5	1.69×10^{-4}	40.5
1.93×10^{-4}	40.4	1.93×10^{-4}	40.3	1.93×10^{-4}	40.4
2.16×10^{-4}	40.0	2.16×10^{-4}	40.2	2.16×10^{-4}	40.2
2.39×10^{-4}	39.8	2.39×10^{-4}	39.9	2.39×10^{-4}	40.1
2.60×10^{-4}	39.7	2.60×10^{-4}	39.8	2.60×10^{-4}	40.0
2.80×10^{-4}	39.6	2.80×10^{-4}	39.7	2.80×10^{-4}	39.8
3.00×10^{-4}	39.5	3.00×10^{-4}	39.7	3.00×10^{-4}	39.8
3.19×10^{-4}	39.5	3.19×10^{-4}	39.6	3.19×10^{-4}	39.7
3.37×10^{-4}	39.5	3.37×10^{-4}	39.5	3.37×10^{-4}	39.6
3.54×10^{-4}	39.4	3.54×10^{-4}	39.5	3.54×10^{-4}	39.5
3.71×10^{-4}	39.4	3.71×10^{-4}	39.5	3.71×10^{-4}	39.5
4.03×10^{-4}	39.4	3.87×10^{-4}	39.4	3.87×10^{-4}	39.4
4.33×10^{-4}	39.4	4.03×10^{-4}	39.4	4.03×10^{-4}	39.4
4.61×10^{-4}	39.3	4.18×10^{-4}	39.4	4.18×10^{-4}	39.3
4.87×10^{-4}	39.2	4.33×10^{-4}	39.3	4.33×10^{-4}	39.4
5.12×10^{-4}	39.2	4.47×10^{-4}	39.3	4.47×10^{-4}	39.4
5.35×10^{-4}	39.3	4.61×10^{-4}	39.2	4.61×10^{-4}	39.4
		4.74×10^{-4}	39.2	4.74×10^{-4}	39.4
		4.87×10^{-4}	39.1	4.87×10^{-4}	39.4
		5.00×10^{-4}	39.1	5.00×10^{-4}	39.3
		5.12×10^{-4}	39.1	5.12×10^{-4}	39.3
		5.35×10^{-4}	39.1	5.23×10^{-4}	39.3
		5.46×10^{-4}	39.2	5.35×10^{-4}	39.3
		5.57×10^{-4}	39.2		
		5.67×10^{-4}	39.2		

Table B-9 Surface tension of P84 in water at 25°C

Trial 1		Trial 2		Trial 3	
Concentration (mol/L)	**γ (mN/m)**	**Concentration (mol/L)**	**γ (mN/m)**	**Concentration (mol/L)**	**γ (mN/m)**
0.00	72.6	0.00	72.2	4.50×10^{-5}	38.7
1.58×10^{-5}	42.4	6.35×10^{-6}	42.6	5.60×10^{-5}	38.4
3.16×10^{-5}	41.7	7.93×10^{-6}	41.9	7.02×10^{-5}	38.3
4.74×10^{-5}	41.1	9.52×10^{-6}	41.7	8.60×10^{-5}	38.0
6.31×10^{-5}	40.7	1.11×10^{-5}	41.5	1.10×10^{-4}	37.9
7.87×10^{-5}	40.4	1.33×10^{-5}	41.1	1.41×10^{-4}	37.6
9.43×10^{-5}	40.2	1.65×10^{-5}	40.9	1.88×10^{-4}	37.3
1.10×10^{-4}	40.0	2.12×10^{-5}	40.6	2.50×10^{-4}	37.1
1.41×10^{-4}	39.7	2.76×10^{-5}	40.3	3.11×10^{-4}	36.8
1.71×10^{-4}	39.5	3.55×10^{-5}	40.1	4.03×10^{-4}	36.6
2.02×10^{-4}	39.2	4.50×10^{-5}	39.8	5.24×10^{-4}	36.4
2.62×10^{-4}	38.9	5.60×10^{-5}	39.6	6.73×10^{-4}	36.3
3.22×10^{-4}	38.6	7.02×10^{-5}	39.3	8.19×10^{-4}	36.2
3.96×10^{-4}	38.4	8.60×10^{-5}	39.0	9.64×10^{-4}	36.2
4.68×10^{-4}	38.3	1.10×10^{-4}	38.7	1.11×10^{-3}	36.2
5.39×10^{-4}	38.3	1.41×10^{-4}	38.4	1.30×10^{-3}	36.2
6.09×10^{-4}	38.1	1.88×10^{-4}	38.1	1.52×10^{-3}	36.2
6.78×10^{-4}	38.1	2.50×10^{-4}	37.8	1.65×10^{-3}	36.2
7.46×10^{-4}	38.0	3.11×10^{-4}	37.5		
8.13×10^{-4}	38.1	4.03×10^{-4}	37.2		
8.79×10^{-4}	38.1	5.24×10^{-4}	37.0		
9.44×10^{-4}	38.0	6.73×10^{-4}	36.8		
1.01×10^{-3}	38.0	8.19×10^{-4}	36.7		
1.07×10^{-3}	38.1	9.64×10^{-4}	36.6		
1.13×10^{-3}	38.1	1.11×10^{-3}	36.6		
1.19×10^{-3}	38.1	1.30×10^{-3}	36.5		
1.25×10^{-3}	38.1	1.52×10^{-3}	36.5		
1.29×10^{-3}	38.1	1.65×10^{-3}	36.5		
1.33×10^{-3}	38.1				
1.36×10^{-3}	38.1				

Table B-10 Surface tension of L121 in water at 25°C

Trial 1		Trial 2		Trial 3	
Concentration (mol/L)	**γ (mN/m)**	**Concentration (mol/L)**	**γ (mN/m)**	**Concentration (mol/L)**	**γ (mN/m)**
0.00	73.7	0.00	73.8	0.00	72.3
1.43×10^{-9}	73.9	1.43×10^{-9}	73.7	1.43×10^{-9}	72.4
2.87×10^{-9}	73.9	1.58×10^{-8}	72.6	1.58×10^{-8}	71.1
4.30×10^{-9}	73.7	4.44×10^{-8}	72.5	4.44×10^{-8}	68.7
5.74×10^{-9}	73.5	7.29×10^{-8}	69.6	7.29×10^{-8}	64.1
7.74×10^{-9}	73.0	1.01×10^{-7}	64.4	1.01×10^{-7}	58.6
1.06×10^{-8}	71.9	1.30×10^{-7}	58.9	1.30×10^{-7}	54.4
1.49×10^{-8}	70.8	1.58×10^{-7}	53.0	1.58×10^{-7}	50.4
4.35×10^{-8}	64.3	1.86×10^{-7}	49.4	1.86×10^{-7}	48.0
7.20×10^{-8}	60.3	2.14×10^{-7}	47.0	2.14×10^{-7}	46.1
1.15×10^{-7}	54.5	2.56×10^{-7}	45.3	2.56×10^{-7}	44.7
1.64×10^{-7}	50.6	3.04×10^{-7}	43.6	3.04×10^{-7}	43.6
2.20×10^{-7}	47.8	3.60×10^{-7}	42.8	3.60×10^{-7}	42.4
2.76×10^{-7}	46.1	4.15×10^{-7}	41.7	4.15×10^{-7}	41.4
3.45×10^{-7}	44.6	4.83×10^{-7}	40.8	4.83×10^{-7}	40.7
4.27×10^{-7}	43.3	5.64×10^{-7}	40.0	5.64×10^{-7}	40.0
5.22×10^{-7}	42.6	6.57×10^{-7}	39.2	6.57×10^{-7}	39.4
6.23×10^{-7}	41.8	7.56×10^{-7}	38.6	7.56×10^{-7}	39.1
7.29×10^{-7}	41.3	8.61×10^{-7}	38.2	8.61×10^{-7}	38.7
8.60×10^{-7}	41.0	9.89×10^{-7}	37.8	9.89×10^{-7}	38.6
1.00×10^{-6}	40.8	1.13×10^{-6}	37.4	1.13×10^{-6}	38.4
1.15×10^{-6}	40.5	1.28×10^{-6}	37.0	1.28×10^{-6}	38.4
1.33×10^{-6}	40.4	1.45×10^{-6}	36.5	1.45×10^{-6}	38.5
1.53×10^{-6}	40.6	1.65×10^{-6}	36.0	1.65×10^{-6}	38.9
1.76×10^{-6}	41.3			2.09×10^{-6}	39.2
1.98×10^{-6}	41.8			2.31×10^{-6}	39.3
2.21×10^{-6}	42.4				

Table B-11 Surface tension of F127 in water at 25°C

Trial 1		Trial 2		Trial 3	
Concentration (mol/L)	**γ (mN/m)**	**Concentration (mol/L)**	**γ (mN/m)**	**Concentration (mol/L)**	**γ (mN/m)**
0.00	68.6	0.00	68.1	0.00	69.6
6.61×10^{-9}	57.0	6.61×10^{-9}	57.6	6.61×10^{-8}	48.2
1.32×10^{-8}	53.8	1.32×10^{-8}	54.2	1.32×10^{-7}	46.3
2.25×10^{-8}	52.1	2.25×10^{-8}	53.5	1.98×10^{-7}	45.5
3.57×10^{-8}	51.0	3.57×10^{-8}	52.7	2.91×10^{-7}	44.5
6.21×10^{-8}	49.5	6.21×10^{-8}	50.5	4.89×10^{-7}	44.0
9.52×10^{-8}	46.5	1.02×10^{-7}	48.8	7.53×10^{-7}	43.5
1.41×10^{-7}	44.0	1.68×10^{-7}	47.8	1.15×10^{-6}	43.1
2.54×10^{-7}	43.9	2.66×10^{-7}	46.2	1.81×10^{-6}	42.7
3.53×10^{-7}	43.0	3.97×10^{-7}	45.0	2.79×10^{-6}	42.2
4.85×10^{-7}	42.6	5.93×10^{-7}	44.0	4.11×10^{-6}	41.8
7.48×10^{-7}	42.2	9.82×10^{-7}	43.6	6.72×10^{-6}	41.4
1.14×10^{-6}	41.9	1.50×10^{-6}	42.8	1.06×10^{-5}	40.8
1.67×10^{-6}	41.5	2.13×10^{-6}	42.2	1.70×10^{-5}	40.4
2.32×10^{-6}	41.1	3.05×10^{-6}	41.8	2.64×10^{-5}	39.9
3.62×10^{-6}	40.6	4.26×10^{-6}	41.2	3.85×10^{-5}	39.4
6.20×10^{-6}	40.0	6.11×10^{-6}	41.2	6.17×10^{-5}	38.9
1.00×10^{-5}	39.5	8.29×10^{-6}	41.0	9.40×10^{-5}	38.4
1.50×10^{-5}	39.0	1.13×10^{-5}	40.4	1.42×10^{-4}	38.0
2.10×10^{-5}	38.6	1.59×10^{-5}	39.9	2.20×10^{-4}	37.8
3.30×10^{-5}	38.0	2.13×10^{-5}	39.6	3.32×10^{-4}	37.8
4.40×10^{-5}	37.5	2.98×10^{-5}	39.9	4.36×10^{-4}	37.9
5.92×10^{-5}	36.9	3.83×10^{-5}	40.2	6.55×10^{-4}	37.1
7.76×10^{-5}	36.7	5.74×10^{-5}	39.1	1.06×10^{-3}	36.3
9.80×10^{-5}	36.5	8.70×10^{-5}	38.9		
1.19×10^{-4}	36.3	1.14×10^{-4}	38.3		
1.40×10^{-4}	36.4				
1.61×10^{-4}	36.0				

Table B-12 Surface tension of P103 in water at 25°C

Trial 1		Trial 2		Trial 3	
Concentration (mol/L)	**γ (mN/m)**	**Concentration (mol/L)**	**γ (mN/m)**	**Concentration (mol/L)**	**γ (mN/m)**
0.00	68.3	0.00	69.2	0.00	69.1
1.68×10^{-10}	67.1	1.68×10^{-9}	67.9	1.68×10^{-9}	68.0
3.37×10^{-10}	67.2	3.37×10^{-9}	67.4	3.37×10^{-9}	66.7
5.05×10^{-10}	67.1	5.05×10^{-9}	66.3	5.05×10^{-9}	64.7
7.40×10^{-10}	67.2	7.40×10^{-9}	63.5	7.40×10^{-9}	62.9
1.08×10^{-9}	67.4	1.08×10^{-8}	59.5	1.08×10^{-8}	59.8
1.41×10^{-8}	67.2	1.92×10^{-8}	57.1	1.92×10^{-8}	57.1
2.25×10^{-8}	64.8	2.76×10^{-8}	56.0	2.76×10^{-8}	56.1
3.43×10^{-8}	59.5	4.10×10^{-8}	53.8	4.10×10^{-8}	52.9
4.77×10^{-8}	54.5	5.77×10^{-8}	50.7	5.77×10^{-8}	50.9
6.44×10^{-8}	50.9	9.12×10^{-8}	46.1	9.12×10^{-8}	46.1
9.12×10^{-8}	45.4	1.24×10^{-7}	43.9	1.24×10^{-7}	43.9
1.21×10^{-7}	41.6	1.74×10^{-7}	42.4	1.74×10^{-7}	42.2
1.54×10^{-7}	40.4	2.57×10^{-7}	41.7	2.57×10^{-7}	41.6
2.04×10^{-7}	39.4	3.55×10^{-7}	41.1	3.55×10^{-7}	41.0
2.70×10^{-7}	38.7	4.68×10^{-7}	40.5	4.68×10^{-7}	40.6
3.51×10^{-7}	38.4	6.27×10^{-7}	39.9	6.27×10^{-7}	40.3
4.32×10^{-7}	37.9	8.46×10^{-7}	39.5	8.46×10^{-7}	39.7
5.92×10^{-7}	37.3	1.12×10^{-6}	39.1	1.12×10^{-6}	39.2
9.04×10^{-7}	36.9	1.42×10^{-6}	38.9	1.42×10^{-6}	39.2
1.21×10^{-6}	36.2	1.84×10^{-6}	38.5	1.84×10^{-6}	39.0
1.50×10^{-6}	35.8	2.38×10^{-6}	38.4	2.38×10^{-6}	38.8
1.78×10^{-6}	35.6	3.01×10^{-6}	38.2	3.01×10^{-6}	38.6
2.06×10^{-6}	35.4	3.60×10^{-6}	37.9	3.25×10^{-6}	38.5
2.19×10^{-6}	35.3				
2.33×10^{-6}	35.1				
2.46×10^{-6}	34.9				

Table B-13 Surface tension of L44 in water at 25°C

Trial 1		Trial 2		Trial 3	
Concentration (mol/L)	**γ (mN/m)**	**Concentration (mol/L)**	**γ (mN/m)**	**Concentration (mol/L)**	**γ (mN/m)**
0.00	69.7	0.00	69.3	0.00	67.0
3.78×10^{-5}	46.3	1.89×10^{-6}	48.4	1.89×10^{-6}	50.4
7.55×10^{-5}	45.6	5.68×10^{-6}	48.3	5.68×10^{-6}	48.8
1.13×10^{-4}	45.2	2.46×10^{-5}	46.7	2.46×10^{-5}	47.3
1.51×10^{-4}	45.0	6.23×10^{-5}	45.7	6.23×10^{-5}	46.1
2.25×10^{-4}	44.4	9.99×10^{-5}	45.3	9.99×10^{-5}	45.5
2.99×10^{-4}	44.2	1.56×10^{-4}	44.9	1.56×10^{-4}	44.9
4.09×10^{-4}	43.4	2.68×10^{-4}	44.1	2.68×10^{-4}	44.1
7.69×10^{-4}	42.7	4.51×10^{-4}	43.7	4.51×10^{-4}	43.5
1.12×10^{-3}	42.1	7.21×10^{-4}	43.0	7.21×10^{-4}	42.9
1.45×10^{-3}	41.8	1.07×10^{-3}	42.6	1.07×10^{-3}	42.5
2.10×10^{-3}	41.4	1.41×10^{-3}	42.0	1.41×10^{-3}	41.9
2.70×10^{-3}	41.2	1.90×10^{-3}	41.6	1.90×10^{-3}	41.4
3.81×10^{-3}	40.8	2.51×10^{-3}	41.1	2.51×10^{-3}	40.8
4.94×10^{-3}	40.6	3.10×10^{-3}	40.8	3.10×10^{-3}	40.5
6.00×10^{-3}	40.4	3.78×10^{-3}	40.6	3.78×10^{-3}	40.1
7.01×10^{-3}	40.3	5.26×10^{-3}	40.3	4.41×10^{-3}	39.8
7.97×10^{-3}	40.1	6.30×10^{-3}	40.1	5.49×10^{-3}	39.7
8.89×10^{-3}	40.0	7.76×10^{-3}	40.0	6.51×10^{-3}	39.3
9.76×10^{-3}	40.0	9.54×10^{-3}	39.8	7.94×10^{-3}	39.3
1.18×10^{-2}	39.6	1.16×10^{-2}	39.7	9.70×10^{-3}	39.1
1.25×10^{-2}	39.5	1.27×10^{-2}	39.3	1.17×10^{-2}	38.8
1.42×10^{-2}	39.3			1.28×10^{-2}	38.7
1.58×10^{-2}	39.1				
1.77×10^{-2}	39.0				

Ethidium Bromide Fluorescence Data

Table B-14 Ethidium bromide – plasmid DNA fluorescence (ex./em. = 535 nm/595 nm) following addition of 16-3-16 at N^+/P^- = 10:1 (I_1) and Pluronic at varying mole fractions (I_2).

Trial 1							
Pluronic	**Pluronic Mole Fraction**	**Fluorescence (RFU)**					
		EtBr + pDNA in water (I_0)	**16-3-16 added (I_1)**	**Pluronic added (I_2)**	**I_1/I_0**	**I_2/I_0**	**Normalized Fluorescence ($I_2/I_0 - I_1/I_0$)**
F87	**0.8**	54.85	4.28	7.17	0.08	0.13	0.05
	0.6	101.16	17.12	22.80	0.17	0.23	0.06
	0.4	113.42	25.92	32.92	0.23	0.29	0.06
	0.2	115.99	53.99	58.74	0.47	0.51	0.04
P84	**0.8**	56.80	5.31	8.88	0.09	0.16	0.06
	0.6	100.41	13.73	21.47	0.14	0.21	0.08
	0.4	119.04	30.92	43.38	0.26	0.36	0.10
	0.2	145.48	47.48	57.39	0.33	0.39	0.07
L121	**0.8**	52.16	4.76	18.38	0.09	0.35	0.26
	0.6	85.69	12.82	44.99	0.15	0.53	0.38
	0.4	104.43	24.25	73.11	0.23	0.70	0.47
	0.2	115.60	38.81	109.09	0.34	0.94	0.61
F127	**0.8**	30.32	5.39	8.12	0.18	0.27	0.09
	0.6	54.95	15.11	25.17	0.27	0.46	0.18
	0.4	78.73	31.31	46.95	0.40	0.60	0.20
	0.2	93.11	51.15	66.84	0.55	0.72	0.17
P103	**0.8**	50.46	3.95	7.68	0.08	0.15	0.07
	0.6	97.73	13.39	24.04	0.14	0.25	0.11
	0.4	130.85	28.48	46.09	0.22	0.35	0.13
	0.2	148.71	47.80	66.35	0.32	0.45	0.12
L44	**0.8**	64.09	4.14	5.52	0.06	0.09	0.02
	0.6	115.10	11.76	13.72	0.10	0.12	0.02
	0.4	116.03	19.37	23.12	0.17	0.20	0.03
	0.2	121.50	30.27	32.61	0.25	0.27	0.02

Table B-14 (cont'd) Ethidium bromide – plasmid DNA fluorescence (ex./em. = 535 nm/595 nm) following addition of 16-3-16 at N^+/P^- = 10:1 (I_1) and Pluronic at varying mole fractions (I_2).

Trial 2							
Pluronic	**Pluronic Mole Fraction**	**Fluorescence (RFU)**					
		EtBr + pDNA in water (I_0)	**16-3-16 added (I_1)**	**Pluronic added (I_2)**	**I_1/I_0**	**I_2/I_0**	**Normalized Fluorescence ($I_2/I_0 - I_1/I_0$)**
F87	**0.8**	52.15	3.96	7.37	0.08	0.14	0.07
	0.6	101.49	15.05	25.03	0.15	0.25	0.10
	0.4	112.95	38.02	55.73	0.34	0.49	0.16
	0.2	123.67	55.36	74.06	0.45	0.60	0.15
P84	**0.8**	55.78	3.63	8.20	0.07	0.15	0.08
	0.6	102.19	12.69	22.93	0.12	0.22	0.10
	0.4	127.89	27.21	45.12	0.21	0.35	0.14
	0.2	147.74	47.90	74.22	0.32	0.50	0.18
L121	**0.8**	42.88	4.12	14.62	0.10	0.34	0.24
	0.6	78.48	11.89	44.05	0.15	0.56	0.41
	0.4	101.85	22.02	68.16	0.22	0.67	0.45
	0.2	100.17	30.44	88.85	0.30	0.89	0.58
F127	**0.8**	29.44	4.44	8.53	0.15	0.29	0.14
	0.6	60.24	16.89	32.38	0.28	0.54	0.26
	0.4	78.75	29.63	50.91	0.38	0.65	0.27
	0.2	95.43	51.33	74.91	0.54	0.78	0.25
P103	**0.8**	54.49	3.54	8.17	0.06	0.15	0.09
	0.6	99.19	14.17	30.09	0.14	0.30	0.16
	0.4	121.13	27.70	48.34	0.23	0.40	0.17
	0.2	140.63	45.52	69.01	0.32	0.49	0.17
L44	**0.8**	49.86	3.45	5.46	0.07	0.11	0.04
	0.6	101.25	12.91	19.05	0.13	0.19	0.06
	0.4	123.98	27.79	35.86	0.22	0.29	0.07
	0.2	137.71	46.38	56.83	0.34	0.41	0.08

Table B-14 (cont'd) Ethidium bromide – plasmid DNA fluorescence (I_0) (ex./em. = 535 nm/595 nm) following addition of 16-3-16 at N^+/P^- = 10:1 (I_1) and Pluronic at varying mole fractions (I_2).

Trial 3							
Pluronic	**Pluronic Mole Fraction**	**Fluorescence (RFU)**					
		EtBr + pDNA in water (I_0)	**16-3-16 added (I_1)**	**Pluronic added (I_2)**	***I_1/I_0***	***I_2/I_0***	**Normalized Fluorescence ($I_2/I_0 - I_1/I_0$)**
F87	**0.8**	57.81	4.24	7.82	0.07	0.14	0.07
	0.6	107.88	19.72	28.62	0.18	0.27	0.09
	0.4	104.78	29.97	43.34	0.29	0.41	0.12
	0.2	146.45	58.72	71.79	0.40	0.49	0.09
P84	**0.8**	49.91	3.53	6.91	0.07	0.14	0.07
	0.6	105.49	13.77	23.27	0.13	0.22	0.09
	0.4	133.38	29.45	44.36	0.22	0.33	0.11
	0.2	151.49	48.69	70.94	0.32	0.47	0.15
L121	**0.8**	51.83	4.79	15.57	0.09	0.30	0.21
	0.6	70.93	10.53	40.44	0.15	0.57	0.42
	0.4	93.52	19.06	63.97	0.20	0.68	0.48
	0.2	127.78	37.97	112.35	0.30	0.88	0.58
F127	**0.8**	31.84	4.84	9.58	0.15	0.30	0.15
	0.6	56.38	15.65	30.57	0.28	0.54	0.26
	0.4	87.52	31.73	50.94	0.36	0.58	0.22
	0.2	107.35	53.46	73.97	0.50	0.69	0.19
P103	**0.8**	51.01	3.55	7.45	0.07	0.15	0.08
	0.6	104.14	13.77	29.57	0.13	0.28	0.15
	0.4	132.22	28.07	49.08	0.21	0.37	0.16
	0.2	140.40	44.89	64.31	0.32	0.46	0.14
L44	**0.8**	48.03	3.79	5.89	0.08	0.12	0.04
	0.6	93.30	11.92	17.50	0.13	0.19	0.06
	0.4	129.06	29.10	37.80	0.23	0.29	0.06
	0.2	144.20	48.48	53.31	0.34	0.37	0.03

Linear Regression Analysis of Interaction Parameter Dependence on EO, PO, and Pluronic mole fraction (MF)

```
Coefficients:
             Estimate Std. Error t value Pr(>|t|)
(Intercept) -34.710807   1.493856 -23.236  < 2e-16 ***
EO           -0.011902   0.005656  -2.105    0.039 *
PO            0.528727   0.024228  21.823  < 2e-16 ***
MF           -7.796975   1.678272  -4.646  1.6e-05 ***
---
Signif. codes:  0 ‘***’ 0.001 ‘**’ 0.01 ‘*’ 0.05 ‘.’ 0.1 ‘ ’ 1

Residual standard error: 3.184 on 68 degrees of freedom
Multiple R-squared:  0.882,    Adjusted R-squared:  0.8768
F-statistic: 169.4 on 3 and 68 DF,  p-value: < 2.2e-16
```

Appendix C

Particle Size Data of Polydisperse Samples

Table C-1 Intensity statistics for hydrodynamic diameter measurements of 0.2 F87/16-3-16/pDNA, 0.2 P84/16-3-16/pDNA, and 0.2 L44/16-3-16/pDNA mixtures

Hydrodynamic diameter (nm)	Mean Intensity %	Standard Deviation Intensity %	Mean Intensity %	Standard Deviation Intensity %	Mean Intensity %	Standard Deviation Intensity %
	0.2 F87/16-3-16/pDNA		0.2 P84/16-3-16/pDNA		0.2 L44/16-3-16/pDNA	
0.4000	0.0	0.0	0.00	0.00	0.0	0.0
0.4632	0.0	0.0	0.00	0.00	0.0	0.0
0.5365	0.0	0.0	0.00	0.00	0.0	0.0
0.6213	0.0	0.0	0.00	0.00	0.0	0.0
0.7195	0.0	0.0	0.00	0.00	0.0	0.0
0.8332	0.0	0.0	0.00	0.00	0.0	0.0
0.9649	0.0	0.0	0.00	0.00	0.0	0.0
1.117	0.0	0.0	0.00	0.00	0.0	0.0
1.294	0.0	0.0	0.00	0.00	0.0	0.0
1.499	0.0	0.0	0.00	0.00	0.0	0.0
1.736	0.0	0.0	0.00	0.00	0.0	0.0
2.010	0.0	0.0	0.00	0.00	0.0	0.0
2.328	0.0	0.0	0.00	0.00	0.0	0.0
2.696	0.0	0.0	0.00	0.00	0.0	0.0
3.122	0.0	0.0	0.00	0.00	0.0	0.0
3.615	0.0	0.0	0.00	0.00	0.0	0.0
4.187	0.0	0.0	0.00	0.00	0.0	0.0
4.849	0.0	0.0	0.00	0.00	0.0	0.0
5.615	0.0	0.0	0.00	0.00	0.0	0.0
6.503	0.0	0.0	0.00	0.00	0.0	0.0
7.531	0.0	0.0	0.00	0.00	0.0	0.0
8.721	0.0	0.0	0.00	0.00	0.0	0.0
10.10	0.0	0.0	0.00	0.00	0.0	0.0
11.70	0.0	0.0	0.00	0.00	0.0	0.0
13.54	0.0	0.0	0.00	0.00	0.0	0.0
15.69	0.0	0.0	0.00	0.00	0.0	0.0
18.17	0.0	0.0	0.00	0.00	0.0	0.0
21.04	0.0	0.0	0.00	0.00	0.0	0.0
24.36	0.0	0.0	0.00	0.00	0.0	0.0
28.21	0.0	0.1	0.00	0.00	0.0	0.1
32.67	0.0	0.1	0.00	0.00	0.1	0.2
37.84	0.1	0.2	0.00	0.00	0.1	0.2
43.82	0.1	0.2	0.00	0.00	0.1	0.2

Table C-1 (cont'd) Intensity statistics for hydrodynamic diameter measurements of 0.2 F87/16-3-16/pDNA, 0.2 P84/16-3-16/pDNA, and 0.2 L44/16-3-16/pDNA mixtures

Hydrodynamic diameter (nm)	Mean Intensity %	Standard Deviation Intensity %	Mean Intensity %	Standard Deviation Intensity %	Mean Intensity %	Standard Deviation Intensity %
	0.2 F87/16-3-16/pDNA		0.2 P84/16-3-16/pDNA		0.2 L44/16-3-16/pDNA	
50.75	0.1	0.2	0.00	0.00	0.1	0.1
58.77	0.3	0.5	0.00	0.00	0.4	0.5
68.06	0.7	1.0	0.00	0.10	1.3	1.1
78.82	1.5	1.7	0.20	0.30	2.8	1.3
91.28	2.8	2.4	0.70	0.70	4.3	1.9
105.7	4.2	3.0	1.80	1.00	4.9	2.9
122.4	5.8	2.6	3.50	0.80	4.8	3.7
141.8	6.9	2.5	5.00	0.80	4.6	4.5
164.2	6.9	3.3	6.00	1.40	4.9	5.0
190.1	6.0	4.0	6.10	1.90	5.4	5.4
220.2	4.7	4.1	5.80	2.10	5.7	6.0
255.0	3.5	4.0	5.50	2.30	6.0	5.8
295.3	3.0	3.3	5.50	2.30	6.6	4.5
342.0	3.4	2.8	6.00	2.20	7.1	3.9
396.1	4.7	3.2	6.90	2.30	7.6	5.2
458.7	6.7	4.4	7.70	2.90	8.0	6.6
531.2	8.5	5.8	8.10	3.40	7.7	7.2
615.1	9.2	6.6	7.70	3.50	6.6	6.9
712.4	8.5	6.5	6.50	3.00	4.7	5.8
825.0	6.4	5.5	4.80	2.50	2.6	3.9
955.4	3.7	3.9	3.10	1.90	1.0	1.7
1106	1.5	2.3	1.90	1.40	0.1	0.3
1281	0.4	1.1	1.10	1.10	0.0	0.0
1484	0.1	0.2	0.60	0.90	0.0	0.0
1718	0.0	0.0	0.40	0.80	0.0	0.0
1990	0.0	0.0	0.20	0.60	0.0	0.0
2305	0.0	0.0	0.20	0.50	0.0	0.0
2669	0.0	0.0	0.20	0.30	0.0	0.0
3091	0.0	0.0	0.30	0.30	0.0	0.0
3580	0.0	0.0	0.50	0.60	0.1	0.1
4145	0.0	0.1	0.80	0.90	0.3	0.5
4801	0.0	0.1	1.10	1.10	0.6	1.2
5560	0.3	0.9	1.80	1.10	1.4	1.9
6439	0.0	0.0	0.00	0.00	0.0	0.0
7456	0.0	0.0	0.00	0.00	0.0	0.0
8635	0.0	0.0	0.00	0.00	0.0	0.0
10000	0.0	0.0	0.00	0.00	0.0	0.0

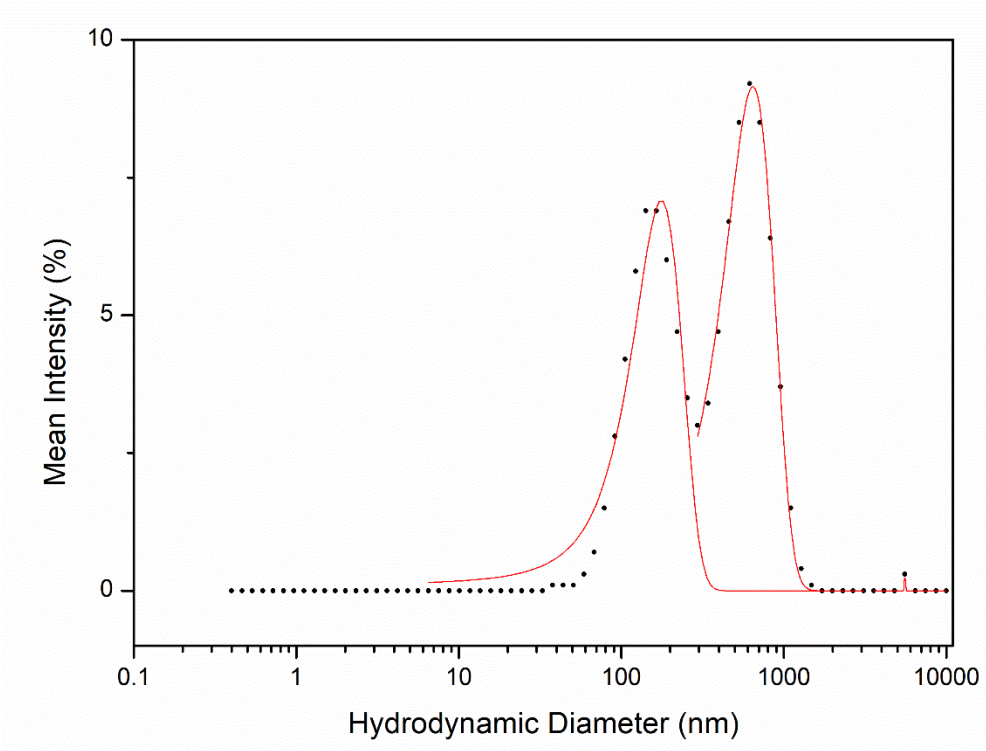

Figure C-1 Curve fitting of particle size distribution of 0.2 mole fraction F87/16-3-16/pDNA mixtures

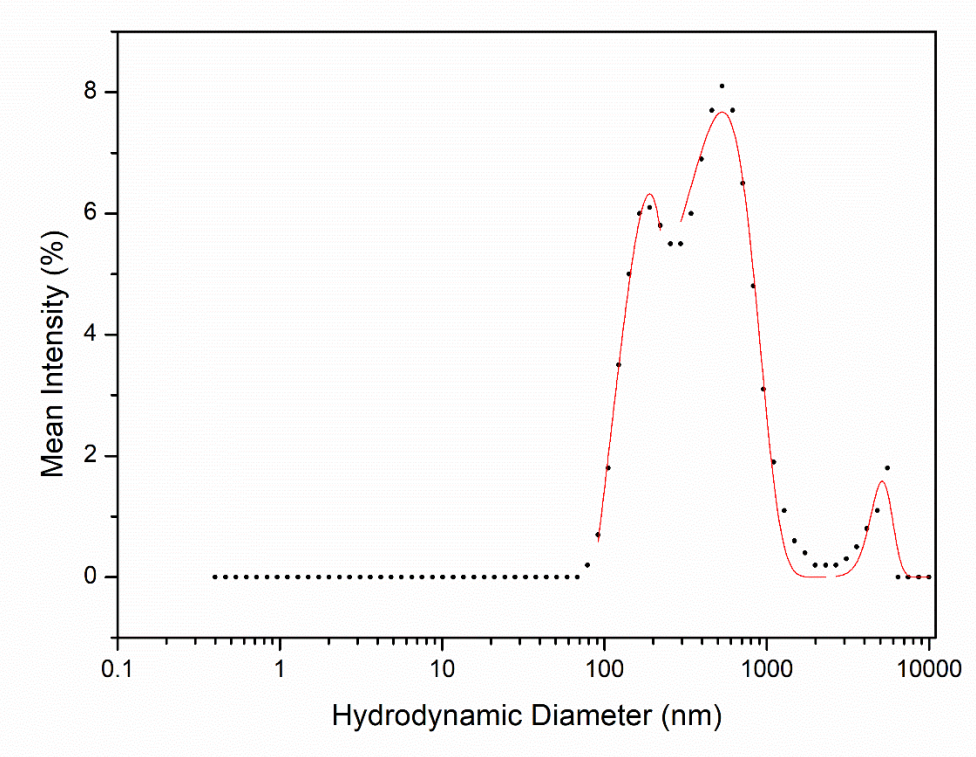

Figure C-2 Curve fitting of particle size distribution of 0.2 mole fraction P84/16-3-16/pDNA mixtures

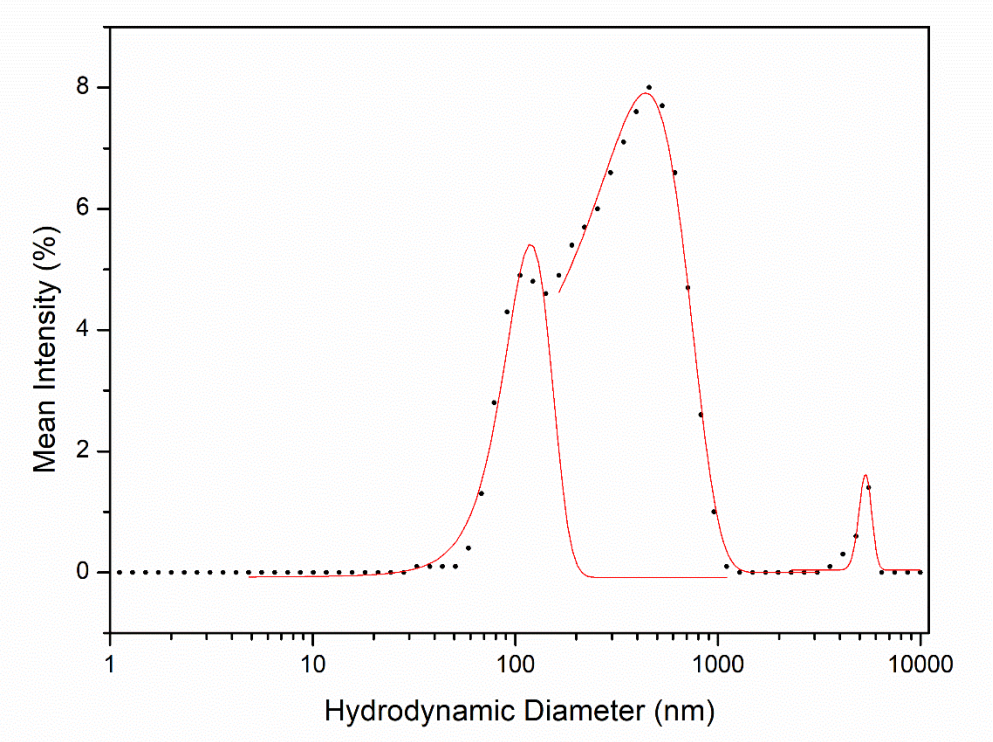

Figure C-3 Curve fitting of particle size distribution of 0.2 mole fraction L44/16-3-16/pDNA mixtures

Table C-2 Particle size of L121/16-3-16/pDNA nanoparticles measured at 25°C. Mean values ± standard deviation for triplicate measurements (n = 3) are reported.

L121 Mole Fraction	Mean hydrodynamic diameter (nm)	Mean PDI
0.2	148.7 ± 21.3	0.16 ± 0.02
0.4	152.1 ± 16.5	0.20 ± 0.03
0.6	158.4 ± 23.6	0.23 ± 0.01
0.8	156.2 ± 63.7	0.27 ± 0.02

Transfection Efficiency and Cell Viability Data

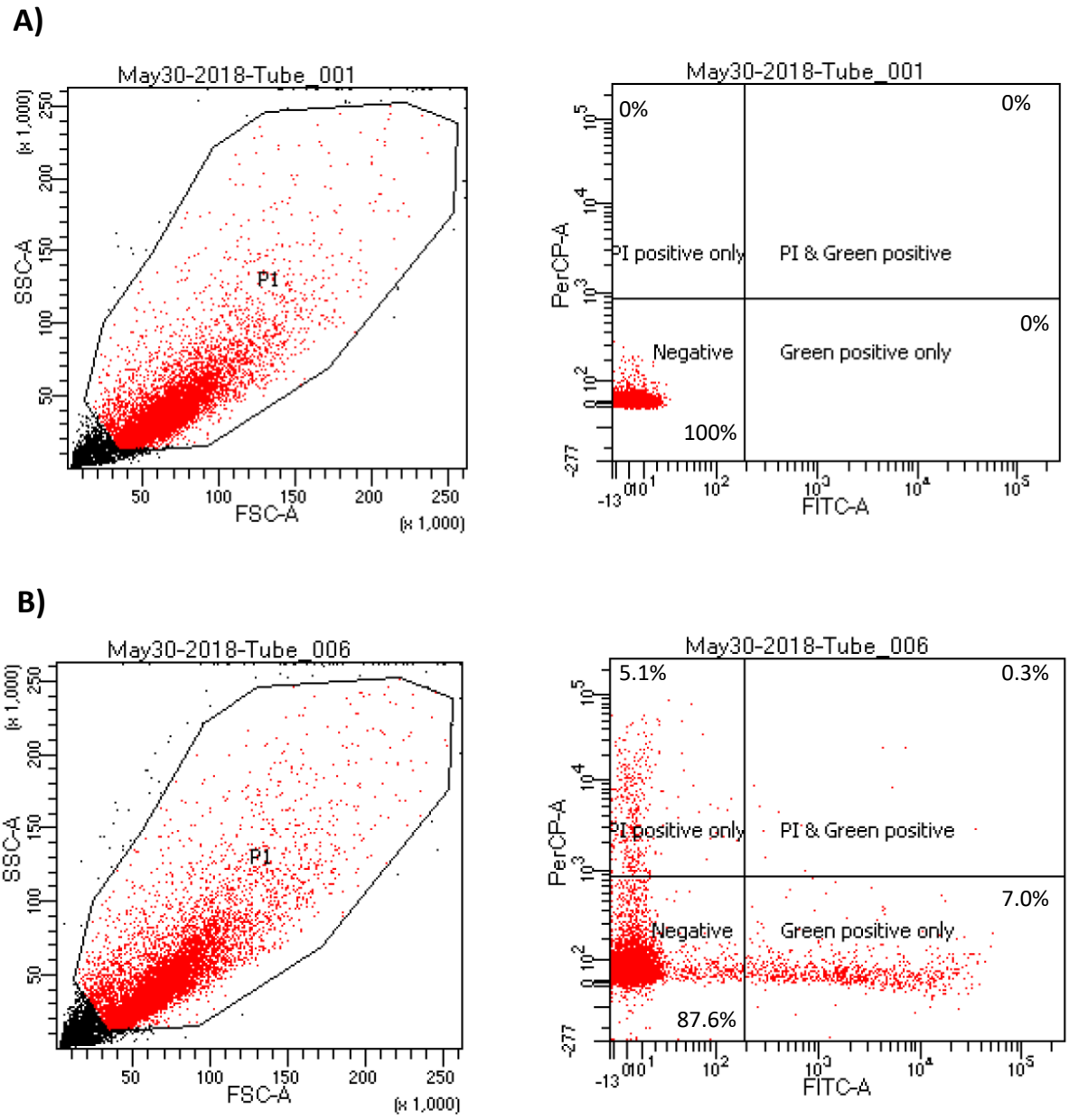

Figure C-4 Sample image of gating used for flow cytometry analysis of transfection samples. Panel A) shows the non-treated, unstained cell sample, and Panel B) is cells treated with the 0.2 F87/16-3-16/pDNA

Table C-3 eGFP expression and propidium iodide staining results from quadrant gating of 10,000 events analyzed through flow cytometry events. Average percent of the total events from each quadrant ± standard deviation are shown.

Treatment	− GFP, + PI (%)	+ GFP, + PI (%)	+ GFP, − PI (%)	− GFP, − PI (%)
0.2 F87/G/P	3.9 ± 1.1	0.2 ± 0.1	7.6 ± 1.0	88.4 ± 1.3
0.4 F87/G/P	3.9 ± 0.8	0.2 ± 0.1	8.0 ± 1.2	87.8 ± 1.7
0.6 F87/G/P	3.6 ± 0.8	0.1 ± 0.0	6.3 ± 0.3	89.9 ± 1.0
0.8 F87/G/P	4.4 ± 1.6	0.1 ± 0.1	5.5 ± 0.6	89.9 ± 1.4
F87 only (no G/P)	2.8 ± 0.7	0.0 ± 0.0	0.0 ± 0.0	97.2 ± 0.7
0.8 F87/G (no P)	3.4 ± 1.4	0.0 ± 0.0	0.0 ± 0.0	96.6 ± 1.4
0.2 F87/G (no P)	3.0 ± 1.7	0.0 ± 0.0	0.0 ± 0.0	97.0 ± 1.7
0.8 F87/P (no G)	2.6 ± 0.7	0.0 ± 0.0	0.0 ± 0.0	97.3 ± 0.7
0.2 F87/P (no G)	2.6 ± 0.5	0.0 ± 0.0	0.0 ± 0.0	97.4 ± 0.5
0.2 P84/G/P	3.3 ± 0.3	0.2 ± 0.1	8.9 ± 0.7	87.6 ± 0.4
0.4 P84/G/P	3.8 ± 0.4	0.2 ± 0.1	7.2 ± 1.4	88.9 ± 1.6
0.6 P84/G/P	3.9 ± 0.2	0.0 ± 0.0	3.9 ± 1.0	92.1 ± 1.1
0.8 P84/G/P	4.7 ± 1.4	0.0 ± 0.0	1.4 ± 1.0	93.9 ± 1.9
P84 only (no G/P)	4.0 ± 2.1	0.0 ± 0.0	0.0 ± 0.0	96.0 ± 2.1
0.8 P84/G (no P)	7.2 ± 1.0	0.0 ± 0.0	0.0 ± 0.0	92.8 ± 1.0
0.2 P84/G (no P)	5.1 ± 1.8	0.0 ± 0.0	0.0 ± 0.0	94.9 ± 1.8
0.8 P84/P (no G)	3.9 ± 1.4	0.0 ± 0.0	0.0 ± 0.0	96.1 ± 1.4
0.2 P84/P (no G)	3.3 ± 0.8	0.0 ± 0.0	0.0 ± 0.0	96.7 ± 0.8
0.2 L121/G/P	4.4 ± 0.7	0.0 ± 0.0	1.3 ± 0.4	94.3 ± 0.3
0.4 L121/G/P	4.7 ± 0.5	0.0 ± 0.0	1.0 ± 0.1	94.3 ± 0.4
0.6 L121/G/P	4.9 ± 0.3	0.1 ± 0.1	3.4 ± 1.4	91.6 ± 1.8
0.8 L121/G/P	4.5 ± 0.3	0.1 ± 0.2	5.2 ± 2.7	90.1 ± 3.0
L121 only (no G/P)	3.2 ± 0.4	0.0 ± 0.0	0.0 ± 0.0	96.7 ± 0.5
0.8 L121/G (no P)	5.2 ± 0.4	0.0 ± 0.0	0.0 ± 0.0	94.8 ± 0.5
0.2 L121/G (no P)	6.0 ± 0.4	0.0 ± 0.0	0.0 ± 0.0	94.0 ± 0.4
0.8 L121/P (no G)	3.2 ± 1.3	0.0 ± 0.0	0.1 ± 0.1	96.8 ± 1.2
0.2 L121/P (no G)	3.8 ± 0.5	0.0 ± 0.0	0.0 ± 0.0	96.2 ± 0.6

Table C-3 (cont'd) eGFP expression and propidium iodide staining results from quadrant gating of 10,000 events analyzed through flow cytometry events. Average percent of the total events from each quadrant ± standard deviation are shown. Average median GFP fluorescence intensity of the live transfected cells (+ GFP, − PI) population ± standard deviation is also reported where applicable.

Treatment	− GFP, + PI (%)	+ GFP, + PI (%)	+ GFP, − PI (%)	− GFP, − PI (%)
0.2 F127/G/P	3.1 ± 0.9	0.0 ± 0.0	0.2 ± 0.1	96.7 ± 1.0
0.4 F127/G/P	3.3 ± 1.0	0.0 ± 0.0	0.1 ± 0.1	96.6 ± 1.0
0.6 F127/G/P	3.1 ± 0.8	0.0 ± 0.0	0.1 ± 0.0	96.9 ± 0.8
0.8 F127/G/P	3.5 ± 1.0	0.0 ± 0.0	0.1 ± 0.1	96.4 ± 1.1
F127 only (no G/P)	2.9 ± 0.3	0.0 ± 0.0	0.0 ± 0.0	97.1 ± 0.3
0.8 F127/G (no P)	3.5 ± 0.7	0.0 ± 0.0	0.0 ± 0.0	96.5 ± 0.7
0.2 F127/G (no P)	3.5 ± 0.5	0.0 ± 0.0	0.0 ± 0.0	96.5 ± 0.5
0.8 F127/P (no G)	3.2 ± 0.6	0.0 ± 0.0	0.0 ± 0.0	96.8 ± 0.6
0.2 F127/P (no G)	2.7 ± 0.8	0.0 ± 0.0	0.0 ± 0.0	97.3 ± 0.9
0.2 P103/G/P	5.2 ± 2.1	0.0 ± 0.0	0.8 ± 0.6	94.0 ± 2.7
0.4 P103/G/P	6.2 ± 3.5	0.0 ± 0.0	0.2 ± 0.1	93.5 ± 3.6
0.6 P103/G/P	3.6 ± 1.1	0.0 ± 0.0	0.2 ± 0.0	96.2 ± 1.1
0.8 P103/G/P	5.9 ± 1.7	0.0 ± 0.0	0.1 ± 0.0	94.1 ± 1.7
P103 only (no G/P)	3.2 ± 0.3	0.0 ± 0.0	0.0 ± 0.0	96.8 ± 0.3
0.8 P103/G (no P)	7.5 ± 4.0	0.0 ± 0.0	0.0 ± 0.0	92.5 ± 4.0
0.2 P103/G (no P)	6.4 ± 3.3	0.0 ± 0.0	0.0 ± 0.0	93.6 ± 3.3
0.8 P103/P (no G)	9.1 ± 6.8	0.0 ± 0.0	0.0 ± 0.0	90.9 ± 6.8
0.2 P103/P (no G)	5.2 ± 2.9	0.0 ± 0.0	0.0 ± 0.0	94.7 ± 2.9
0.2 L44/G/P	3.7 ± 0.9	0.2 ± 0.1	9.1 ± 1.0	87.0 ± 1.2
0.4 L44/G/P	5.7 ± 3.5	0.3 ± 0.1	10.5 ± 1.7	85.2 ± 1.6
0.6 L44/G/P	3.5 ± 0.8	0.2 ± 0.0	10.8 ± 2.3	85.5 ± 1.6
0.8 L44/G/P	3.8 ± 0.9	0.3 ± 0.1	12.4 ± 0.5	83.5 ± 1.5
L44 only (no G/P)	3.2 ± 0.8	0.0 ± 0.0	0.0 ± 0.0	96.8 ± 0.8
0.8 L44/G (no P)	4.8 ± 1.3	0.0 ± 0.0	0.0 ± 0.0	95.2 ± 1.4
0.2 L44/G (no P)	3.8 ± 0.8	0.0 ± 0.0	0.0 ± 0.0	96.2 ± 0.8
0.8 L44/P (no G)	3.1 ± 1.1	0.0 ± 0.0	0.0 ± 0.0	96.9 ± 1.1
0.2 L44/P (no G)	3.3 ± 0.8	0.0 ± 0.0	0.0 ± 0.0	96.7 ± 0.8
No Treatment	3.0 ± 0.9	0.0 ± 0.0	0.0 ± 0.0	97.0 ± 0.9
23 µM 16-3-16	52.1 ± 13.1	0.0 ± 0.0	0.0 ± 0.0	47.9 ± 13.1
pDNA only	3.0 ± 1.2	0.0 ± 0.0	0.0 ± 0.0	96.9 ± 1.2
16-3-16 only	4.8 ± 2.2	0.0 ± 0.0	0.0 ± 0.0	95.2 ± 2.2
16-3-16/pDNA 10:1	4.2 ± 1.5	0.3 ± 0.2	8.8 ± 1.7	86.7 ± 2.2
Lipofectamine+pDNA	4.3 ± 1.8	0.7 ± 0.5	20.3 ± 4.6	74.7 ± 4.4
Lipofectamine only (no pDNA)	2.8 (n=1)	0.0 (n=1)	0.0 (n=1)	97.2 (n=1)

Cell Viability

Table C-4 Comparison of cell viability following treatment with F87 transfection nanoparticles determined by two different methods (resuzarin reduction, and propidium iodide staining).

	Cell Viability by Method		
Treatment	**CellTiter Blue (n=3) (%, normalized to untreated control)**	**Propidium Iodide (% of total events)**	
0.8 F87	96.9 ± 3.0	95.4 ± 1.7	(n = 3)
0.6 F87	96.0 ± 5.6	96.3 ± 0.9	(n = 3)
0.4 F87	96.1 ± 7.2	95.9 ± 0.8	(n = 3)
0.2 F87	94.6 ± 9.0	96.0 ± 1.2	(n = 3)
1 (F87 only)	96.2 ± 3.2	97.2 ± 0.7	(n = 3)
0.8 F87 (no 16-3-16)	94.3 ± 3.0	97.3 ± 0.7	(n = 3)
0.2 F87 (no 16-3-16)	95.2 ± 5.9	97.4 ± 0.5	(n = 3)
0.8 F87 (no pDNA)	93.8 ± 2.5	96.6 ± 1.4	(n = 3)
0.2 F87 (no pDNA)	86.8 ± 5.4	97.0 ± 1.7	(n = 3)
16-3-16 only	97.4 ± 5.7	95.2 ± 2.2	(n = 9)
16-3-16/pDNA 10:1 (no F87)	93.9 ± 11.2	95.5 ± 1.5	(n = 12)
Lipofectamine + pDNA	98.0 ± 6.1	95.0 ± 2.2	(n = 12)
Lipofectamine only	99.2 ± 2.6	-	
Gemini (conc. = 23μM)	55.8 ± 5.8	47.9 ± 13.1	(n = 12)
DMSO	1.3 ± 1.7	-	
pDNA only	100.0 ± 1.1	97.0 ± 1.2	(n = 5)

Results of Dunnett's test for comparing transfection efficiency of Pluronic/16-3-16/pDNA treatments to the 16-3-16/pDNA complex (0GP) as a control

```
Dunnett's test for comparing several treatments with a control :
    95% family-wise confidence level

$`0GP`
                  diff      lwr.ci     upr.ci    pval
0.2F127-0GP -8.6233333 -12.9972871 -4.2493795 6.6e-07 ***
0.2F87-0GP  -1.1600000  -5.5339538  3.2139538  1.0000
0.2L121-0GP -7.5233333 -11.8972871 -3.1493795 1.7e-05 ***
0.2L44-0GP   0.2866667  -4.0872871  4.6606205  1.0000
0.2P103-0GP -7.9866667 -12.3606205 -3.6127129 4.3e-06 ***
0.2P84-0GP   0.1033333  -4.2706205  4.4772871  1.0000
0.4F127-0GP -8.6833333 -13.0572871 -4.3093795 5.0e-07 ***
0.4F87-0GP  -0.7400000  -5.1139538  3.6339538  1.0000
0.4L121-0GP -7.7666667 -12.1406205 -3.3927129 8.0e-06 ***
0.4L44-0GP   1.7700000  -2.6039538  6.1439538  0.9876
0.4P103-0GP -8.5300000 -12.9039538 -4.1560462 8.4e-07 ***
0.4P84-0GP  -1.6133333  -5.9872871  2.7606205  0.9959
0.6F127-0GP -8.7140000 -13.0879538 -4.3400462 4.4e-07 ***
0.6F87-0GP  -2.4333333  -6.8072871  1.9406205  0.8060
0.6L121-0GP -5.3400000  -9.7139538 -0.9660462  0.0057 **
0.6L44-0GP   1.9900000  -2.3839538  6.3639538  0.9587
0.6P103-0GP -8.6133333 -12.9872871 -4.2393795 6.2e-07 ***
0.6P84-0GP  -4.8666667  -9.2406205 -0.4927129  0.0173 *
0.8F127-0GP -8.7036667 -13.0776205 -4.3297129 4.9e-07 ***
0.8F87-0GP  -3.2300000  -7.6039538  1.1439538  0.3631
0.8L121-0GP -3.5400000  -7.9139538  0.8339538  0.2297
0.8L44-0GP   3.5900000  -0.7839538  7.9639538  0.2119
0.8P103-0GP -8.7080000 -13.0819538 -4.3340462 5.6e-07 ***
0.8P84-0GP  -7.3466667 -11.7206205 -2.9727129 2.7e-05 ***
LP-0GP      11.5566667   8.7903354 14.3229979 < 2e-16 ***

---
Signif. codes:  0 '***' 0.001 '**' 0.01 '*' 0.05 '.' 0.1 ' ' 1
```

Results of Dunnett's test for comparing transfection efficiency of Pluronic/16-3-16/pDNA treatments to that of Lipofectamine/pDNA (LP)

```
Dunnett's test for comparing several treatments with a control :
    95% family-wise confidence level

$LP
                  diff    lwr.ci     upr.ci    pval
0.2F127-LP -20.180000 -24.55395 -15.806046 < 2e-16 ***
0.2F87-LP  -12.716667 -17.09062  -8.342713 9.3e-13 ***
0.2L121-LP -19.080000 -23.45395 -14.706046 < 2e-16 ***
0.2L44-LP  -11.270000 -15.64395  -6.896046 9.8e-11 ***
0.2P103-LP -19.543333 -23.91729 -15.169380 < 2e-16 ***
0.2P84-LP  -11.453333 -15.82729  -7.079380 4.6e-11 ***
0.4F127-LP -20.240000 -24.61395 -15.866046 < 2e-16 ***
0.4F87-LP  -12.296667 -16.67062  -7.922713 6.1e-12 ***
0.4L121-LP -19.323333 -23.69729 -14.949380 < 2e-16 ***
0.4L44-LP   -9.786667 -14.16062  -5.412713 1.4e-08 ***
0.4P103-LP -20.086667 -24.46062 -15.712713 < 2e-16 ***
0.4P84-LP  -13.170000 -17.54395  -8.796046 2.1e-13 ***
0.6F127-LP -20.270667 -24.64462 -15.896713 < 2e-16 ***
0.6F87-LP  -13.990000 -18.36395  -9.616046 2.9e-14 ***
0.6L121-LP -16.896667 -21.27062 -12.522713 < 2e-16 ***
0.6L44-LP   -9.566667 -13.94062  -5.192713 4.5e-08 ***
0.6P103-LP -20.170000 -24.54395 -15.796046 < 2e-16 ***
0.6P84-LP  -16.423333 -20.79729 -12.049380 < 2e-16 ***
0.8F127-LP -20.260333 -24.63429 -15.886380 < 2e-16 ***
0.8F87-LP  -14.786667 -19.16062 -10.412713 2.1e-15 ***
0.8L121-LP -15.096667 -19.47062 -10.722713 3.3e-16 ***
0.8L44-LP   -7.966667 -12.34062  -3.592713 5.0e-06 ***
0.8P103-LP -20.264667 -24.63862 -15.890713 < 2e-16 ***
0.8P84-LP  -18.903333 -23.27729 -14.529380 < 2e-16 ***
0GP-LP     -11.556667 -14.32300  -8.790335 < 2e-16 ***

---
Signif. codes:  0 '***' 0.001 '**' 0.01 '*' 0.05 '.' 0.1 ' ' 1
```

Results of Dunnett's test for comparing cell viability of Pluronic/16-3-16/pDNA treatments to the no treatment (NT) control

```
  Dunnett's test for comparing several treatments with a control :
    95% family-wise confidence level

$NT
                    diff     lwr.ci     upr.ci   pval
0.2F127-NT  -0.13082500  -9.302782   9.041132 1.0000
0.2F87-NT   -1.03415833 -10.206115   8.137798 1.0000
0.2L121-NT  -1.46415833 -10.636115   7.707798 1.0000
0.2L44-NT   -0.95415833 -10.126115   8.217798 1.0000
0.2P103-NT  -2.22749167 -11.399448   6.944465 1.0000
0.2P84-NT   -0.50415833  -9.676115   8.667798 1.0000
0.4F127-NT  -0.35749167  -9.529448   8.814465 1.0000
0.4F87-NT   -1.14749167 -10.319448   8.024465 1.0000
0.4L121-NT  -1.70749167 -10.879448   7.464465 1.0000
0.4L44-NT   -1.27082500 -10.442782   7.901132 1.0000
0.4P103-NT  -3.27082500 -12.442782   5.901132 0.9987
0.4P84-NT   -0.92082500 -10.092782   8.251132 1.0000
0.6F127-NT  -0.08815833  -9.260115   9.083798 1.0000
0.6F87-NT   -0.74082500  -9.912782   8.431132 1.0000
0.6L121-NT  -2.01415833 -11.186115   7.157798 1.0000
0.6L44-NT   -0.75082500  -9.922782   8.421132 1.0000
0.6P103-NT  -0.65415833  -9.826115   8.517798 1.0000
0.6P84-NT   -1.00749167 -10.179448   8.164465 1.0000
0.8F127-NT  -0.51115833  -9.683115   8.660798 1.0000
0.8F87-NT   -1.57082500 -10.742782   7.601132 1.0000
0.8L121-NT  -1.68082500 -10.852782   7.491132 1.0000
0.8L44-NT   -1.15082500 -10.322782   8.021132 1.0000
0.8P103-NT  -2.88215833 -12.054115   6.289798 0.9998
0.8P84-NT   -1.72082500 -10.892782   7.451132 1.0000
OGP-NT      -1.51582500  -7.316680   4.285030 1.0000
D-NT       -49.15990833 -54.960763 -43.359054 <2e-16 ***
Gonly-NT    -1.78305389  -8.048693   4.482585 1.0000
LP-NT       -2.00915833  -7.810013   3.791696 0.9992
Ponly-NT    -0.06749167  -7.630881   7.495897 1.0000

---
Signif. codes:  0 '***' 0.001 '**' 0.01 '*' 0.05 '.' 0.1 ' ' 1
```

Transfection Nanoparticle Composition

Table C-5 Pluronic mole fraction in mixed micelles (X_1) at concentrations used in *in vitro* transfection experiments (c > CMC of the mixture). X_1^{stock} is calculated for c = 0.5 mM, the total surfactant concentration within the transfection mixtures, and X_1^{well} is calculated for the total surfactant concentration (indicated below for each condition) following dilution with 2 mL of cell culture medium in the well at the start of treatment.

Pluronic	Mole fraction Pluronic ($\alpha_{Pluronic}$)	Δ ($\Delta = f_2CMC_2 - f_1CMC_1$)	X_1^{stock}	Total surfactant concentration in transfection well (μM)	X_1^{well}
F87	**0.2**	0.642	0.200	9.47	0.211
	0.4	0.028	0.400	12.6	0.401
	0.6	-0.421	0.600	18.9	0.595
	0.8	-0.724	0.800	37.9	0.797
P84	**0.2**	0.273	0.200	9.47	0.205
	0.4	-0.026	0.400	12.6	0.399
	0.6	-0.134	0.600	18.9	0.598
	0.8	-0.309	0.800	37.9	0.799
L121	**0.2**	23.5	0.208	9.47	0.711
	0.4	1.34	0.401	12.6	0.426
	0.6	1.34	0.601	18.9	0.617
	0.8	-0.033	0.800	37.9	0.800
F127	**0.2**	2.44	0.201	9.47	0.248
	0.4	1.19	0.401	12.6	0.423
	0.6	0.09	0.600	18.9	0.601
	0.8	-0.45	0.800	37.9	0.798
P103	**0.2**	2.70	0.201	9.47	0.254
	0.4	1.13	0.401	12.6	0.422
	0.6	2.71	0.601	18.9	0.633
	0.8	0.114	0.800	37.9	0.800
L44	**0.2**	0.243	0.200	9.47	0.204
	0.4	-0.001	0.400	12.6	0.400
	0.6	-0.245	0.600	18.9	0.597
	0.8	-0.243	0.800	37.9	0.799

Bootstrap method

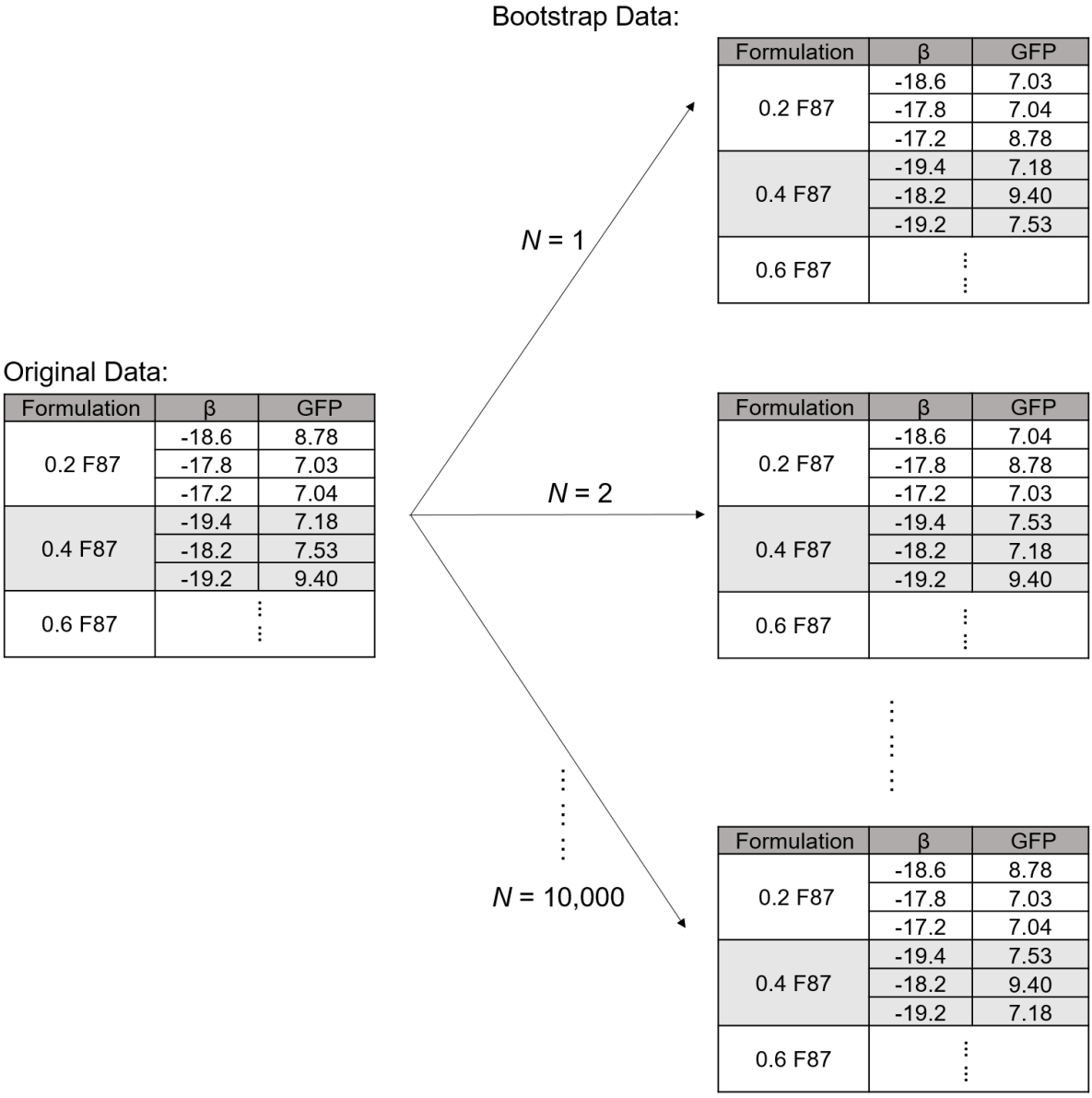

Figure C-5 Example illustration of random assignment of transfection observations to an interaction parameter using a bootstrap method.

Appendix D

Copyright Permission

JOHN WILEY AND SONS LICENSE TERMS AND CONDITIONS

May 28, 2020

This Agreement between Samantha Shortall ("You") and John Wiley and Sons ("John Wiley and Sons") consists of your license details and the terms and conditions provided by John Wiley and Sons and Copyright Clearance Center.

License Number	4827950651579
License date	May 14, 2020
Licensed Content Publisher	John Wiley and Sons
Licensed Content Publication	Wiley Books
Licensed Content Title	Surfactant Science and Technology, 3rd Edition
Licensed Content Author	Drew Myers
Licensed Content Date	Oct 1, 2005
Licensed Content Pages	1
Type of Use	Dissertation/Thesis
Requestor type	University/Academic
Format	Print and electronic
Portion	Figure/table
Number of figures/tables	2
Will you be translating?	No
Title	Relationship Between Transfection Efficiency and Mixed Micelle Characterization of Pluronic and Gemini Surfactant – Based Gene Therapy Carriers
Institution name	n/a
Expected presentation date	Jun 2020
Portions	Figure 6.1 Figure 7.8
Requestor Location	Samantha Shortall 200 University Ave. W. Waterloo, ON N2L 3G1 Canada Attn: Samantha Shortall
Publisher Tax ID	EU826007151
Total	**0.00 CAD**
Terms and Conditions	

ELSEVIER LICENSE
TERMS AND CONDITIONS

May 28, 2020

This Agreement between Samantha Shortall ("You") and Elsevier ("Elsevier") consists of your license details and the terms and conditions provided by Elsevier and Copyright Clearance Center.

License Number	4837831043376
License date	May 28, 2020
Licensed Content Publisher	Elsevier
Licensed Content Publication	Elsevier Books
Licensed Content Title	Engineering of Nanobiomaterials
Licensed Content Author	Ana M.S. Cardoso,Sandra G. Silva,M. Luísa do Vale,Eduardo F. Marques,Maria C. Pedroso de Lima,Amália S. Jurado
Licensed Content Date	Jan 1, 2016
Licensed Content Volume	n/a
Licensed Content Issue	n/a
Licensed Content Pages	30
Start Page	227
End Page	256

Type of Use	reuse in a thesis/dissertation
Portion	figures/tables/illustrations
Number of figures/tables/illustrations	1
Format	both print and electronic
Are you the author of this Elsevier chapter?	No
Will you be translating?	No
Title	Mixed Micelle Characterization of Pluronic and Gemini Surfactant – Based Gene Therapy Carriers and a Connection to Transfection Efficiency
Institution name	n/a
Expected presentation date	Jun 2020
Portions	Figure 7.5
Requestor Location	Samantha Shortall 200 University Ave. W. Waterloo, ON N2L 3G1 Canada Attn: Samantha Shortall
Publisher Tax ID	GB 494 6272 12
Total	0.00 CAD

Order Date	20-Aug-2020	Type of Use	Republish in a thesis/dissertation
Order license ID	1057113-1	Publisher	FUTURE MEDICINE LTD
ISSN	1748-6963	Portion	Image/photo/illustration

LICENSED CONTENT

Publication Title	Nanomedicine	Publication Type	e-Journal
Article Title	Interactions between DNA and Gemini surfactant: impact on gene therapy: part I.	Start Page	289
		End Page	306
Date	01/01/2006	Issue	3
Language	English	Volume	11
Country	United Kingdom of Great Britain and Northern Ireland	URL	http://www.futuremedicine.com/loi/nnm
Rightsholder	Future Medicine Ltd.		

REQUEST DETAILS

Portion Type	Image/photo/illustration	Distribution	Worldwide
Number of images / photos / illustrations	1	Translation	Original language of publication
Format (select all that apply)	Print, Electronic	Copies for the disabled?	No
Who will republish the content?	Academic institution	Minor editing privileges?	No
Duration of Use	Life of current edition	Incidental promotional use?	No
Lifetime Unit Quantity	Up to 499	Currency	CAD
Rights Requested	Main product		

NEW WORK DETAILS

Title	Mixed Micelle Characterization of Pluronic and Gemini Surfactant-Based Gene Therapy Carriers and a Connection to Transfection Efficiency	Institution name	University of Waterloo
		Expected presentation date	2020-08-20
Instructor name	Samantha Shortall		

ADDITIONAL DETAILS

Order reference number	N/A	The requesting person / organization to appear on the license	Samantha Shortall

REUSE CONTENT DETAILS

Title, description or numeric reference of the portion(s)	Figure 2	Title of the article/chapter the portion is from	Interactions between DNA and Gemini surfactant: impact on gene therapy: part I.
Editor of portion(s)	Ahmed, Taksim; Kamel, Amany O; Wettig, Shawn D	Author of portion(s)	Ahmed, Taksim; Kamel, Amany O; Wettig, Shawn D
Volume of serial or monograph	11	Issue, if republishing an article from a serial	3
Page or page range of portion	289-306	Publication date of portion	2016-02-01

SPRINGER NATURE LICENSE
TERMS AND CONDITIONS

May 28, 2020

This Agreement between Samantha Shortall ("You") and Springer Nature ("Springer Nature") consists of your license details and the terms and conditions provided by Springer Nature and Copyright Clearance Center.

License Number	4837831459644
License date	May 28, 2020
Licensed Content Publisher	Springer Nature
Licensed Content Publication	Journal of Molecular Medicine
Licensed Content Title	Linear closed mini DNA generated by the prokaryotic cleaving-joining enzyme TelN is functional in mammalian cells
Licensed Content Author	Jochen Heinrich et al
Licensed Content Date	Jan 1, 2002
Type of Use	Thesis/Dissertation
Requestor type	academic/university or research institute
Format	print and electronic
Portion	figures/tables/illustrations
Number of figures/tables/illustrations	1

Will you be translating?	no
Circulation/distribution	1 - 29
Author of this Springer Nature content	no
Title	Mixed Micelle Characterization of Pluronic and Gemini Surfactant – Based Gene Therapy Carriers and a Connection to Transfection Efficiency
Institution name	n/a
Expected presentation date	Jun 2020
Portions	Figure 2A
Requestor Location	Samantha Shortall 200 University Ave. W. Waterloo, ON N2L 3G1 Canada Attn: Samantha Shortall
Total	0.00 CAD